Technical Report

TR-99-06

Main Report
Volume II

Deep repository for spent nuclear fuel

SR 97 – Post-closure safety

November 1999

Svensk Kärnbränslehantering AB
Swedish Nuclear Fuel
and Waste Management Co
Box 5864
SE-102 40 Stockholm Sweden
Tel 08-459 84 00
+46 8 459 84 00
Fax 08-661 57 19
+46 8 661 57 19

SKB

Main Report
Volume II

Deep repository for spent nuclear fuel

SR 97 – Post-closure safety

November 1999

Contents

Volume 1

Volume II

9 Canister defect scenario

9.1 Introduction

The premises for the canister defect scenario are the same as for the base scenario, except for one important point: A few canisters are postulated to have initial defects so that the isolation function can be said to be jeopardized already at repository closure.

Otherwise, as for the base scenario, the situation in brief is that the repository is assumed to be designed according to specifications, and present-day conditions in the surroundings are assumed to persist. The evolution in and around the majority of canisters, which are assumed to be undamaged, is thereby expected to be the same as for the base scenario and is therefore not dealt with in the canister defect scenario.

Instead, all relevant aspects of the evolution of the damaged canisters are dealt with in detail, along with radionuclide migration from damaged canisters in buffer/backfill, geosphere and biosphere. A much more detailed description of groundwater flow and biosphere conditions is required for radionuclide migration than was the case in the base scenario.

An overview of the processes and dependencies that are analyzed in detail in the canister defect scenario is given in section 9.4. This section also describes the structure of Chapter 9, based on the system of processes and dependencies. Much in the subanalyses paves the way for the concluding analysis of radionuclide transport.

9.2 Initial state

The initial state of the repository is thus assumed to be the same as in the base scenario, except that a few canisters are postulated to have undetected defects so that the isolation function can be said to be jeopardized already at repository closure.

9.2.1 Initial canister defects

An estimation of the size and frequency of initial defects must be based on assumptions and reasoning. Statistically relevant data on defects and frequencies cannot be built up until experience has been gained from a large number of canisters that have been sealed and then inspected. Even such a body of data would be of limited value, since the canisters that are discovered to have defects would be discarded or repaired, and can therefore not be used directly to estimate the frequency of defective canisters which escape detection.

The fundamental reasoning in judging the size and extent of the initial defects is firstly that there are only a few events that could lead to an initial defect, and secondly that the defect must be small enough so that there is a reasonable likelihood that it will escape detection. If a defect does occur, it is therefore most probable that it will be in the weld between the lid and body of the canister. The other welds in the canister shell are easier to inspect, since inspection can be performed both internally and externally and furthermore in a non-radioactive environment.

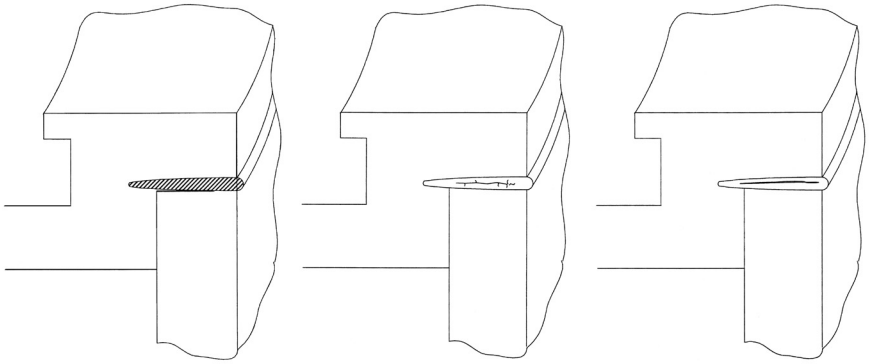

Figure 9-1. *Illustration of initial canister defects caused by lack of fusion, cracking and discharges in the electron beam gun /from Punshon, 1997/.*

Welding defects that could cause a penetrating defect are identified in Punshon /1997/:

- Lack of fusion, meaning that the weld has not fused in both lid and body. This may be caused by e.g. thermal expansion of the material or incorrect angle of the welding gun.
- Cracking in the welded joint can occur during repairs of an unsuccessful joint.
- Discharges in the electron beam welder can give rise to metal fume that temporarily breaks the electron beam and causes a hole in the weld.

All of these defects can be detected with ultrasonic testing. Technology for minimizing the risk of these defects and methods for checking that the sealing welds meet the established requirements are being developed in SKB's Canister Laboratory. Figure 9-1 illustrates the different defects.

In order for a defect to go undetected, it must be small, presumably not larger than 1 mm^2.

There is today no real way to estimate the number of canisters with initial defects. The design requirements for the canister say that no more than one canister out of a thousand may leave the Encapsulation Plant with a weld that fails to meet the acceptance criteria for the nondestructive testing /Werme, 1998/. In SR 97, it is therefore postulated that no more than 0.1 percent of the canisters have initial defects. The real number of canisters with initial defects is expected to be lower.

9.2.2 Data for calculations of radionuclide transport

In the canister defect scenario, it is postulated as a reasonable case that one canister out of a total of about 4,000 has passed through quality inspection with a penetrating defect of 1 mm^2 in size. Both circular holes (cracks and discharges) and circumferential defects (lack of fusion) are discussed in the following sections.

In the pessimistic case, it is assumed that five canisters (i.e. about 0.1 percent) have such defects.

9.3 Boundary conditions

The external conditions in the canister defect scenario are postulated to be the same as in the base scenario, i.e. in brief:

- Present-day climatic conditions are assumed to prevail in the future.
- Land uplift and its influence on groundwater flows, biosphere etc. is included.
- Present-day site-specific biospheres are assumed to persist, except for the effects of land uplift on the biosphere.
- Rock-mechanical changes take place only as a result of aseismic processes, i.e. earthquakes are not included.
- No human intrusions occur.

The boundary conditions are described in greater detail in the base scenario, section 8.3.

9.4 Overview of processes and dependencies

All processes and dependencies that occur in the base scenario, Chapter 8, also occur in the canister defect scenario. In the case of canisters with penetrating defects, a number of additional processes also occur, most inside the damaged canister. Figure 9-2 shows processes in common with the base scenario in black and additional processes in the canister defect scenario in red.

The course of events starts when water from the buffer, either as a liquid or as vapour, enters a damaged canister. This leads to a cycling of water and gas in the interior of the canister, with strong couplings to some important chemical processes. Water coming in contact with the insert leads to iron corrosion. This leads to the formation of hydrogen gas, which affects both chemical and hydraulic conditions inside the canister, for one thing by counteracting further influx of water. If the gas pressure becomes high enough, gas may be released as a pulse through the buffer and on out into the geosphere. In time, the corrosion may also have mechanical consequences. For one thing, the build-up of solid corrosion products in the gap between insert and copper canister may cause mechanical stresses that may further damage the copper shell. For another, extensive iron corrosion may reduce the mechanical strength of the cast iron insert. Water in a damaged canister might also have consequences for the radiation-related evolution: Neutrons from the fuel may be slowed down by attenuation (moderation) in the water to energies that favour neutron-induced fission of above all U-235 and Pu-239 in the fuel. Fission liberates new neutrons, and the process could, under very unfavourable conditions, become self-sustaining. The system is then said to be critical.

If the water penetrates all the way in to the fuel, corrosion of cladding tubes and other metal parts in the fuel also occurs. The metal parts contain radionuclides that are released by the corrosion.

If the cladding tubes have penetrating defects, either initially or as a result of corrosion, water can come into contact with the fuel matrix. Radionuclides on the surface of the fuel matrix may then dissolve in water and become available for migration, and the fuel matrix may dissolve, releasing matrix-bound radionuclides. The chemical form of the nuclides in contact with water in the interior of the canister is determined by speciation

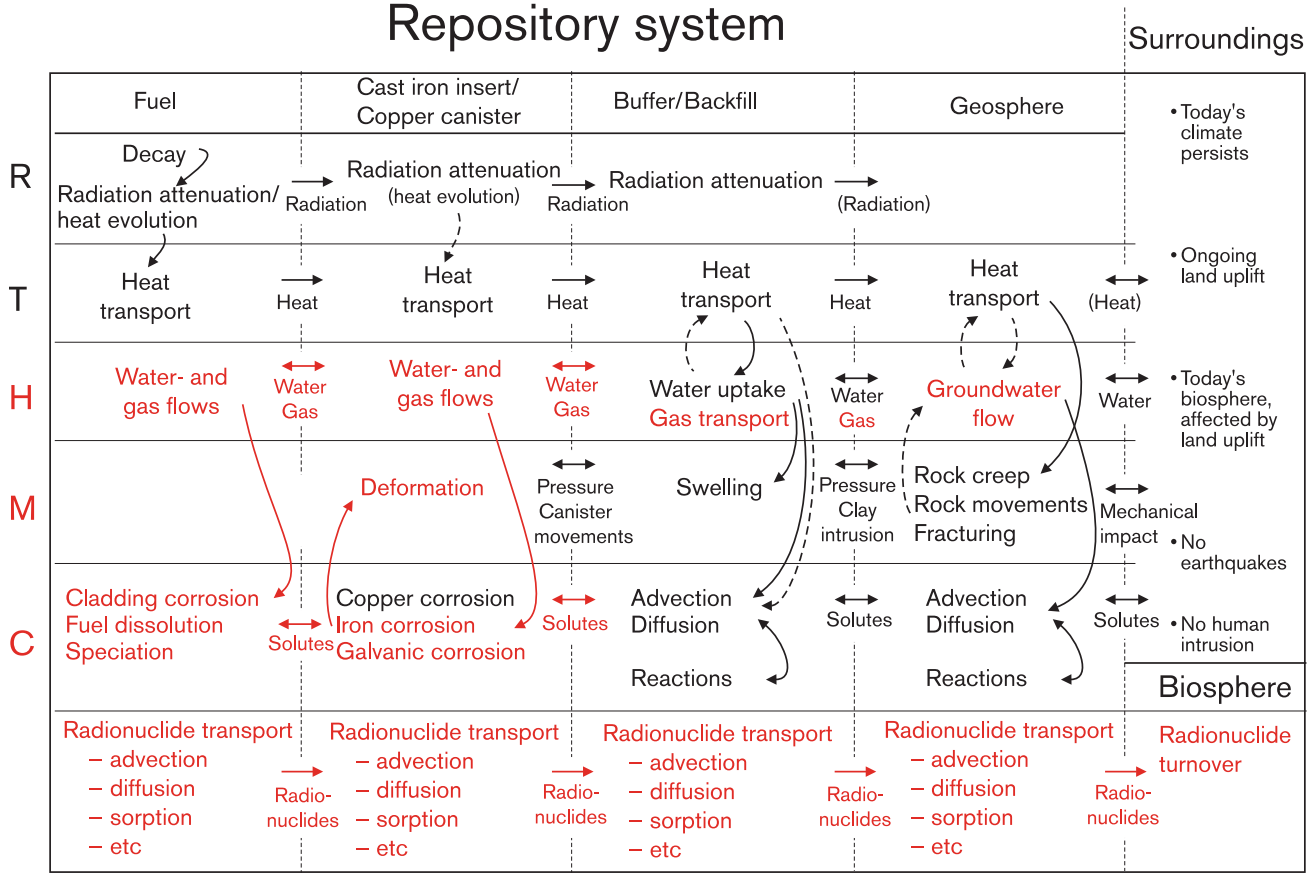

Figure 9-2. *The main features of the process system for the canister defect scenario in the geosphere. Red processes follow a different course or have a different scope than in the base scenario.*

processes, which for example determine whether the nuclides will remain as solutes or be precipitated as solid phases. Speciation is determined by the chemical environment in the canister, which is in turn affected strongly by the iron and iron corrosion.

Dissolved radionuclides (solutes) can be transported out of the canister, mainly by diffusion, through the hole in the canister to the buffer. There as well, radionuclide transport takes place principally by diffusion. Transport through the buffer is also greatly affected by sorption. In the geosphere, radionuclides may be further transported with the flowing groundwater – advection. Matrix diffusion also occurs here, i.e. radionuclides diffuse into the stagnant water in the microfractures in the rock and are thereby retained from the flowing water. Another mechanism of crucial importance for radionuclide transport in the geosphere is sorption, whereby radionuclides can adhere to the surfaces of the fracture system and the rock matrix. Finally, radioactive decay affects the radionuclide content of the entire system and must therefore be included in the description of transport phenomena.

9.4.1 Structure of the reporting

The structure of the reporting of the canister defect scenario is similar to that of the base scenario, which follows a relatively strict subdivision into radiation-related, thermal, hydraulic, mechanical and thermal evolution. The subdivision has been modified slightly in the canister defect scenario. Furthermore, there is an additional, lengthy section on radionuclide transport which is based on the material in the preceding sections. The main headings in the canister defect scenario are as follows:

Radiation-related evolution, criticality

Beyond what is described in the base scenario, the question of criticality needs to be addressed in the canister defect scenario. This is done in section 9.5.

Thermal evolution

The thermal evolution of buffer and rock is expected to be the same as in the base scenario around both intact and damaged canisters.

In a defective canister, thermal conductivity and thereby temperature evolution could be affected by intruding water. However, liquid water is not expected to occur in significant quantities in a defective canister for thousands of years, according to section 9.6. By then, the decay heat flux has declined to such a low level that the temperature elevation in the canister is very small. For this reason, a minor change in thermal conductivity in the canister will be of no importance.

Therefore, the thermal evolution is not dealt with in the canister defect scenario.

Hydromechanical evolution in defective canister and buffer

Section 9.6 deals with water ingress in a damaged canister with subsequent iron corrosion and hydrogen gas generation. The section also discusses how the increasing gas pressure counteracts the influx of water and how hydrogen gas at sufficiently high pressures can penetrate through the buffer. The mechanical evolution in the canister is also dealt with: Iron corrosion leads to formation of magnetite, which is less dense than iron and thereby occupies a larger volume. An extensive build-up of corrosion products in the canister leads to mechanical stresses.

Chemical evolution in defective canister

Section 9.7 deals with various aspects of the chemical evolution in a defective canister, including:

- Iron corrosion.
- Corrosion of the cladding tubes around the fuel pellets and other metal parts in the fuel assemblies.
- Dissolution/conversion of the fuel matrix, a process that determines the rate of release of many radionuclides.
- Chemical speciation of radionuclides. The chemical form of the radionuclides is of crucial importance for their solubility in water, which is in turn crucial for the releases of radionuclides from the canister.

Hydraulic evolution in the geosphere

Section 9.8 deals with the hydraulic evolution in the geosphere at the three repository sites in much greater detail than in the base scenario. This is necessary to provide an adequate description of radionuclide transport in the geosphere.

Transport processes in the repository

Section 9.9 deals with transport processes for radionuclides in canister, buffer/backfill and geosphere.

Radionuclide turnover in the biosphere

Section 9.10 deals with the biosphere processes that are of importance for radionuclide transport in different ecosystems in the biosphere.

Radionuclide transport

Section 9.11 presents integrated calculations of radionuclide transport in canister, buffer/backfill, geosphere and biosphere. The chain of models used for calculation of radionuclide transport is presented. Many of the premises for the calculations come from previous sections in the presentation of the canister defect scenario. The section ends with the presentation of a number of calculation cases and a discussion of the calculation results.

9.4.2 Data for calculations of radionuclide transport

The analysis of the canister defect scenario includes calculations of radionuclide transport in canister, buffer/backfill, geosphere and biosphere. A large quantity of data used in the calculations is obtained as a result of the initial analyses that precede the analysis of radionuclide transport. These data are reported directly in the relevant section as follows:

- Canister defects, section 9.2.2.
- Delay time, section 9.6.2.
- Fuel dissolution rate, section 9.7.4.
- Radionuclide solubilities, section 9.7.6.
- Groundwater flows and advective travel times, section 9.11.2.
- Transport data in buffer and geosphere, section 9.9.
- Biosphere conversion factors, section 9.10.3.

Data for transport calculations are reported under the heading “Data for calculations of radionuclide transport” in each section. As was seen in Chapter 4, an attempt is always made in the choice of data to find a set of reasonable values and a set of values that will give pessimistic results in the calculations. The choice of data is explained more fully in the Data Report.

9.5 Radiation-related evolution, criticality

9.5.1 Introduction

The radiation-related evolution is assumed to be essentially the same for a damaged and an undamaged canister, i.e. radiation levels in and around the canister are affected very marginally by a defect in the copper canister with accompanying water ingress.

One important question concerning the radiation-related evolution must be investigated in detail, however: Might the conditions in a damaged canister under any circumstances possibly be such that a fission process becomes self-sustaining? Here it is important to study different fuel types, burnups and hydraulic conditions inside the canister.

Neutrons with suitable energy can cause nuclear fissions particularly in uranium-235, plutonium-239 and plutonium-241 in the spent fuel. If water enters a defective canister, neutrons can be moderated (slowed down) to suitable energies. Under very unfavourable circumstances, this could result in a self-sustaining chain reaction. The system is then said to be critical.

Of crucial importance for the criticality conditions in a system is the effective multiplication constant, k_{eff}. An average of 2.5–3 new neutrons are formed in each fission. They can be captured by other atomic nuclei in the fuel, in the canister material or in the surroundings. K_{eff} indicates how many of the new neutrons give rise to a new fission. If k_{eff} has a value of exactly **one**, a critical state is achieved and a self-sustaining chain reaction is obtained. If k_{eff} is less than one, neutrons must be supplied in some other way to keep the reaction going. If k_{eff} is greater than one, a steadily increasing number of fissions is obtained.

Agrenius /1999/ calculates criticality conditions in the canister for different conditions. The following material is taken from that report.

9.5.2 Premises

The criticality conditions have been calculated assuming the canister design described in section 6.3. The calculations have been done for BWR fuel of type SVEA-64 with a mean enrichment of 3.6 percent U-235 and for PWR fuel of type F17x17 with a mean enrichment of 4.2 percent U-235.

These fuels provide coverage from a criticality viewpoint of the fuel types expected to occur in an actual repository. The reference fuel in SR 97 (BWR, SVEA 96) is less prone to criticality.

The requirement from a criticality viewpoint is that k_{eff} may not exceed 0.95, after uncertainties in the determination of the value have been taken into account.

The calculations are done for a situation where the fuel is postulated to be placed in canisters where the cavity in the insert has been filled with water and where the canisters are surrounded by bentonite externally.

9.5.3 Calculations

Unspent fuel has a reactivity (tendency to become critical) that is dependent upon its enrichment, among other factors. Fissionable material in the fuel is consumed during operation, which is why reactivity declines with burnup.

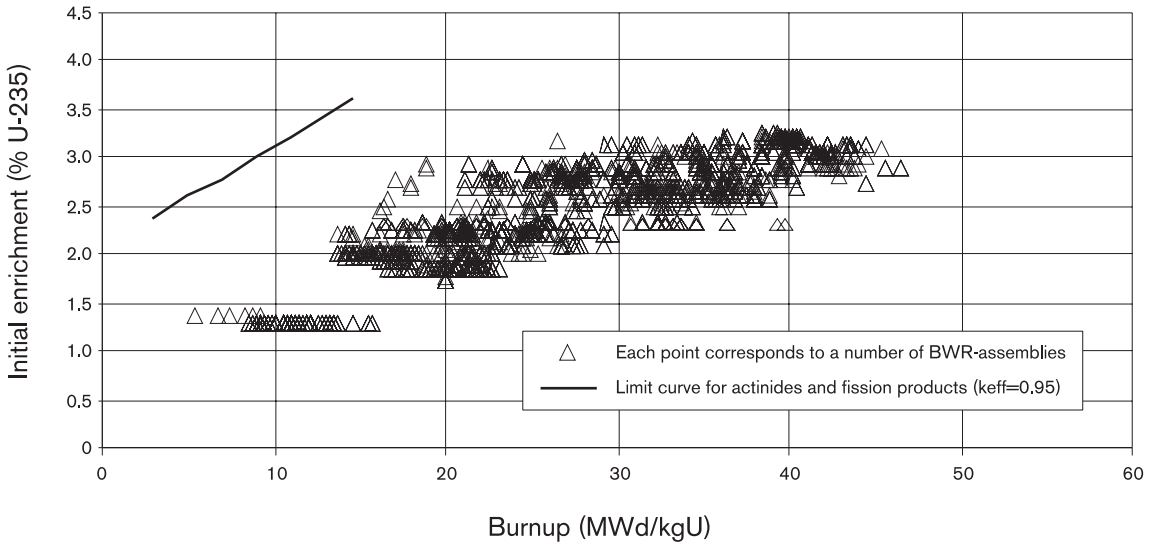

Figure 9-3. *Limit curve and fuel data for BWR fuel.*

Knowing how k_{eff} is dependent upon enrichment and burnup, it is possible to calculate what combinations of these factors give a k_{eff} of 0.95 in the canister geometry.

Figure 9-3 shows a curve with combinations of enrichment and burnup that give a k_{eff} of 0.95 for BWR fuel. Fission products that absorb neutrons and thereby lower reactivity are included in the calculation.

Before the calculations were done, uncertainties in burnup determination were analyzed. Effects of uneven burnup in the fuel assembly, of extracted fuel rods, varying spacing between channels, gap width between assembly and channel, eccentric placement, and cavities and porosities in the insert were also analyzed. The calculations were done with margin for uncertainties in all these factors.

The properties of all BWR fuel in CLAB as per 31 December 1998 are also plotted in Figure 9-3. All fuel assemblies lie below the limit curve in the graph and can thereby be accepted from a criticality viewpoint for placement in the canister. The equivalent limit curve and CLAB inventory for PWR fuel are shown in Figure 9-4. The graphs show that all fuel that is currently being stored in CLAB meets the criticality requirements with good margin.

9.5.4 Long-term perspective

Since the deep repository must function for a very long time, it is imperative to analyze how the long-term evolution of the repository could affect the risk of criticality. Processes of potential importance are:

- Reactivity changes due to radioactive decay.
- Corrosion and other chemical processes that affect canister, canister insert, fuel material and fuel geometry.
- Local accumulation of fissile material.

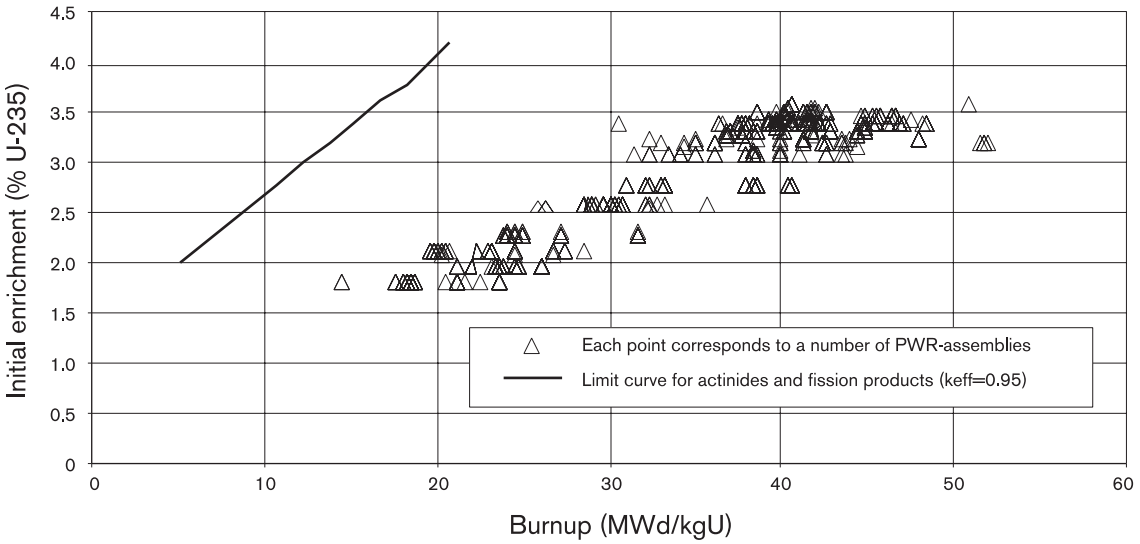

Figure 9-4. *Limit curve and fuel data for PWR fuel.*

Radioactive decay

Reactivity declines at an early stage due to decay of Pu-241. In a very long time perspective, reactivity rises once again due to decay of actinides, which reduces neutron absorption. Reactivity in the deep repository is, however, never greater than for the fuel composition 40 days after operation, which is used in the calculations.

Corrosion

Corrosion of the canister insert could reduce the dimensions of the fuel channels due to build-up of corrosion products. The calculations of this case show that reactivity decreases sharply if the channels are filled with corrosion products and the fuel is intact. The absorbing action of the iron reduces k_{eff} to approximately 0.5.

If the same calculation is done with the geometry that gives the highest reactivity, the resulting k_{eff} is 0.7 for BWR fuel and 0.65 for PWR fuel.

The conclusion is that corrosion of the canister insert counteracts the occurrence of criticality.

Local accumulation of fissile material

Hicks and Green /1999/ have summarized studies of criticality in repositories for radioactive waste. The conclusion is that the probability of a local accumulation of critical mass is low, and that even if one should form the consequences would be small.

9.5.5 Conclusions

The analyses show that the spent BWR and PWR fuel that is present in CLAB and that which comes from the Swedish nuclear power plants can be disposed of in the canisters with good margin to criticality, even if the canisters should for some reason be filled completely or partially with water. Future changes in isotope composition, material or geometry are not predicted to reduce the margin to criticality.

9.6 Hydromechanical evolution in defective canister

The hydraulic evolution in a canister with a damaged copper shell underlies all essential processes that distinguish the evolution of a damaged canister from that of an undamaged one: Ingress of water is a prerequisite for corrosion of the copper canister, which in turn gives rise to production of hydrogen gas. Water is also a prerequisite for corrosion of the fuel's metal parts, fuel dissolution and radionuclide transport.

Due to the fact that the corrosion processes both consume water and generate hydrogen, strong couplings exist between the chemical and the hydraulic evolution, which must therefore be described in a single context. Certain aspects of the mechanical evolution must also be dealt with in parallel with the hydrochemical processes.

This section deals with water ingress in the canister, consumption of water and build-up of hydrogen gas pressure as a consequence of iron corrosion and release of gas from the interior of the canister through the buffer to the geosphere. The build-up of solid corrosion products between the cast iron insert and the copper shell is also described, along with the consequences in the form of enlargement of the initial defect.

The processes are important for the function of a repository. In order for radionuclides to be transported out of the spent fuel, there must be a continuous water pathway between the fuel and the groundwater in the rock, with the exception of nuclides that are transported with gas. Consumption of water in the canister means that it can take a very long time before such a water pathway forms.

The description is based on two new model studies of the hydromechanical evolution in a canister with a damaged copper shell, one by Bond et al /1997/ and one by Takase et al /1999/. A series of regimes are first described in the following, which is also what is modelled in the studies. Then a likely composite sequence of events, composed of the various interim sequences, is sketched.

9.6.1 Corrosion data

The reaction rate for iron corrosion is in several ways crucial for the subsequent course of events if water enters the canister. The corrosion rate determines the rate of formation of hydrogen gas and solid corrosion products, and is thereby very important for the hydraulic and mechanical evolution in the canister. The rate also governs the consumption of water in the canister. This indirectly influences radionuclide transport, which requires a continuous water pathway between the fuel and the hole in the canister.

Data on the corrosion rate are needed for the quantitative treatment of the hydraulic evolution. The corrosion process is discussed in detail in section 9.7.2. Based on that account, 0.1 μm/y can be used as a reasonable point of departure for the discussions below, both for liquid water and for hydrogen gas saturated with water vapour.

9.6.2 Hydraulic evolution in canister

In the event of a penetrating defect in the canister's copper shell, water can be driven through the buffer and into the canister by the difference between the internal gas pressure in the canister and the groundwater pressure. When water comes into contact with the iron insert, it will corrode. The iron corrosion consumes the intruding water, at the same time as hydrogen gas is generated and the gas pressure in the canister increases. The pressure differential across the buffer is thereby reduced and the rate of influx of water decreases.

The flow of water in a damaged canister is dependent on the size and shape of the defect, the permeability of the buffer and the pressure differential between the groundwater and the interior of the canister. For a circular hole with an area of 1 mm^2, the flow can be calculated to be 5.5 ml/y with typical values for the properties of buffer and groundwater. For a crack around the circumference of the canister body, also with an area of 1 mm^2, the inflow is 1.2 l/y /Bond et al, 1997/. In the first case, the canister cavity (approx. 1 m^3) would be filled in 180,000 years, and in the second case in 850 years. The shape of the hole is thus of great importance for the inflow rate. These calculations assume that no counterpressure is built up in the canister.

In reality, hydrogen gas from corrosion of the iron insert is expected to cause a pressure build-up in the canister, which in turn reduces the inflow. Ingress of water into the canister, coupled with water consumption and pressure build-up, has been modelled by both Bond et al /1997/ and Takase et al /1999/ for a variety of conditions. Most calculations in these studies apply to 5 mm^2 defects. In some cases reported below, the results have been rescaled to apply to 1 mm^2, since this value has been assigned to the size of the initial defect investigated in the canister defect scenario.

With a corrosion rate of 0.1 μm/y and a 1 mm^2 circular hole, the calculations show that no water volume will ever be built up, since all intruding water is consumed by corrosion. The pressure in the canister gradually approaches the groundwater pressure asymptotically. The pressure in the canister is 4 MPa after about 4,500 years and 4.9 MPa after about 11,000 years.

If the defect is larger and/or the corrosion rate is lower, water will accumulate in the canister. With a corrosion rate of 0.01 μm/y and a 5 mm^2 circular hole, the shell-insert gap is filled with water in approximately 3,000 years, assuming that the holes in both the shell and the insert are situated at the top. After that, water can run into the channels in the insert. The water level in the insert's channels is calculated to reach one decimetre after approximately 6,000 years. The level is then expected to fall as the increasing hydrogen gas pressure reduces the inflow of water and corrosion consumes the water that has already entered.

After approximately 11,000 years, the canister is once again calculated to be free of liquid water. In this case, the gas pressure in the canister reaches 5 MPa after approximately 7,000 years, at which point the inflow ceases. Due to continued corrosion, the pressure after about 15,500 years has risen to 10 MPa. When the pressure reaches the sum of the groundwater pressure (5 MPa) and the buffer's swelling pressure (assumed to be 5 MPa in this study), gas can leave the canister through the buffer (see further section 9.6.5). The water level in the gap and the insert and the pressure in the canister for this case are shown in Figure 9-5. Corrosion is assumed to occur globally, where either liquid water or water vapour exists, in both cases at the same rate.

To verify the results in Bond et al /1997 /, Takase et al /1999/ conducted a study of the coupled progression water ingress-corrosion-gas formation with similar qualitative conclusions. The numerical results also agree well for most of the calculation cases. Figure 9-6 shows the results from Takase et al /1999/ for the same modelling as that illustrated in Figure 9-5.

The conclusion from the two studies is that intruding water in a canister will be consumed and dry conditions will prevail for long periods of time. The course of the process is, however, strongly dependent on the value of the corrosion rate and the size of the defect in the shell.

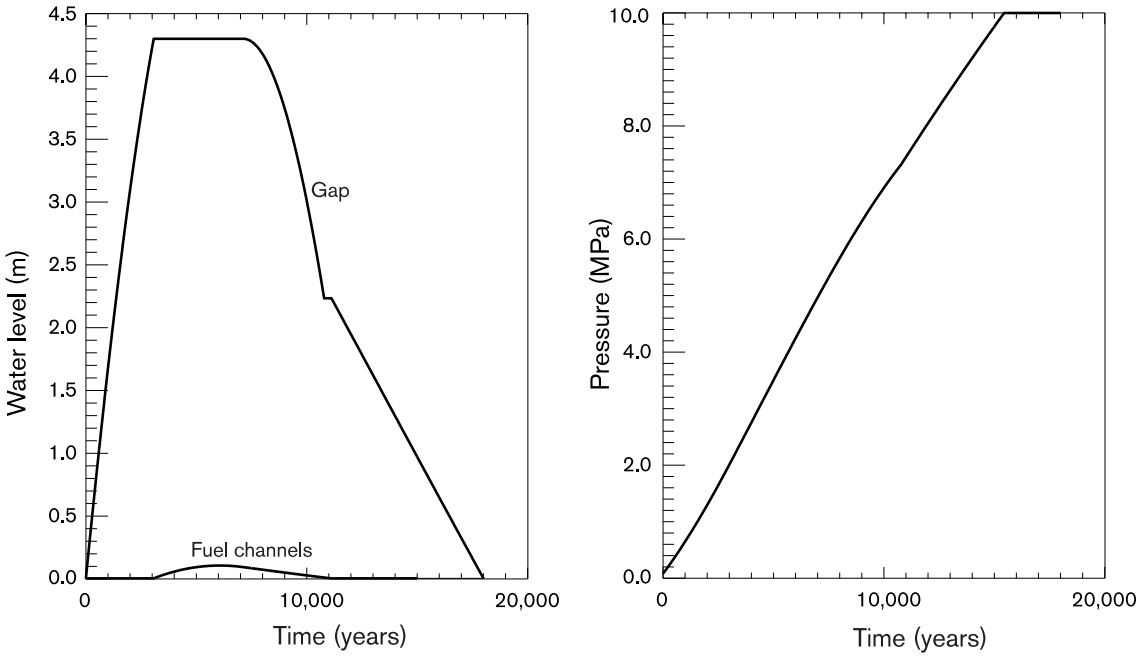

Figure 9-5. *Hydraulic progressions in a canister with a corroding insert.*

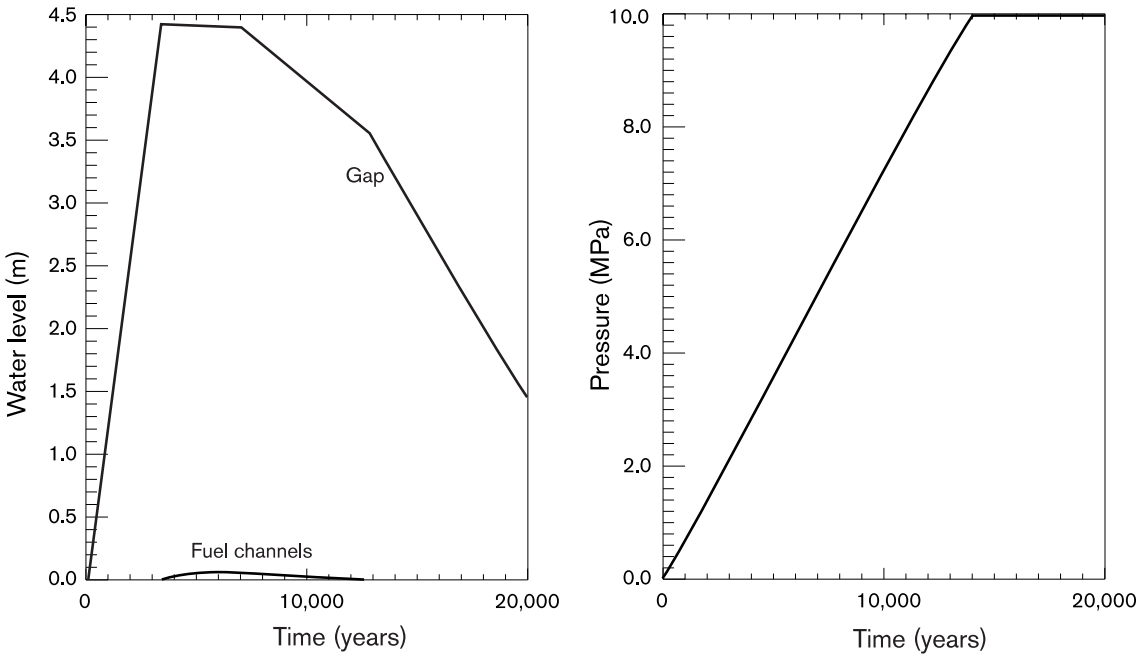

Figure 9-6. *Calculation by Takase et al /1999/ of same progression as in Figure 9-5.*

If the defect in the shell instead takes the shape of a circumferential crack, also with an area of 1 mm^2, the course of events is radically different. The inflow of water is then about 200 times higher, and there is not enough time for any counterpressure to build up before the canister cavity has filled with water. A high gas pressure can therefore build up rapidly in the limited cavity that has not been filled with water.

9.6.3 Water ingress via diffusion; local corrosion

When the gas pressure in the insert reaches the groundwater pressure, the inflow of water to the canister will cease. Water can then continue to enter by diffusion, thus sustaining corrosion. Diffusion is very slow; with a 1 mm^2 circular hole and a corrosion rate of 0.1 µm/y, the inflow is about 10^{-5} l/y. It is probable that due to the limited ingress of water, corrosion will only take place next to the defect in the canister. The size of the area around the defect that is expected to corrode as a result of inward diffusion of water is calculated in Bond et al /1997/. The model study shows that it is likely that corrosion will take place over an area with a radius of approximately five centimetres from the defect in the copper shell assuming a corrosion rate of approximately 0.1 µm/y and a circular hole of 1 mm^2. The corrosion area will in this case be proportional to the area of the defect.

Inward transport of water and corrosion are also dependent on the canister-insert distance. The diffusion calculation assumes an initial gap of 1 mm, which decreases with time as it is filled with corrosion products so that the water transport rate and the corrosion area also diminish.

9.6.4 Mechanical effects of corrosion products

When the insert corrodes, a layer of magnetite will be built up between insert and shell. Magnetite has a lower density than iron, so the corrosion products will exert a pressure between insert and shell. The effects of this are analyzed in Bond et al /1997/ if a) corrosion takes place over the entire outer surface of the insert (global corrosion), and b) if corrosion occurs locally around the defect in the copper shell.

Local corrosion: If corrosion occurs locally around the defect in the copper shell, the calculations show that the shell is severely deformed around the defect without the defect itself becoming enlarged. Figure 9-7 shows the strain in the shell for a 0.5 mm expansion of the copper shell with a corrosion radius of 4 cm. This is roughly equivalent to the probable corrosion radius given a 1 mm^2 circular hole and a corrosion rate of 0.1 µm/y. With the given assumptions and material properties, this is expected (in a longer time perspective) to cause a circular disc of the same size as the corrosion area to be "punched" out of the shell.

The shell is projected to fail when the strain has reached approximately 20 mm. The density ratio between magnetite and iron is 2.1:1, and with a corrosion rate of 0.1 µm/y the time to failure can be calculated to be approximately 200,000 years.

In the model studies, local corrosion (circular hole) never resulted in stresses that affect the integrity of the insert.

Global corrosion: If corrosion takes place over the entire outer surface of the insert, the pressure from the corrosion products causes strain of the whole copper shell. With a corrosion rate of 0.1 µm/y, the stresses after approximately 23,000 years lie around

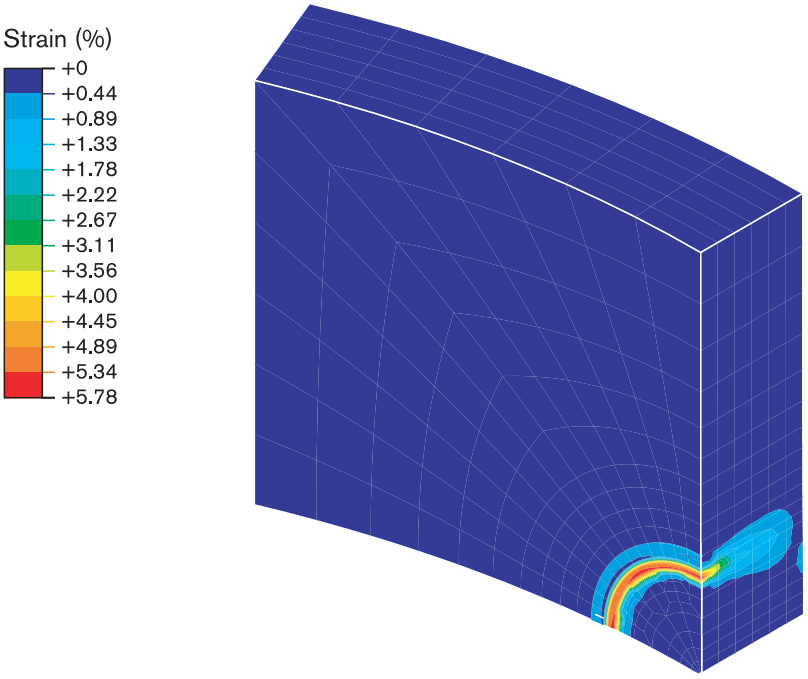

Figure 9-7. *Plastic strain in the copper shell for the case with a 4 cm corrosion radius and a 0.5 mm load /Bond et al, 1997/. The copper shell undergoes plastic strain in the outer part of the corrosion area.*

100 MPa generally in the shell, and 2.5 times higher near the defect (circular hole). No significant enlargement of the defect has then occurred, according to the calculations.

At the same time, enough stress has built up to cause local plastic deformation in the rim of the insert lid, but the stresses don't affect the strength of the insert.

In a longer time perspective with global corrosion, the build-up of corrosion products causes deformation of the copper shell, where the greatest strains occur around the canister lid. After approximately 200,000 years of global corrosion, the lid is expected to come loose.

After approximately 500,000 years, the insert is expected to have corroded completely. Corrosion has then only been assumed to take place from the outer surface of the insert. The strain in the body of the copper shell is still less than 20 percent, which means that it is not expected to crack. The material can take about 40 percent strain, see section 8.8.2. The very slow strain means that failure can occur earlier. But this is of no importance in the analysis, since the canister's barrier function is neglected when the global corrosion starts after 200,000 years.

In this situation the insert has lost its mechanical strength. The fuel channels are expected to be filled with corrosion products, so that the canister is expected to be deformed marginally by external loads.

To determine how global corrosion affects buffer and rock, the mechanical stresses in canister, buffer and 10 cm of the rock have been calculated for the situation where the insert has corroded completely. The radius of the copper shell is then calculated to have been deformed 55 mm. The properties of the buffer enable it to absorb most of the stresses from the canister without transmitting them to the rock in this situation. The buffer has been deformed locally at the bottom, see Figure 9-8.

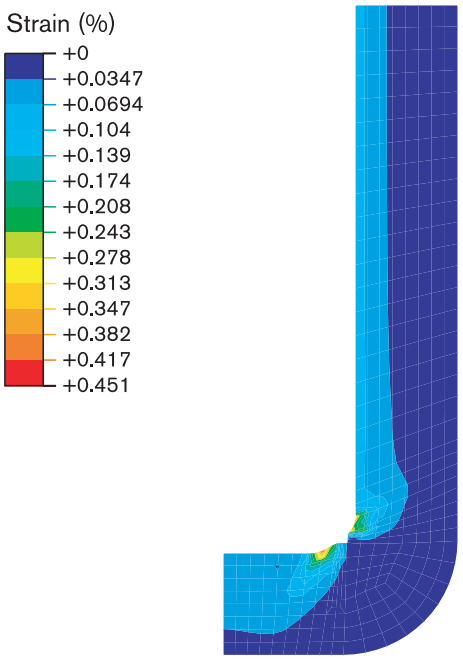

Figure 9-8. *Maximum plastic strain in the buffer for the case with corrosion over the entire surface of the insert.*

The maximum compressive stresses in the rock are around 4 MPa, and the tensile stresses around 1.4 MPa. The compressive stresses are judged not to affect the rock. The tensile stresses could cause local cracks in the lower corner of the deposition hole. Figure 9-9 shows the stresses in the rock.

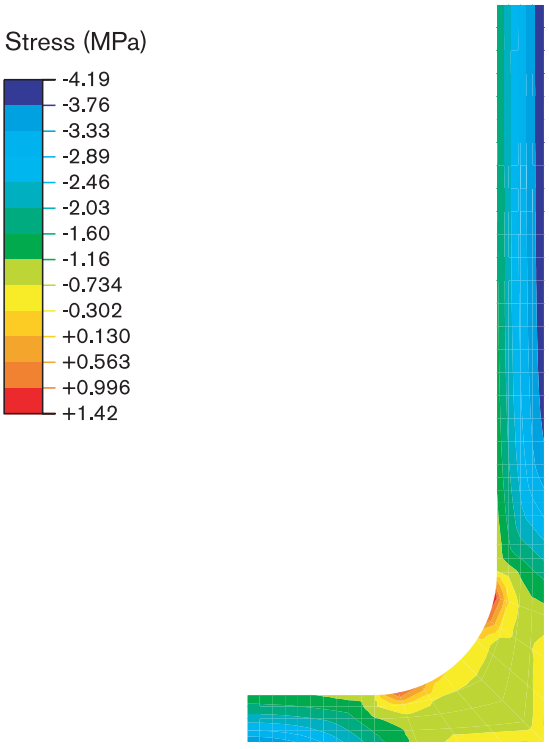

Figure 9-9. *Maximum stresses in the rock for the calculation case with corrosion over the entire surface of the canister.*

9.6.5 Gas transport through buffer

Corrosion of the insert produces hydrogen gas in accordance with:

$$3Fe + 4H_2O \rightarrow Fe_3O_4 + 4H_2$$

The total surface area of the insert is approximately 34 m^2. A corrosion rate of 0.1 µm/y then gives a gas production of $1.5 \cdot 10^{-2}$ m^3/y (STP) with global corrosion.

With local corrosion, all intruding water is expected to be consumed by the corrosion. The inflow of water is calculated according to section 9.6.3 to be about 10^{-5} l/y for a 1 mm^2 defect and a corrosion rate of 0.1 µm/y. This is equivalent to a hydrogen gas production of $1.2 \cdot 10^{-5}$ m^3/y (STP).

In the water-saturated state, the buffer is impenetrable to flowing gas and a gas pressure is therefore expected to build up in the canister cavity. The gas can dissolve in water and diffuse through the buffer out to the rock. However, solubility and diffusivity are relatively low, which means that transport capacity is limited. Wikramaratna et al /1993/ calculate the diffusive transport capacity to be approximately $2 \cdot 10^{-6}$ m^3/y for a 1 mm^2 defect at an internal gas pressure of 15 MPa. This is not sufficient to remove gas generated by either global or local corrosion.

Several experiments have shown that bentonite does not allow gas to pass until the pressure in the canister exceeds the sum of the swelling pressure and the groundwater pressure, i.e. about 12–14 MPa /Pusch et al, 1985; Horseman et al, 1997; Tanai et al, 1997/. 14 MPa pressure in the canister cavity is equivalent to a gas volume of 140 m^3 at STP.

When the pressure reaches this value, a transport pathway is formed through the buffer and gas is released. The experimental results can be interpreted as showing that a system of microfractures is formed due to rupturing of the clay. The pressure falls and the gas production rate determines the further course of events.

- If the pressure falls to a sufficiently low value, the transport pathway closes. This so-called "shut-in pressure" is dependent on the swelling pressure. At normal swelling pressure, 7–8 MPa, the shut-in pressure is 3–5 MPa, according to very preliminary estimates. After that, gas once again migrates solely by diffusion, see Figure 9-10. If gas production continues long enough, a cycle is obtained with successive gas pulse releases and pressure build-ups.
- If, on the other hand, gas production is high enough to sustain a higher pressure, the gas transport pathway is expected to remain open.

The buffer's gas transport capacity is the subject of investigations.

Most of the water in the buffer is strongly bound to the clay mineral and very difficult to remove with a flowing gas /Rodwell et al, 1999/. Furthermore, the swelling pressure causes any gas transport pathway that may have opened to close when gas transport ceases. A gas transport pathway through the buffer is therefore not judged to influence its other properties.

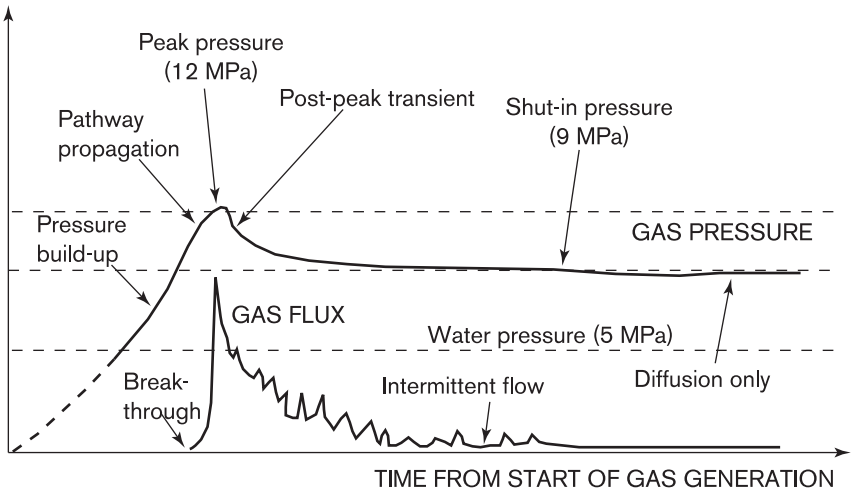

Figure 9-10. *Temporal course of gas transport through bentonite. The timescale in the figure is relative and dependent on the rate of pressure build-up.*

9.6.6 Sequence of events

The previous sections describe hydraulic and mechanical processes separately. Here follows a coupled description.

The processes in a defective canister are very slow and in principle impossible to verify experimentally. The course of events is also heavily dependent on several of the relevant parameters, above all the corrosion rate and the size of the defect in the copper shell.

Two sequences of events are described in the following: one for a 1 mm^2 circular hole, the other for an equally large circumferential crack. In both cases, the corrosion rate is assumed to be 0.1 µm/y.

The sequence of events described here is based on the line of reasoning in Bond et al /1997/, assuming in the main case a corrosion rate of 0.1 µm/y and a defect with an area of 1 mm^2.

Circular hole

Time up to about 11,000 years: Water is expected to flow into the canister driven by the pressure differential between the groundwater in the rock and the gas in the canister cavity. The corrosion rate is sufficiently high to consume all water. After about 11,000 years, the pressure in the canister is projected to reach 5 MPa, after which water is transported into the canister by diffusion of water vapour.

11,000 to 18,000 years: Water diffuses in around the defect and corrosion is only expected to occur locally in a radius of about 5 cm around the defect. After about 18,000 years, the corrosion products are projected to have filled the 2 mm wide gap between insert and shell, and the shell will begin to expand. Gas production is low in this time interval, since the inward transport of water is slow.

18,000 to 200,000 years: The corrosion products around the defect are expected to expand the copper shell. After approximately 200,000 years, the copper shell is projected to fail and a hole as big as the corrosion area will be created. Gas production is still low in this time interval.

200,000 to 400,000 years: When a larger hole has formed, water transport into the canister will increase once again, and it is probable that the entire surface of the insert will corrode. At this point it is not impossible that gas production will reach the maximum value of $1.5 \cdot 10^{-2}$ m^3/y (STP). The maximum pressure increase will then be about 1 MPa in 700 years, which means that the gas can probably not escape by diffusion and gas release can be expected in the buffer. The strains will now be greatest around the canister lid, and after about 400,000 years the lid is expected to come loose.

400,000 to 700,000 years: The global corrosion continues, and after appoximately 700,000 years the insert has corroded through to the fuel channels. The strain in the body of the copper shell is still less than 20 percent, which means it is not expected to crack. After approximately 700,000 years, gas production is projected to decline due to the fact that nearly all iron has been consumed and the gas releases through the buffer cease. The buffer has been deformed locally at the bottom. The rock is mainly subjected to compressive stresses and is not judged to be damaged. The tensile stresses that occur around the deposition hole are very local.

Circumferential defect

The course of events if the breach takes the form of a circumferential defect has not been modelled in Bond et al /1997/ or Takase et al /1999/. The following description is therefore more summary.

Time up to about 800 years: The transport resistance in a circumferential defect is much less than in a circular hole. This means that the gap between insert and shell fills very quickly, and even the fuel channels are expected to be filled with water. If no counter-pressure builds up, the whole canister could be filled in about 850 years. However, corrosion causes a pressure increase of approximately 2 kPa/y (based on empty canister), which means that the inflow of water will cease before the canister is completely filled with water.

800 to about 60,000 years: Water is now available in the canister, and since corrosion of the insert will not be controlled by the availability of water, the whole surface of the insert can corrode. No transport of water in through the defect is expected in this time interval. 16 grams of water is consumed every year by corrosion, which means that the canister will be empty after about 60,000 years (assuming it was almost full to begin with). Providing there is no hindrance to transport between channels and gap, corrosion will take place evenly over the entire surface of the insert. In 60,000 years, 6 mm of iron will corrode, giving a net growth of 6.6 mm of magnetite. The gap will be filled and the corrosion products will expand the whole copper shell 5.6 mm.

Due to the water, the free space for gas is small and the pressure will therefore increase rapidly. When the pressure inside the canister exceeds the sum of the swelling pressure and the hydrostatic pressure, a gas channel will be opened in the buffer. This channel will then remain open as long as there is water left in the canister, in other words for the entire time interval.

If the defect in the copper shell is in the bottom weld instead of the lid weld, which is deemed unlikely, the course of events will be different. Then water can be expelled when the gas pressure exceeds the hydrostatic pressure in the rock. The water will then disappear much faster, and no transport of hydrogen gas through the buffer is expected. This is because water can be expelled from the canister when the internal pressure exceeds the hydrostatic pressure, while gas cannot be expelled until the internal pressure exceeds the sum of the hydrostatic pressure and the buffer's swelling pressure.

60,000 to 200,000 years: During this period, there is no liquid water in the canister and corrosion is expected to control the inward diffusion of water vapour in the same way as for the case with a circular hole. This could possibly be a more favourable geometry from a mechanical point of view, but the possibility cannot be ruled out that corrosion will occur locally and that a larger defect will be formed when the copper shell has been strained to the failure limit.

200,000 to 400,000 years: The course of events is judged to be the same as in the case with a circular hole.

400,000 to 700,000 years: The course of events is judged to be the same as in the case with a circular hole. However, all iron is projected to be consumed slightly earlier than in the case with a circular hole, due to the longer early period with global corrosion.

Uncertainties

Calculations over hundreds of thousands of years are speculative and provide at best an illustration of what may happen.

Corrosion of the iron insert causes magnetite to form with hydraulic and mechanical properties that are crucial to the evolution of a damaged canister. The material data used in the analysis come from magnetite formed in open systems. In a defective canister, magnetite will form under high pressure, which could have two consequences:

1. The hydraulic conductivity is so low that the canister is sealed and the inflow of water is stopped.
2. The pressure causes the magnetite to spread over the canister surface instead of building up locally.

These processes would be favourable for the long-term function of the canister, but not enough data are available today to allow them to be taken into account.

The corrosion rate of 0.1 μm/y is well-established experimentally, but it is still doubtful whether the value can be extrapolated to hundreds of thousands of years.

Other important factors are the size and shape of the defect in the copper shell. If defects occur, they are expected to be small, in which case size is of limited importance for the sequence of events: A smaller defect gives a smaller corrosion radius, but is nevertheless expected to lead to bursting of the copper shell at the same time, since the time is only dependent on the corrosion rate.

9.6.7 Data for calculations of radionuclide transport

The hydromechanical evolution in a damaged canister furnishes data for a) the time it takes for a continuous water pathway between the fuel and the outside of the canister to be formed, called the delay time, and b) the time it takes for the internal evolution to have caused the small initial defect to suddenly grow to a larger defect. Radionuclide transport begins when the continuous water pathway has formed, but is restricted by the small initial defect. When the defect has grown larger, it is assumed that the canister no longer offers any resistance to radionuclide transport. Both reasonable and pessimistic estimates are needed for both times.

In accordance with the account in section 9.6.6, 200,000 years is chosen as a reasonable value for the time when the initial defect grows to a larger defect. Up to this time, no liquid water is expected to be present in the canister and no radionuclide transport occurs. When the initial defect grows into a larger defect, it is assumed that water can also enter freely, and 200,000 years is therefore the reasonable time when a continuous water pathway is expected to form.

It is pessimistically assumed that a continuous water pathway is formed after only 300 years. The above calculation, which gives 850 years as the shortest time to fill the canister with water, has then been modified with pessimistic data for the buffer's hydraulic conductivity as well. It is pessimistically assumed that the corrosion rate of the iron is 1 μm/y, which gives full defect growth in 20,000 years.

9.7 Chemical evolution in defective canister

9.7.1 Overview

The chemical evolution in a damaged canister differs radically from that in an intact canister in that intruding water gives rise to several important chemical reactions, chiefly:

- corrosion of the cast iron insert,
- corrosion of the fuel's Zircaloy cladding and other metal parts, release of radionuclides in these parts,
- dissolution of the fuel matrix with release of radionuclides, and
- release of instant release fraction.

The chemical evolution is also controlled by the composition of the water that enters via the buffer. According to the base scenario, the buffer's pore water can at early stages contain elevated carbonate and sulphate concentrations. Later, the intruding water is expected to have a composition that is very close to the natural groundwater composition on the site in question.

The composition of the intruding water and the ensuing reactions together determine the chemical environment in the canister. The chemical environment in turn determines how released radionuclides speciate, i.e. which chemical form they assume, and thereby also to what extent they occur in dissolved form, accessible for transport, or are precipitated in the canister. Speciation is of decisive importance for radionuclide migration from a damaged canister.

The four above processes and the speciation of radionuclides in a canister with damaged copper shell are described in the following. The descriptions should be regarded in the light of the preceding section, which discusses the prerequisite for their taking place at all: ingress of water.

9.7.2 Corrosion of the cast iron insert

Groundwater at repository depth is oxygen-free. The cast iron insert will therefore corrode anaerobically, with hydrogen generation and magnetite formation:

$$3Fe + 4H_2O \rightarrow Fe_3O_4(magnetite) + 4H_2$$

The corrosion process is described in detail in the Process Report and in Blackwood et al /1994/.

The equilibrium pressure for hydrogen in the reaction is approximately 100 MPa. This means that equilibrium can never be expected in a deep repository, since the buffer is expected to release gas at considerably lower pressure, see section 9.6.

A magnetite layer is expected to be built up on the iron surface. When the layer has reached a thickness of 0.7–1 µm, the corrosion rate is expected to be around 0.1 µm/y. The subsequent corrosion rate has been shown to be independent of several important factors /Blackwood et al, 1994/:

- Further growth of the magnetite layer does not affect the rate. This is interpreted as meaning that additional magnetite forms a layer with poor adhesion due to a precipitation reaction of iron in solution, while the inner layer is formed by direct reaction with the metal surface.
- The rate is independent of whether the water occurs as a liquid or a gas saturated with water vapour.
- The rate is not affected by carbonate, nitrate or ammonia in the water.
- Increased concentrations of hydrogen gas or iron ions do not affect the rate, which indicates that the transport rate across the inner magnetite layer controls the process.

The corrosion rate increases with increasing sulphate concentration and ionic strength. At sulphate concentrations of 0.1 M, the rate is around 1 µm/y after 4,000 hours.

A constant corrosion rate of 0.1 µm/y is therefore considered to be a reasonable estimate of the long-term evolution, provided water is available. The uncertainty in this value is relatively small, and 0.01 and 1 µm/y are set as extreme lower and upper bounds.

The importance of corrosion of the cast iron insert for the hydromechanical evolution in the canister was explored in the preceding section. The corrosion process and its products are also of importance for the redox conditions in the canister, and thereby for e.g. the speciation of radionuclides, see section 9.7.6.

9.7.3 Corrosion of metal parts and cladding tubes

The fuel assemblies consist of fuel pellets of uranium dioxide, cladding tubes of Zircaloy and other structural elements of, among other things, stainless steel and the nickel alloys Inconel and Incoloy /Repository System Report/.

Metal parts

The metal parts are highly corrosion-resistant, but no real studies of the long-term corrosion resistance of the fuel's structural parts have been conducted. The influence of the corrosion products on the chemical environment in the canister is deemed to be negligible in comparison with the effects of iron corrosion.

The corrosion's importance lies in the fact that the nickel alloys and the stainless steel contain a certain quantity of radioactive activation products from reactor operation, above all Co-60, Ni-59, Ni-63 and Nb-94.

In SR 97 it is pessimistically assumed that the entire nuclide inventory in the fuel's metal parts is released immediately on contact with water. However, both Ni-59 and Nb-94 have such long half-lives that a more reasonable estimate of the corrosion rate would nevertheless lead to release of most of the inventory before the nuclides decay.

Cladding tubes

The cladding tubes of Zircaloy enclose the spent fuel, and as long as the tubes are intact no nuclides can be released from the fuel. Zircaloy is passivated by a thin surface layer of zirconium oxide, which has very low solubility in water. The corrosion rate of Zircaloy can be estimated at 2 nm/y, which would give a life of about 400,000 years /Process Report/.

There are great uncertainties attached to the long-term corrosion resistance of Zircaloy, since all experimental observations come from short-term experiments. It is also conceivable that the cladding tubes will be penetrated by local corrosion much earlier.

The cladding tubes' barrier function is therefore neglected in the radionuclide transport calculations in SR 97. All tubes are assumed to be initially defective. The transport resistance in the defects is also neglected. This resistance is of limited importance if the defect in the copper shell is so small that it dominates. If the defect in the copper shell is large, however, the Zircaloy cladding could comprise an important transport resistance.

9.7.4 Dissolution of the fuel matrix

The majority of radionuclides in the fuel lie embedded in the fuel matrix of uranium dioxide and cannot be released until the matrix has been dissolved or converted. A description of the dissolution/conversion of the fuel matrix is therefore needed in a safety assessment.

Under normal conditions in the repository (reducing environment, neutral to alkaline pH), uranium dioxide has very low solubility in water. If solubility is assumed to be the limiting factor, dissolution of the fuel matrix will proceed very slowly. Based on this, a solubility-limited model for the release of radionuclides from the fuel can be formulated.

In addition to this dissolution mechanism, it is also conceivable that oxidants formed by radiolysis of water around the fuel matrix could cause conversion of the fuel so that embedded radionuclides are released. Based on this, a model for fuel conversion resulting from radiolytic oxidation can be devised. This makes a further contribution to fuel dissolution, since the former mechanism always occurs.

Solubility-limited model

The uranium dioxide which the fuel matrix consists of has a given water solubility in the chemical environment in a water-filled, damaged canister. If the uranium concentration in the groundwater in the surrounding rock is lower, uranium in solution can be transported out, leading to gradual dissolution of the fuel matrix.

The solubility of uranium dioxide in fuel can be estimated at 10^{-7} M /Bruno et al, 1997/, and the water turnover rate in the canister can be estimated at between 0.01 and 1 litre/year, depending on the size of the defect in the canister shell. A canister contains around 10,000 moles of uranium. With these data, a dissolution of between one ten-millionth and one hundred-thousandth of the fuel is obtained in a million years.

Model with radiolytic oxidation

In a solubility-limited model, it is assumed that radiolytically produced oxidants are not of any importance for the fuel conversion process. The large quantity of reducing species in the canister, above all Fe(II) and Fe(0), could conceivably "neutralize" the effects of the oxidants formed by radiolysis.

However, such a mechanism has not yet been experimentally or theoretically proved. In SR 97, a model is therefore used that assumes that the fuel matrix is dissolved as a consequence both of its "own" solubility and of the oxidants produced by radiolysis of water.

A model that describes a radiolytic oxidation was first used in the SKB 91 safety assessment. There it was assumed that the oxidation and thereby the release of radionuclides was proportional to the α dose rate in the fuel. The proportionality constant was derived from the release rate of strontium-90 from fuel leach tests under oxidizing conditions / Werme et al, 1990/. Similar models have been used in the TVO-92 /Vienoet al 1997/ and SITE-94 /SKI, 1996/ studies, and most recently in the TILA-99 safety assessment /Vieno and Nordman, 1999/.

The model has been refined for use in SR 97 /Eriksen, 1999; Eriksen, 1996/. The new model quantifies:

- radiolysis processes in the water between fuel and cladding,
- a series of reactions between different radiolysis products in the water and between radiolysis products and dissolved hydrogen from corrosion of the insert, and
- reactions between oxidants and the uranium dioxide, i.e. the direct cause of fuel dissolution.

Radiolysis processes: Both α and β radiolysis are included. The β radiolysis tends to produce radicals, while the a radiolysis produces molecular species. The calculations are performed with a constant dose rate that corresponds to the conditions at the time of deposition ($1{,}29 \cdot 10^{18}$ eV/($dm^3 \cdot s$), i.e. 685 Gy/h).

The radiolytic reactions are assumed to take place in a 100 µm wide water layer around the fuel pellets. The cladding is assumed to be defective so that water can leak in, but due to the slow corrosion of the cladding it is assumed to enclose the fuel for very long times. Because of the thin water layer, no concentration gradients are expected for radiolytically produced species, since diffusion across 100 µm is rapid.

Chemical reactions in water: Approximately forty reactions between different radiolysis products, dissolved hydrogen and water are included in the calculations. Reactions and reaction data come from established databases for modelling of radiolysis /Ross et al, 1992; Draganic et al, 1991/.

Reactions between uranium dioxide and oxidants: Oxidation of uranium dioxide caused by hydrogen peroxide and molecular oxygen, H_2O_2 and O_2, is calculated in the model. The reactions are assumed to be of the first order, i.e. the reaction rate is directly proportional to the concentration of the reacting species. The rate of the reactions is extrapolated from experimentally measured values.

Calculations

The model calculations are performed with Macksima-Chemist, a standard program for modelling of radiolysis /Carver et al, 1979/. For the reactions in the aqueous phase, NDRL/NIST Solution Kinetics Database /Ross et al, 1997/ has been used, together with constants for carbonate reactions from Draganic et al /1991/. Reaction rates for the reaction between O_2 and UO_2 have been taken from Torrero /1995/, and the rate for the reaction between H_2O_2 and UO_2 has been taken from Gimenez /1996/ and Shoesmith and Sunder /1992/.

Simulations with the model show that the system quickly reaches a steady state where the dissolution rate is determined by the partial pressure of the hydrogen in the canister and the dose rate. Figure 9-11 shows the dissolution rate as a function of hydrogen gas pressure. In the base case, the rate corresponds to the dissolution of a fraction of 10^{-8} of

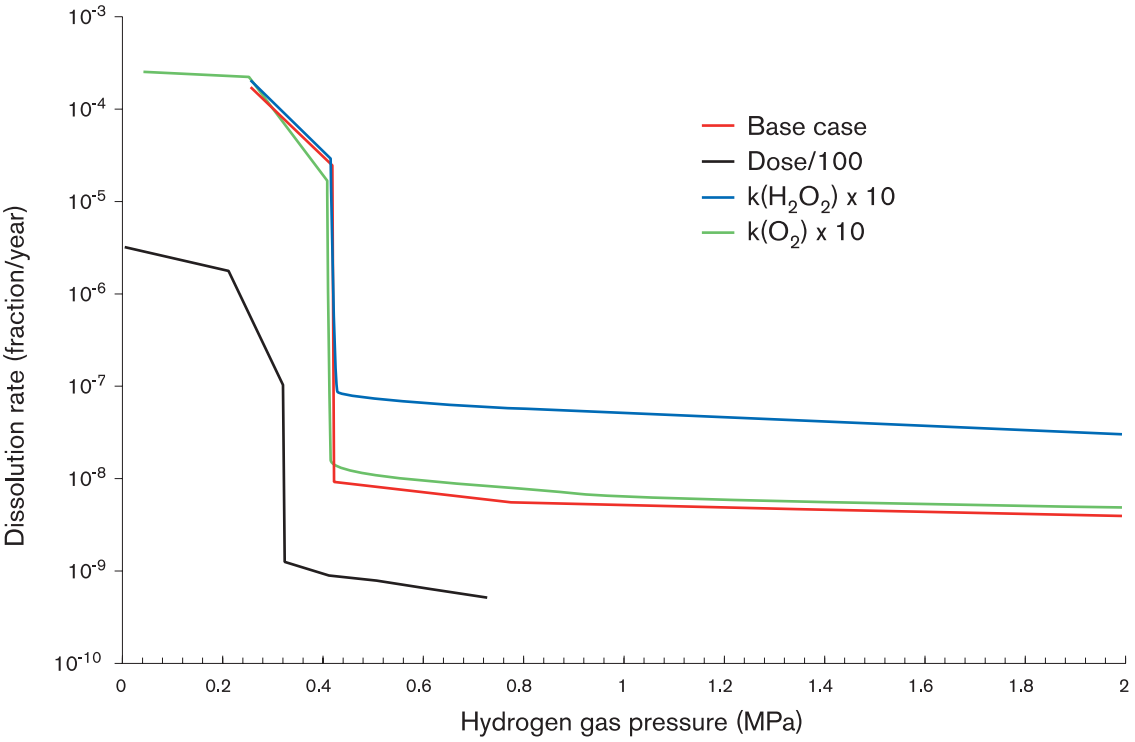

Figure 9-11. *Dissolution rate as a function of hydrogen gas pressure at constant dose rate for:*
- *the base case,*
- *100 times lower dose rate,*
- *ten times higher reaction rate between hydrogen peroxide and uranium dioxide,*
- *ten times higher reaction rate between oxygen molecules and uranium dioxide.*

the fuel every year at the hydrogen gas pressure expected in the canister (around 5 MPa according to section 9.6). The initial dose rate and reference values of all reaction parameters have been used here.

The hydrogen concentration is of crucial importance, since hydrogen reacts with the OH radical to form atomic hydrogen:

$$OH + H_2 \rightarrow H_2O + H$$

Atomic hydrogen in turn reacts with H_2O_2 and O_2, i.e. the oxidants are consumed by atomic hydrogen instead of reacting only with the fuel.

Variations and uncertainties

As mentioned, the model includes some forty-odd reactions between different radiolysis products in the water. It has not been possible to pinpoint a few reaction parameters that are crucial for the model's predictions. However, a number of variations have been carried out to ascertain the importance of different factors:

- A reduction of the dose rate by a factor of 100 (6.9 Gy/y) leads to a reduction of the conversion rate for the matrix by a factor of ten, see Figure 9-11. The sum of the α and β dose rates declines by approximately a factor of 100 in 10,000 years. The ratio between the α and β dose rates changes over time. The effects of this have not been analyzed in detail. The change counteracts the positive effect of the reduced total dose.
- The dissolution rate is almost linearly dependent on the assumed reaction rate between uranium dioxide and H_2O_2, but hardly at all on the reaction with O_2, Figure 9-11.

Uncertainties in reaction rates: The rates of the reactions between uranium dioxide and the oxidants and O_2 have been taken from experimental measurements. Measured values of reaction rates vary between different experiments /Bruno et al, 1998/ by approximately a factor of ten up and down from the value chosen in the model. The importance of this has been tested with variation analyses.

Few measurements of the rate for the reaction between uranium dioxide and H_2O_2 are reported. Measurements have for technical reasons been made at much higher oxidant concentrations than those used in the calculations. An important question is therefore the reasonableness of the extrapolation of reaction rates to low concentrations. The reactions are assumed to be of the first order. Other values of the reaction order have, however, been reported. Schoesmith and Sunder /1992/, for example, find values between zero and one depending on the H_2O_2 concentration in the water. This is explained by the fact that degradation of the hydrogen peroxide is included as a competing reaction.

If the reaction were to be of a higher order, the extrapolation to lower oxidant concentrations would give such low oxidation rates that chemical dissolution would dominate, i.e. the situation with a solubility-limited model would be approached. If, on the other hand, the reaction were to be of a lower order than one, the extrapolation to low oxidant concentrations would give considerably higher rates.

Uncertainties surrounding physical premises: Will the fuel-clad gap really be filled with water? The gap is 100 μm at fabrication, but decreases as the fuel is oxidized, owing to the build-up of secondary uranium phases of lower density. If the cladding disappears, the free space will be much larger.

Uncertainties surrounding the exchanges in the radiolysis reactions and for the rates of the reactions between the radiolytic species: The uncertainties for the reactions that are used in the calculations are small in comparison with many others, above all geometry and reaction rates between uranium and oxidants.

Comparisons

A solubility-limited model gives a dissolution/conversion rate of between approximately 10^{-11} and 10^{-13} (fraction of inventory per year), the oxidation model for SR 97 gives 10^{-8}. The rate of the SKB 91 model is time-dependent. In the original reference, approximately 45 percent of the fuel has been converted after one million years and around 70 percent after ten million years /Werme et al, 1990/. The big differences do not have to be of any decisive importance for safety. For many radionuclides, not even the assumption of an immediately dissolved fuel matrix results in any radical changes in release rates from a repository, for several reasons:

- Some nuclides in the fuel accumulate on the surface of the fuel and are therefore released even if the matrix is stable.
- Other nuclides are present in the structural parts of the fuel and are released as they corrode, which is judged to be a faster process than matrix dissolution.
- Several matrix-bound nuclides, such as plutonium, have very low individual solubilities and precipitate in solid phases if the matrix is dissolved rapidly. This results in a very slow release of such nuclides.

Nuclides that occur in low concentrations in the fuel, e.g. Ra-226 and Am-241, are however affected considerably by different matrix conversion rates, since a low conversion rate means that it takes a very long time for such a nuclide to reach its saturation concentration in the canister. In the case of Am-241, a conversion rate of 10^{-8} means that it will never reach its saturation concentration. Ra-226 is produced by chain decay in the fuel matrix as long as the matrix (U-238) remains. The fuel dissolution rate is here decisive for the rate at which Ra-226 is released in the canister. In the calculations of radionuclide transport, the importance of fuel dissolution is shown in section 9.11.10 with a special case where the fuel is assumed to dissolve immediately when it comes into contact with water.

Natural analogy

The model used for the SKB 91 safety assessment greatly overestimates the oxidation rate for the fuel. Based on the assumptions in SKB 91, the long-term fuel dissolution rate is such that complete dissolution can be expected in about 170 million years. In the long term, conditions in the fuel should be comparable to those at the uranium deposit at Cigar Lake, which is still largely intact after more than a billion years.

The model for SR 97 is an attempt to give a more complete and realistic description of the radiolytic oxidation of the fuel. If the assumptions in the SR 97 model were to be applied to Cigar Lake, this would result in complete oxidation in 100 million years. This suggests that models with radiolytic oxidation overestimate oxidation over long periods of time.

Data for calculations of radionuclide transport

Based on the above results, a rate that corresponds to the dissolution of a fraction of 10^{-8} of the fuel matrix every year has been chosen for the calculations of radionuclide transport in SR 97.

9.7.5 Dissolution of gap inventory

Most of the radionuclides in the fuel are evenly distributed in the UO_2 matrix and are released as the fuel dissolves (see preceding section). A small fraction of the inventory of a few radionuclides has during reactor operation segregated to the fuel-clad gap and possibly also to grain boundaries in the fuel.

On contact with water, these radionuclides can rapidly go into solution. The quantity of released activity is determined by the solubility and the availability of segregated material. A study of release from segregations in fuel has been done by Johnson and Tait /1997/. Realistic and conservative data have been selected from that report for the nuclide transport calculations in SR 97 /Data Report/.

9.7.6 Chemical speciation of radionuclides

In solubility calculations, a solubility-limiting phase is assumed for each radioelement. The thermodynamically most stable phase (which would result in the lowest solubilities) is not always chosen; rather, phases are chosen which can be formed with great certainty under the prevailing conditions. The solubility calculations determine not only the value of the radioelement's solubility, but also speciation in the aqueous phase. Speciation is of importance for solubility, but also for the radionuclide's transport properties in buffer and rock.

In preparation for SR 97, extensive efforts were made to determine solubilities and the uncertainties associated with them:

- Evaluation of the importance of the natural composition of the groundwater and the relative importance of different species, in order to get an idea of which complexes and solid phases will dominate.
- A comprehensive literature survey of concentrations of (stable isotopes of) the important radioelements, in order to determine the reasonableness of the calculated solubilities.
- Survey of available data from fuel leach tests of concentrations of non-natural radioelements to get an idea from there as well of the reasonableness of the calculated solubilities.
- Calculation of solubilities with the equilibrium model EQ3NR for all three reference waters in SR 97, plus an assumed bentonite pore water.
- Comparison of the calculated results with natural concentrations, concentrations in leachates and results from other safety assessments.
- A sensitivity/uncertainty study to determine which factors are important for each radionuclide. The three site-specific groundwaters in SR 97 are very different from each other, and the solubility calculations with these waters therefore give a picture of how the radionuclide solubilities might vary between different sites. Besides the calculations for the different reference waters, the importance of reasonable variations of the most important parameters (pH, Eh, carbonate concentration and temperature) have been studied. As far as temperature is concerned, 25ºC has been chosen as the reference and 60ºC and 15ºC have been used as variations.

Table 9-1. Solubility-limiting phases, speciations and solubilities for the three repository sites in SR 97.

Element	Solubility-limiting phase	Dominant species	Aberg Reasonable (mol/l)	Beberg Reasonable (mol/l)	Ceberg Reasonable (mol/l)	All sites Pessimistic (mol/l)
Ag	AgCl	$AgCl_x^{y-}$	$2.96 \cdot 10^{-5}$	$9.39 \cdot 10^{-7}$	$7.12 \cdot 10^{-7}$	$3 \cdot 10^{-5}$
Am	$AmOHCO_3$	$Am(OH)_2^+$, $AmCO_2^+$, $AmOH^{2+}$	$6.87 \cdot 10^{-7}$	$9.36 \cdot 10^{-8}$	$9.34 \cdot 10^{-8}$	$7 \cdot 10^{-6}$
Cm	$CmOHCO_3$	$CmOH^{2+}$	$2.22 \cdot 10^{-7}$	$2.02 \cdot 10^{-9}$	$9.01 \cdot 10^{-10}$	$2 \cdot 10^{-6}$
Ho	$Ho_2 (CO_3)_2$	$HoCO_3^+$, $Ho(CO_3)_2^-$	$6.27 \cdot 10^{-6}$	$5.58 \cdot 10^{-6}$	$5.58 \cdot 10^{-6}$	$6 \cdot 10^{-5}$
Nb	Nb_2O_5	NbO_3^-	$1.37 \cdot 10^{-3}$	$1.37 \cdot 10^{-3}$	$1.39 \cdot 10^{-3}$	$4 \cdot 10^{-2}$
Ni	NiO	Ni^{2+}, $NiCO_3$,	high	high	high	high
Np	$Np(OH)_4$	$Np(OH)_4$, $Np(OH)_3CO_3^-$ $Np(HPO_4)_4^{6-}$	$5.87 \cdot 10^{-8}$	$1.05 \cdot 10^{-7}$	$5.87 \cdot 10^{-8}$	$2 \cdot 10^{-7}$
Pa	$Pa_2 O_5$	PaO_2OH	$3.16 \cdot 10^{-7}$	$3.16 \cdot 10^{-7}$	$3.16 \cdot 10^{-7}$	$4 \cdot 10^{-7}$
Pd	PdO	$Pd(OH)_2$	$4.21 \cdot 10^{-9}$	$4.17 \cdot 10^{-9}$	$4.18 \cdot 10^{-9}$	$8 \cdot 10^{-9}$
Pu	$Pu(OH)_4$	$Pu(OH)_4$, $PuCO_3^+$, Pu^{3+}	$6.56 \cdot 10^{-9}$	$5.35 \cdot 10^{-10}$	$1.38 \cdot 10^{-10}$	$3 \cdot 10^{-6}$
Ra	$RaSO_4$	Ra^{2+}, $RaSO_4$	$2.86 \cdot 10^{-7}$	$5.02 \cdot 10^{-7}$	$1.20 \cdot 10^{-4}$	$2 \cdot 10^{-4}$
Se	$FeSe_{(2)}$/ Selenium	HSe^-	$2.59 \cdot 10^{-9}$	$2.59 \cdot 10^{-9}$	$2.59 \cdot 10^{-9}$	high
Sm	$Sm_2 (CO_3)_2$	$SmCO_3^+$, $Sm(CO_3)_2^-$	$2.13 \cdot 10^{-6}$	$8.03 \cdot 10^{-7}$	$8.03 \cdot 10^{-7}$	$2 \cdot 10^{-5}$
Sn	SnO_2	$Sn(OH)_4$, $Sn(OH)_5^-$	$5.52 \cdot 10^{-10}$	$6.03 \cdot 10^{-10}$	$4.68 \cdot 10^{-9}$	$1 \cdot 10^{-5}$
Sr	Celestite/ Strontianite	Sr^{2+}	$6.88 \cdot 10^{-3}$	$3.09 \cdot 10^{-3}$	$1.21 \cdot 10^{-4}$	$4 \cdot 10^{-2}$
Tc	TcO_2	$TcO(OH)_2$	$7.67 \cdot 10^{-9}$	$7.92 \cdot 10^{-9}$	$7.67 \cdot 10^{-9}$	$5 \cdot 10^{-8}$
Th	$Th(OH)_4$	$Th(OH)_4$, $Th(HPO_4)_3^{2-}$	$1.22 \cdot 10^{-9}$	$1.22 \cdot 10^{-9}$	$1.22 \cdot 10^{-9}$	$2 \cdot 10^{-9}$
U	UO_2	$U(OH)_4$	$1.28 \cdot 10^{-7}$	$1.29 \cdot 10^{-7}$	$1.29 \cdot 10^{-7}$	$2 \cdot 10^{-7}$
Zr	ZrO_2	$Zr(OH)_4$	$2.48 \cdot 10^{-9}$	$2.51 \cdot 10^{-9}$	$2.51 \cdot 10^{-9}$	$3 \cdot 10^{-9}$

The entire study is reported in Bruno et al /1997/. Based on that report, site-specific reasonable and pessimistic data have been chosen for the nuclide transport calculations, see the Data Report. The pessimistic values have been chosen on the basis of the results of the variation analyses. Table 9-1 shows solubility-limiting solid phases, speciation and site-specific solubilities.

Below is a brief account of solubilities used for the different radioelements, based on Bruno et al /1997/ and the Process Report.

Carbon, Chlorine, Krypton, Iodine and Cesium

It is not likely that any of these elements form solid phases with such a low solubility that it is of any importance in the safety assessment.

Carbon could be limited by isotope exchange in carbonates (calcite). However, it is difficult to determine with certainty to what extent this happens, so no solubility limitation is used for carbon in SR 97.

Nickel

Sulphides, silicates and mixed oxides with iron and nickel all have very low solubilities. However, it is difficult to guarantee that any of these phases will be formed in the repository, and therefore the nickel concentration is assumed to be limited by the solubility of nickel oxide (NiO). The solubility decreases with increasing pH, but is relatively independent of other parameters. In all reference waters in SR 97, however, the solubility of nickel is so high that it is of no practical importance. In the aqueous phase, the free nickel ion and the carbonate complex $NiCO_3$ dominate.

Selenium

Under the conditions that prevail in the repository, the selenium concentration will be controlled by the solubility of the iron selenides FeSe and $FeSe_2$. A lowering of the pH by one unit increases the solubility by an order of magnitude. In all reference waters, however, the solubility of selenium is very low, below 10^{-8} mol/l. In the aqueous phase, selenium occurs as HSe^-. The argument is based on the fact that selenium will not be oxidized irreversibly in the repository. If this were the case, its solubility would be very high. The consequences of this are studied in a separate calculation case.

Strontium

Celestite and strontianite are the two least soluble strontium phases under repository conditions. However, due to their relatively high solubilities, strontium will never be solubility-limited. The free ion Sr^{2+} dominates in the aqueous phase.

Zirconium

In SR 97 it is assumed that the zirconium concentration is limited by the solubility of the amorphous zirconium oxide ZrO_2. This phase has very low solubility, and the solubility is insensitive to variations in the groundwater composition. The hydroxide complex $Zr(OH)_4$ dominates in the aqueous phase.

Niobium

Nb_2O_5 has been posited as the solubility-limiting phase for niobium in SR 97. Nb solubility increases with increasing pH, resulting in a very high solubility in the reference water for Ceberg. The hydroxide complexes $Nb(OH)_6^-$ and $Nb(OH)_5$ dominate in solution. There are gaps in the thermodynamic database for niobium, making the calculated solubilities and the speciations very uncertain. However, the relatively high solubility values, together with the small inventory, mean that Nb solubility is not an important barrier function.

Technetium

Technetium occurs in metallic form in the fuel, and the solubility of the metal is very low. Despite the fact that the metal is stable under repository conditions, it is scarcely formed by precipitation reactions. The oxide $TcO_2 \cdot xH_2O$ is therefore assumed to be the solubility-limiting phase. The solubility of this phase is independent of variations in groundwater composition, but is affected by the temperature in such a manner that a reduction from 60ºC to 15ºC reduces the solubility by an order of magnitude. The complex $TcO(OH)_2$ dominates in the aqueous phase.

Palladium

Like technetium, palladium occurs in metallic form in the spent fuel, but here as well the more readily soluble oxide is used as the solubility-limiting phase in SR 97. It is very insensitive to variations in groundwater composition. The neutral hydroxide complex $Pd(OH)_2$ dominates, but the chloride complex $PdCl_4^{2-}$ can be important at lower pH and higher chloride concentrations.

Tin

SnO_2 is posited as the solubility-limiting phase. The solubility of this phase increases with pH. In Bruno et al /1997/, its solubility increases sharply with temperature. However, this is due to an error in the temperature correction for the dominant complex. More recent studies /Amaya et al, 1997/ have shown that the solubility of tin can be higher than that given in Bruno et al /1997/. The pessimistic solubility used in SR 97 is therefore still relevant. The hydroxide complexes $Sn(OH)_5^-$ and $Sn(OH)_4$ dominate in the aqueous phase.

Radium

The most stable radium phase is radium sulphate. Changes in pH and temperature influence solubility, but not to any significant extent. The concentration of sulphate in the water is of great importance for radium solubility, however, which means that the solubility limit in the very ion-poor (sulphate-poor) Ceberg water is much higher than in the other reference waters. The quantity of radium in a canister is, however, so small that it is unlikely that the concentration will ever reach the saturation limit for radium sulphate in any of the reference waters. It is, on the other hand, likely that radium will be precipitated together with some other substance, such as calcite, which could lower the radium concentration in the canister. This is not dealt with in the calculations in SR 97, however. The free radium ion dominates in the aqueous phase.

Thorium

The thorium concentration is limited by the solubility of $Th(OH)_4$. In SR 97, the solubility of thorium is calculated based on the amorphous phase. Its solubility is in principle unaffected by variations in the groundwater composition. The hydroxide complex $Th(OH)_4$ dominates in the aqueous phase. Thorium can form strong phosphate complexes, but the phosphate concentrations in Swedish groundwaters are so low as to be of no importance.

Protactinium

Pa_2O_5 has been set as the solubility-limiting phase for protactinium in SR 97. Its solubility is not affected by variations in the groundwater composition. The thermodynamic database for protactinium that has been used in this analysis is not as complete as it should be, however, especially for the redox equilibrium Pa(IV)/Pa(V). The calculated solubility of Pa_2O_5 is $3 \cdot 10^{-7}$ mol/l, while the solubility of PaO_2 under similar conditions is $5 \cdot 10^{-11}$ mol/s /Berner, 1994/. The solubility of protactinium in SR 97 is therefore pessimistic. The complex PaO_2OH dominates in the aqueous phase, but this also presumes that protactinium is pentavalent.

Uranium

Under the conditions that prevail in the repository, uranium is always expected to precipitate as tetravalent phases. Uranium dioxide has a solubility of approximately 10^{-10} mol/l, but in SR 97 the solubility of a hypothetical phase called UO_2(fuel) is used instead. Its solubility is based on measurements of uranium concentrations in solutions from fuel leach tests. The reason for this choice is that uranium dioxide in the spent fuel can be slightly oxidized on the surface due to radiolysis oxidants: (UO_{2+x} where $0 < x < 0.35$). This phase gives a very pessimistic value of the solubility. The value is insensitive to changes in the groundwater composition and is only marginally affected by the temperature. $U(OH)_4$ dominates in the aqueous phase.

Neptunium

As with uranium, the tetravalent form of neptunium is stable under repository conditions. The amorphous hydroxide $Np(OH)_4$ is posited as the solubility-limiting phase. In contrast to uranium, however, carbonate complexes can be important in the aqueous phase, which means that the solubility of neptunium is affected by the carbonate concentration in the water. In the aqueous phase, $Np(OH)_4$ dominates at lower carbonate concentrations and $Np(OH)_3\ CO_3^-$ at higher ones.

Plutonium

The amorphous hydroxide $Pu(OH)_4$ is posited as the solubility-limiting phase. Its solubility is on the order of 10^{-10} mol/l and increases relatively rapidly with falling Eh/pH. This is due to a stabilization of trivalent plutonium in the aqueous phase.

Under the redox conditions that naturally prevail on the three sites in SR 97, a tetravalent solid plutonium phase is stable. It is, however, possible that the cast iron insert can affect the redox conditions in such a way that the tetravalent phase is destabilized and that a trivalent phase will control the solubility of plutonium. In order to obtain a reasonable estimate of the solubility of plutonium under these conditions, a trivalent phase should therefore be chosen: Data for $PuOHCO_3$ /from Puigdomenech and Bruno, 1991/ then give a solubility that is lower than for the tetravalent phase. It has not been fully ascertained whether plutonium will form tri- or tetravalent solid phases, and values from the tetravalent phase are used in SR 97.

Speciation in the aqueous phase is also sensitive to variations in Eh/pH. The free trivalent ion Pu^{3+} and the carbonate complex $PuCO_3^+$ dominate under strongly reducing conditions, while the tetravalent hydroxide complex $Pu(OH)_4$ (aq) dominates at higher redox potential.

Americium and curium

Americium and curium have similar chemical properties, and the hydroxycarbonates $AmOHCO_3$ and $CmOHCO_3$ are solubility-limiting phases. The solubility of these phases decreases with increasing pH and carbonate concentration, but the effect is relatively limited in the studied ranges. The phases are probably formed as co-precipitates with each other, which further limits the solubility of curium. However, credit is not taken for this effect in SR 97. $AmOH^+$, $AmCO_3^+$ and $Am(OH)_2^+$ dominate in the aqueous phase for americium and $CmOH^+$ for curium.

Conclusions regarding solubilities

"Reliable", pessimistic solubility-limiting phases have been chosen throughout in the solubility calculations in SR 97. The actual concentrations of radionuclides in a water-filled canister can in many cases be several orders of magnitude lower than those used in the radionuclide transport calculations. The sensitivity analyses that have been done with respect to the composition of the groundwater show that the solubilities are in most cases relatively insensitive to even substantial changes in water composition. This is important, since the groundwater composition in the repository will change during its lifetime.

9.7.7 Data for calculations of radionuclide transport

How data for fuel dissolution and solubilities have been chosen for calculations of radionuclide transport is summarized in the following.

Fuel dissolution

A rate that corresponds to the dissolution of a fraction of 10^{-8} of the fuel every year has been chosen for the calculations of radionuclide transport in SR 97. The consequences of other assumptions regarding fuel dissolution are illustrated with special cases.

Dissolution of gap inventory (IRF)

Best estimates of the fraction of activity in the inventory that is instantly released (IRF = Instant Release Fraction) for different nuclides in the spent fuel are estimated from measurements of release of fission gases from representative Swedish BWR fuel, combined with results from dissolution tests on LWR and CANDU fuel /Johnsson and Tait, 1997/. Pessimistic values are estimated by choosing the highest values of IRF that have been determined in these studies. For the nuclides that only occur on the metal parts (Nb-94, Ni-59 and Ni-63), it is assumed that all activity is instantly released, even though the metal has a limited dissolution rate. For C-14, however, lower IRF values are posited, since a large portion of the activity is present in the fuel and in the fuel cladding /Antilla, 1992/.

Table 2-3 in Appendix 2 shows the used values of IRF. The values are not correlated with other input data to the transport models.

Solubilities

Solubilities are calculated for different species in the reference waters for Aberg, Beberg and Ceberg (see Chapter 8) and for a special bentonite water with the aid of the speciation code EQ3NR /Bruno et al, 1997/. Bruno et al have also studied the sensitivity of the solubilities to variations in pH, Eh, carbonate concentration and temperature. The choice of solubilities for the transport calculations is discussed in the Data Report.

Reasonable values of the solubilities are selected from the solubilities that have been calculated for a given reference water, but if the solubility of a given substance is higher in the bentonite water, this value is chosen as the reasonable one.

In view of the uncertainty in the future chemical environment inside the canister, the pessimistic solubilities are chosen by choosing for a given substance the highest solubility that has been calculated for any of the different water compositions. If the sensitivity calculations show that the solubilities could be even greater, these values are chosen.

The proposed solubilities, as well as the solubility-limiting phase for the reasonable values, are shown in Table 9-1, as well as Table 2-5 in Appendix 2. The solubilities are dependent on the chemical composition of the pore water and are thereby theoretically correlated with other input data that are dependent on the chemical conditions (sorption and diffusivity data). But due to the uncertainty in groundwater chemistry and the different conditions that can simultaneously prevail inside the canister and out in the rock, this correlation is not particularly strong.

9.8 Hydraulic evolution in the geosphere

Groundwater flow and the change of flow in time are determined by the hydraulic properties of the geosphere and the conditions in the surroundings, above all precipitation, which is in turn dependent on the climate. Since these factors are postulated to be the same as in the base scenario, the same hydraulic evolution as in the base scenario is also expected, i.e.

- an initial transient phase where the geosphere is resaturated with water after repository closure,
- followed by a long-term phase where conditions resemble the undisturbed, natural conditions that prevailed before the repository was built. These conditions are expected to be essentially unchanged over a long period of time, with the exception of minor effects of known trends such as land uplift.

Thus, the description of the hydraulic evolution on the regional scale for the three sites that is given in the base scenario (section 8.7.2) is valid for the canister defect scenario as well.

A more detailed description of the long-term phase is required on a local scale for the canister defect scenario than was given in the base scenario. The higher resolution is important to provide a good description of possible radionuclide transport from the repository.

This section provides a summary of detailed modellings of the steady-state phase on a local scale for Aberg, Beberg and Ceberg. First, the modelling approach and the numerical model used are described, followed by a review of the individual sites. The emphasis here is on the different base cases and model variants that have been analyzed, along with comparisons of results.

9.8.1 Approach and modelling tools

Approach

Couplings between models and data for modelling of groundwater flow in the geosphere are discussed in the Data Report, see Figure 9-12. Modelling of groundwater flow is divided into a regional and a local model. The local model is a refinement of the level of detail nearest the repository.

Geophysical data and other available information from e.g. lineament interpretations and analysis of borehole cores are used to devise a geological structural model, see Figure 9-12. The structural model is a compilation of the locations and geometries of the fracture zones on a site, sometimes also a quantitative description of the hydrogeological properties of the zones. The structural model is in part the product of expert judgement and therefore contains qualitative uncertainties. These are discussed in detail in the Data Report.

Based on the structural model, the hypothetical repository is positioned in the available rock volume. The consequences of the layout are studied in the safety assessment with the aid of models for groundwater flow on a local scale and radionuclide transport.

Geophysical data and structural models are also used for statistical hydrogeological descriptions for use on both the regional and local scales. The descriptions summarize data that are needed to set up numerical models, e.g. information on boreholes, interpreted conductivity values and inferred statistical properties for both fracture zones and intact rock (rock mass). Expert judgement yield qualitative uncertainties at this stage as well, see the Data Report.

Based on the hydrogeological description and boundary conditions, groundwater flow on the regional scale is simulated. The results from the regional model are used as boundary conditions in the local model. The boundary conditions and the hydrogeological description on a local scale comprise input data for the local model. The local model in turn furnishes results that are used for calculations of radionuclide transport in canister, buffer, geosphere and biosphere, see Figure 9-12.

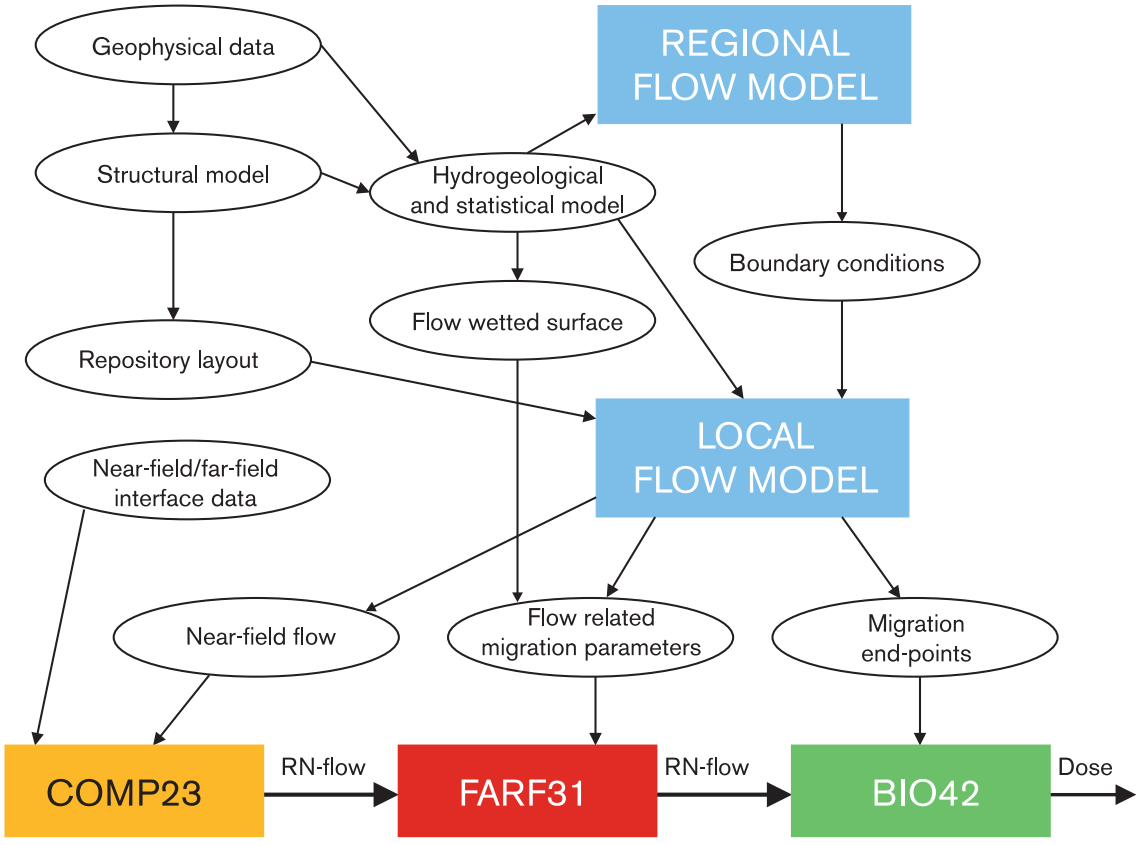

Figure 9-12. *Couplings between data and models for groundwater flow on the regional and local scale.*

Modelling tools

The primary quantities that are calculated with the models on the local scale are:

- groundwater flux (Darcy velocity) at repository depth [$m^3/(m^2 \cdot year)$],
- travel paths and advective travel times from canister positions to the boundary between geosphere and biosphere (years),
- coordinates for exit points at the ground surface.

The advective travel time is a theoretical quantity that is used to transfer calculation results from hydromodels to transport models. The transport models use the travel times to calculate the time for transport of solutes from repository depth to the surface. These solute residence times are often several orders of magnitude longer than the advective travel times.

The following models have been used to calculate the quantities:

- HYDRASTAR, a finite difference model for stochastic continuum simulation of groundwater flow and advective transport.
- CHAN3D, a channel network model for simulation of groundwater flow and transport,
- FracMan/MAFIC/PAWorks, a software package for stochastic simulation of groundwater flow and transport in discrete fracture networks,
- NAMMU, a continuum model for groundwater flow and transport based on the finite element method.

HYDRASTAR is the primary model used in SR 97 on the local scale; the other models have been used for supplementary studies. HYDRASTAR is described in brief below; other models are described in the SR 95 safety report /SKB, 1995/.

HYDRASTAR is a finite difference model for stochastic continuum simulation of groundwater flow in three dimensions. The flow is driven by differences in hydraulic head; density-driven flow arising from differences in salinities cannot be calculated. The model has been verified in a number of studies, see e.g. Norman /1991/, Morris and Cliffe /1994/ and Walker et al /1996/.

Hydraulic conductivity is described as a spatially correlated stochastic process and is assumed to be log-normally distributed with a given correlation structure. The necessary parameters for the description are obtained by geostatistical analysis. The host rock can be divided into domains with different mean values for hydraulic conductivity, permitting the differentiation of rock mass domains from more conductive domains, such as fracture zones. The generated hydraulic conductivity fields can be conditioned on measured conductivity values from borehole tests. An empirical method based on data from Äspö is used for upscaling of hydraulic conductivity data from measurement scale to discretization scale /Rhén et al, 1997/.

Advection is simulated in the model using inert particles that are transported through the calculated velocity field. The travel times are calculated with constant flow porosity, pessimistically assumed to be 10^{-4}. Andersson et al /1998/ recommend values in the range 10^{-4}–10^{-2} for all three sites. The travel times are therefore presumably longer in reality than those calculated in SR 97, see further sections 9.8.3 and 9.9.7.

9.8.2 Model implementation

The application of HYDRASTAR on the local scale for the three sites is described in the following. A more detailed discussion for Aberg, Beberg and Ceberg is found in Walker and Gylling /1998/, Gylling et al /1999a/ and Walker and Gylling /1999/. Figures in section 8.7.2 show the model areas on both the regional and local scales for the three sites. Much of the input data can be found in section 6.5 and in the Repository System Report.

For each site, the rock is divided into rock mass (rock domain) and fracture zones (conductor domain). Fracture zones represent geometrically deterministic structures with relatively higher hydraulic conductivity, while the rock mass represents the more or less intact rock between the structures. The subdivision into rock mass and fracture zones is based on the geological structural model that has been devised for the site. The hydrogeological properties (hydraulic conductivity) do not only differ between fracture zones and rock mass, but may also differ between different volumes in the rock mass.

HYDRASTAR's model volume is discretized into cubical elements, all of the same size. The model descriptions are summarized in Table 9-2. The parameter values are taken from section 3.5 in Walker and Gylling /1998/ for Aberg, section 3.5 in Gylling et al /1999a/ for Beberg and section 3.5 in Walker and Gylling /1999/ for Ceberg. The mean hydraulic conductivities vary between fracture zones at each site, as shown by the range of variation of the mean hydraulic conductivity between different fracture zones. The ranges represent the fracture zones with the lowest/highest mean hydraulic conductivities. The hydraulic conductivity at Aberg is reduced by a factor of ten below –600 metres above sea level (m.a.s.l.). At Beberg, the hydraulic conductivity is reduced by a factor of 12.3 below –100 m.a.s.l. The correlation structure is described with exponential isotropic models for all sites.

In Table 9-2, SRD (site-scale rock domain) designates domains in the horizontal plane, see Figure 9-13 and Figure 9-14. Aberg and Beberg have different mean conductivity values in the horizontal plane. Ceberg, however, has the same mean conductivity in the entire horizontal plane, with a depth dependence in several discrete steps.

Table 9-2. Important model parameters for the three sites.

	Aberg	Beberg	Ceberg
Element size (m)	25	35	35
Area, depth (m)	2,400 x 2,200, 1,250	4,130 x 5,355, 1,505	6,510 x 4,290, 1,190
Mean of $\log_{10}$K (m/s) for rock mass	SRD1: –8.0 SRD2: –7.1 SRD3: –8.8 SRD4: –7.5 SRD5: –7.6 Other: –8.5	SRD northern: –6.4 SRD southern: –6.8 SRD other: –7.2	+110 to 0: –7.4 0 to –100: –8.9 –100 to –300: –9.9 under –300: –10.1
Range of variation for mean of $\log_{10}$K between different fracture zones (m/s)	–8.3 to –5.3	–7.5 to –4.3	–9.6 to –6.9
Standard deviation of $\log_{10}$K for rock mass and fracture zones	1.6	0.8	1.1
Correlation length (practical range) (m)	97	247	68

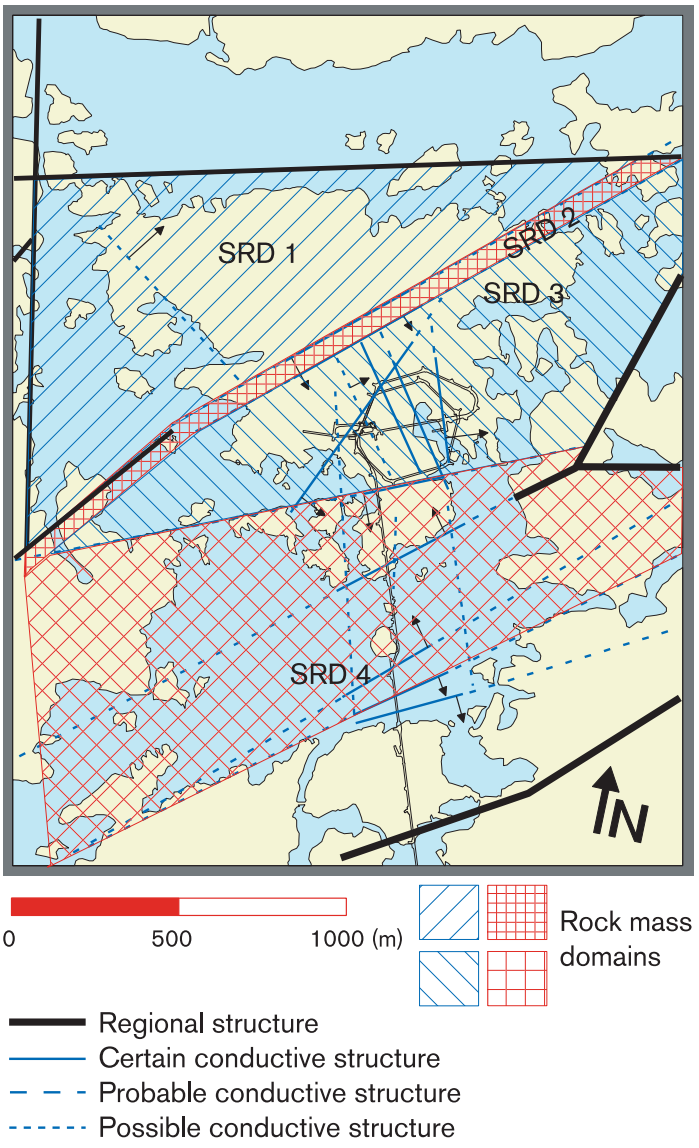

Figure 9-13. *Aberg rock mass domains in HYDRASTAR.*

As is evident from Table 9-2, the conductivity values for the rock mass at repository depth in Ceberg are more than two orders of magnitude lower than the corresponding values for Aberg and Beberg. The difference in conductivity values between rock mass and fracture zones is also smallest for Ceberg.

The conductivity values in the fracture zones are summarized in section 6.5 and described in greater detail in the Repository System Report. Minor adaptations of data to the HYDRASTAR model's parameterization have been done, see the relevant background report.

The repository layouts for the three sites are described in detail in Munier et al /1997/ and are based on the principle that the repository should avoid fracture zones. The backfilled tunnels are assumed to have a hydraulic conductivity of 10^{-10} m/s, while the EDZ (excavation-disturbed zone) is neglected. With the chosen element sizes (25 and 35 metres, respectively), the effect of this approximation is negligible. The EDZ is, however,

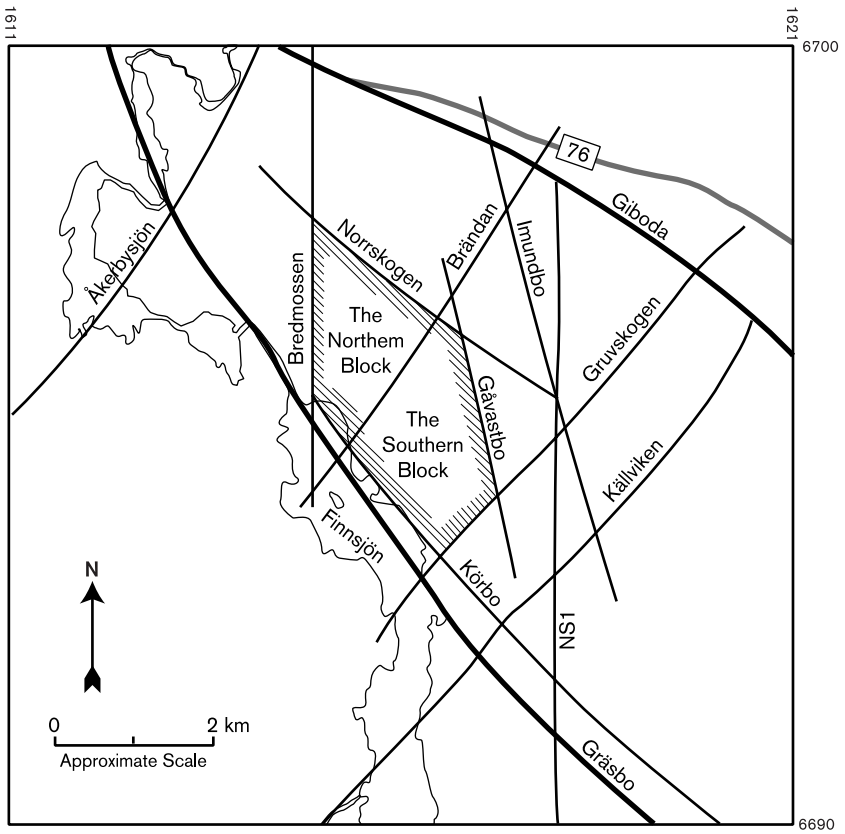

Figure 9-14. *Beberg rock mass domains in HYDRASTAR.*

included in the analysis of the near-field flows, see section 9.9.4. The individual deposition holes are not modelled in HYDRASTAR. More than one hundred representative canister positions spread out over each repository site are used to groundwater fluxes and travel times from repository depth to the biosphere.

The hypothetical repository for Aberg is "stacked" in two levels at –500 and –600 m.a.s.l. In Beberg, the entire repository is positioned at –600 m.a.s.l., and in Ceberg at –500 m.a.s.l.

The boundary conditions for the local models are obtained from the regional model calculations described in section 8.7.2. Since the local models do not handle density-driven flow, special cases without saline water have been used to calculate the boundary conditions in the regional models for Aberg and Beberg. The boundary conditions from the regional models are transferred as hydraulic head on the six sides of the local models.

9.8.3 Aberg base case and variants

For Aberg, a base case in accordance with the above model application plus five variants have been studied:

1. Alternative boundary conditions.
2. Upscaling of hydraulic conductivity.
3. Anisotropy in statistical description of hydraulic conductivity.
4. Hydraulic conductivity conditioned on measurement data.

5. Deterministic simulation with constant hydraulic conductivity within each individual domain for rock mass (rock domain) and fracture zones (conductor domain).

The variants have been chosen by a group of experts to shed light on questions regarding model application and system properties.

The first variant shows how variations in the regional model affect the boundary conditions for the local model. Among other things, regional calculations with stochastic conductivity and with or without density-driven flow have been analyzed. Since HYDRASTAR cannot handle density-driven flow, it is of interest to try to simulate this effect by using density-compensated head (environmental head) as a boundary condition from the regional model, which includes density-driven flow. Environmental head as a boundary condition closely approximates systems where the density gradient is nearly vertical /Follin, 1999; Lusczynski, 1961/, such as at Aberg. Simplified hydrostatic boundary conditions are also analyzed. For variant 1, only one realization has been calculated for each treated case. Variant 1.2 in Figure 9-15 represents the case with a regional model with stochastic conductivity and boundary conditions transferred as environmental head.

The second variant shows whether the results are sensitive to the discretization scale to which the measured conductivities are rescaled. A 50-metre discretization scale has been used in variant 2 instead of a 25-metre scale.

There are indications from Aberg that the hydraulic conductivity is anisotropic /e.g. Rhén et al, 1997/, i.e. that the conductivity has different magnitudes in different directions at the same location. Even though HYDRASTAR cannot simulate this effect, the behaviour can be partially approximated by a model with stochastic anisotropy in hydraulic conductivity /Bergman and Walker, 1998/. Stochastic anisotropy entails that the correlation lengths (see Table 9-2) are different in different directions. This variant analyzes the effects of a correlation length increased by a factor of two (variant 3.1) and ten (variant 3.2) in the northwesterly direction.

Variant 4 provides an alternative model description of the heterogeneity. In the base case the calculation model is divided into domains for rock mass and fracture zones with given statistics. In variant 4 the model consists of only one domain with a geometric mean conductivity of $2 \cdot 10^{-8}$ m/s. The variance and correlation length (practical range) of $\log_{10}K$ are 3.1 and 122 metres, respectively. The individual conductivity values have been conditioned on measured field values. Conditioning entails that the stochastic simulation of conductivity values preserves the measured values at the measurement points. The correlation structure determines the influence of the measured values on the surrounding simulated values. With sufficiently many measured values and a relatively long correlation length, the geological structure can be recreated in the model.

In variant 5, no variability of hydraulic conductivities within rock mass and fracture zones has been assumed, that is, the hydraulic conductivities are deterministic. The purpose is to study the effect of the absence of spatial variability versus the explicitly defined structures, and to study the upscaling methodology. By comparing the total flow over the model boundaries in variant 5 and the base case, an indication is obtained of the consistency of the upscaling method.

Figure 9-15 shows the results for travel times and groundwater fluxes for base case and variants. The results represent ensemble statistics for all realizations and canister positions. For variant 1, only the case with boundary conditions transferred as environmental head from a regional model with stochastic conductivity is presented (variant 1.2). Variant 3.2 is not included in the figure, but is very similar to variant 3.1.

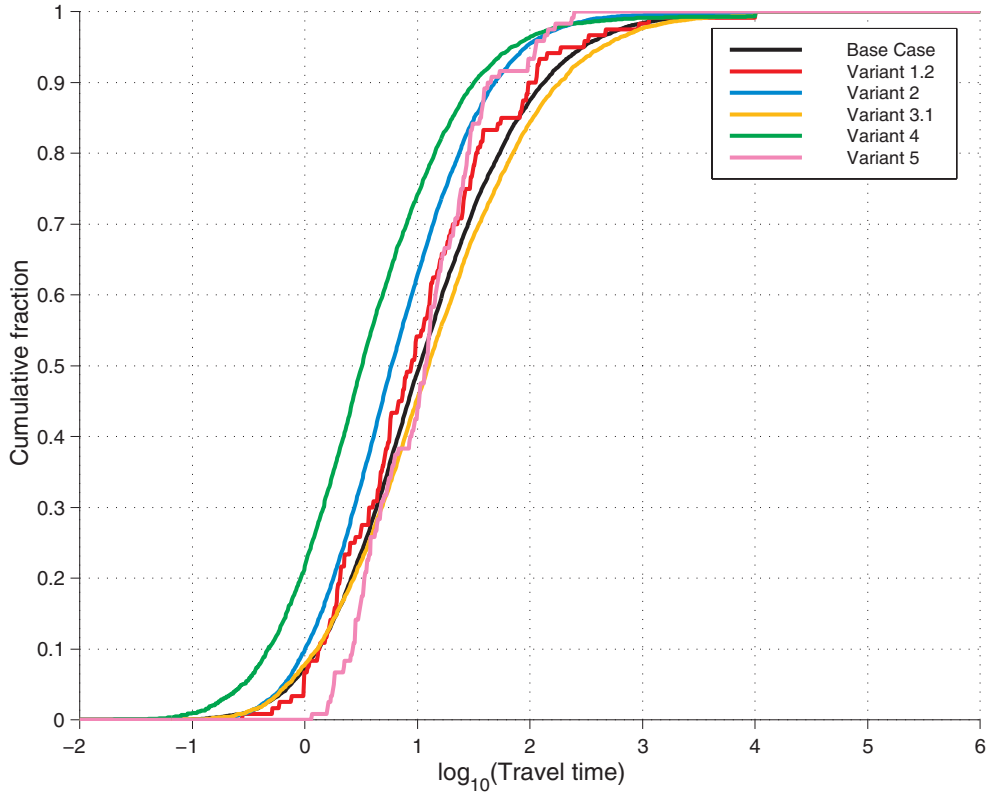

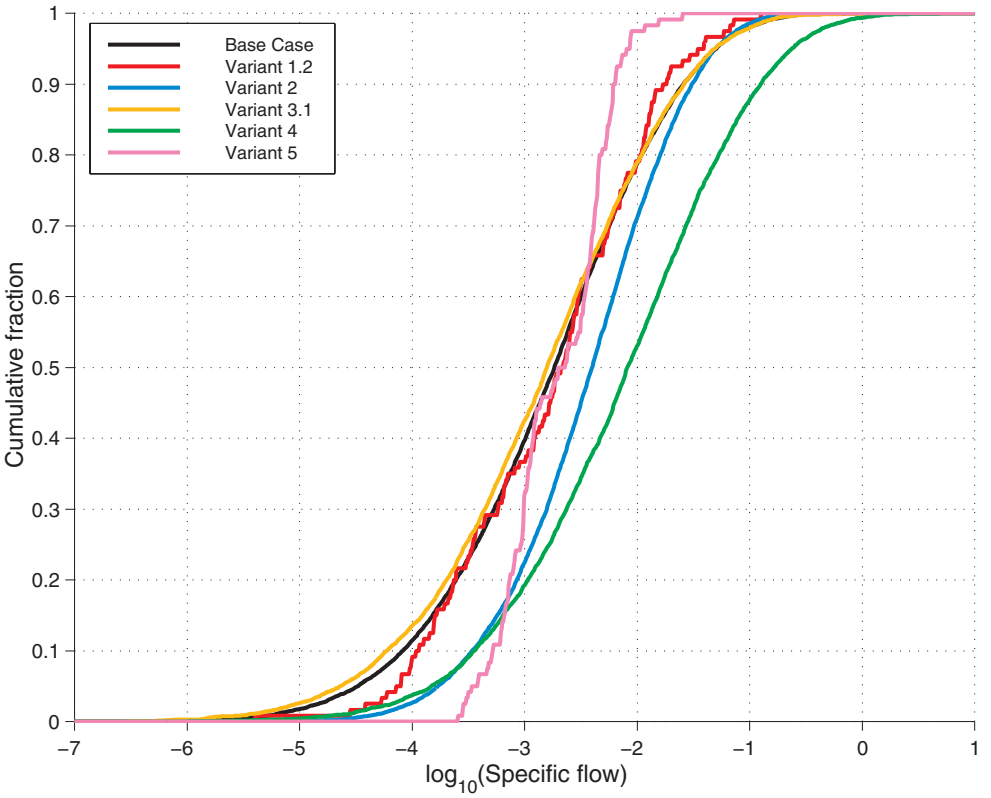

Figure 9-15. *Comparison of a) travel times (years) and b) groundwater flux [$m^3/(m^2 \cdot y)$] at repository depth between base case and variants. The simulation of travel times was interrupted at 10,000 years.*

Figure 9-15 shows that the base case and variants are for the most part very similar in terms of both the location and spread of the distributions. In variant 5 (deterministic hydraulic conductivities), however, the spread is much smaller because the spatial variability in hydraulic conductivity is neglected except for the large-scale variation represented by the different domains for rock mass and fracture zones. Variant 1.2 (alternative boundary conditions), which is based on a single realization, also results in less variation than the base case.

The results in variant 1 indicate that the effect of salinity, included using environmental heads, only marginally affects travel times, groundwater fluxes and fraction of particles reaching the surface. Numerical studies of Aberg that handle density-driven flow fully /Svensson, 1997a; 1997b/ indicate greater effects of neglected density dependence. More than an order of magnitude higher values of groundwater flux are predicted in HYDRASTAR's base case than in the model by Svensson /1997b/.

Concerning transport from a single canister, the distributions in Figure 9-15 represent the uncertainty in travel time implied by the natural variability combined with the random canister position. The figure shows that this uncertainty is much greater than the uncertainty represented by the different variants. The overall conclusion of these comparisons is thus that effects of spatial variability dominate over the uncertainties that stem from assumptions regarding other properties of the system.

Analysis of single canister positions results in narrower distributions, see Walker and Gylling /1998/. This indicates that some of the range of variation seen in Figure 9-15 is due to differences between different starting positions. The analysis of single canister positions also shows that different canister positions in the repository have systematically different mean travel times and groundwater fluxes. This type of information could be used to optimize the repository to some extent by avoiding unfavourable canister positions. As mentioned, this has not been done in SR 97. In this type of optimization, HYDRASTAR's discretization with elements on a scale of 25–30 metres is a limitation. Single structures on scales smaller than the discretization scale are not resolved in the model, and positioning of canisters can therefore not be done with greater accuracy than this scale.

To compare the calculation results with observed conditions at Aberg, the advective travel time can be estimated as:

$$t_w = \frac{L\varepsilon_f}{Ki}$$

where

L = 500 m is the length of the travel path,
ε_f = 10^{-4} is the flow porosity,
K = 10^{-7} m/s is the hydraulic conductivity, and
i = 10^{-3} is the hydraulic gradient.

The approximation gives a travel time of t_w = 16 years. This order of magnitude agrees well with the results from HYDRASTAR. The conductivity value represents fracture zones at Aberg, the gradient applies at repository depth at Aberg (section 8.7.2). The estimate of flow porosity is highly uncertain and has been pessimistically set at 10^{-4}, both in the back-of-the-envelope calculation above and in the model calculations. A more realistic porosity can thereby have a greater influence on the result than the assumptions made in the different variants.

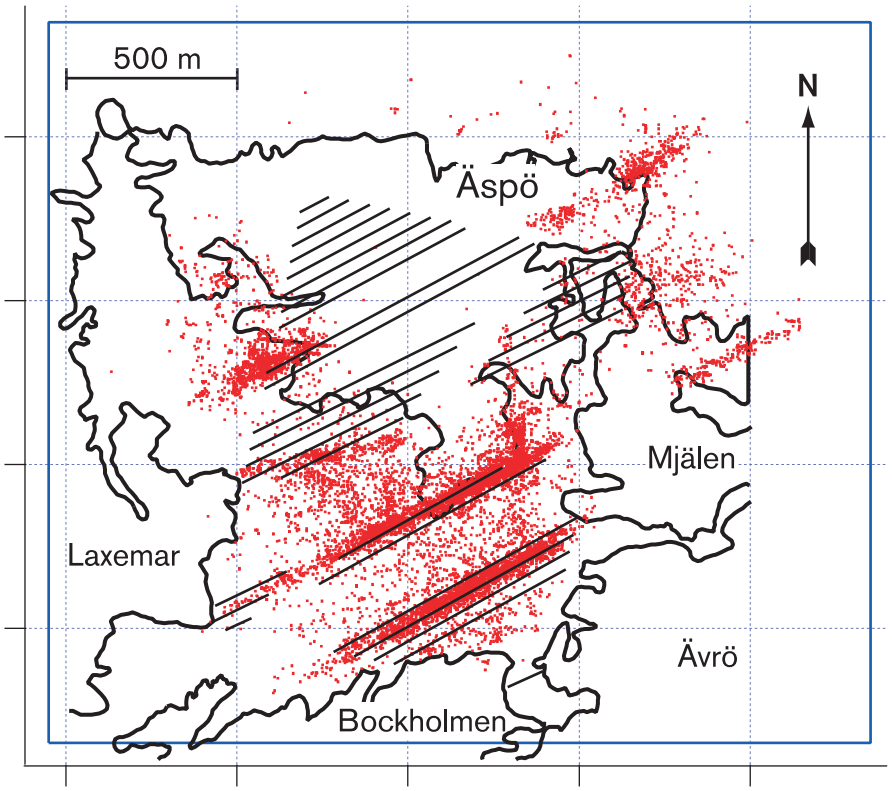

Figure 9-16. *Exit points for Aberg's base case. Repository tunnels at –500 m.a.s.l. are shown projected on the surface.*

As mentioned above, the advective travel times alone do not provide all information needed to obtain the residence time for solutes in the geosphere. In section 9.9.7 it is shown how such times can also be calculated roughly, and that the short travel times at Aberg do not conflict with observations of very old water at repository depth. The short travel times at Aberg are a result of the upward-directed flow pattern, which gives short travel paths.

The exit points at the upper model boundary for the base case are shown in Figure 9-16. Exit points for all canister positions and realizations are indicated in the figure. The fracture zones tend to concentrate the location of the exit points.

9.8.4 Conceptual uncertainty at Aberg

A special project, the Alternative Models Project (AMP), has been carried out to analyze conceptual model uncertainty. Aberg has been modelled with the stochastic continuum model HYDRASTAR /Widén and Walker, 1999/, the discrete fracture network model FracMan/MAFIC/PAWorks /Dershowitz et al, 1999/, and with the channel network model CHAN3D /Gylling et al, 1999b/.

In AMP, strict modelling premises have been applied in order to ensure that the results should be comparable. Compared with the above HYDRASTAR simulations, the most important difference is that only a part of the repository has been included in the AMP models. Comparisons between travel times, groundwater fluxes and F factors have been made. Travel times and groundwater fluxes are discussed below; the F factor, which greatly affects retention of transported radionuclides, is further discussed in section 9.9.7.

The analysis shows that all models give consistent travel times and fluxes at repository depth, see Figure 9-17. The results for median travel time and median flux are in particular very similar. The spread is greater in HYDRASTAR than in the two other models, however. This can be explained for FracMan by the fact that the results only represent a portion of the repository compared with the repository in the other two models.

Furthermore, only approximately 40 percent of the canister positions in FracMan are connected with water-bearing fractures. Finally, only a small number of realizations have been done, which can affect the reliability of the statistics. The smaller spread in CHAN3D is due to the fact that the travel time from each canister position is represented by the median value of a number of particles released at the point in question, see further Gylling et al /1999b/. Even though the spread is greater in HYDRASTAR than in FracMan and CHAN3D, the models predict values of very similar magnitude for the shortest travel times and the highest fluxes.

The exit points are also predicted similarly in the three models. Taken together, this indicates that the problem premises rather than the chosen model determine the result, i.e. that the conceptual uncertainty is low. Furthermore, it can be observed that HYDRASTAR's base case and variants in Figure 9-15 cover virtually the entire range of variation of results calculated with the different models in the alternative model project.

9.8.5 Beberg base case and variants

For Beberg, a base case in accordance with the above model application plus four variants that shed light on different assumptions have been analyzed:

1. Boundary conditions from a regional model, including salinity.
2. Alternative conductive structures.
3. Alternative hydrogeological interpretation.
4. Deterministic simulation with constant hydraulic conductivity within each individual domain for rock mass and fracture zones.

In the regional model, Hartley et al /1998/ observed that the flow pattern at the repository was downward-directed due to transient salinity effects. This resulted in long travel times from repository depth to model boundaries with times of hundreds of years for certain particles. In variant 1, the conditions are translated from a regional model with salinity to environmental head for use as a boundary condition in HYDRASTAR.

In a separate study within SR 97, Saksa and Nummela /1998/ have made assessments of the structural models used. For Beberg, it was found that certain additional zones may exist that were not included in the original structural model used in the base case. These structures are included as fracture zones in variant 2. In addition, three zones from the original structural model are included that were not included in the base case because their evaluated conductivities are lower than that of the surrounding rock mass. All new zones in variant 2 are assumed to have a hydraulic conductivity equal to the mean conductivity of the zones used in the base case.

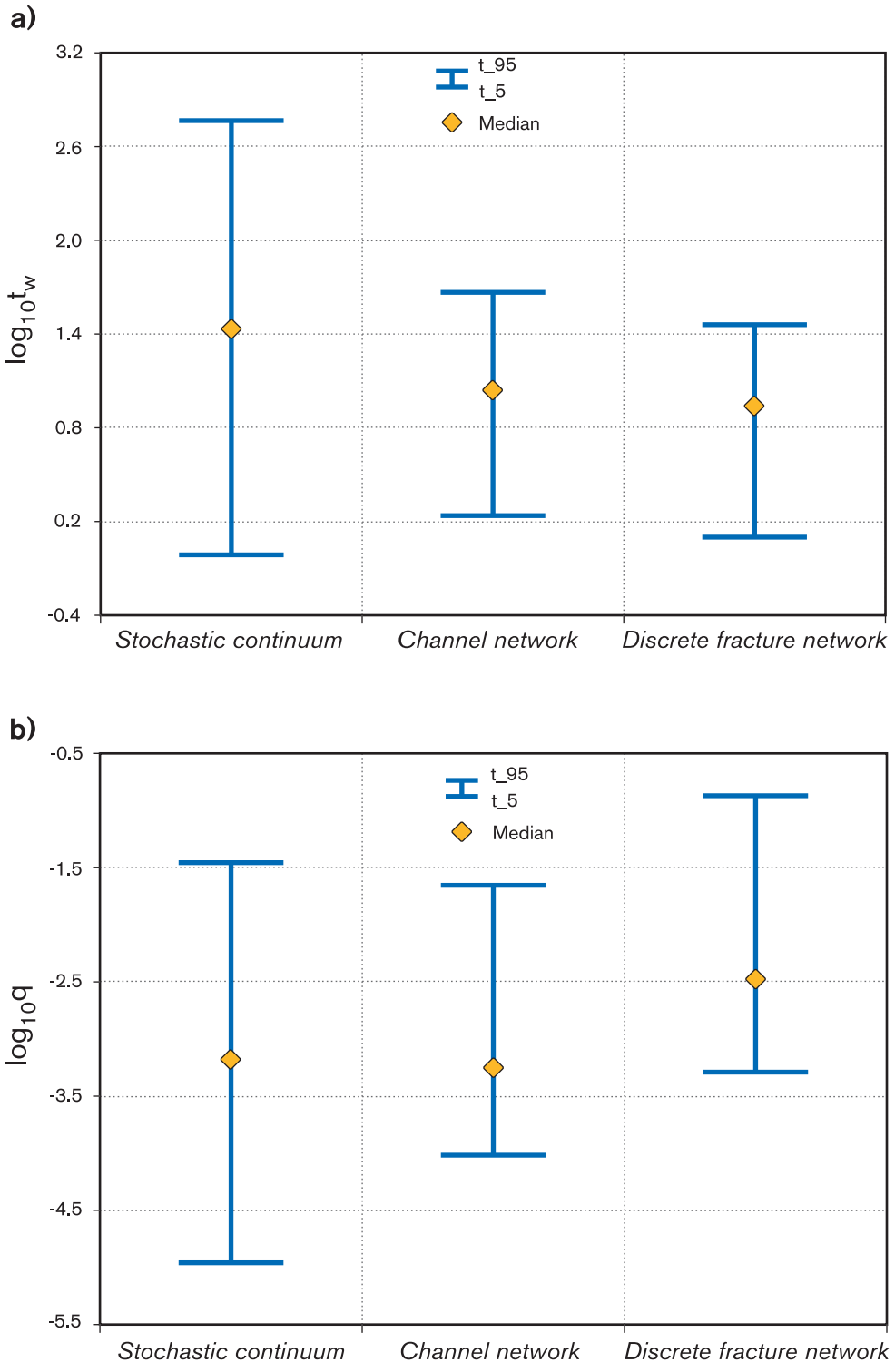

Figure 9-17. *Ensemble results for a) travel times (years) and b) groundwater fluxes [$m^3/(m^2 \cdot y)$] at repository depth in the AMP models. Results for 5th percentile, median and 95th percentile.*

In the regional model, Hartley et al /1998/ also investigated an alternative to the base case hydrogeological interpretation of Beberg. The alternative model is investigated on a local scale in variant 3. The differences compared with the base case are that zone 2 is regarded as a three-part conductive structure with a low-permeability core, five other structures terminate at the bottom of zone two, and a different depth dependence for the conductivity of the rock mass is used. Environmental head is used as a boundary condition in this variant as well.

Variant 4 is a deterministic variant, i.e. no variability of hydraulic conductivities within rock mass and fracture zones has been assumed. The purpose is to investigate the effect of the absence of spatial variability versus the explicitely defined structures, and to study the upscaling methodology.

The results for travel times and groundwater fluxes for the base case and all variants are shown in Figure 9-18. The results presented represent ensemble statistics for all realizations and canister positions.

Figure 9-18a shows that the fraction of particles that reach the surface in variants 1 and 3 is much lower than the fraction in the base case and variant 2. However, the particles that reach the upper surface in the variants with mainly downward-directed flow have travel times of the same order of magnitude as in the other variants. Figure 9-18 also indicates that the spread in travel time within the different variants and the base case is comparable when the particles that do not reach the surface in variants 1 and 3 are neglected.

The comparison of groundwater fluxes in Figure 9-18 shows that all variants are very similar. However, variant 4 (deterministic hydraulic conductivities) has as expected much less variation in the flux values. Figure 9-18 also indicates that the base case and variant 2 (additional zones) are almost identical as regards travel times and fluxes. Certain differences in travel paths arise due to the additional zones, however.

In a separate study, NAMMU has been used to study the effects of density-driven flow at Beberg /Marsic and Hartley/. A conductivity field corresponding to variant 4 for HYDRASTAR has been used in the simulation. The results indicate on comparison with equivalent results from HYDRASTAR that the use of environmental head as a boundary condition at Beberg is a valid representation of the effects of density-driven flow.

The results of the base case in Figure 9-18 are comparable to the corresponding results from SKB 91 /SKB, 1992/. The travel times in SR 97 are slightly shorter due mainly to the slightly higher conductivity values used in SR 97. In SKB 91, the rock was not divided into different domains for rock mass; furthermore, other upscaling procedures and a different depth dependence for the hydraulic conductivity were used.

Figure 9-19 shows discharge areas for the base case and for variant 1.

In the base case, the location of the exit points is determined by the regional structures and the gradient towards the northeast. In variant 1, the effect of the downward-directed flow is added, which results in a high proportion of exit points at the model's lower boundary.

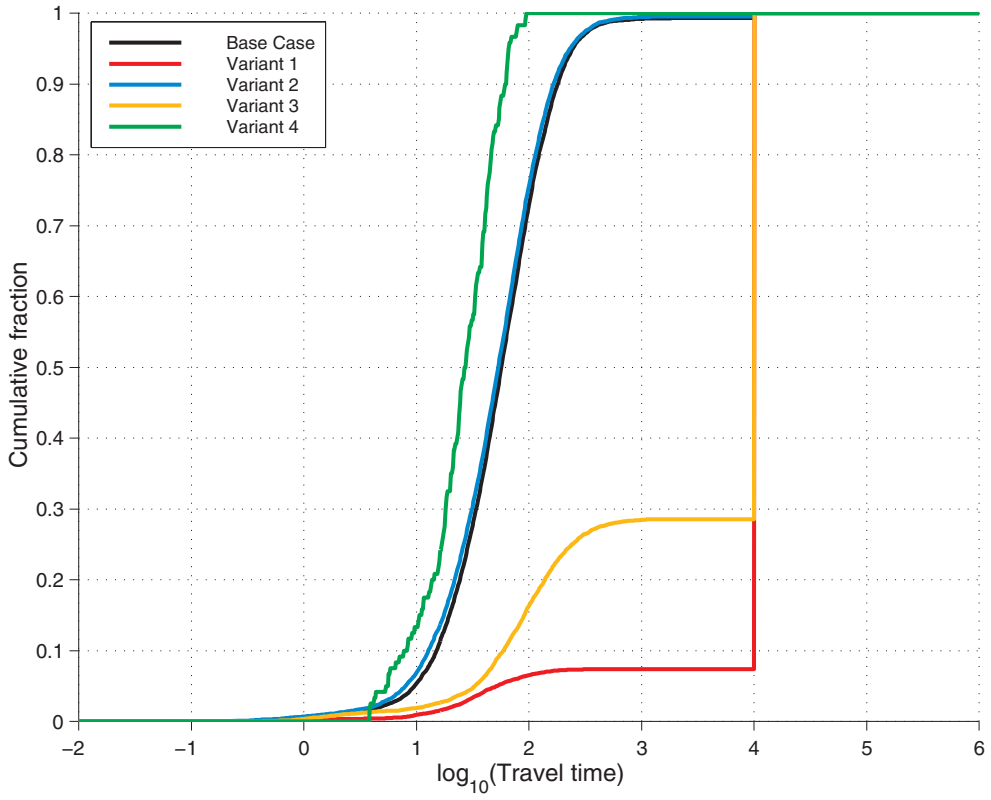

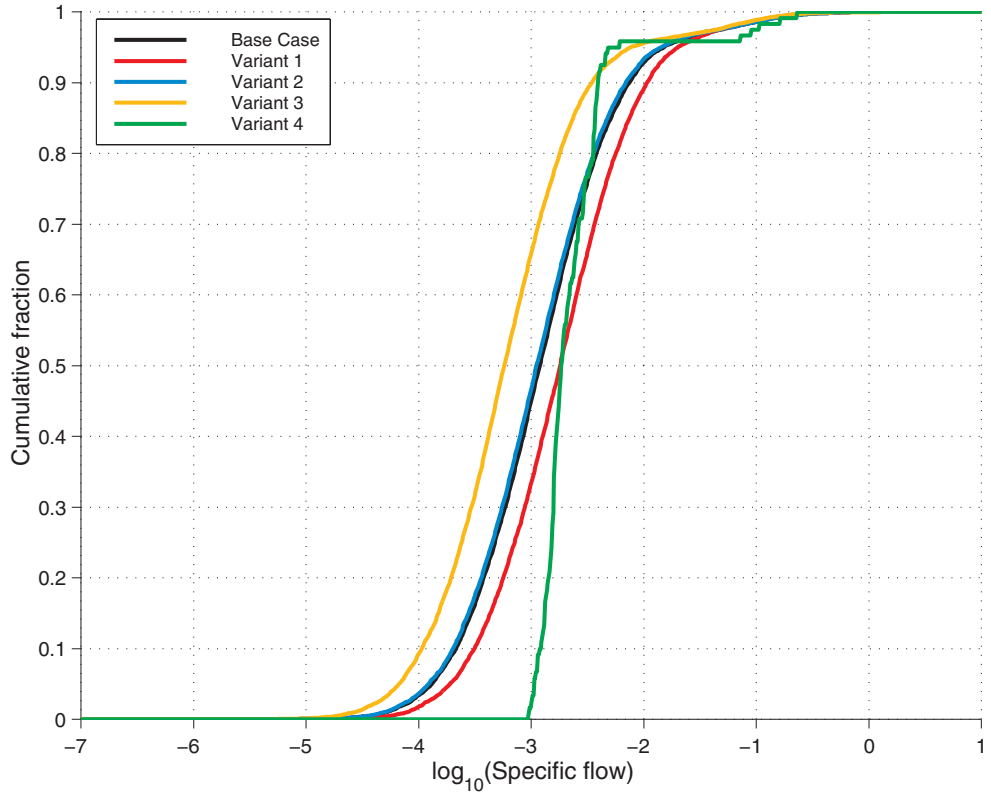

Figure 9-18. *Comparison of a) travel times (years) and b) groundwater flux [$m^3/(m^2 \cdot y)$] at repository depth for base caseand variants at Beberg. The simulation of travel times was interrupted at 10,000 years.*

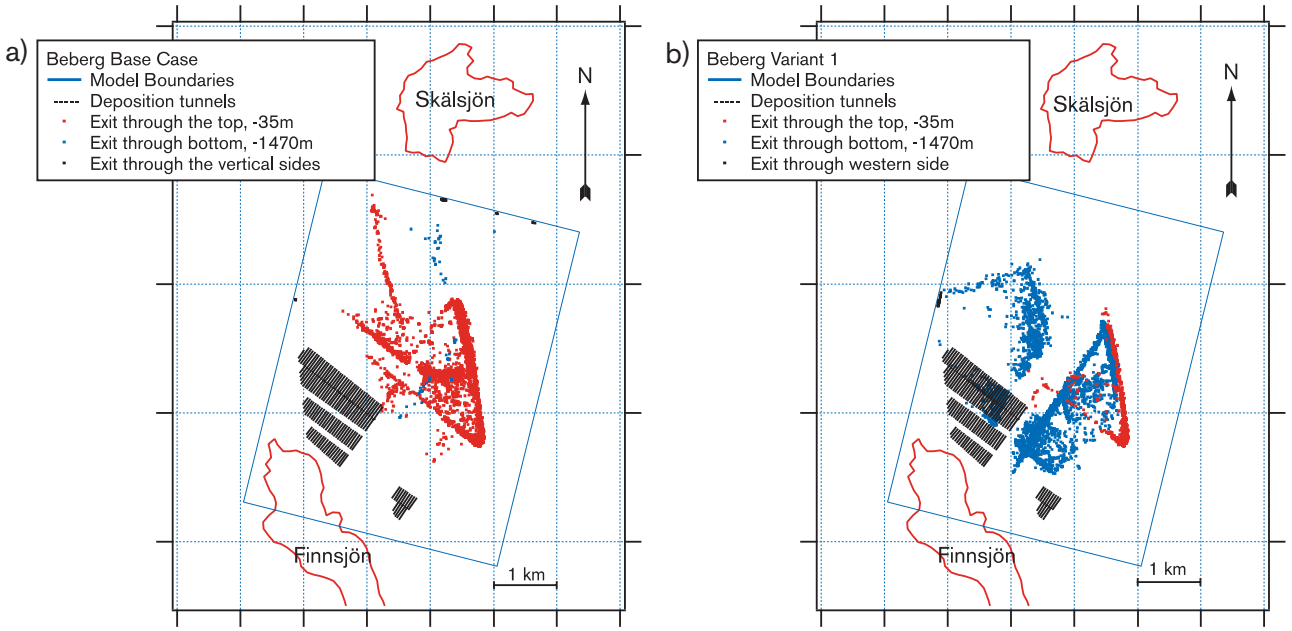

Figure 9-19. *Exit points for Beberg's a) base case and b) variant 1. Repository tunnels at –600 m.a.s.l. are shown projected on the surface.*

9.8.6 Ceberg base case and variants

For Ceberg as well, a base case and a number of variants have been analyzed:

1. Contrast in hydraulic conductivity between domains for rock mass and fracture zones increased by a factor of 100.
2. Alternative conductive structures.
3. Increased variance in hydraulic conductivity.
4. Deterministic simulation with constant hydraulic conductivity within each individual domain for rock mass and fracture zones.

In the base case, the difference in conductivity between rock mass and fracture zones is small. Due to a limited data quantity, Walker et al /1997/ propose that all fracture zones be modelled with identical hydraulic properties. However, analysis of individual zones indicates that higher conductivities are possible for certain fracture zones /Walker et al, 1997/. The first variant sheds light on the effects of a hundred-fold increase in hydraulic conductivity for all fracture zones.

The second variant sheds light on the effect of alternative conductive structures. It is assumed that all fracture zones, intrusive dykes and topographical lineaments are high-conductivity zones. As for variant 1, it has been assumed that the contrast between the domains for rock mass and fracture zones is increased by a factor of a hundred compared with the base case. The geographic location of these additional fracture zones is taken from Saksa and Nummela /1998/, who have evaluated uncertainties in geological structural models for all three sites.

The present version of HYDRASTAR has a limitation in that the same variance for hydraulic conductivity must be specified for both rock mass and fracture zones. The variance used for the base case is based on data for rock mass, which are more abundant

and also considered more reliable. If data for fracture zones were used, however, the variance would increase considerably. Variant 3 illustrates this case with a variance for hydraulic conductivity ($\log_{10}$ scale) increased to 2.0. It should be pointed out that this is a purely hypothetical case inasmuch as the variance for the rock mass also increases; there is no support for such an increase in the rock mass.

The last variant is deterministic, i.e. no variability of hydraulic conductivities within rock mass and fracture zones has been assumed. The purpose of this variant is to study the effect of the absence of spatial variability versus the explicitly defined structures, and to study the upscaling methodology more closely.

Figure 9-20 shows the results for travel times and groundwater fluxes for base case and variants. The results represent ensemble statistics for all realizations and canister positions.

Figure 9-20 indicates that the base case does not cover all variants as well as at Aberg and Beberg. This is particularly true of the travel times, where all variants except variant 4 (deterministic hydraulic conductivities) have shorter travel times than the base case. Variant 2 (alternative conductive structures) is extreme in this respect, with a higher proportion of very short travel times. The differences between the variants are, however, still less than the difference within the base case and within individual variants.

Variant 4 (deterministic hydraulic conductivities) and the base case are very similar with respect to travel times, while the spread in flux is much less in variant 4 than in the base case. This indicates that even though the variability of the rock mass in the base case results in greater spread of fluxes than in the deterministic case, it is mainly differences in the location of the canister positions that determine the spread of travel times.

Exit points for all the base case's canister positions and realizations are shown in Figure 9-21. The exit points are separated into four distinct areas. Two areas, in the west and in the east along the Husån river, contain particles that reach the surface. The area at the southern boundary contains both particles that reach the surface and particles that exit through the southern boundary. The area in the middle of the model contains particles that exit through the lower boundary, i.e. at the bottom of the model. These particles reflect a regional, downward-directed flow pattern. A total of about 90 percent of the particles reach the surface.

9.8.7 Comparison between the sites

Travel times and groundwater fluxes in the base cases for the three sites are compared in Figure 9-22. Aberg has the shortest mean travel time but the greatest spread in the distribution. It is followed by Beberg and Ceberg, which has the longest mean travel time and the smallest spread when particles that do not reach the surface are neglected.

For groundwater flux, Aberg and Beberg have mean values of the same order of magnitude, while Ceberg is roughly two orders of magnitude lower. Here as well, Aberg has the greatest spread while Ceberg has the least.

When the results in Figure 9-22 are compared, it should be remembered that the base cases for Aberg and Ceberg represent today's expected conditions, while Beberg's base case is a hypothetical situation that can represent possible future conditions when non-saline water has replaced today's saline waters. Once again it is pointed out that the travel times do not correspond to the groundwater's actual residence time, see discussion in 9.9.7.

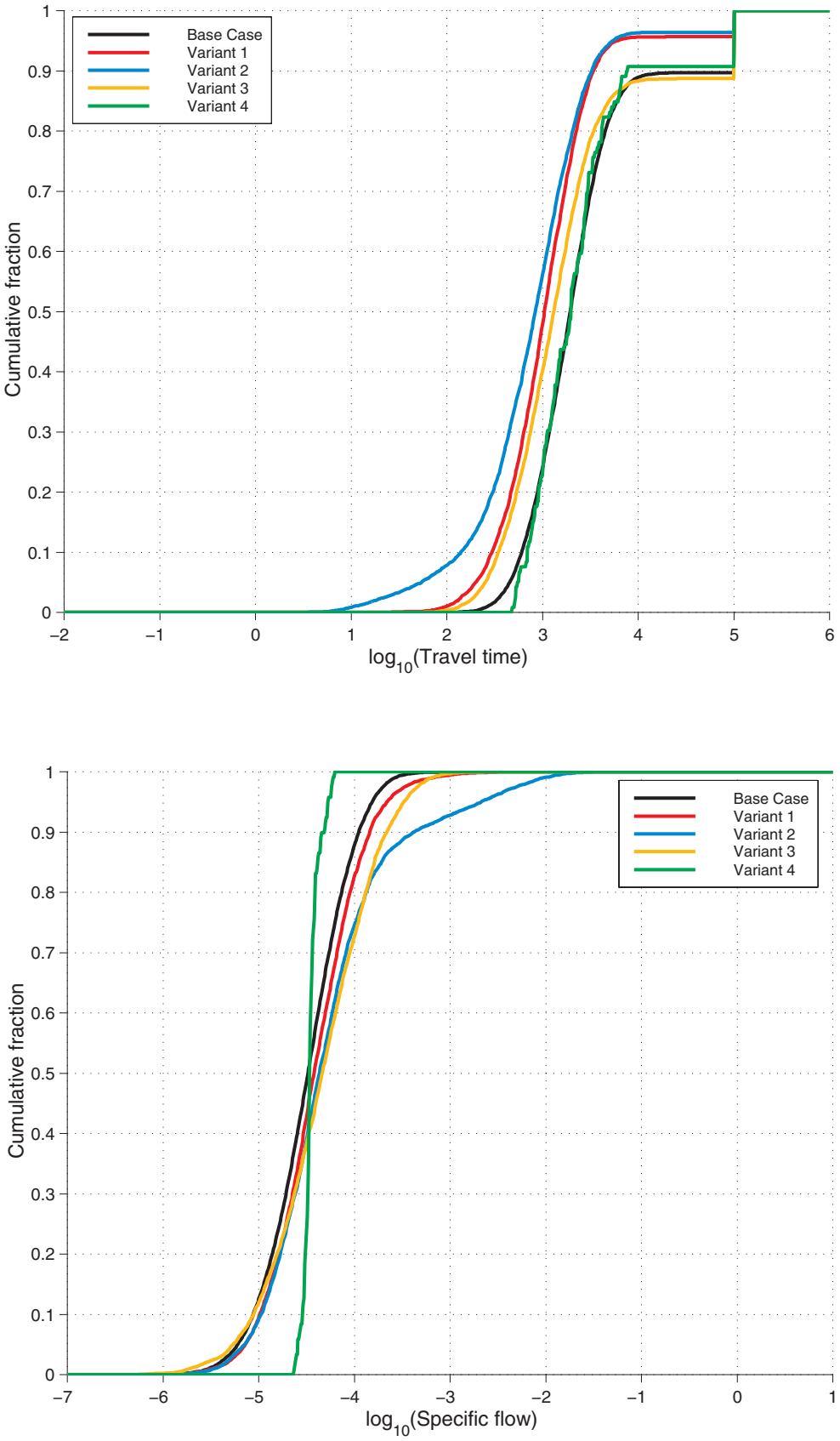

***Figure 9-20**. Comparison of a) travel times (years) and b) groundwater flux [$m^3/(m^2 \cdot y)$] at repository depth for base case and variants at Ceberg. The simulation of travel times was interrupted at 100,000 years.*

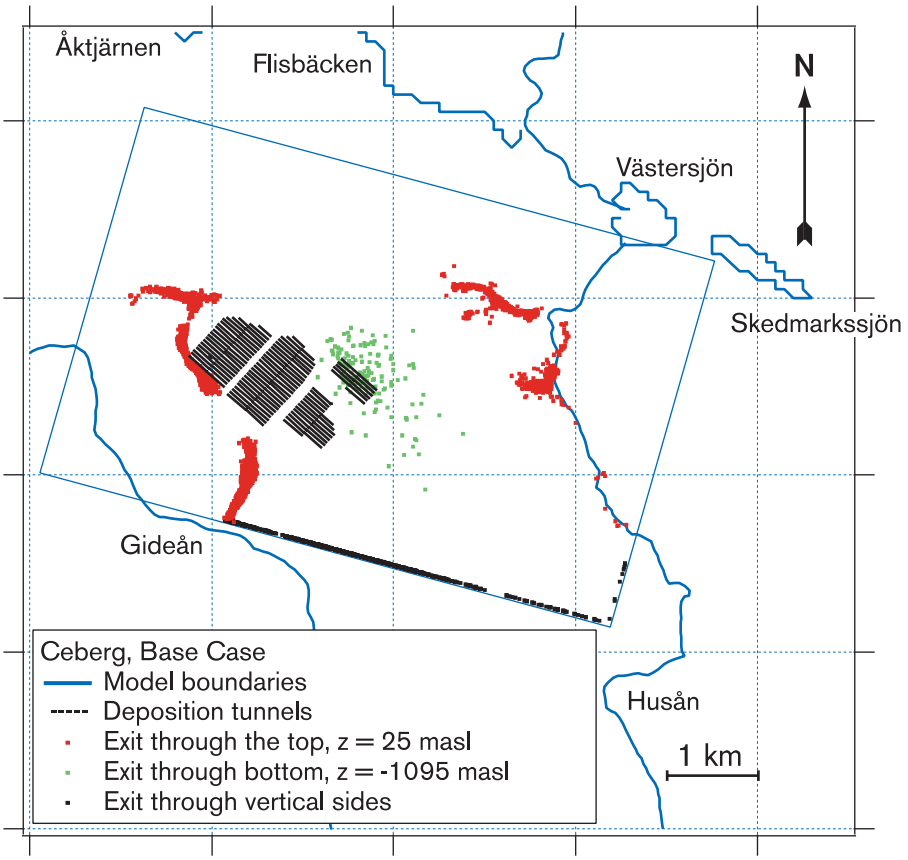

Figure 9-21. *Exit points for base case in Ceberg. Repository tunnels at –500 m.a.s.l. are shown projected on the surface.*

A comparison of the total flow through the models for the base cases and the deterministic variants indicates that the upscaling procedure for the mean and variance of the hydraulic conductivity is acceptable for all three sites. Comparison with corresponding flows in the regional models shows that the transfer of boundary conditions from regional model to local model works acceptably for the purposes of the analysis.

9.8.8 Uncertainties

The purpose of the local models is to provide an understanding of the hydraulic conditions at the site in question. The models are subject to various types of uncertainties. One can distinguish between uncertainties due to:

- the chosen conceptual model,
- spatial variability, and
- incomplete data on the site's geological structures and incomplete knowledge of other controlling properties.

A more detailed description of all uncertainties associated with the description of groundwater flow is given in the Data Report.

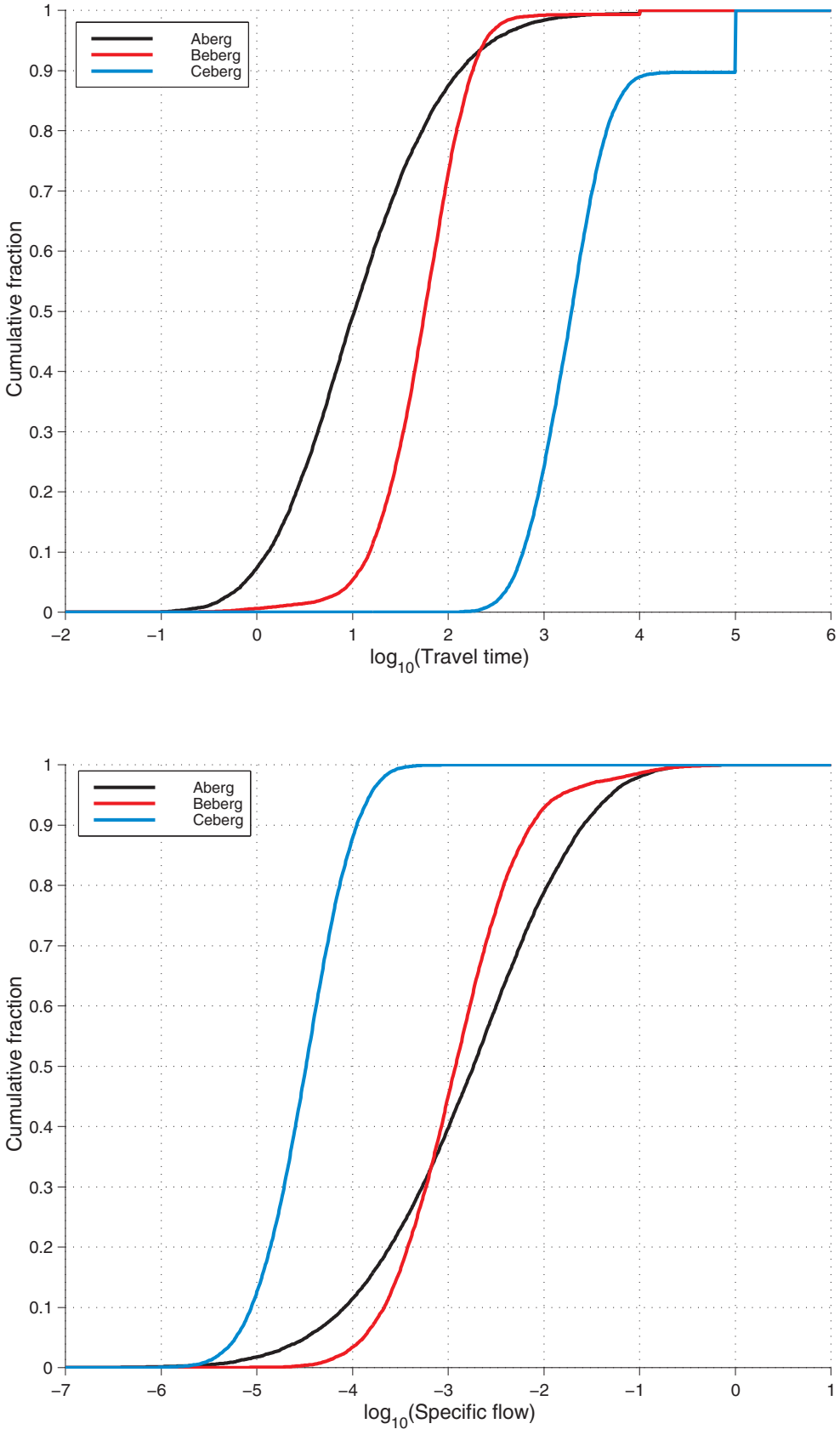

Figure 9-22. *Comparison of a) travel times (years) and b) groundwater flux [$m^3/(m^2 \cdot y)$] at repository depth for base cases at Aberg, Beberg and Ceberg.*

The importance of **conceptual uncertainty** is primarily analyzed for Aberg. Three different models for groundwater flow and advective transport are used to analyze how the choice of conceptual model for description of the rock's hydrogeological properties affects the result. The different conceptual models give similar results.

Spatial variability means that the properties of the rock are only known in a statistical sense: we don't know the properties of the rock at every point. The resulting uncertainty is handled quantitatively using multiple Monte Carlo realizations, all equally probable, of the rock's properties and resulting groundwater flow. The results are expressed statistically with distributions. It is shown for all sites that the heterogeneity of the geosphere, in combination with the randomly chosen position of a damaged canister, gives rise to the greatest uncertainties in travel times and groundwater fluxes.

Uncertainties due to **incomplete data and knowledge of system properties** are analyzed by comparing a base case with a number of variants. The base case usually represents the expected hydraulic situation, while the variants shed light on different assumptions regarding properties and alternative interpretations of underlying data. In SR 97, a group of experts has prioritized a set of variants. Additional motives for the different variants are given in the relevant background report. The results show that the differences between different variants are usually small. The exception is salinity effects, which at Beberg control the dominant flow direction.

The time variation at the boundaries has been neglected in all local models. The models describe today's conditions; the effects of land uplift are neglected, despite the fact that this phenomenon is included in the canister defect scenario. For Beberg, however, the transient evolution is described on the regional scale /Hartley et al, 1998/, while a supplementary modelling on the local scale for Aberg has included transient effects /Svensson, 1999/. Svensson's study shows that the quantities that are propagated to radionuclide calculations are only changed marginally by land uplift in comparison with effects of other uncertainties.

The calculated differences in travel times and groundwater fluxes between the different sites are consistent with the differences in hydrogeological conditions/data presented in Walker et al /1997/. Although factors such as boundary conditions and length of travel paths influence the results, the underlying difference in hydraulic conductivity between the sites can to some extent explain the results. This is particularly true of the differences between Ceberg and the two other sites; when Aberg and Beberg are compared, where the conductivity values are more similar, the influence of gradient and location of the discharge areas become more important.

An interesting follow-up question is whether the differences in model results between the sites represent actual physical differences in underlying hydrogeological conditions, or whether they are caused by differences in investigation methodology (number of measurements, measurement method, etc.). Part of the answer is suggested by a comparison with the results of previous analyses. Gideå (Ceberg) and Finnsjön (Beberg) were analyzed in the KBS-3 project as well /SKB, 1983/. The same data that were used for Ceberg in KBS-3 have been used in SR 97, while the database for Beberg has been increased between KBS-3 and SR 97. Similar investigation methodology and evaluation of all sites were used in the KBS-3 project. As in SR 97, a calculated difference in groundwater flux at repository depth of approximately two orders of magnitude emerged when Beberg and Ceberg were compared. This indicates that systematic differences in investigation methodology between the sites in SR 97 are of subordinate importance for the results of the safety assessment. However, it has not been possible in SR 97 to fully quantify how much of the differences in calculated results is due to actual, physical differences between the sites and how much to differences in investigation methodology.

Confidence in the fact that HYDRASTAR is adequate for its purpose in SR 97 is discussed in section 9.11.3, along with other central models for quantification of radionuclide transport. The discussion around HYDRASTAR is largely based on the above account of uncertainties.

9.9 Transport processes in the repository

9.9.1 Overview

The processes that can lead to dissolution of radionuclides in a damaged canister have been discussed in previous sections. Radionuclides dissolved in water can be transported in the interior of the canister, primarily by diffusion, and thereby reach the buffer via the defect.

After water saturation, radionuclide transport in the buffer is expected to take place solely by diffusion in the buffer's pores, possibly also on the surfaces of the clay particles. Neither advection nor colloid transport occur, due to the properties of the buffer. Radionuclides can be sorbed to the surfaces of the montmorillonite. A crucial factor for this is the chemical form of the radionuclide, which is determined by the chemical environment in the buffer by the process of speciation.

In the rock, radionuclides can be transported by the flowing groundwater, advection. Diffusion can also be important under stagnant conditions. An important aspect of this is matrix diffusion, i.e. radionuclides diffuse in the stagnant water in the micropores in the rock and are thereby retained and transported more slowly than the flowing water. The timescale for advection in relation to the timescale for matrix diffusion determines the relative importance of the latter process. Sorption, where radionuclides sorb (adhere) to the surfaces of the fracture system and the rock matrix, is also crucial for radionuclide transport. Matrix diffusion and sorption are the two most important retention processes for radionuclides in the geosphere. Another factor that can be of importance for retention is sorption on colloidal particles and transport with them. The chemical environment in the water determines what speciation (chemical form) the radionuclides will have, which is crucial particularly for the sorption phenomena. Some nuclides can be transported in the gas phase.

Finally, radioactive decay influences the entire system's content of radionuclides and must therefore be included in the description of transport phenomena.

9.9.2 Transport processes in canister cavity

Released radionuclides can be transported in the interior of the canister and escape through a damaged copper shell. Radionuclides dissolved in water inside the canister can be transported either by accompanying the moving water, advection, or by diffusing in the water. Transport in water is the dominant means of transport for radionuclides. Certain nuclides may occur in gas form in the canister, and can then be transported in the gas phase as well. These include above all C-14, Rn-222 and Kr-85.

The geometry of the transport pathways inside a damaged canister is determined by the original geometry of the canister and the fuel and by the changes to which corrosion has led. In order for water to come into contact with fuel and permit release and transport of radionuclides, there must be penetrating defects in both the cast iron insert and the

Zircaloy cladding. Even if such defects have occurred, remaining structures can be expected to constitute significant transport barriers, both to inflow of water and to outflow of dissolved nuclides. The structure of the four-metre-long cladding tubes, the other metal parts of the fuel, the cast iron insert and the copper canister prevent efficient transport. Products from corrosion of the copper canister in particular can be expected to impede transport. The surfaces of all these structures may also have good sorption properties for certain radionuclides.

There are great uncertainties surrounding water/gas flux in the interior of the canister and corrosion of the cast iron insert and the fuel's metal parts. An assessment of e.g. the geometric conditions and thereby the geometry of the transport pathways will therefore also be uncertain. The sorption properties of the materials in a damaged canister are difficult to judge as well.

Radionuclide transport in the interior of the canister is therefore pessimistically simplified in the safety assessment in the following way: After a certain "delay time" has passed since the breach occurred in the canister's copper shell, the entire void in the canister at closure, approximately 1 m^3, is assumed to be filled with water. The length of the delay time is determined on the basis of the size of the breach in the copper shell and the subsequent water turnover and corrosion (see section 9.6).

After the delay time, all water in the canister is assumed to be available for the fuel dissolution process, i.e. to be in direct contact with all fuel without being impaired by Zircaloy cladding or other structures. The water is assumed to be thoroughly mixed, i.e. there are no concentration differences between different parts of the interior of the canister. The fuel dissolution process (see 9.7) then determines the rate of release of matrix-bound radionuclides. Segregated nuclides and radionuclides in the structural parts of the fuel are assumed to be instantly released for dissolution in water at the end of the delay time. Solubility-limited nuclides are precipitated if the nuclide's concentration in the water exceeds its solubility (see 9.7). Sorption of radionuclides to the internal parts of the canister is neglected.

Transport of radionuclides through the breach in the copper shell is modelled as diffusion with an assumed geometry of the breach.

Data for calculations of radionuclide transport

Because the model assumes that the water in the canister is thoroughly mixed, no data are needed to describe the processes there. Data for inventory, size of canister defect, delay time, fuel dissolution, speciation and dissolution/precipitation have been discussed in previous sections.

9.9.3 Transport processes in buffer/backfill

Advection

Due to the low hydraulic conductivity of the buffer material, all transport of solutes in the buffer after water saturation is expected to take place by diffusion.

The backfill has a hydraulic conductivity and a diffusivity that lie in a range where both diffusion and advection can be important transport mechanisms. Calculations /Moreno, 1999/ show, however, that even with a very high flow through the backfill, the outward transport of radionuclides will be no more than twice as great than in the case with diffusion only, so advection can be neglected in the buffer as well.

Diffusion and sorption in the backfill

Transport through the buffer is mediated by different diffusion mechanisms. The mechanisms are described more thoroughly in Yu and Neretnieks /1997/ and the Process Report.

It has been established that certain cations may have high diffusivities (be transported efficiently). A possible explanation of this phenomenon is the theory of surface diffusion. The process is handled by assigning higher diffusivity values to the elements Cs, Sr and Ra.

When bentonite has such high density that the electrical double layers between two planes are superimposed, a phenomenon known as anion exclusion occurs. Anions cannot penetrate into the interlamellar pores due to the electrostatic forces between the negatively charged surfaces and the anion. Anion exclusion significantly reduces the porosity available for diffusion. The effect of anion exclusion becomes less at high salinities, and in crushed rock/bentonite mixtures it is negligible.

Radionuclides may be sorbed to the surfaces of the montmorillonite /Yu and Neretnieks, 1997; Process Report/. In calculations of radionuclide transport, the sorption equilibrium is normally described as a linear relationship between the sorbed concentration and the concentration in solution, with a distribution coefficient K_d. When the concentration of the species in solution is low, which is normally the case for radionuclides, the linear approximation gives a satisfactory result. However, the distribution coefficient K_d is a measured value that only applies for the conditions under which the particular value was measured, and it cannot really be extrapolated to other conditions. The uncertainty in the process description must therefore be handled by the choice of K_d values.

Of crucial importance for sorption and diffusion is the chemical form of the radionuclide, which is determined by the chemical environment in the buffer via the process of speciation. It is affected by the speciation the nuclide had at the boundary of the buffer, i.e. inside the canister (see section 9.7.6), but also by the chemical conditions in the buffer. The data that are used for diffusion and sorption are based on one (or more) water compositions that can occur in the buffer.

Yu and Neretnieks /1997/ hold a detailed discussion of different experimental methods and how the results can be interpreted. Ochs /1997/ examines and summarizes the uncertainties surrounding diffusion and sorption in bentonite.

Data for calculations or radionuclide transport

Yu and Neretnieks /1997/ and Ochs /1997/ have evaluated different published measurements of diffusion and sorption properties in water-saturated bentonite and critically evaluated different sources of error. The value of the parameters depends on, among other things, the ionic strength of the pore water. Ochs /1997/ points out, however, that the pore water in the bentonite will have a high ionic strength, regardless of the composition of the surrounding groundwater, since the bentonite contains soluble impurities such as $CaSO_4$ and NaCl. The redox capacity of the buffer and the large quantity of iron in the canister further prevent oxidizing conditions from existing in the buffer. For most substances, the porosity is given by the bentonite's specification, but for certain substances the porosity must be reduced to account for anion exclusion. With these premises, element-specific values of distribution factors (K_d) and effective diffusivity (D_e) are chosen from the best estimate values given by Yu and Neretnieks /1997/. Pessimistic K_d values are obtained by choosing the lowest values in the uncertainty

intervals given. Table 2-6 in Appendix 2 shows which values have been chosen. The values are dependent on the chemical composition of the pore water and are thereby in principle correlated with other input data that are dependent on the chemical conditions.

The backfill is assumed in the analysis to consist of a mixture of 15 percent bentonite and 85 percent crushed rock. Sorption data (K_d) are obtained by proportionally weighting the values for bentonite and rock by 15 and 85 percent, respectively. The ionic strength of the pore water in the bentonite portion is assumed to be the same as in the groundwater in the rock, which for a best estimate entails saline conditions for Aberg and non-saline conditions for Beberg and Ceberg. Since the bentonite only occurs in mixed form, no ion exclusion effects arise. The diffusivity can therefore be chosen as the diffusivity in water (around 10^{-10} m^2/s). The porosity is determined essentially by the bentonite's porosity and is set equal to 30 percent. In practice, the transport properties of the backfill are of little importance. Pessimistic values are therefore chosen. Data are shown in Table 2-7 and 2-8 in Appendix 2. The values are dependent on the composition of the pore water and are thereby in principle correlated with other input data that are dependent on the chemical conditions.

Colloid transport in buffer and colloid release

The buffer acts as an effective barrier to any colloids that may form inside the canister cavity /Process Report/. This function has been demonstrated experimentally.

Montmorillonite from the expanding buffer can intrude into fractures around the deposition hole. The groundwater in the fractures could then erode the buffer and thereby give rise to clay colloids in the groundwater, but experiments conducted on laboratory scale with granitic groundwater show negligibly small concentrations /Process Report/.

Colloid transport in the buffer and colloid release from the surface of the buffer are therefore neglected in the calculation of radionuclide transport.

9.9.4 Mass transfer between buffer/backfill and geosphere

The mass transfer from buffer and backfill to the flowing groundwater in the rock takes place by diffusion. The efficiency of the transfer is thereby dependent on the geometry of the contact interface between the flow paths that have direct or indirect contact between buffer and backfill.

The mass transfer can be described with the concept equivalent flow rate (Q_{eq}) /Moreno and Gylling, 1998/. The equivalent flow rate is not an actual flow rate, but is calculated with boundary layer theory so that the mass transfer rate corresponds to the product of the equivalent flow rate and the concentration of the radionuclide on the boundary between buffer/backfill and the flowing groundwater. The equivalent flow rate (Q_{eq}) is dependent on the geometry (length, width and porosity) of the contact interface with the flow path, on the diffusivity and on the flux of the groundwater surrounding the deposition hole.

There are no additional uncertainties regarding the processes (diffusion) that control the mass transfer, but uncertainties arise indirectly from the uncertainties in geometry and groundwater flow. Since the rock is heterogeneous, both geometry and groundwater flux vary between different canister positions. Furthermore, there may be several flow paths in the rock that have contact with buffer and backfill.

Data for calculations of radionuclide transport

In the calculation of radionuclide transport, it is assumed /Moreno and Gylling, 1998/ that radionuclides escaping through the buffer out to the flowing groundwater in the geosphere can exit via four different pathways, Figure 9-23:

1. directly into a fracture intersecting the deposition hole opposite the breach in the canister,
2. into the EDZ assumed to surround the deposition tunnel,
3. via the tunnel's backfill and further into a fracture zone that is assumed to intersect the tunnel,
4. via diffusion through the rock into an assumed fracture zone in the rock.

The groundwater fluxes, q_o, that are calculated with the stochastic-continuum model on the site scale for each site (see section 9.8) are used to estimate the fluxes for these different paths. The reasonable estimate is chosen as the median of the base case for a particular site, while the pessimistic case is chosen as the 95th percentile of the variant that has the highest fluxes for the same site. The difference between sites is considerable.

The difference between the reasonable estimate and pessimistic values for groundwater fluxes reflects the reasonable variation on the site. The groundwater flux is dependent on the canister position. The calculated statistical distribution within and between realizations can be used in probabilistic analysis. The difference between variants (for the same site) is relatively small, so the statistical distribution can be based on the base cases calculated for the different sites. The spread stems mainly from the spatial variation within a realization. The spatial variation does not constitute an uncertainty in itself, but results in an uncertainty since it is not possible to predict which canister(s) will have

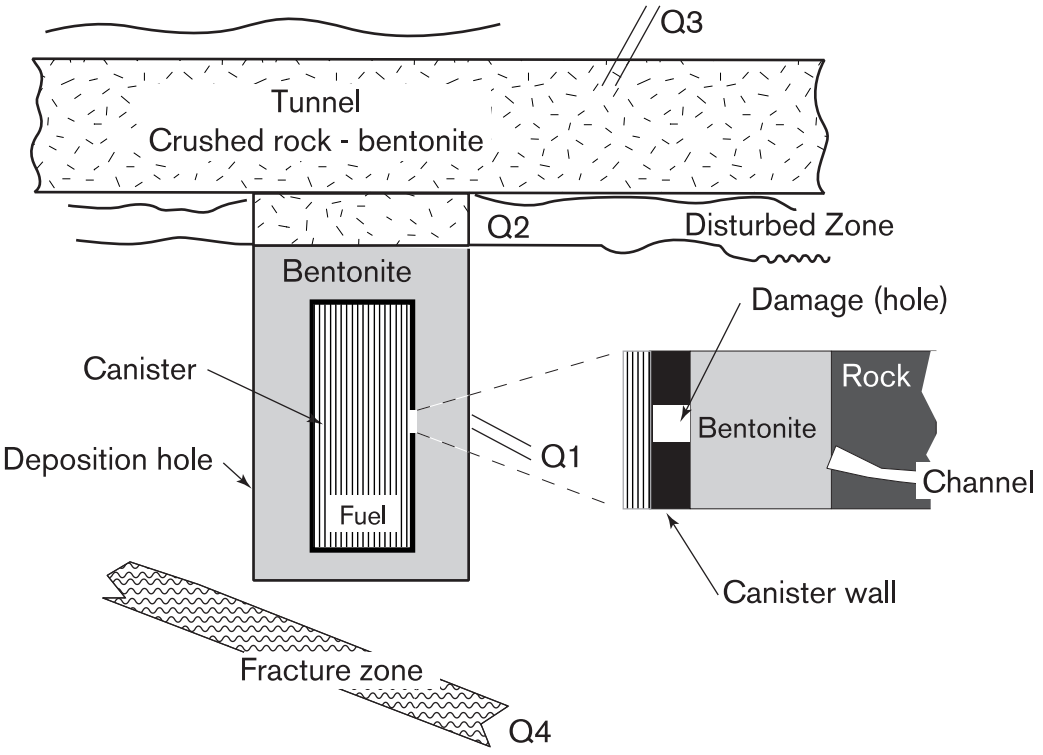

Figure 9-23. *Schematic illustration of the different transport pathways (Q1–Q4) dealt with in the near-field modelling.*

initial defects. The location of canister positions with high flux varies between different realizations, even though there are certain areas that always have higher or lower flux. No attempt has been made to make use of the knowledge about flux distribution by choosing only positions with low flux.

The groundwater flux that has been calculated with the continuum model is a mean value for a block of about 30x30x30 m^3. The fluxes for the different contact pathways are calculated as different multiples of q_0. The flux for a fracture that intersects the deposition hole (q_1) is assumed as a reasonable estimate to be the same as q_0, but comparison with results from a discrete network model (see section 9.8) suggests that q_1 may be about five times q_0. The pessimistic estimate of q_1 is therefore assumed to be $5q_0$. It is assumed that the flux in the EDZ in the tunnel floor (q_2) can be ten times greater than the mean flux and at most 100 times greater than the mean flux /Data Report/. The fluxes at a fracture zone intersecting the tunnel (q_3) or at a fracture zone inside the rock (q_4) are of little importance. Reasonable values are assumed to be $q_3=q_4=100\ q_0$, while pessimistic values are assumed to be $q_3=1{,}000\ q_0$ and $q_4=10{,}000\ q_0$. The porosity is assumed to amount to a maximum of 10^{-3} in the contact pathway with the fracture zones, while lower values are used for the contact pathway between fracture and deposition hole.

Tables 2-9 and 2-10 in Appendix 2 report the input data that are used. The groundwater flux in the near field is correlated with the travel time in the geosphere. High flux often means short travel time.

9.9.5 Diffusion/matrix diffusion in the geosphere

When the groundwater moves, diffusion in the flowing water can be neglected. However, the rock located between the fractures in which the groundwater flows contains micro-fractures with stagnant groundwater where radionuclides can diffuse in, a phenomenon known as matrix diffusion /Process Report/. Matrix diffusion entails that radionuclides diffuse into the stagnant water in the rock's microfractures and are thereby retained and transported more slowly than the flowing water. Of even greater importance is the fact that matrix diffusion provides an opportunity for sorption on the rock matrix.

The existence of an interconnected system of microfractures in granitic rock has been verified by tests both in the laboratory /Skagius and Neretnieks, 1985; Skagius, 1986/ and in the field /Birgersson and Neretnieks, 1988/. In water with low ionic strength, anions have a lower diffusion into the matrix than equivalent uncharged particles with otherwise identical properties. This is due to an ion exclusion effect where the negatively charged anions are repelled from the negatively charged pore surfaces and therefore have a smaller effective volume available for diffusion /Ohlsson and Neretnieks, 1997/. Diffusion of cations that undergo ion exchange can be reinforced by the phenomenon of surface sorption. In this case, the radionuclides diffuse into the sorbed solid phase as well /e.g. Skagius, 1986/.

The importance of matrix diffusion for transport of radionuclides is determined not only by the diffusion and sorption properties of the matrix, but also by the geometry of the fractures and the magnitude of the flow (the advective velocity) in the fractures, see further below.

Matrix diffusion is a process that is difficult to quantify and thereby burdened with relatively great uncertainties. Even though it has been possible to demonstrate diffusion into the rock mass in laboratory tests, it is much more difficult to demonstrate this conclusively under field conditions. Natural analogues in the form of geological

formations with elevated natural radioactivity can be used to verify matrix diffusion as a process that has taken place over long timespans. Analogues such as those at Palmottu in Finland, Alligator Rivers in Australia and Cigar Lake in Canada offer an opportunity for improved process understanding /Miller et al, 1994/.

Data for calculations of radionuclide transport

Diffusivity in the rock matrix is element-specific. Data are estimated from diffusion experiments /Johansson et al, 1996/, with tritiated water (HTO) and with some cations in saline water, performed on rock material from Äspö (Aberg). Diffusivities for other substances are obtained /Ohlsson and Neretnieks, 1997/ by scaling with the diffusivity of the different substances in free water and by taking into account the potential for anion exclusion and for surface diffusion. A reasonable estimate is obtained by taking all these effects into account, while pessimistic values are obtained by not taking into account (uncertain) processes that lead to high diffusivities, and by consistently choosing an unfavourable water composition.

The diffusivity values theoretically apply for unlimited penetration depth. For reasons of symmetry, however, matrix diffusion cannot occur unimpeded further than to half the size of the rock matrix block. This size is indirectly related to the flow-wetted surface area per volume rock /Andersson et al, 1998/. For model reasons, the maximum penetration depth is therefore set equal to two metres for Aberg and Beberg and 20 metres for Ceberg, which is roughly equal to the distance between conductive fractures on these sites. The actual penetration depth for sorbing nuclides will be much shorter, and there is moreover reason to believe that matrix porosity and diffusivity vary in space. The theoretically maximum values used should therefore not be accorded any great importance.

Tables 2-11 and 2-12 in Appendix 2 show the proposed input data. The values are dependent on the composition of the pore water and are thereby in principle correlated with other input data that are dependent on the chemical conditions.

9.9.6 Sorption in the geosphere

Sorption, where radionuclides sorb (adhere) to the surfaces of the fracture system and the rock matrix, is also crucial for radionuclide transport. The term sorption embraces a number of different retention processes and mechanisms that result in the adherence of a substance (radionuclide) on the solid surfaces of the rock or on another material, e.g. clay mineral, that may be present on the fracture surfaces /Process Report/.

The strength of sorption is dependent on the chemical properties of the ions and the presence of any complexing agents. A large number of experimental, nuclide-specific studies of sorption have been conducted /Carbol and Engkvist, 1995/. These tests are usually performed as batch tests where an aqueous solution of the nuclide in question is allowed to come to equilibrium with the solid rock material. If the sorption is linear, completely reversible and equilibrium exists, a distribution coefficient (K_d) can be estimated for the particular water composition. The assumption of linearity is usually fulfilled at the low concentrations that are of interest, while the assumption of equilibrium is fulfilled if the sorption has a timescale that is substantially shorter than the timescale for transport by advection and dispersion.

Sorption by surface complexation can theoretically also be described with surface complexation models. Such models are general and well-founded, but require a large quantity of difficult-to-determine data. Results of various experiments with surface

complexation models have therefore not been used to replace the distribution coefficients (K_d values), but rather to increase our understanding of the sorption mechanisms and determine what they are dependent on, i.e. how reliable sorption can be considered to be /Carbol and Engkvist, 1995; Olin and Lehikoinen, 1997/.

Data for calculations of radionuclide transport

Element-specific sorption data for the geosphere in the form of K_d values are obtained by evaluating various experimental databases while taking into account the composition of the groundwater at the different sites /Carbol and Engkvist, 1997/. The composition of the groundwater affects the speciation of the substances and is thereby of great importance for sorption. The K_d values are mainly affected by differences in salinity, whereby higher salinity results in poorer sorption. Differences in rock types between the sites are of less importance.

Values for saline water are chosen for Aberg, while values for non-saline water are chosen for Beberg and Ceberg. An obviously pessimistic choice is to always choose the lowest K_d values that have been observed, regardless of water composition. At Ceberg, however, non-saline conditions can be expected to exist in the future as well (see base scenario, section 8.9.2). The lowest non-saline K_d values are therefore chosen as a pessimistic case for Ceberg.

The proposed values are shown in Table 2-13 in Appendix 2. The values are dependent on the composition of the pore water and are thereby in principle correlated with other input data that are dependent on the chemical conditions.

9.9.7 Advection/dispersion and mass transfer between fractures and rock matrix

Radionuclides can be transported with the flowing groundwater /Process Report/. This transport is usually divided into advection and dispersion, but the subdivision is dependent on the studied scale and is relatively arbitrary. The advective component describes the mean transport, while the dispersive component takes into account effects of heterogeneity in the rock and velocity variations on scales smaller than that described by advection. Dispersion also normally includes pure molecular diffusion in water. Dispersion is a model concept rather than an actual process.

The conceptual uncertainties surrounding advection are very small. The naturally occurring spatial variability in hydraulic conductivity means that groundwater flow and advective velocities also vary in space, which leads to uncertainty. This uncertainty is handled (see section 9.8) by describing the groundwater flow with a stochastic model, by analyzing different variants and by studying different conceptualizations for groundwater flow (discrete fracture model, channel network model, and stochastic continuum description).

A large-scale mixing is obtained in the models, since different transport pathways have different groundwater flow. This large-scale mixing is the dominant component in what is known as dispersion. The explicit modelling of these velocity variations enables the description of dispersion in the radionuclide transport model to be minimized to small-scale velocity variations. Dispersion will thereby be of only subordinate importance for radionuclide transport.

The transport of radionuclides through the rock takes place by advection in the open fractures. If the substances that are dissolved in the water do not interact with their surroundings, their transport velocity is determined by the velocity of the water, which can be expressed as the flux divided by the flow porosity. If the substances can furthermore diffuse into the rock matrix and sorb there as well, this will give rise to a considerable retardation, and the resulting "transport velocity" will essentially be determined by the flux and the geometry of the fractures, as well as by the diffusion and sorption properties of the matrix. The flow porosity is of subordinate importance here.

The geometry- and flow-related portion of the transport is controlled by the F factor:

$$F = \frac{a_r L}{q}$$

where a_r is the flow-wetted surface area per unit volume of rock, L is the length of the transport pathway and q is the groundwater flux. Alternatively, the F factor can be expressed as the product of the advective travel time and the flow-wetted surface area per volume of water, $t_w a_w$, see e.g. /Andersson et al, 1998/. The latter formulation is used in the model FARF31, section 9.11.2, which is included in the calculation chain.

For a more detailed discussion of this subject, see Neretnieks /1980/, Olsson et al /1995/, Moreno et al /1995/, Elert /1997/, Andersson et al /1998/.

Transit times at Aberg

The model-calculated advective travel times can be used to estimate transit times for transport of aqueous solutes (or water molecules) from repository depth to the surface. Then matrix diffusion must also be taken into account, i.e. the fact that water molecules and solutes can diffuse into microfractures in the rock where the water is virtually stagnant. In actuality, a large portion of the rock's cavities are such microfractures, and water molecules and solutes will spend most of their transit time in these microscopic pores.

The transit time for non-sorbing solutes from repository depth to the surface can be estimated with the aid of the F factor by Neretnieks /1993/:

$$t_{transport} = t_w + F^2 D_e \varepsilon_p$$

where

D_e = $3 \cdot 10^{-6}$ m^2/y is the diffusivity for e.g. chloride ions at Aberg, and
ε_p = $5 \cdot 10^{-3}$ is the porosity in the rock matrix.

The F factor can be estimated either as $a_r L/q$ or as the product $a_w t_w$ according to the preceding section.

In section 9.8.3, the advective travel time t_w at Aberg is estimated to be 160 years with a reasonable flow porosity of 10^{-3} $m^3/(m^2 \cdot y)$. With $a_w = 10^3$ m^{-1} (reasonable value in the Data Report, compensated for the higher flow porosity), the F factor is 160,000 y/m.

With a_r = 1 m^{-1} (reasonable value according to the Data Report), L = 500 m and q = $2 \cdot 10^{-3}$ (reasonable value according to the Data Report), the F factor is 250,000 y/m.

These two estimates of the F factor give, with the above formula, transit times of 540 years and 1,100 years, respectively. This demonstrates that the model-calculated advective travel times at Aberg are compatible with observations of very old waters at repository depth.

The above formula presumes an unlimited penetration depth in the rock matrix, which is not necessarily valid. With a limited penetration depth, the transit times for solutes are shorter. On the other hand, the age of the observed water at repository depth at Aberg is given by the transit time down to repository depth. This means that the advective travel time for the inflow should be used for the calculation. Aberg is located in a discharge area, and the travel time from the surface to repository depth is much longer than that from repository depth to the surface. Only the latter is calculated in the local model. This reinforces the conclusion that the model-calculated travel times at Aberg are compatible with observations of very old waters at repository depth.

Data for calculations of radionuclide transport

The site-scale stochastic continuum models calculate advective travel times from different canister positions and through the geosphere for the site in question, see section 9.8. Reasonable travel times are chosen as the median in the base case of the stochastic continuum model's results, while the pessimistic time is chosen as the 95th percentile of the variant that has the shortest travel times. The difference between sites is considerable. The difference is essentially due to differences in interpreted hydraulic conductivity, see discussion in section 9.8.

The difference between reasonable estimate and pessimistic values for travel times reflects the spatial variation on the site. The travel time is dependent on the canister position. The calculated distribution of travel times can be used in probabilistic analysis. The difference between variants (for the same site) is relatively small, which means that the statistical distribution can be based on the base cases calculated for the different sites. The spread stems mainly from the spatial variation within a realization. This does not constitute an uncertainty in itself, but results in an uncertainty since it is not possible to predict which canister(s) will have initial defects. The location of canister positions with short travel times varies between different realizations, even though there are certain areas that always have short or longer travel times. No attempt has, however, been made to make use of the knowledge about travel time distribution by choosing only positions with long travel times.

The size of the flow-wetted surface area per volume of rock (a_r) is determined /Andersson et al, 1998/ from evaluations of a few site-specific tracer tests, geological characterization, hydraulic testing and modelling. For the most part, the value of the flow-wetted surface area is determined from assessments of the conductive fracture frequency, which are in turn based on the hydraulic tests. Pessimistic values of the flow-wetted surface area are chosen a factor of ten lower than the value that corresponds to the best estimate. The flow-wetted surface area per volume of rock (a_r) is converted to flow-wetted surface area per volume of water (a_w) by dividing it by the flow porosity (10^{-4}) used in the calculation of advective travel times (t_w). The F factor, the product $a_w t_w$, is thereby independent of the flow porosity. The flow porosity therefore has little influence on the transport calculations.

The calculation of the F factor using the method described here presumes in principle that the groundwater flux is evenly distributed within the elements in the continuum description. F factors calculated with the continuum model and with the discrete network

model are, however, relatively similar /Data Report/. It is therefore reasonable to use the assumed values of t_w and a_w, even though this comparison does not constitute formal proof.

Hydrodynamic dispersion along the transport pathways has only a secondary influence on retardation through the geosphere, compared with the large variation in F factors /Andersson et al, 1988/. Literature data for Peclet numbers fall within the range 2–40 /Elert et al, 1992/. Ten is chosen as a reasonable estimate and two as a pessimistic value, regardless of site. For rapid releases of long-lived nuclides, however, the retardation is less if low dispersion (high Peclet numbers) is assumed.

The chosen data are shown in Table 2-14 in Appendix 2. The groundwater flux is correlated with the travel time in the geosphere. High flux often means short travel time (low F factor).

9.9.8 Colloid transport in the geosphere

Sorbing radionuclides could in principle be transported more or less unretarded with the velocity of the water if they adhered to colloidal particles in the groundwater /Process Report/.

Observations in nature show that colloids are present in deep groundwaters in the form of mineral particles containing e.g. silicon, aluminium and iron. There are also measurements that suggest that mineral particles can be transported hundreds of metres as colloids /Hofmann, 1989/. Such particles can adsorb radionuclides, and colloids are found in nature with e.g. uranium and thorium /Miekeley et al, 1992/. Plutonium has been analyzed in contaminated groundwater from underground nuclear weapons tests on the nuclear weapons test site in Nevada in the United States, and colloids have been found there as well /Kersting, 1999/. The samples are taken 1.3 km from the centre of the blasts. Although these observations are the subject of heated debate, they support the view that colloids can transport radionuclides long distances in the rock.

The concentration of colloids at repository depth in Swedish bedrock is low /Laaksoharju et al, 1995/. This is because deep groundwater is highly mineralized, i.e. contains a great deal of dissolved salts.

If the uptake of radionuclides on colloidal particles is reversible, this can be handled by a reduction of the K_d value, where the reduction is inversely proportional to the concentration of colloids and the sorption tendency on the colloids. The reduction is, however, negligible at maximum colloid concentrations in Swedish rock /Allard et al, 1991/. Even if the nuclide adheres irreversibly, calculations summarized by Allard et al /1991/ show that the process can be neglected due to the low natural concentration of colloids.

Based on the above reasoning, SKB has not found reason to develop any special transport model for this mechanism.

9.9.9 Radionuclide transport in the gas phase

Radionuclide transport in the gas phase is handled by scoping calculations, see section 9.11.2.

9.10 Radionuclide turnover in the biosphere

Migration of radionuclides from the repository to man and nature in the vicinity of the repository is analyzed in the canister defect scenario. For this reason, a much more detailed analysis of biosphere conditions is required than for the base scenario.

Compared with the repository system (fuel, canister, buffer/backfill and geosphere), the biosphere is considerably more heterogeneous, complex and changeable. It is therefore difficult to carry out as strict and exhaustive a process description for the biosphere as for other parts of the system. Radionuclide turnover in the biosphere is, however, controlled by a limited set of processes that can be described in general terms.

The quantitative description is dependent on which ecosystem the processes take place in. To quantify radionuclide turnover for the safety assessment, the migration in a number of typical ecosystems is first calculated for uniform radionuclide releases to them, after which the dose to humans is estimated. The calculations give an ecosystem-specific dose conversion factor (EDF) for each ecosystem and nuclide. The EDF expresses the continuous dose load (Sv/y) to humans in the surroundings resulting from a continuous radionuclide release to the ecosystem (Bq/y) with a duration of 10,000 years. The unit for the EDF is thereby Sv/Bq.

For application in the safety assessment's calculations, the three repository sites are divided into smaller areas and each area is classified as one of the typical ecosystems. Site-specific and time-dependent releases of radionuclides to the biosphere can then be converted to estimated doses to man. This is carried out as the final step in the coupled calculation of radionuclide transport, section 9.10.

This section includes the following:

- a general description of the most important groups of processes that control radionuclide turnover in the biosphere,
- determination of EDFs for a number of typical ecosystems, and
- division of the three repository sites into typical ecosystems.

The biosphere section concludes with a discussion of the results achieved.

9.10.1 Processes in the near-surface ecosystems

When groundwater from great depth reaches quarternary deposits on top of the rock, the admixture of near-surface groundwaters increases. The transport velocities are often higher, since the deposits are relatively permeable. This means that the deep groundwater can be diluted and dispersed greatly in the near-surface groundwater. When the water reaches a watercourse, lake or sea, further dilution takes place by mixing with currents. Dilution and dispersal are dependent on precipitation, evapotranspiration and transport of water masses with watercourses or currents. Solutes such as radionuclides follow the deep groundwater's dilution and dispersal at the surface.

Chemical, physical and biological processes in the surface ecosystems can precipitate solutes or cause them to be absorbed in particles and organisms. The transition from anoxic (oxygen-free) to oxygenated conditions affects the properties of many solutes.

The high concentration of organic substances, e.g. humus, also causes many solutes to react with or be adsorbed to particles.

Organisms, especially plants and microbes, can actively absorb solutes and thereby retain and accumulate e.g. radionuclides. The finer fractions in the loose deposits, such as clays, can also sorb the solutes in the water in the same way as in the bentonite buffer in the deep repository. This causes retardation or even accumulation in the discharge areas.

Particle-bound substances have different transport properties, for example heavier particles can sediment in lakes and seas, resulting in a downward transport through the water. Particles can also be moved by powerful water currents, wind, ice movements or collapses. Organisms such as mussels and sponges can filter large quantities of water and thereby immobilize the particles in organic material.

All substances that have been immobilized in organisms via active uptake or sorption will be further transported in the biological food webs. The organism may be eaten by another organism, which thereby ingests the foreign substances. Some substances tend to be bound in organisms and can be enriched on every such passage, a phenomenon known as biomagnification.

All organisms actively seek out or exploit nutrient-rich areas. Plants steer their root growth to nutrient-rich areas, animals can locate or hunt suitable food. Bacteria can also move towards more nutrient-rich areas. All organisms react to plentiful nutrition by reproducing until they are limited by some resource. This means that biological processes can lead to increased concentrations of substances, unlike most physical and chemical processes which equalize differences in the concentration of substances.

Most organisms also influence the physical and chemical environment around them. Plants, bacteria and fungi secrete acids or organic complexing agents to liberate substances bound to e.g. mineral particles. This enables them to exploit limited nutrients efficiently. At the same time, other substances are affected, such as radionuclides, which can also be mobilized and absorbed in e.g. plants. Plants can transport substances to the surface via their root systems. Worms can also move solid material from deeper to shallower deposits. They also affect the chemical environment due to the fact that oxygen can more readily be transported in sediments and penetrated up by worms.

The scope of the biological processes is determined by the composition of the ecosystems, which in turn is influenced by climate (temperature, precipitation and insolation), availability of water and nutrients (nitrogen, phosphorus, iron, etc.) and oxygen conditions. The ecosystem composition is also greatly affected by natural disturbances (e.g. ice erosion, landslides and fires), but also by various human activities (e.g. agriculture and forestry) as well as by the interaction between different organisms (e.g. invasion by alien species).

In summary, there are two contradirectional forces at work in the surface ecosystems: On the one hand dilution and dispersal with the surface water, on the other hand accumulation and precipitation via chemical and biological processes. Both forces are important for radionuclide transport.

9.10.2 Calculation of ecosystem-specific dose conversion factors (EDFs)

The processes that were described in general terms in the preceding section will be of different quantitative importance for radionuclide migration in different ecosystems. In SR 97, radionuclide migration and dose load are modelled in a number of typical ecosystems according to Bergström et al /1999/:

- Coast and archipelago area.
- Lake.
- Running water, stream, river.
- Wetlands, peat bogs.
- Agricultural land.
- Well.

Forest has been assumed to be equivalent to peatland, which is judged to be pessimistic.

Two coupled models are used in the calculations. The first is a transport model for calculating the turnover of radionuclides in the typical ecosystem. The second is used to calculate how man is exposed to radiation from radionuclides, given the turnover.

Radionuclide migration in the compartments of the system

In the transport model, the ecosystem is divided into a number of compartments, e.g. water, soil and sediment. The radionuclides are assumed to be homogeneously distributed within a compartment. The flow of nuclides between the compartments is described with transfer coefficients that can be estimated with the aid of data from the site in question (such as water turnover) and the properties of the nuclides (e.g. sorption on different materials). The content of radionuclides in the different compartments is calculated as a function of time in the model.

In the calculation, the system receives a continuous input of 1 Bq/y of each radionuclide, and the course of events during 10,000 years is simulated. After that time the system has usually reached a steady state where the continuous inflow is balanced by radioactive decay, losses to sinks such as sediments or export over the system boundary with e.g. a water flow. The situation that has then been established with specific concentrations of radionuclides in the different compartments is the result of the calculation with the transport model.

Radiation dose to man

The specific concentrations are used to calculate the radiation dose to man. Both internal exposure from radionuclides that are inhaled or ingested in the form of contaminated food and external exposure via direct radiation from nuclides in the surroundings are calculated.

The concentration of radionuclides in foodstuffs (e.g. fish and potatoes) is calculated with distribution coefficients that describe the concentration in organisms in relation to the concentration in the compartments where they occur. The size of these factors is dependent on, among other things, the specific nuclides involved and the properties of the

organisms. For many nuclides there are data from field measurements or laboratory investigations that can be used to calculate the distribution coefficient, for others the coefficient is derived from comparisons with similar nuclides.

It is assumed in the model that humans live solely on foodstuffs produced locally. Their intake of contaminated foodstuffs is thus not diluted by other foods. Nor has any allowance been made for the loss of radionuclides in connection with cleaning or preparation of the food items, see further Bergström et al /1999/.

Performance of calculations

Both models are devised in the program ACTIVI, which is a subroutine in BIOPATH /Bergström et al, 1982/, which is also used in the actual calculation. The variation in the EDF, depending on uncertainties and variations in input data, is calculated in the program PRISM /Gardner et al, 1983/.

The EDF values are thus determined probabilistically and the results are statistical distributions. They can be utilized directly for probabilistic analyses and to estimate reasonable and pessimistic EDFs. The mean of the distribution is taken as the reasonable value, and the value that 99 percent of the realizations fall short of, the 99th percentile, is taken as the pessimistic value.

The models for the EDFs for the typical ecosystems (modules) lake, running water, coastal area (open coast and archipelago), agricultural land and peatland are described in Bergström et al /1999/. In addition, exposure from contaminated groundwater via wells is modelled. Turnover of radionuclides in forestland has not been modelled, since data are lacking for most nuclides except cesium. In SR 97, the EDF for peatland is used for forestland, which is judged to be pessimistic.

Following are general descriptions of the models of the most important typical ecosystems in the calculations of radionuclide transport in section 9.10, namely peat bog and well. The coastal area ecosystem is also described, since it is used in the scenario that handles climate change. The models of all typical ecosystems are described in detail in Bergström et al /1999/.

Peat bogs – wetlands

Many solutes, including most radionuclides, have a strong tendency to be absorbed by and accumulate in peat. The typical ecosystem for peatland deals with radionuclides that reach peat bogs and wetlands from outflows of groundwater. The distribution of radionuclides in the peat is assumed to be homogeneous. Important processes are adsorption of radionuclides to peat, the processes that occur in the soil when the peat is used as soil conditioner, and uptake in organisms. The total adsorption and concentrations in peat are determined by the peat quantity present in the area. The precipitation is the only site-specific information used in the calculations. The peat is used for cultivation or is burned in heating plants and private households.

Man is exposed via consumption of milk, meat, cereals, vegetables and root crops, and by inhaling radionuclides present in dust from the peat and in off-gases from peat combustion. Direct radiation from the peat is also taken into account. The greatest dose contributions for most nuclides come from cultivated crops. This is true, for example, of Ra-226, which can dominate the total long-term risk picture.

Peatland is the ecosystem that gives the highest EDFs for most radionuclides, which means that peat-rich areas are potentially the worst from this point of view. Peatlands occur widely and are formed naturally as a consequence of land uplift in marine areas or drying-up of lakes. There is therefore a high probability that discharge will take place to a wetland during some period. Exposure to radionuclides from peatland requires one additional measure, however, such as land drainage and peat cutting or cultivation. Peatlands can therefore function for long periods of time (thousands of years) as an effective barrier to radionuclides that reach the near-surface ecosystems. On the other hand, the doses will be higher if radionuclides are released for some reason.

Such long-term changes within an ecosystem are not taken into account in today's models, which are by nature equilibrium models that presume constant conditions. Refining the models to make them time-dependent could yield time-dependent EDFs which would be lower for long periods than the time-constant values used now.

Well

The well is assumed to contain groundwater contaminated with radionuclides from the deep repository. The well is described as a reservoir where the water turnover rate is assumed to be the mean capacity for existing wells on the site in question. All sorption is disregarded in the well itself. The water in the well is used as drinking water for humans and cattle and for irrigation of a small garden plot where vegetables are grown for consumption by the local residents. The amount of precipitation that is mixed with the irrigation water is site-specific. Important processes in irrigation are retention of nuclides in soil and on plants, transport in the soil of soil organisms and redistribution of absorbed radionuclides to the edible parts of the plants.

Humans are exposed by consumption of drinking water, cultivated vegetables and root crops, and by milk and meat from cattle that have drunk contaminated water. External exposure from the garden plot and inhalation of dust from the same are also taken into account.

Coastal area

The typical ecosystem for coast deals with the Swedish Baltic Sea coast. The module has two parts for handling both an archipelago and an open coast, with water exchange between the two. The inflow of radionuclides can occur in the archipelago or directly to the open coast. The water in the different parts is assumed to be homogeneously mixed. Important processes are water turnover, uptake in biota, and sedimentation and its opposite: resuspension. Water turnover is site-specific and is dependent on the volumes of the areas and their openness to the sea, as well as weather and water level variations. Uptake in biota is calculated with distribution coefficients, as for the lake and running water modules.

Exposure is assumed to occur via consumption of fish, aquatic plants (algae) and milk and meat from cattle that have drunk of the water and eaten contaminated aquatic plants.

The coastal area generally gives low EDFs, due to the large water exchange and a limited use of the water; it is not used as drinking water, for example. The effect of the water exchange is probably exaggerated, since a large portion of the radionuclides will probably be bound to particles, which have a longer retention time than water. If the groundwater with radionuclides passes through the sediments instead of, as in the current model, discharging directly into the recipient, a large portion will probably be bound in the

sediments by the processes that occur there (see above). This gives lower concentrations in the water, i.e. lower EDFs, for a long period. Since sediments that have accumulated radionuclides for a long time are exposed to wave surging due to land uplift, higher concentrations may be released during a brief timespan. This can lead to higher EDFs than the calculated values. The effect of this is currently being investigated in the safety assessment for SFR, the SAFE Project /Andersson et al, 1998a; 1998b/.

9.10.3 Data for calculations of radionuclide transport

The calculations of radionuclide transport in section 9.10 require EDFs for the different typical ecosystems, plus a classification of the land area above the repository into typical ecosystems.

EDFs

The results of the calculations of the ecosystem-specific dose conversion factors for well, agricultural land, peatland, coast, lake, river are shown in Figure 9-24. For comparison, the figure also contains dose conversion factors for direct intake of the different nuclides with food.

It can be seen that the EDFs for many of the typical ecosystems differ by a factor that is largely independent of the radionuclide. The shape of these curves is furthermore similar to that for direct intake. The reason for the similarities is that varying dilution is the factor that most differentiates the modules from each other, and this factor affects all nuclides equally. In the cases of peatland and agricultural land, accumulation takes place over a long period of time and the dilution is slower, which is why these ecosystems depart from the pattern.

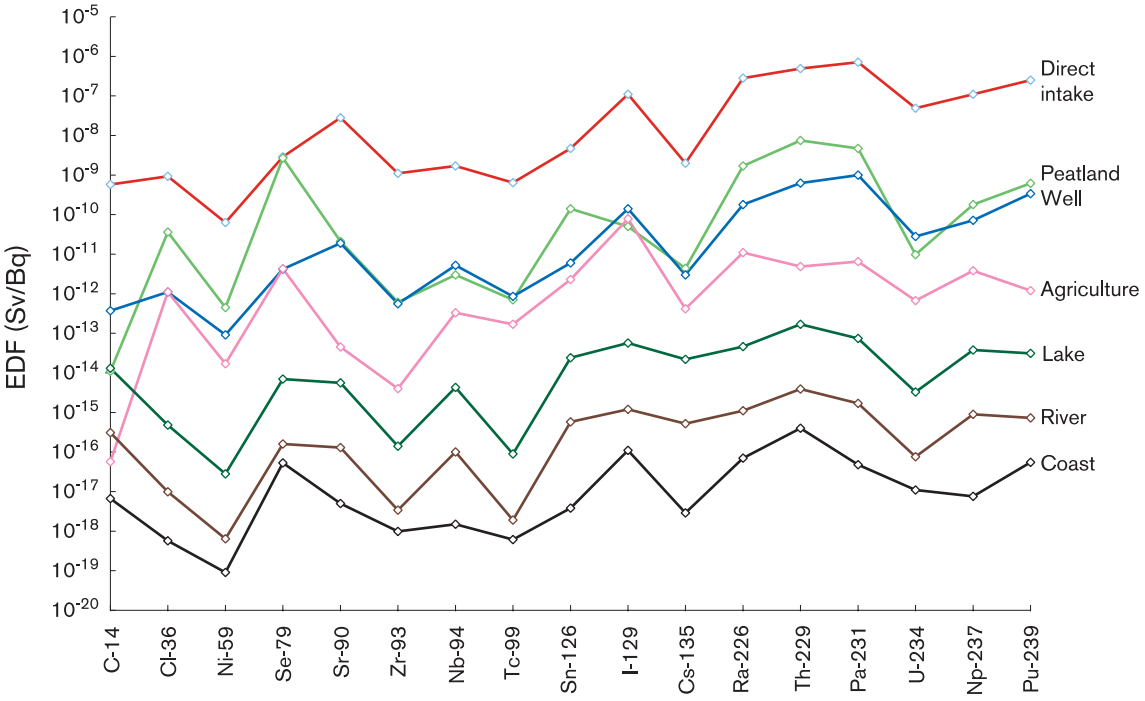

Figure 9-24. *EDFs for a selection of radionuclides in different typical ecosystems representative of Aberg, Beberg and Ceberg. Direct intake refers to the dose conversion factor for ingestion with food. For a complete list see Nordlinder et al /1991/.*

Description and classification of the sites' typical ecosystems

In order to use the EDFs, the different sites must be divided into different typical ecosystems. This classification is described for the three sites in Nordlinder et al /1999/. The land surface is divided into subareas (250 x 250 metres), and each subarea is associated with a typical ecosystem with the aid of available maps (green and yellow map). If several ecosystems are possible, the one expected to give the highest doses is chosen. If there is a well (registered in the well registry) in the area, the well module is chosen, since the well is expected to be the dominant transport pathway. The peatland module is pessimistically used for the forest, for which there is no model.

Aberg: The typical ecosystem for archipelago and open coast dominates today. Forestland and peatlands also comprise a large portion of the ecosystems. Small parts of the area are agricultural land, while lakes are lacking. There are three wells in the area today with a mean capacity of 300 litres per hour.

Land uplift is expected to change the situation, and in 2,000–5,000 years peatland will probably be the dominant ecosystem (see the base scenario).

Beberg: Forest is the dominant ecosystem, followed by wetlands and agricultural areas. There are also lakes and watercourses. In addition, there are four wells with a mean capacity of 1,000 litres per hour. Since forestland is pessimistically replaced by peatland in the modelling, the EDF for peatland will dominate.

Land uplift and drying-up of lakes are not expected to alter the present-day situation appreciably.

Ceberg: The site is drained by two major watercourses. Small areas of cultivated land occur along one of them. Peatlands and forests are the dominant ecosystems. As a result, the peat ecosystem dominates in the area. Watercourses and agricultural land also occur frequently. There are two wells with an average capacity of 500 litres per hour within the area.

Land uplift is not expected to affect the distribution of the dominant ecosystems at Ceberg.

9.10.4 Discussion

Which acceptance criterion?

In calculations of EDFs, it is assumed for the typical ecosystems peatland, agriculture and well that releases of radionuclides to the biosphere are dispersed within a local area of roughly the same size as the subareas that were used to subdivide the biosphere on the three sites (250 x 250 metres). It is assumed that residents produce all their food and get all their drinking water within this area.

For at least these three typical ecosystems, the calculations thus include the most exposed individuals within a large region. The acceptance criterion which the calculation results should be compared with when these EDFs are used is thus a risk of 10^{-5}, i.e. a risk for the most exposed individuals in a population. Expressed in dose, this risk is equivalent to $1.5 \cdot 10^{-4}$ Sv/y for an exposure that is certain to occur.

For the typical ecosystems coast, lake and running water, large populations may be exposed in some cases, which makes it more reasonable to compare with a risk of 10^{-6}, which is equivalent to a dose of $1.5 \cdot 10^{-5}$ Sv/y for an exposure that is certain to occur.

Uncertainties

The employed methodology of dividing the sites into subareas enables the uncertainties in the near-surface ecosystems to be separated into the question of which ecosystem will be the discharge area, and uncertainties in input data for the calculation models for each typical ecosystem.

The greatest uncertainties lie in the identification of which typical ecosystem will be relevant. An improved understanding of which ecosystems are reasonable to expect and how near-surface transport of radionuclides takes place ought to reduce the uncertainties considerably. An accurate description of the near-surface ecosystems in future site investigations may contribute towards reducing the uncertainties regarding calculated EDFs. However, the changeableness of the biosphere sets the ultimate limit on the accuracy of biosphere descriptions that will be used to estimate radionuclide turnover far into the future.

The calculation models for each typical ecosystem need to be revised. A model needs to be developed for forestland. Forestland probably has EDFs between those of agricultural land and peat bogs for most radionuclides. For this reason, classifying forest as peatland probably leads to an overestimation of potential doses.

The highest EDFs are obtained for the typical ecosystems peatland, well and agricultural land. In the well case, drinking water is the dominant exposure pathway for actinides. With regard to the more bioavailable chlorine, iodine and cesium isotopes, consumption of foodstuffs gives higher doses than consumption of water in the well case.

The probabilities of the different exposure pathways in the different ecosystems also need to be evaluated. Peatland, for example, requires several steps of human activity before high EDFs arise. Several steps of human activities are required before exposure takes place in the well case as well. Agricultural land, on the other hand, may represent a reasonable and natural course of events, as may discharge in surface water.

Taken together, this means that the consequences estimated in SR 97 probably overestimate the risks considerably. With site-specific input data, a better understanding of the dominant ecosystems and revised calculation models, most of the EDFs can probably be reduced.

Coming work

- The design of the entire biosphere model needs to be reviewed in the light of the regulations from SSI that recently entered into force.
- The current biosphere model needs to be augmented with a description of a forest ecosystem for future safety assessments.
- Methods for classification of a potential repository site into different typical ecosystems need to be refined for future site investigations.

9.11 Calculations of radionuclide transport

9.11.1 Introduction

Calculations of radionuclide transport constitute a large part of the safety assessment for a deep repository. The calculations are supposed to describe a large number of coupled processes in the repository, the surrounding rock and the biosphere. They require a large body of data, and the body of results is large and complex. Calculations of radionuclide transport for the canister defect scenario are reported in this section. The purpose of the calculations is, in brief, to:

- describe radionuclide transport quantitatively for this scenario,
- illustrate the importance of uncertainties in input data and show which data have the greatest influence on the calculation results,
- compare the risk caused by the repository at the three sites with given acceptance criteria,
- illustrate the importance of the individual barriers in the repository system.

First the calculation models are reported, together with the confidence that they fulfil their purpose. Reference is made to all data included in the analysis, after which a number of calculation cases are formulated with a view towards the above purposes. The calculation results are reported, along with some analytically calculated results. The section is concluded with a discussion of results.

The calculation results are reported up to a time period of one million years, in accordance with SKI's draft regulations. However, the results are judged differently for different time periods, in accordance with SSI's regulations and the discussion in section 2.2.1. All calculation cases are presented in greater detail in Lindgren and Lindström /1999/.

9.11.2 Description of the transport models

Radionuclide transport is calculated with the near-field model COMP23, the far-field transport model FARF31, and the dose model BIO42. Input data to the models come from various more or less complex model calculations or data analyses of different conditions or phenomena.

COMP23

The near-field model COMP23 is a so-called compartment model and is based on the NUCTRAN model /Romero, 1995; Romero et al, 1999/. COMP23 calculates how nuclides in a damaged canister are released from the fuel, how they may be precipitated due to solubility limitations, how the nuclides diffuse through the breach in the canister and on out through the buffer, and how they are transferred along different pathways to the flowing groundwater in the rock's fractures, see Figure 9-25.

The calculations require information on the radionuclide inventory which is changed by radioactive decay. Information on half-lives and decay chains is required to quantify this.

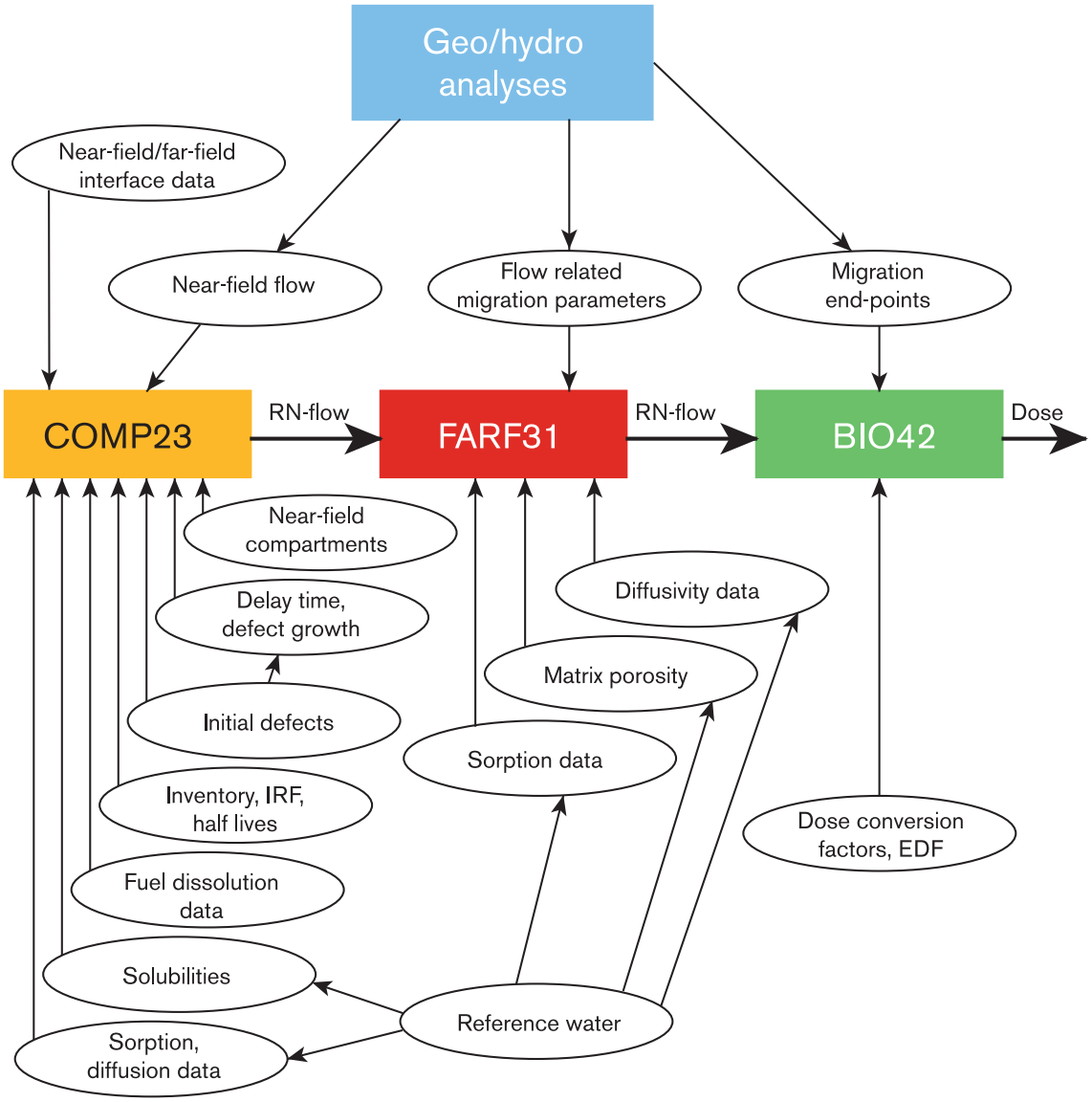

Figure 9-25. *Models (rectangles) and data (ellipses) used for radionuclide transport.*

In order for release and transport out of the canister to be possible, there must be a breach in the canister and there must be a continuous water pathway between the breach and the fuel. The size of the breach limits the release. After a breach has occurred, a delay time passes before the continuous water pathway has been formed. COMP23 thereby needs information on the size and growth of the breach, as well as on the delay time.

Most radionuclides in the spent fuel occur in solid form in and on the fuel. There are also radionuclides in metal parts and in the fuel cladding. If the fuel and metal parts are surrounded by water, nuclides can be released to the water. In COMP23, this release is handled by two mechanisms: instant release of a given fraction, IRF (instant release fraction), of the inventory specific for each nuclide, and release of the nuclides inside the uranium dioxide matrix at a constant rate R equivalent to the rate of dissolution/ conversion of the uranium dioxide matrix.

The concentration of a given radionuclide depends on the available void volume in the canister, how much has been released and how much has been transported out of the canister. COMP23 checks that the concentration of the radionuclides does not become greater than the solubility of the nuclide. It is pessimistically assumed that different isotopes of the same substance must each reach the solubility limit before they are precipitated.

Transport through the buffer is described with the processes diffusion, sorption and chain decay. No solubility limits are modelled in the buffer. COMP23 uses element-specific values for distribution factors (K_d), effective diffusivity (D_e) and porosity (ε).

Transport through the buffer out to the flowing groundwater in the geosphere can continue via four different pathways, Figure 9-26:

1. directly into a fracture intersecting the deposition hole opposite the breach in the canister,
2. into the excavation damaged zone (EDZ) assumed to surround the deposition tunnel,
3. via the tunnel's backfill and further into a fracture zone that is assumed to intersect the tunnel,
5. via diffusion through the rock into an assumed fracture zone in the rock.

To describe this transport, information is needed on the transport properties (sorption and diffusion) of the backfill and the rock, and on the mass transfer to the flowing groundwater in the rock. In COMP23, the mass transfer is described with equivalent flow rates (Q_{eq}) for the different transport pathways (see section 9.10.2). Q_{eq} is dependent

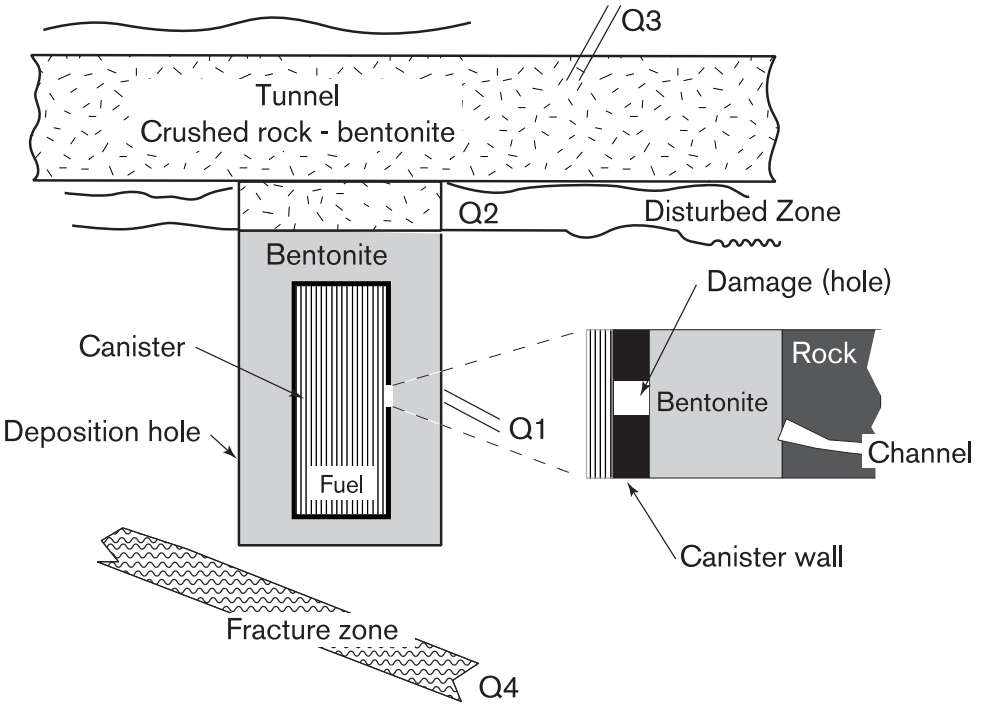

Figure 9-26. *Schematic illustration of the different transport pathways (Q1–Q4) dealt with in the near-field model COMP23.*

on the geometry (length, width and porosity) of the contact interface with the flow path and on the size of the groundwater flux, see Moreno and Gylling /1998/. Since the rock is heterogeneous, groundwater flow varies in space. The different canister positions will therefore have different values of Q_{eq}.

FARF31

The model FARF31 /Norman and Kjellbert, 1990/ is used to calculate transport of the released radionuclides through the rock. The model calculates radionuclide transport along the imagined flow path travelled by a fictitious particle following the groundwater flow through the rock. Since the rock is heterogeneous, groundwater flow varies in space. The different canister positions will therefore be coupled to different flow paths with different properties.

Geosphere transport describes how large a portion of the release (Bq/y) from COMP23 reaches the biosphere. The exit points of the different travel paths also determine where the release in the biosphere will take place.

FARF31 is one-dimensional, handles advection and dispersion along the flow path, matrix diffusion combined with sorption on the rock matrix, and radioactive chain decay. Dispersion is described with a constant dispersivity and expressed as a Peclet number. Retardation in the rock is dependent on the flow velocity in the fracture, which is described with the travel time t_w, and the F factor, which takes into account the exchange between nuclides in the water and in the rock matrix. The F factor can be expressed as the product of the advective travel time and the flow-wetted surface area per volume of water in the transport pathway ($t_w \cdot a_w$), but other descriptions are also possible, see section 9.9.7 and Andersson et al /1998/. In order to describe matrix diffusion and sorption in the rock's micropore structure, information is required on matrix diffusivity (D_e), matrix porosity (ε), maximum penetration depth and sorption values (K_d) for the different nuclides.

BIO42

The biosphere modelling is aimed at describing the turnover of any released radionuclides in the biosphere in order to make it possible to estimate the radiological consequences for potentially exposed humans and for the environment. The ultimate dose calculation is performed with the model BIO42, which calculates a dose by multiplying the release from the geosphere (Bq/y) calculated with FARF31 by an "ecosystem-specific dose conversion factor" (EDF) (Sv/Bq). The dose conversion factor is determined by which type of "biosphere module" the release takes place to. Type of module can either be specified directly or be determined as a function of where the release takes place.

The actual biosphere modelling takes place in connection with the determination of dose conversion factors for the different module types. The modules currently being used are well, lake, coast (sea), agricultural land and peat. Each site is first divided into typical modules for different ecosystems, and ecosystem-specific dose conversion factors are calculated for each typical module. This analysis lies outside of the actual BIO42 model, however.

9.11.3 Confidence in the models for groundwater flow and transport

Confidence that the models in the safety assessment with the data used correctly describe relevant physical processes is important for confidence in the results of the model calculations. The models for groundwater flow and radionuclide transport are used directly to quantify the repository's safety in release calculations, and here the question of confidence is particularly important.

The question of how the models used in the safety assessment can be validated has also been analyzed and discussed in different international contexts. In the INTRAVAL Project /NEA/SKI, 1996/ with participants from regulatory authorities and nuclear waste organizations from all over the world, nuclide transport models were compared with results from different tracer tests conducted in Sweden and other countries. No definite conclusions could be drawn, however, since it is not possible experimentally to completely simulate transport of sorbing radionuclides under natural groundwater flows. The models were not rejected, but the comparison does not conclusively prove that the models are accurate.

SKI has, together with the US Nuclear Regulatory Commission, published a White Paper entitled "Regulatory perspectives on model validation in high-level radioactive waste management programs" /NRC/SKI, 1999/. The regulatory authorities conclude that validation is not an absolute, but something that must be evaluated. Validation entails judging the completeness of the scientific data, trying to describe all processes that have a major influence on the results, and judging whether the models are sufficiently accurate for their intended use. A sitting working group within the OECD Nuclear Energy Agency /NEA, 1999/ finds that models are used for decisions. Confidence in the model must be in parity with the importance of the decision. Sufficient confidence does not mean that all relevant questions have to be answered and resolved. It is enough to show that unresolved questions do not have a crucial bearing on the decision in question, and that there are good prospects for solving the problems, if necessary, in connection with later decisions in the development of the deep repository.

The transport models cannot in detail predict exactly how much, when and where the migration of radionuclides from a damaged canister will occur. Nor are such exact predictions necessary. The purpose of the calculations is primarily to check that release and transport do not lead to consequences that exceed the limits set by the acceptance criteria. It is therefore important that the models do not underestimate the releases to the biosphere, whereas exact predictions regarding the location of the transport pathways or when release will occur are less important. Confidence in a model calculation is based on an assessment of whether all relevant processes are described, whether the mathematical processing is correct, and whether the model data are supported by results from different experiments and field investigations. Deficiencies in the detailed understanding of a process can be handled by choosing data and otherwise simplifying the description of the process so that the consequences (release and transport) are not underestimated.

Greater realism is striven for in the modelling of groundwater flow than in the subsequent modelling of radionuclide transport. The reason for this is that a model for groundwater flow that can explain observed conditions on the site provides greater confidence in the safety assessment as a whole. In order to inspire confidence, models of groundwater flow should therefore be able to explain observed conditions. The search for a modelling that with certainty does not underestimate the safety-related consequences nevertheless leads to a pessimistic handling of certain aspects of the groundwater modelling as well.

HYDRASTAR

Confidence that a model of groundwater flow describes the conditions on a site sufficiently accurately is dependent on:

- confidence in the mathematical handling of the flow equations,
- confidence in the method used to translate input data to a three-dimensions hydraulic description of the rock in the model,
- quality in the hydraulic input data to the model.

The two first points are classified as conceptual uncertainties, the last belongs to data uncertainties. The material for the discussion of confidence below is largely taken from the discussions of uncertainties surrounding the hydromodelling in section 9.8.8.

Conceptual uncertainties

In HYDRASTAR, groundwater flow is described by Darcy's law and hydraulic conductivity is described as a continuous, spatially correlated stochastic process. The former description is well-founded, while the latter can be discussed. On scales relevant for the groundwater modelling in the safety assessment, the permeability of crystalline fractured rock is non-continuous; certain volumes of the rock may, for example, be almost completely impervious.

The view that the rock is non-continuous has led to the formulation of discrete fracture network models, which agrees better with an intuitive picture of the properties of the rock. The AMP study (section 9.8.4) shows however that both views lead to very similar results for Aberg. This indicates that the effects of the conceptual uncertainty are limited. Modelling of field tests at Aberg /Walker et al, 1996/ indicates that HYDRASTAR can explain observed conditions on the site. This also suggests that HYDRASTAR's conceptualization is suitable for its purpose.

Density-drive flow is neglected in HYDRASTAR. A study for Beberg /Marsic and Hartley, 1999/ shows, however, that boundary conditions given as density-compensated head (environmental head) can recreate the effects of density-driven flow sufficiently well.

Another simplification in the HYDRASTAR simulations in SR 97 is that the time variation at the boundaries has been neglected. A study for Aberg /Svensson, 1999/ shows, however, that the effect of the simplification is small compared with other uncertainties in the modelling.

Data uncertainties; water-bearing structures

Uncertainties in data on the site's geological structures can also affect the assessment of confidence in the model. The existence, direction, size and properties of major water-bearing structures may be known with great certainty within certain well-investigated rock volumes, while there may be great uncertainty regarding the same structures, and others, in less well-investigated rock volumes. The feasibility of interpreting field data is also affected by the complexity of the geology. Spatial variability is usually great in both identified major fracture zones and the rock mass between the zones.

A considerable uncertainty also lies in the determination of the interconnected network of water-bearing structures. The connectivity between geologically interpreted structures and hydraulic structures is not clear-cut.

Uncertainties of this type are handled in SR 97 by analyzing different model variants with different assumptions regarding data and properties. Here as well, the overall result is that the variants are well-covered by the base case they are compared with and that confidence in the model in this respect can therefore be regarded as good.

Verification

In order to be able to have confidence in a model, it must also be verified, in other words it must have been proved to produce the right calculation results. HYDRASTAR has been verified in a number of studies, see e.g. Norman /1991/ and Morris and Cliffe /1994/.

Conclusion

Based on the above discussion, the judgement is made that confidence in HYDRASTAR for use in SR 97 is good.

COMP23

It has not been possible to test the whole near-field model COMP23 against experimental results. However, the model has been used to describe the propagation of a redox front at the natural analogue Poços de Caldas /Romero, 1995/. Confidence in the model must nevertheless essentially be based on confidence in how its different processes have been chosen, described and coupled together.

The numerical simplifications in COMP23 have been verified by comparison with a more general numerical model /Romero, 1995; Lindgren and Widén, 1998/.

COMP23 handles all the processes that have been identified in the process description. The process description is in turn based on many years of analysis by different researchers and organizations. It is not deemed likely that there are any completely new, unknown processes that influence the transport processes in the near field of the final repository, see discussion in section 5.8. The uncertainty thereby relates rather to how the transport processes are described and what data are used.

A large part of the confidence in COMP23 stems from confidence in the description of processes that determine the premises for transport. This has already been discussed in previous sections.

- The inventory varies, but can be determined with sufficiently good precision (see section 6.2.4).
- The description of fuel dissolution and data is based in part on experimental data, but some parts of the model have not yet been able to be fully supported experimentally (section 9.7)
- The description of dissolution/precipitation is based in part on experimental data and in part on analysis of uncertainties (section 9.7). The description of the chemical evolution in the canister (section 9.7) and in the buffer (section 8.9) could, however, be made more detailed. The description of the process in COMP23, where solubilities are only checked inside the canister and for each isotope separately, is pessimistically simplified.

- There are considerable uncertainties regarding the size and growth of the defect (see section 9.6) which are handled by studying different cases.
- Knowledge of and data for chain decay is good and fully adequate for the purpose of the modelling (see section 8.5).

The basis for describing confidence in the description of the transport processes in COMP23 is discussed in section 9.10.2.

- The great uncertainties that exist surrounding transport in the canister are handled by assuming thorough mixing in the canister. Diffusion through the defect, and the limitation of outward transport caused by a small defect, take place according to well-known mathematical relationships. The uncertainty pertains instead to the shape of the defect (see above).
- Experimental data show that the buffer is so impervious that advection can be neglected, making diffusion the dominant transport process through the buffer (section 8.7.3).
- Experiments on a laboratory scale show negligibly small concentrations of released colloids (see the Base Scenario, section 8.9.3, and the Process Report). Colloid release is therefore not modelled in COMP23.
- A large number of diffusion and sorption tests have been conducted in bentonite and similar clays, see the Process Report. Interpretation of these data can be complicated, and there are different theories concerning the details of the transport processes. However, the uncertainty can be handled by choice of data, see section 9.9.3.
- The mass transfer between buffer and rock is controlled by known processes (diffusion and advection). The uncertainties relate to the geometry and the groundwater flow. The uncertainties for these are relatively great, see section 9.8, but are handled with variant cases. The stylized geometry assumed in COMP23 could be made more realistic.

COMP23 with associated data is deemed to be sufficiently reliable for SR 97. The model and data can be improved and the uncertainties can probably be reduced. No such changes are expected to have any crucial effect on the results of the transport calculations, however.

FARF31

Transport models similar to FARF31 have been used to describe different trace tests. In Sweden, tests have for example been carried out in the Stripa Mine /Gnirk, 1993; Olsson and Gale, 1995/, in Finnsjön /Ahlbom et al, 1992/ and at the Äspö HRL /Gustafson and Ström, 1995; Elert, 1999/. Similar analyses have been performed internationally, for example within the framework of the INTRAVAL Project (see above). However, transport processes that have a great impact on the results of tracer tests, such as different dispersion phenomena, are of less importance for transport of long-duration releases of sorbing radionuclides, while the tracer tests are little affected by matrix diffusion and sorption, which are of great importance for nuclide transport. The comparisons cannot, however, be used as direct evidence for the suitability of the models for the needs of the safety assessment. Confidence in FARF31 must therefore be based to a large extent on confidence in the manner in which its various component processes have been chosen, described and coupled together.

Like COMP23, FARF31 handles all the relevant processes that have been identified in the process description. Nor is there reason in the case of FARF31 to expect that there should be any completely new, unknown processes that influence the transport processes in the geosphere. The uncertainty is therefore concerned more with how the transport processes are described, and what data are used.

The basis for describing confidence in the description of the transport processes in FARF31 is discussed in section 9.10.2.

- Measured colloid concentrations in granitic groundwater justify neglecting colloid transport.
- Since sorption is a collective term for several processes, it can be asserted that the conceptual understanding varies. There is a wealth of experimental data from laboratory tests, but the process is much more difficult to determine in the field. Given all uncertainties, K_d values are chosen in safety assessments so that retention capacity is not overestimated.
- There are certain uncertainties surrounding the actual process of diffusion in the rock matrix, but these uncertainties are handled by choosing data pessimistically. The porosity of the rock matrix is a bigger source of doubt. It has been demonstrated in many laboratory tests, but is more difficult to determine directly in the field. Further theoretical and experimental studies of the importance of varying matrix porosity may be warranted.
- Advection and transfer between flowing groundwater and the rock matrix are burdened with relatively great uncertainties. For one thing, the groundwater flow itself is heterogeneous and uncertain (see section 9.8), and for another there are uncertainties surrounding the geometry of the contact interface between flow path and rock. The geometric description in FARF31 ("flow-wetted surface area") and migration along flow paths without mixing is geometrically simplified. The uncertainty in flow is handled by studying different models and different variants (see section 9.8), while the uncertainty in the rest of the geometry is handled by pessimistic choices of data.

FARF31 with associated data is deemed to be sufficiently reliable for SR 97. The model and data can be improved, and the uncertainties will probably be reduced. There is a potential for improvements, especially regarding the handling of the groundwater flow and its geometric distribution in the rock, that could lead to less pessimistic estimates of the geosphere's retarding capacity.

Biosphere models

Uncertainties in the biosphere modelling are discussed in section 9.9 and in Bergström et al /1999/.

Compared with the repository system, the biosphere is much more complex and changeable, and the biosphere models contain considerable simplifications of the mechanisms for turnover in the ecosystems.

For many radionuclides, empirical data that can be used in the calculation of transfer factors are available from accidents or nuclear bomb tests in which the transfer of radionuclides has been measured. However, these data are the result of the combined effect of different processes that affect radionuclide transport, and it is difficult to distinguish the importance of individual processes. This is particularly true when data

come from situations involving episodic atmospheric deposition or release in surface water, while the source of radionuclides from a deep repository will be groundwater during long periods of time. The transfer factors therefore need to be broken down into general mechanisms (e.g. food uptake) and exposure-specific mechanisms (e.g. water-soil transfer) in order to be able to be used in other exposure situations.

Numerical results in international validation studies have been within a few orders of magnitude of measured values and have usually overestimated them (BIOMOVS, 1993; BIOMOVS II, 1996; VAMP, 1996/. In general, the model concepts and tools used by SKB have yielded good results in these international comparisons.

In the calculation of the EDFs for the safety assessment, pessimistic assumptions are made regarding the migration of radionuclides in the biosphere and people's habits and food intake.

Confidence is therefore good that the calculated EDFs do not underestimate doses to humans, despite the fact that the mechanisms in some ecosystems are inadequately described.

9.11.4 Reference to data used to analyze radionuclide transport

In order to determine suitable input data to the transport models, information is needed from many disciplines. Data have been chosen after compilation and analysis of a large number of background studies, see the Data Report.

Appendix 2 reports all input data to the transport models that have been used in the canister defect scenario. Table 9-3 shows an overview of the available data with reference to the text section where the choice of data is discussed. Input data to the models given as reasonable values and usually also as defensible pessimistic estimates. In some cases, calculated statistical distributions are also given for input data, but as a rule the uncertainty is not defined with greater precision than as a range between best estimate and pessimistic values. Some data are dependent on the chemical (speciation) and/or radioactive properties of the radioactive substance and are therefore element- or nuclide-specific. Some data are dependent on site-specific conditions and are therefore different for Aberg, Beberg and Ceberg.

In the choice of data it is also necessary to take into account whether different parameters are or may be correlated. Hydrogeochemical conditions and groundwater flow in particular determine the values of one or more of the groups of input data that are used directly in the models, see Table 9-3. By taking correlations into account, unreasonable combinations of parameter values can also be avoided.

9.11.5 Choice of calculation cases

According to section 9.11.1, the purpose of the radionuclide calculations is to:

- describe radionuclide transport quantitatively for this scenario,
- illustrate the importance of uncertainties in input data and show which data have the greatest influence on the calculations results,

- compare the risk caused by the repository at the three sites with given acceptance criteria,
- illustrate the importance of the individual barriers in the repository system.

Based on this, a number of calculation cases are formulated.

Reasonable cases

A point of departure for quantifying the performance of a deep repository on the three sites is a case where reasonable values are chosen for all pertinent data. As has been seen, these data are often cautiously chosen, and the consequences are therefore probably overestimated even in the "reasonable" cases.

Table 9-3. Available data for the transport models. (R = Reasonable data, P = Pessimistic data, D = Calculated distribution, E = Element/nuclide-specific data, S = Site-specific data).

Parameter	R	P	D	E	S	Correlation with other data	Section
Near field							
Inventory	X			X			6.2.4
IRF	X	X		X			9.7.7
Fuel dissolution rate	X						9.7.7
No. of defects	X	X					9.2.2
Defect size	X						9.2.2
Defect growth	X	X				Delay time	9.6.7
Delay time	X	X				Defect growth	9.6.7
Solubilities	X	X		X	X	Groundwater composition	9.7.6
Sorption in bentonite	X	X		X	X	Groundwater composition	9.9.3
Diffusivity in bentonite	X			X	X	Groundwater composition	9.9.3
Porosity in bentonite	X			X	X	Groundwater composition	9.9.3
Backfill	X			X	X	Groundwater composition	9.9.3
Specific groundwater flux at repository depth	X	X	X		X	Determined by groundwater model (certain correlation with travel time)	9.8 and 9.9.7
Q_{eq}-related parameters (q_i, e_i)	X	X				q_i are multiples of q_0	9.9.4
Geosphere							
Matrix porosity	X			X	X	Groundwater composition	9.9.5
Matrix diffusivity	X	X		X	X	Groundwater composition	9.9.5
Sorption	X	X		X	X	Groundwater composition	9.9.6
Advective travel time, t_w	X	X	X		X	Determined by groundwater model (certain correlation with groundwater flux)	9.8 and 9.9.7
Flow-wetted surface area per volume of water, a_w	X	X			X	Product $a_w t_w$ not dependent on flow porosity	9.9.7
Maximum penetration depth	X	X			X		9.9.5
Peclet number	X	X					9.9.7
Biosphere							
Choice of module	X	X			X	Exit points determined by groundwater model	9.10.3
EDF for chosen module	X	X		X	X		9.10.3

Uncertainty analyses

Since all data are burdened with uncertainties, the reasonable calculation case must be supplemented with cases that illustrate the importance of the uncertainties.

For this reason, calculations are also made of cases where groups of parameters related to:

1) canister defects,
2) the fuel,
3) the buffer and backfill material,
4) fracture and flow conditions around the deposition holes,
5) chemical conditions in the geosphere,
6) fracture and flow conditions in the geosphere,
7) the biosphere,

are chosen pessimistically, while all other data are assigned reasonable values.

Risk calculations

The acceptance criterion for the repository is a risk measure, i.e. not only consequences, but also probabilities of various consequences must be estimated. Simple probabilistic calculations are therefore also carried out for the three repository sites.

Special cases

In addition, a number of special calculations cases are reported, formulated to illustrate extreme assumptions such as that the fuel dissolves immediately, that the canister is omitted, etc.

9.11.6 What happens in the transport models?

The transport models are devised to ensure that the calculated releases will not be underestimated. The models therefore provide a simplified and pessimistic picture of the evolution. Here follows a brief description of the processes that are quantified in the transport models, as an introduction to the presentation of the results of the calculation cases.

1. No releases occur from the canister before a continuous water pathway has been formed between the fuel and the breach in the copper shell. Radioactive decay reduces the radionuclide content and total radiotoxicity of the fuel.

2. As soon as a continuous water pathway has formed, the instant release fraction of the inventory dissolves in the water in the canister void. If the solubility limit is reached, the concentration of the dissolved nuclide in the water does not increase further. The nuclides dissolved in the water begin to diffuse out of the canister.

   The release rate of nuclides embedded in the fuel is determined by the rate of fuel dissolution. Here as well, the solubilities of the nuclides limit the concentration that can occur in the water.

3. The nuclides are sorbed with varying effectiveness in the buffer and the diffusion and sorption properties determine the time for diffusion through the buffer. If this time is shorter than or comparable to the half-life of the nuclide, it passes out into the rock.

4. In the rock, the nuclide's sorption properties, together with the rock's transport properties (the flow and the fracture structure), determine the time for transport through the rock to the biosphere. Just as in the buffer, the half-life of the nuclide determines whether it passes through the geosphere before decaying.

5. In the biosphere, the nuclide gives rise to a dose that is dependent on its inherent radiotoxicity and its turnover in the biosphere type to which it is released. Both of these factors are included in the EDF.

In general, nuclides with a relatively high instant release fraction also tend to be readily soluble and relatively mobile in both buffer and rock. Several percent of the inventory of I-129, for example, is instantly released; iodine has very high solubility and is not sorbed in either buffer or rock. Plutonium isotopes, on the other hand, lie completely embedded in the fuel matrix, have low solubility and are sorbed strongly in both buffer and rock. Isotopes of uranium, thorium and americium have similar properties to plutonium. Furthermore, as a simplified, general rule the mobile nuclides are less radiotoxic.

Figure 9-27 illustrates schematically the fact that long-term radiotoxicity is dominated by those nuclides that have both low solubility and low mobility in buffer and rock.

The above description provides a general picture of the sequence of events and consequences. The quantitative details are determined by the input data chosen in a calculation case. The following account of different calculation cases is focused on the nuclides that make the greatest contribution to the releases. Many of the most toxic nuclides – such as isotopes of americium, plutonium and thorium – are not seen in the results, since the retarding capacity of the repository is very good for these nuclides.

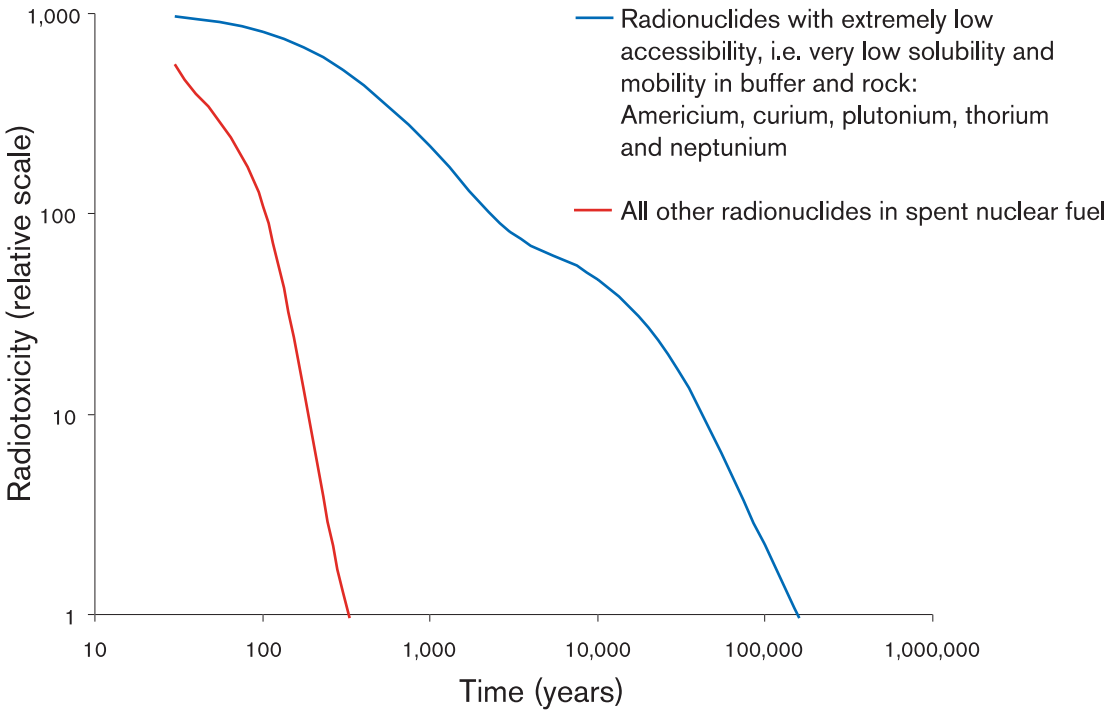

Figure 9-27. *Radiotoxicity of spent nuclear fuel broken down into nuclides with extremely low accessibility and other nuclides /Hedin, 1997/.*

9.11.7 Reasonable cases for Aberg, Beberg and Ceberg

All calculations cases are reported in greater detail in Lindgren and Lindström /1999/. Figure 9-28 shows the results of the calculations for Aberg, where all data have been chosen as reasonable. The calculation thereby applies to **one** canister, with an initial defect that has grown after 200,000 years so that a continuous water pathway has been formed to the fuel. Fuel dissolution and radionuclide transport thereby also start after 200,000 years. Many radionuclides have decayed completely by this time. Only very long-lived nuclides, and above all those that have an instant release fraction, are released. The damaged canister is emplaced in a deposition hole with median values for groundwater fluxes and advective travel times.

The biosphere is a peat bog with reasonable EDFs. With today's flow situation at Aberg, most releases are expected to occur to the Baltic Sea. The ongoing shoreline displacement means that the releases from a few thousand years in the future can be expected to occur to land areas. The peat bog is the "land module" that is calculated to give the highest doses, at the same time as it cannot be regarded as improbable. It has therefore been chosen as the reasonable case in the long term for Aberg.

The releases from the near field are dominated by nickel-59, a radionuclide with a half-life of 75,000 years located in the fuel's structural parts. These are assumed to be completely dissolved by corrosion, rendering the entire inventory of Ni-59 accessible for transport.

The fraction of readily mobile fission products I-129 and Cs-135 present on the surface of the fuel pellets is released instantly from the fuel and diffuses relatively rapidly through the buffer.

Further in the future, the releases from the near field will be dominated by radium-226, a naturally occurring radionuclide that is formed by chain decay of uranium-238 in the fuel matrix.

Of the four possible release pathways to the rock (Figure 9-26), the dominant ones are Q1, i.e. rock fractures that are assumed to exist immediately opposite the defect in the canister, and Q2, the fractured zone around the periphery of the tunnel created by tunnel blasting.

The releases from the geosphere are also dominated by Ni-59 at Aberg. The maximum release from the geosphere is around $1/30^{th}$ of that from the near field. In the case of I-129 and Cl-36, which also contribute to the geosphere release, the entire release from the near field passes through, even in the reasonable case. Ra-226, with a half-life of 1,600 years, decays almost completely in the geosphere in the reasonable case.

The curves that show biosphere dose for the different nuclides have the same shape as the release curves from the geosphere. The relative importance of different nuclides is, on the other hand, different in the biosphere curves, which are obtained by multiplying the geosphere curves by the nuclide-specific EDFs. The biosphere dose at Aberg is dominated by I-129 and Se-79.

The doses for all times are far below doses from natural background radiation in Sweden.

The biosphere figures also show a dose limit of 0.15 mSv/y. This is the dose that is equivalent to a risk of 10^{-5}/y for certain exposure. 10^{-5}/y is the risk limit from SSI which SKB has interpreted as the relevant one to use for the well and peat modules in SR 97, see section 9.10.4.

The equivalent cases for Beberg, Figure 9-29, and Ceberg, Figure 9-30, are very similar, especially for the near-field releases. The geosphere's retention properties for e.g. Ni-59

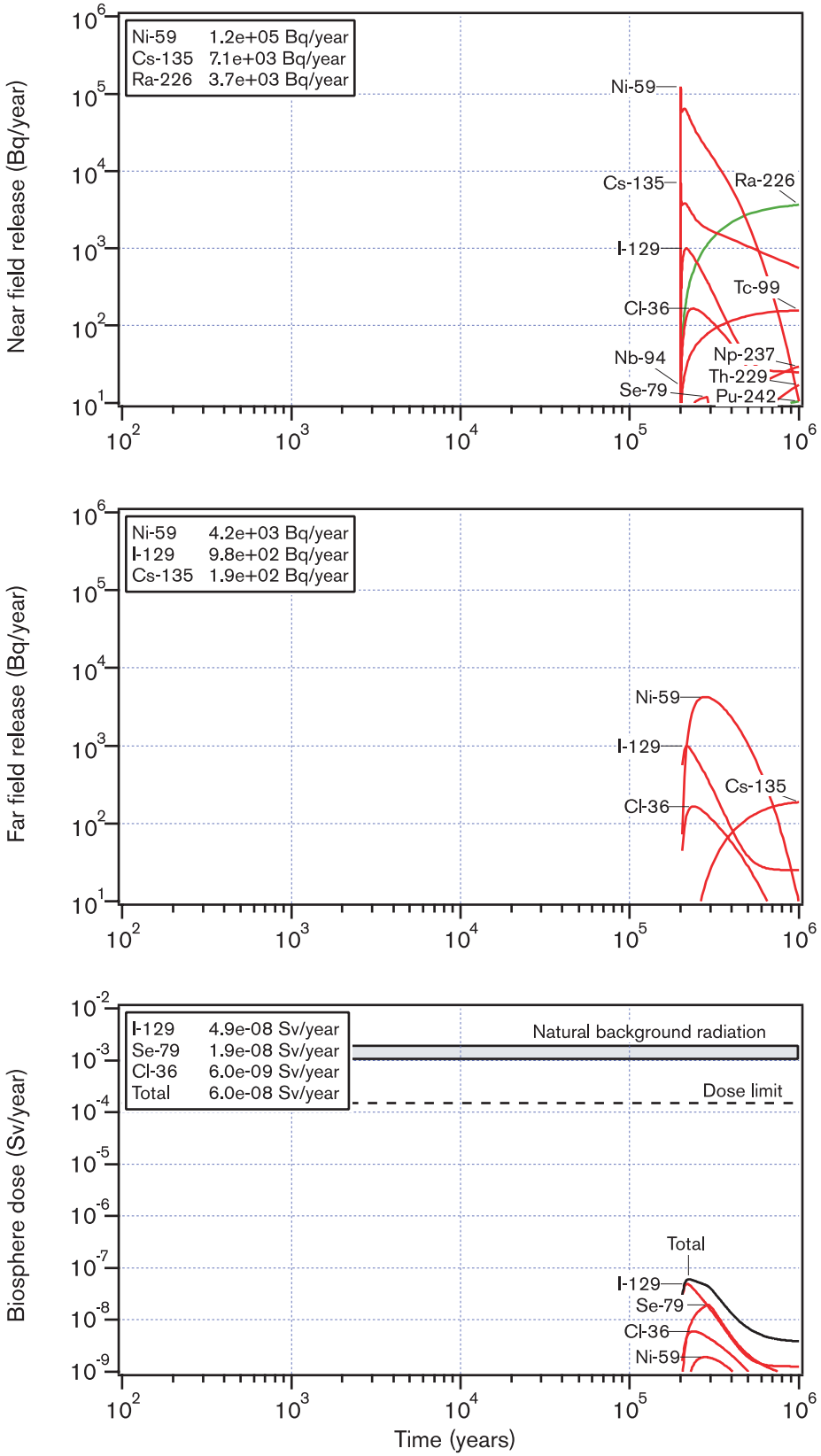

Figure 9-28. *Releases from near field and far field and doses in the biosphere as a function of time in Aberg. All data chosen as reasonable. The inset boxes show maximum releases and doses for dominant nuclides.*

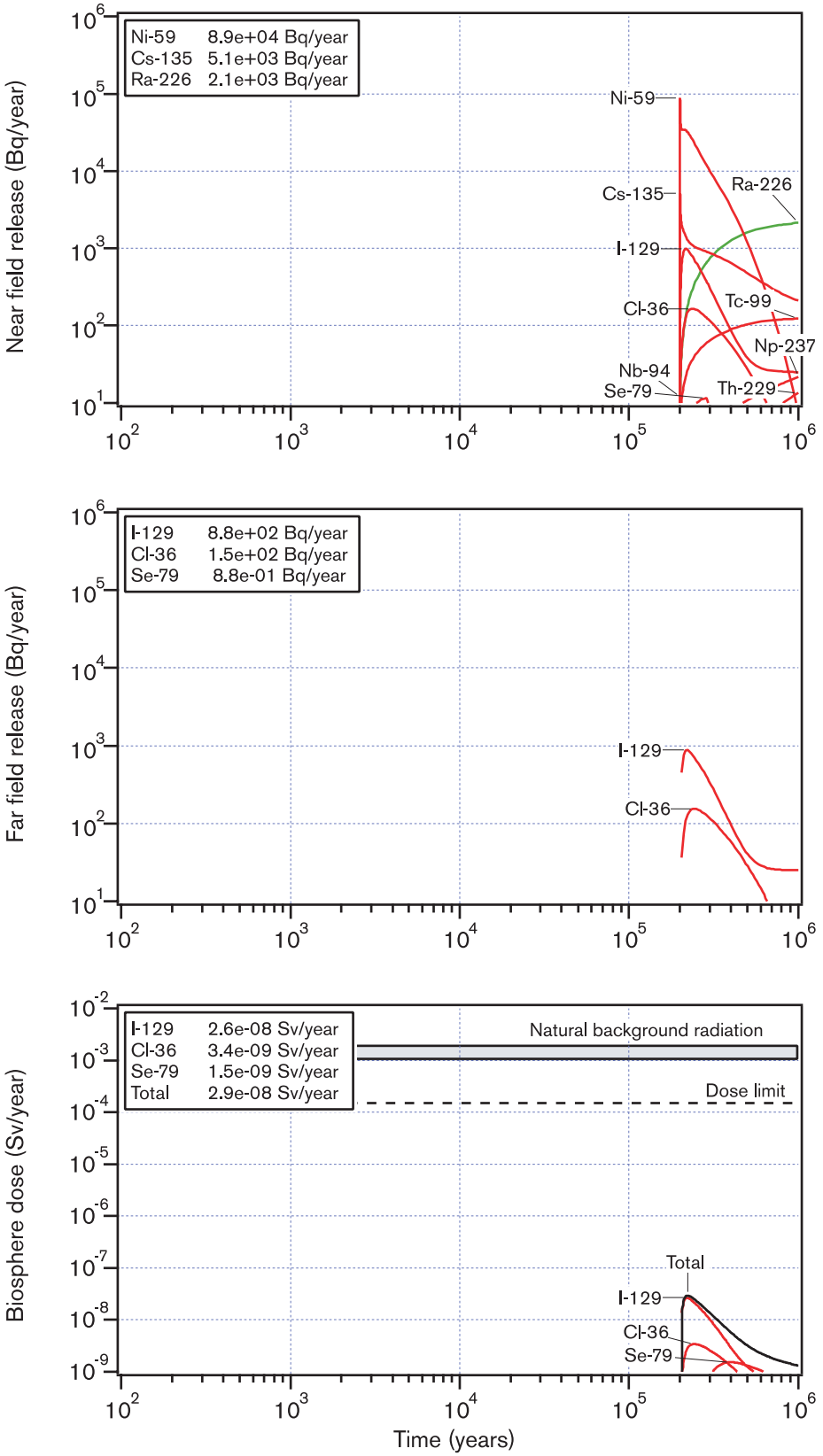

Figure 9-29. *Reasonable case for Beberg.*

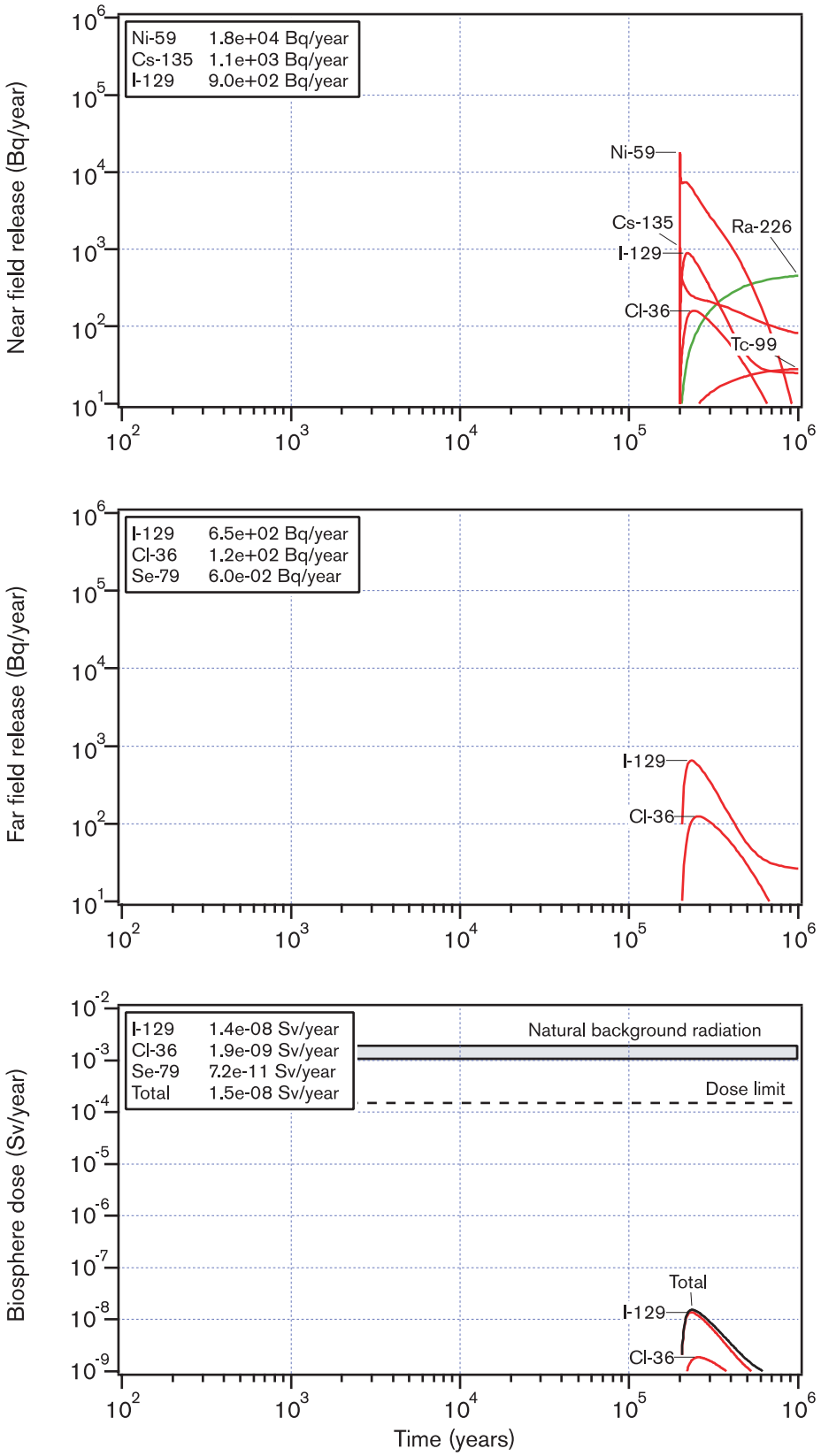

Figure 9-30. *Reasonable case for Ceberg.*

and Cs-135 are better in Beberg and Ceberg. Here the geosphere releases are dominated by the readily mobile nuclides I-129 and Cl-36, where, as in Aberg, almost the entire near-zone releases passes through the geosphere.

The dose curves (peat bog in Beberg and Ceberg as well) are similar on all sites, since I-129 dominates.

9.11.8 Uncertainty analysis

All input data to the radionuclide transport calculations are burdened with uncertainties. As described earlier, uncertainties have been quantified by determining not only reasonable values, but also pessimistic values for nearly all input data. To analyze the influence of data uncertainties on the calculation results, cases are calculated where data related to different parts of the repository are systematically given pessimistic values.

The work of determining reasonable and pessimistic data is very extensive and is described thoroughly in the Data Report. Parts of the work are summarized in previous sections under the headings "Data for calculations of radionuclide transport" and in Appendix 1. In those cases where statistical distributions are available as a basis for choice of data, pessimistic data have been chosen as the 95th percentile, i.e. the value for which 95 percent of the cases in the underlying calculations gave a more favourable result.

The effects of using different combinations of reasonable and pessimistic data are shown in the following, without repeating the reasons for the choices of data. Only doses in the biosphere (peat ecosystem) are presented for these cases. First follows a detailed analysis for Aberg, supplemented by a couple of important cases for the other sites, followed by a summary for all the sites. As a point of departure for the discussion, biosphere doses for thoroughly reasonable data at Aberg are once again shown in Figure 9-31.

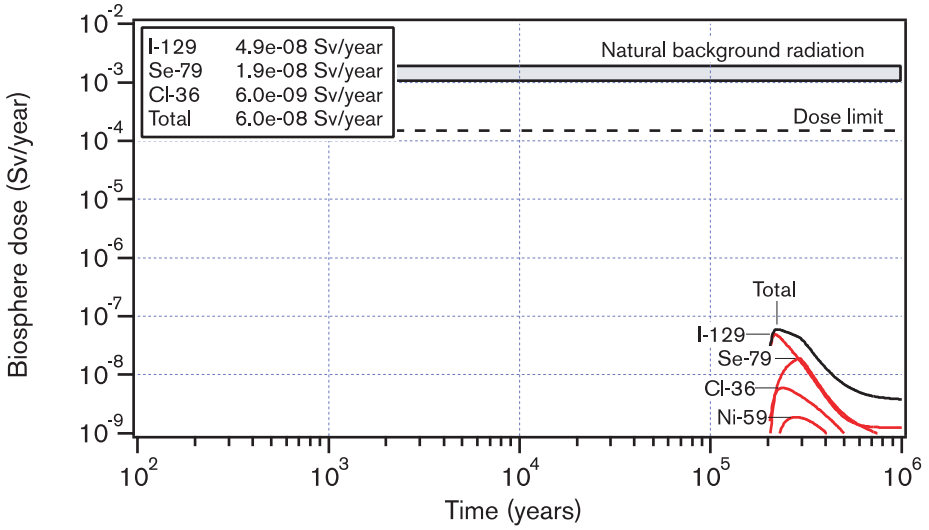

Figure 9-31. *Doses in the biosphere as a function of time in Aberg. All data chosen as reasonable. The inset boxes show maximum releases and doses for dominant nuclides. The dose limit of 0.15 mSv/y corresponds to a risk of 10^{-5}/y, interpreted as applicable to the most exposed individuals whose exposure is simulated in the biosphere models for peat.*

Canister-related data

Figure 9-32 shows doses in the biosphere as a function of time with pessimistic data for canister damages and otherwise reasonable data at Aberg.

In this case, five canisters are pessimistically assumed to be initially damaged, compared with one in the reasonable case. The initial canister defect gives rise to a continuous water pathway to the fuel after only 300 years, and the defect is assumed to have grown so that the copper canister offers very limited transport resistance after 20,000 years. In the reasonable case, a continuous water pathway is not formed until after 200,000 years, by which time the defect is also assumed to have grown so that canister resistance is little.

During the interval from 300 to 20,000 years, the defect is small (1 mm^2) and greatly limits the releases.

In the case with pessimistic data for canister damages as well, the doses in the biosphere are dominated by long-lived, non-sorbing nuclides, and the doses lie far below the limit values. The increase in maximum dose compared with the reasonable case comes almost entirely from the fact that the number of damaged canisters has increased from one to five. The long-lived nuclides do not decay appreciably between 20,000 and 200,000 years, so it is of little importance for the maximum dose when the larger defect arises.

An extreme and unrealistic case where the canister has a large hole initially is described in section 9.11.10.

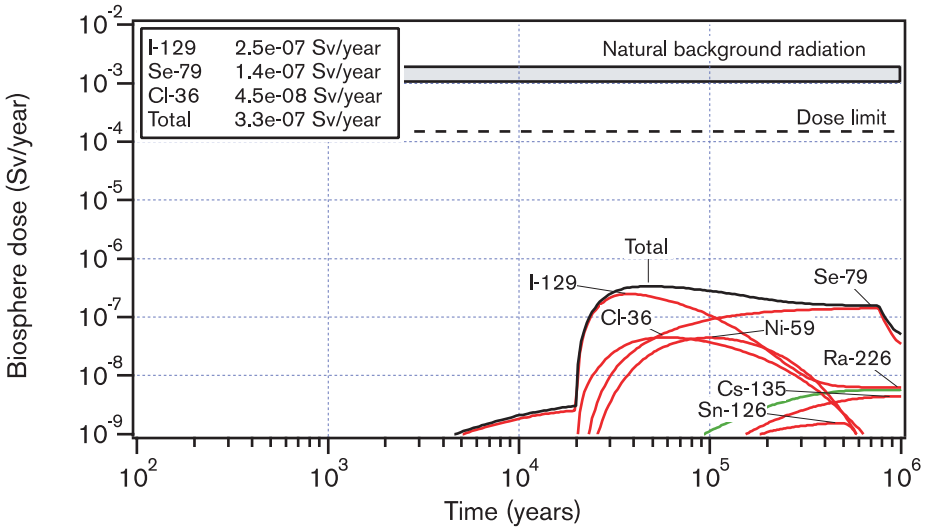

Figure 9-32. *Pessimistic data for number of damaged canisters, delay time and defect growth for Aberg.*

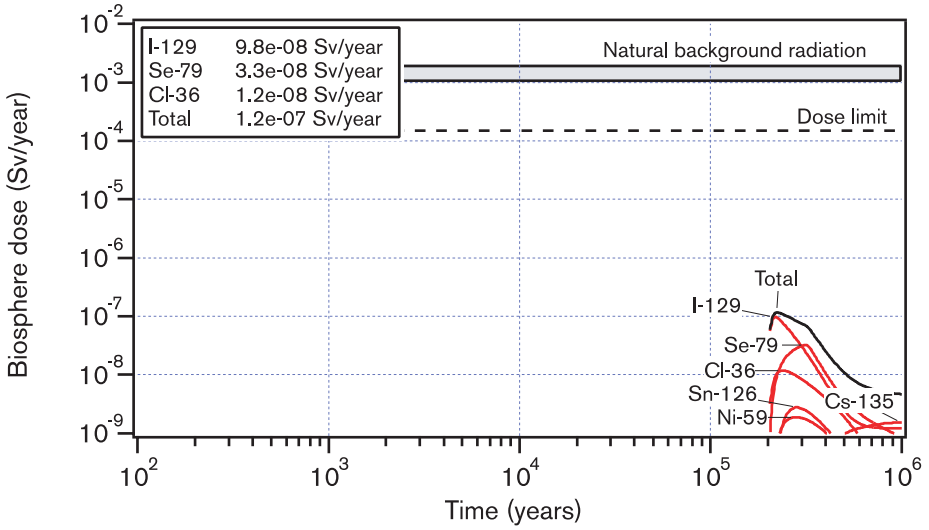

Figure 9-33. *Pessimistic data for instant release fraction and solubilities for Aberg.*

Fuel-related data

The effects of assuming pessimistic solubilities and values for the instant release fraction (IRF) are shown in Figure 9-33.

The difference compared with the thoroughly reasonable case is very small. The higher values for the instant release fractions of I-129 and Cl-36, both twice as high as for the reasonable case, influence the results in the figure.

The changes in solubilities between reasonable and pessimistic values do not influence the results other than for Se-79. Most poorly soluble nuclides – such as isotopes of plutonium, americium and thorium – lie embedded in the fuel matrix. Whether or not the solubility limit is reached for such nuclides is determined by the fuel dissolution rate and the nuclide-specific solubilities and inventories. The fuel dissolution rate is too low for the solubility limits to be reached in the reasonable case for most nuclides. A change to pessimistic solubilities therefore does not affect the results. The releases from the near field of actinides such as uranium, plutonium and thorium increase, but are still very small.

Two extreme and unrealistic variations with instant fuel dissolution and infinite solubilities, respectively, are presented in 9.11.10.

Sorption data in buffer and backfill

The effect of pessimistically chosen sorption data for buffer and backfill is illustrated in Figure 9-34.

Nuclides that are not sorbed in the buffer, such as I-129 and Cl-36, are not affected. The releases of sorbing nuclides – such as Ni-59, Sn-126 and Ra-226 – increase, but I-129 still dominates the total dose. The changes in sorption in the backfill have a negligible impact on the results.

An extreme and unrealistic case where the buffer's diffusion resistance has been neglected is shown in section 9.11.10.

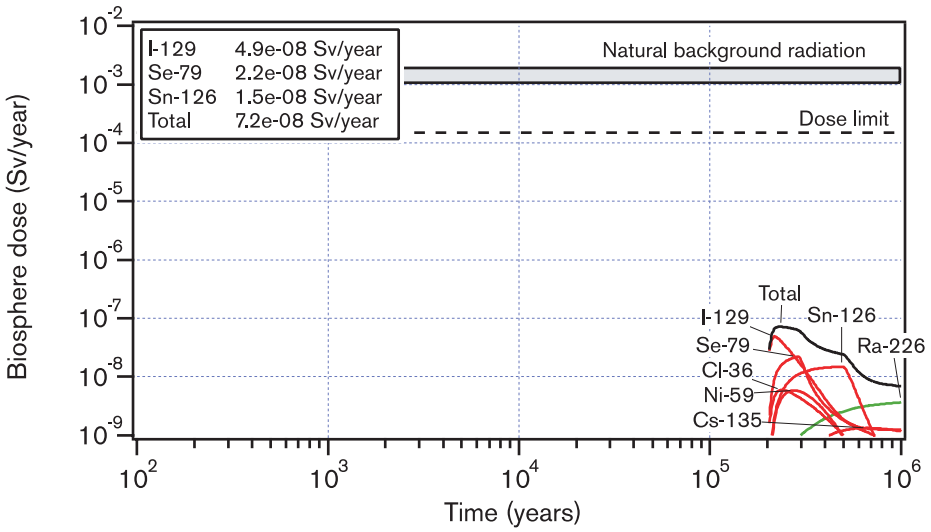

Figure 9-34. *Pessimistic sorption data in buffer and backfill for Aberg.*

Data related to the boundary layer between buffer and rock

The transport of radionuclides across the boundary layer between buffer and rock is determined by the groundwater flux and the properties of the fractures/fracture zones that are in contact with buffer/backfill, see section 9.9.4. Figure 9-35 shows the effect of using pessimistic values for these data. Instead of the median value of the flux, $2 \cdot 10^{-3} m^3/(m^2 \cdot y)$, from the base case in the hydromodelling, the 95th percentile, i.e. $10^{-1} m^3/(m^2 \cdot y)$, is chosen pessimistically.

The flux and the properties of the fractures in the near field together determine what capacity the rock has to transport nuclides away from buffer and backfill.

If this capacity, expressed as a nuclide-specific transport resistance, is great, the size of the canister defect or the buffer's transport resistance will control the total transport through the near field. If the boundary layer's transport resistance is great, this can constitute the limiting factor.

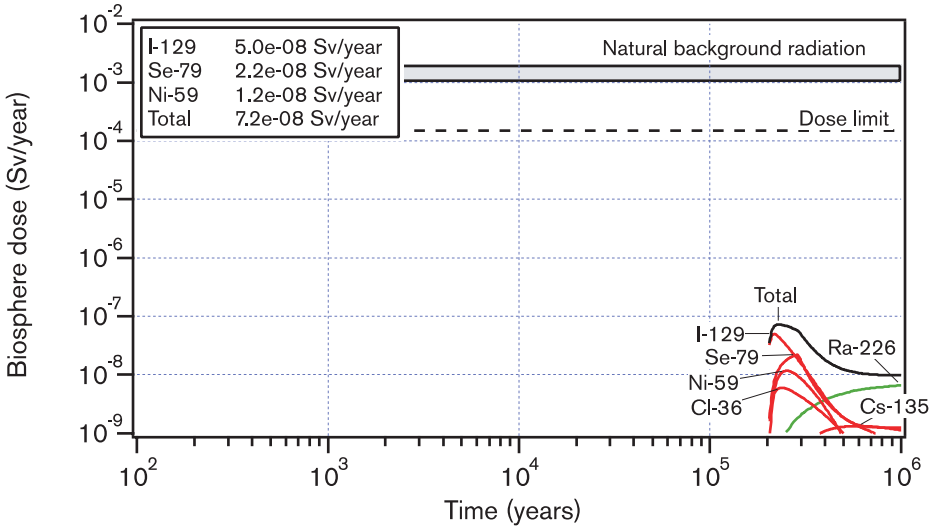

Figure 9-35. *Pessimistic data for transport between buffer and rock for Aberg.*

With all data reasonable at Aberg, the boundary layer is limiting for many nuclides. I-129 and Cl-36 comprise exceptions, where the buffer transport resistance dominates. With pessimistic data for the boundary layer, it is not limiting for any nuclide. The effect is illustrated in Figure 9-35. I-129 and Cl-36 are unchanged compared with the reasonable case, while the releases of e.g. Ni-59, Cs-135 and Ra-226 increase when pessimistic data are chosen for the properties of the boundary layer.

Finally, it should be noted that the span between reasonable and pessimistic data for the flux reflects an actual variability within a site.

Chemical transport data in the geosphere

Figure 9-36 shows biosphere doses with pessimistic sorption and diffusivity data in the geosphere for the saline water at Aberg.

Retention is affected strongly for all sorbing nuclides when pessimistic data are substituted for reasonable data at Aberg.

This is clear in Figure 9-37 for Ni-59, Cs-135, Th-229 and Ra-226. This is also the first of the cases reported this far where the maximum biosphere dose is caused by a nuclide other than I-129. During virtually the entire time radionuclide transport occurs, the dose is dominated by Ra-226. The maximum dose is still less than one-hundredth of the dose limit.

The effect of choosing pessimistic sorption and diffusivity data at Beberg and Ceberg is considerably less dramatic. Reasonable data pertain to non-saline water for both sites, while pessimistic data apply to saline water in Beberg and non-saline water in Ceberg, see section 9.9.

The reason the effects are less at these sites is not mainly due to the fact that pessimistic chemical transport data are more favourable than in Aberg. Pessimistic data for Beberg are actually the same as for Aberg. The big effect at Aberg is due to the fact that flow-related transport data, which together with chemical transport data determine retention for sorbing nuclides, are less favourable.

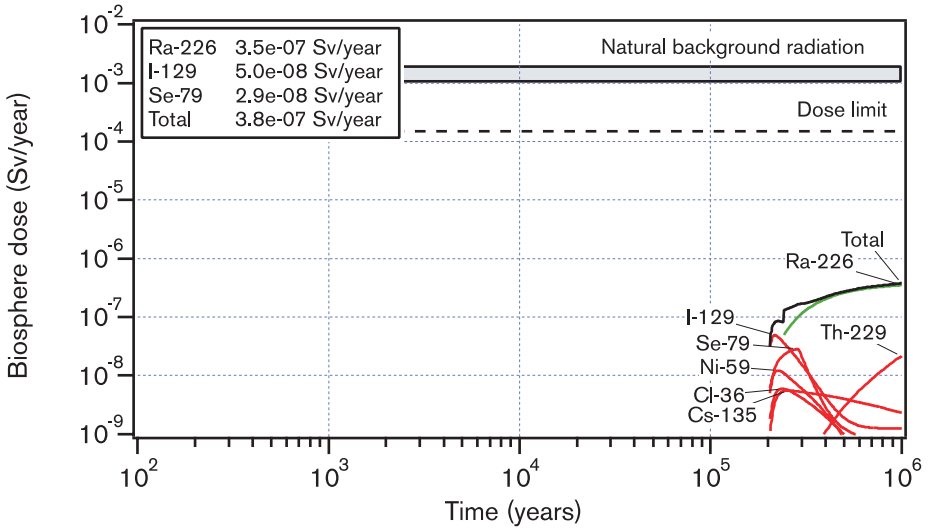

Figure 9-36. *Pessimistic sorption and diffusivity data in the geosphere for Aberg.*

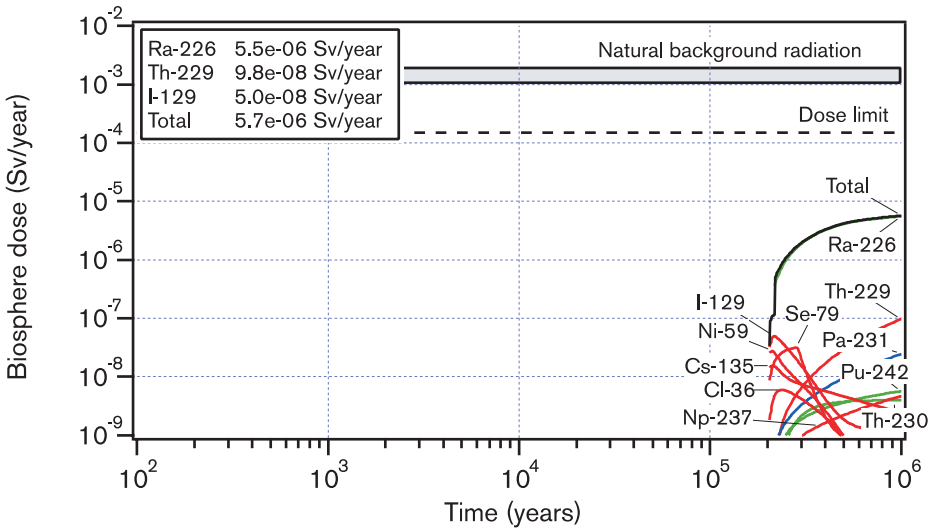

Figure 9-37. *Pessimistic values of flow-related data in the geosphere for Aberg.*

For these nuclides, retention capacity at Aberg is good when data are reasonable, while pessimistically chosen chemical data cause a sharp reduction in retention capacity. See further the discussion in section 9.11.11.

Flow-related data in the geosphere

Figure 9-37 shows how uncertainties in flow-related data in the geosphere at Aberg affect the results. What is most important here is the F factor, i.e. the product of the flow-wetted surface area a_w and the advective travel time t_w, see section 9.9.7.

Peclet number and maximum penetration depth were also chosen pessimistically in this case, but the effect of this is small.

The effects on all sorbing nuclides are even more striking here. The reason is the same as above: Pessimistically chosen flow-related data result in much poorer retention properties at Aberg, which means that the transit time for Ra-226 is short compared with the nuclide's half-life.

The maximum dose is roughly one-twentieth of the dose limit. In actual fact, retention is nearly non-existent for the long-lived nuclides shown in the figure for this case. Figure 9-37 is almost identical to Figure 9-50, section 9.11.10, where retention in the geosphere has been completely neglected as an extreme case. The effects for Beberg and particularly Ceberg are considerably less dramatic, see Figures 9-38 and 9-39.

Table 9-4. Reasonable and pessimistic values for advective travel times and flow-wetted surface area. Only one pessimistic value for a_w could be estimated for Ceberg. The same value is used as "reasonable" in the calculations.

	Advective travel time (years)		**Flow-wetted surface area (m^{-1})**	
	Reasonable	Pessimistic	Reasonable	Pessimistic
Aberg	10	0.8	10^4	10^3
Beberg	60	3.3	10^4	10^3
Ceberg	2,000	400	10^3	10^3

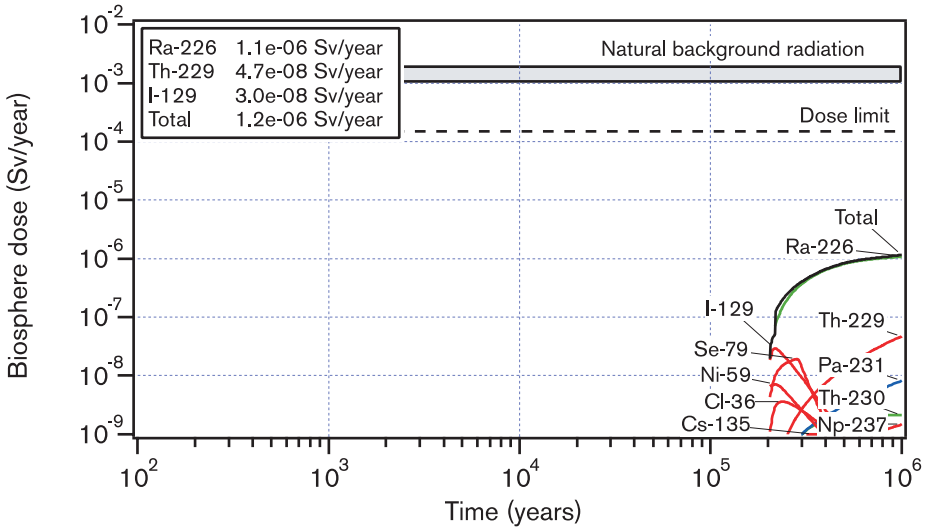

Figure 9-38. *Pessimistic values of flow-related data in the geosphere for Beberg.*

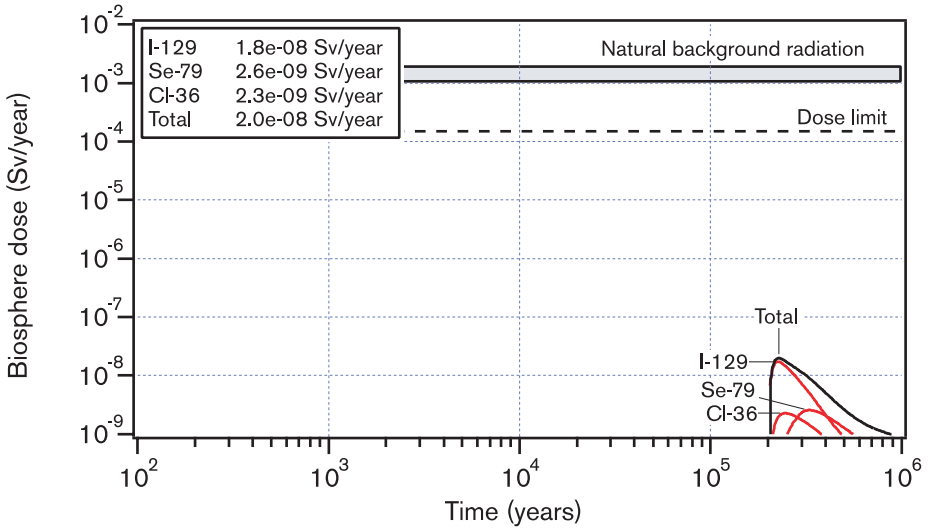

Figure 9-39. *Pessimistic values of flow-related data in the geosphere for Ceberg.*

The difference between reasonable and pessimistic values for the advective travel times reflects the natural variability at the particular site. The variability is a result of the fact that different positions in the repository have different properties, and of the stochastic nature of the rock. The former factor can be influenced to some extent by active choices of canister positions, the latter can in principle not be influenced.

The natural variability in travel time at Aberg in particular thus leads to large variations in retention of sorbing nuclides, see further the discussion in section 9.11.11.

Biosphere data

Figure 9-40 shows the effect of choosing pessimistic biosphere data for Aberg. In the reasonable case, the biosphere module has been assumed to be a peat bog and reasonable dose conversion factors for such a module have been used. In the pessimistic case, the module that gives the highest conversion factor for each nuclide has been chosen. The conversion factor has furthermore been calculated pessimistically. The result in Aberg for most nuclides is release to a peat bog for the pessimistic case as well, but with pessimistically chosen conversion factors in this module.

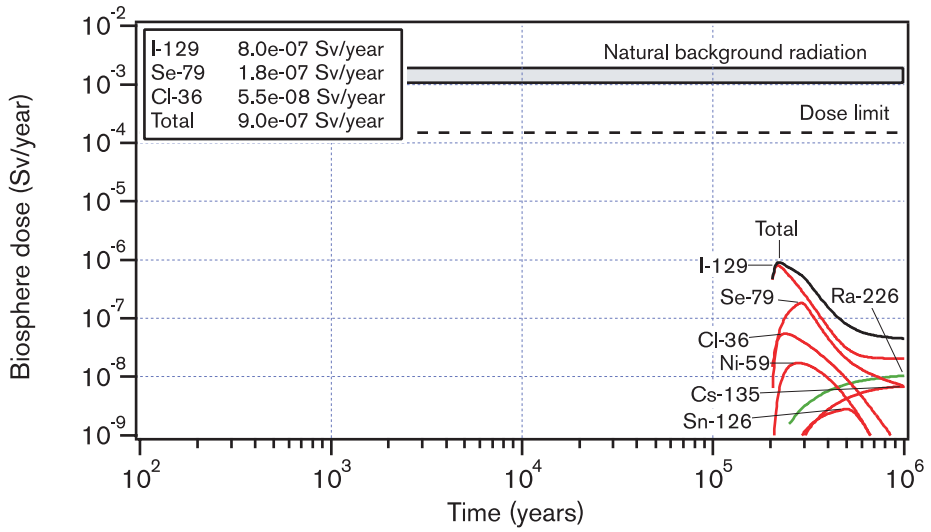

Figure 9-40. *Pessimistic values of biosphere data for Aberg.*

The figure shows that the doses increase by around a factor of ten for most radionuclides. This is a direct consequence of the fact that the pessimistic EDFs for peat bog are around ten times higher than the reasonable ones.

Summary Aberg, Beberg and Ceberg

Regardless of which data group is chosen pessimistically in the uncertainty analyses above, the maximum dose lies below the dose limit. Figure 9-41 is a compilation of how variations in each individual parameter influence the result at each of the sites.

The figure shows the change (increase) in maximum dose if a particular parameter is changed from a reasonable to a pessimistic value. The maximum dose pertains to the time up to one million years after deposition.

The figure shows that the greatest effects for Aberg are obtained for the number of initially defective canister, the F factor (the product $t_w \cdot a_w$) and the dose factors in the biosphere (EDFs). Many of the other parameters have little influence on the result if they are varied, starting with the thoroughly reasonable case. The result is in agreement with the above discussion of the different parameter groups. The effects of varying the F factor are mainly caused by a poorer retention of Ra-226.

The estimated number of initially damaged canisters could be improved with data and experience from future canister fabrication. The influence of the uncertainties in the F factors differs between the three sites. Here the result can thus be influenced by choice of site. Within a site, the uncertainties can in part be reduced by investigating the site thoroughly, but a large part of the spread in F factors is caused by spatial variability within the site. This can only be partially reduced by suitable choices of canister positions etc. The uncertainties surrounding the EDFs should be able to be reduced with increased understanding of, and thereby improved modelling of, radionuclide migration in the biosphere.

These simple uncertainty analyses are complemented by the risk analyses in the next section, where effects of combinations of reasonable and pessimistic data are systematically investigated.

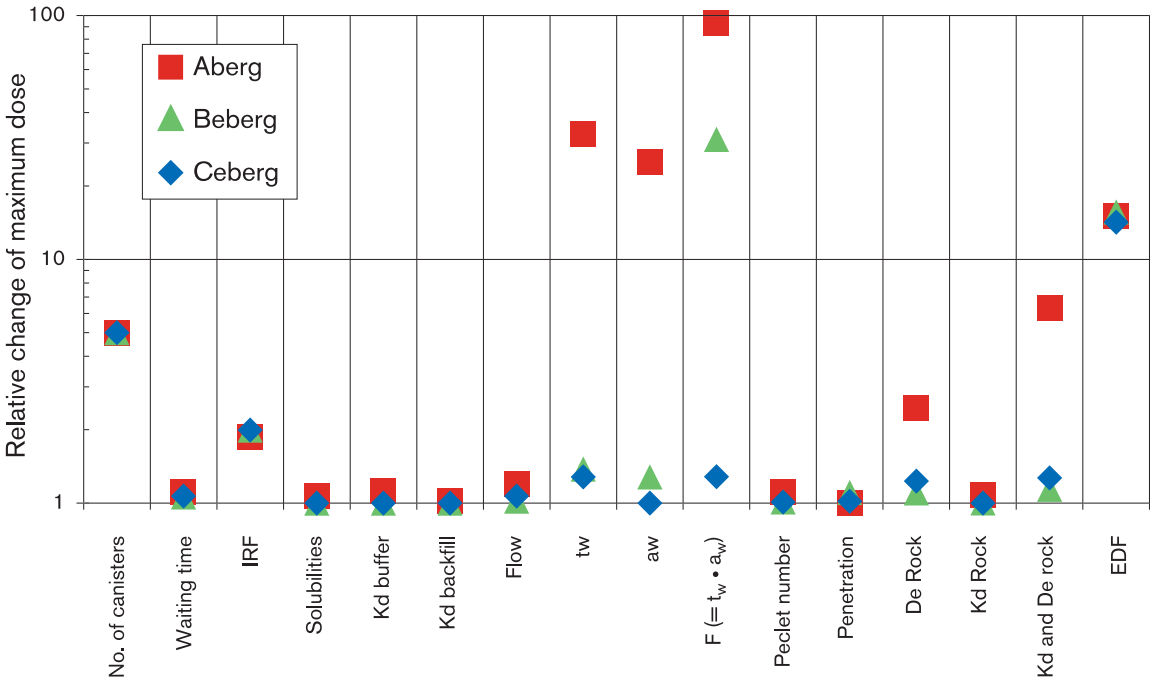

Figure 9-41. *The effect of varying different parameters based on the thoroughly reasonable case.*

9.11.9 Risk analyses

The stipulated criterion for repository safety is a risk measure, i.e. a summation of products of probabilities and consequences for different alternatives for repository evolution.

Calculations reported so far show only the consequence in the form of dose for different choices of data for the models. To be able to calculate a risk, the probability of different data sets must also be estimated.

As noted in Chapter 4, probability distributions are only available for a limited portion of the underlying data, such as certain flow-related data in the geosphere. Only reasonable and pessimistic values are available for the large majority of data, but no estimate of associated probabilities.

The pessimistic values are chosen throughout to serve as an absolute upper limit for the respective parameter's (negative) influence on the calculation result. Many pessimistic data must therefore be regarded as highly improbable. Reasonable data are also often cautiously chosen; in many cases, further research, more accurate measurements, etc. may lead to more positive data.

Based on the above, a probability of 0.9 is assigned to reasonable data and 0.1 to pessimistic data in the majority of cases where no distributions are available. The situation is illustrated in Figure 9-42. Instead of guessing what a whole distribution looks like, a rough estimate is made of the probability of reasonable versus pessimistic data. (The graduation of the x axis is arbitrary in this illustration; reasonable and pessimistic values can sometimes differ by several orders of magnitude.)

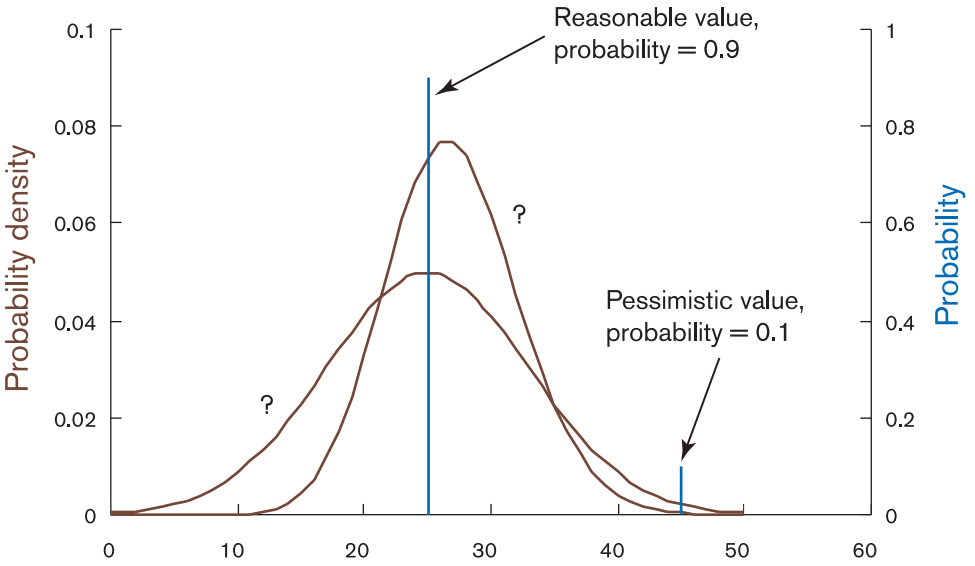

Figure 9-42. *Reasonable and pessimistic values, with probabilities of 0.9 and 0.1, respectively, are used for input data where distributions are lacking.*

A probabilistic calculation is carried out for the three repository sites with data as follows:

- Calculated correlated distributions are used for advective travel times and groundwater fluxes.
- Only pessimistic values are used for delay time, fracture geometries around deposition holes, Peclet number and maximum diffusion penetration depth in the rock matrix. The reason is technical and related to limitations in current versions of the calculation programs. The influence of the difference between pessimistic and reasonable values on the calculation result is limited for these parameters.
- For remaining data, i.e. number of broken canisters, solubilities, IRFs, sorption data in bentonite, sorption data in backfill, diffusion and sorption data and flow-wetted surface area in the geosphere, as well as EDFs in the biosphere, probabilities of 0.9 and 0.1 are assigned to reasonable and pessimistic data, respectively.

Groundwater fluxes and advective travel times are correlated, according to the results of the hydrological calculations. Other input data to the probabilistic calculation are not correlated, which is not entirely correct. Co-variations can occur between different nuclides as regards e.g. EDFs so that these data should at least be partially correlated. There is, however, nearly always one nuclide that completely dominates the maximum dose in a given realization. By not correlating such data, more realizations will contain a pessimistic value for at least one nuclide, which makes it pessimistic not to include such correlations.

The nuclides in the risk calculation are reduced for capacity reasons to those which might conceivably under some circumstances make significant contributions to the maximum dose, namely Ni-59, Nb-94, Sn-126, I-129, Pu-239 and the decay chain U-238 → U-234 → Th-230 → Ra-226.

The results in the form of a dose distribution function are depicted in Figures 9-43 and 9-44. The figures differ in that different biosphere modules have been used: a peat bog in Figure 9-43 and a site-specific well in Figure 9-44.

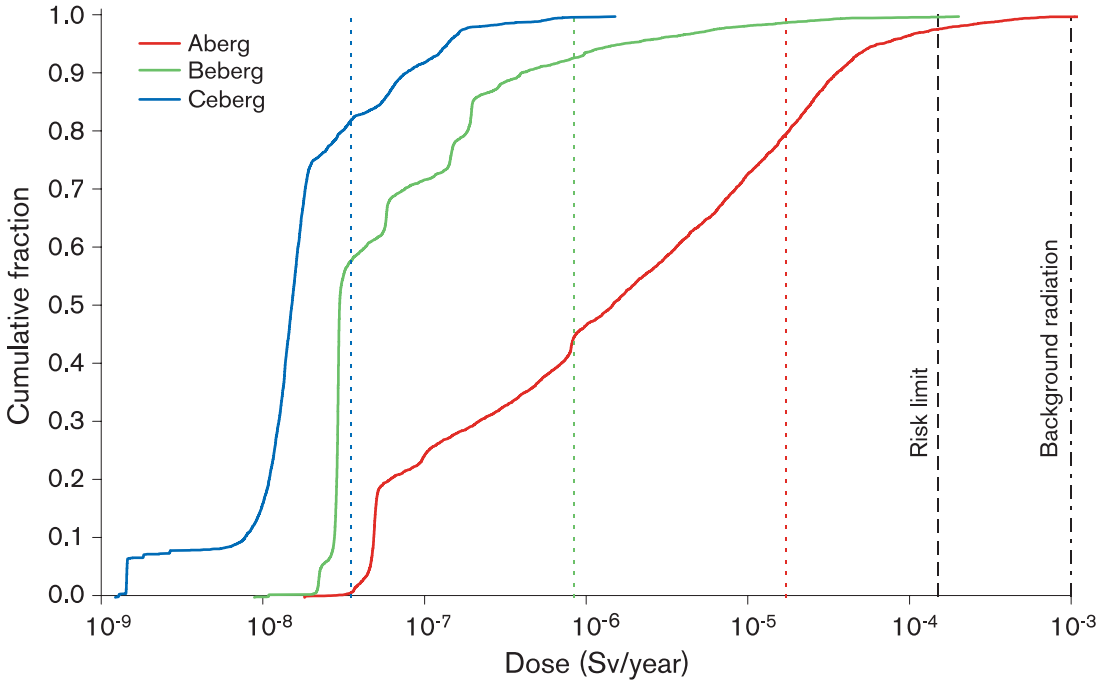

Figure 9-43. *Probabilistic results for site-specific peat bogs. The coloured vertical lines show the mean values of the different distributions, i.e. the calculated risk on the three sites.*

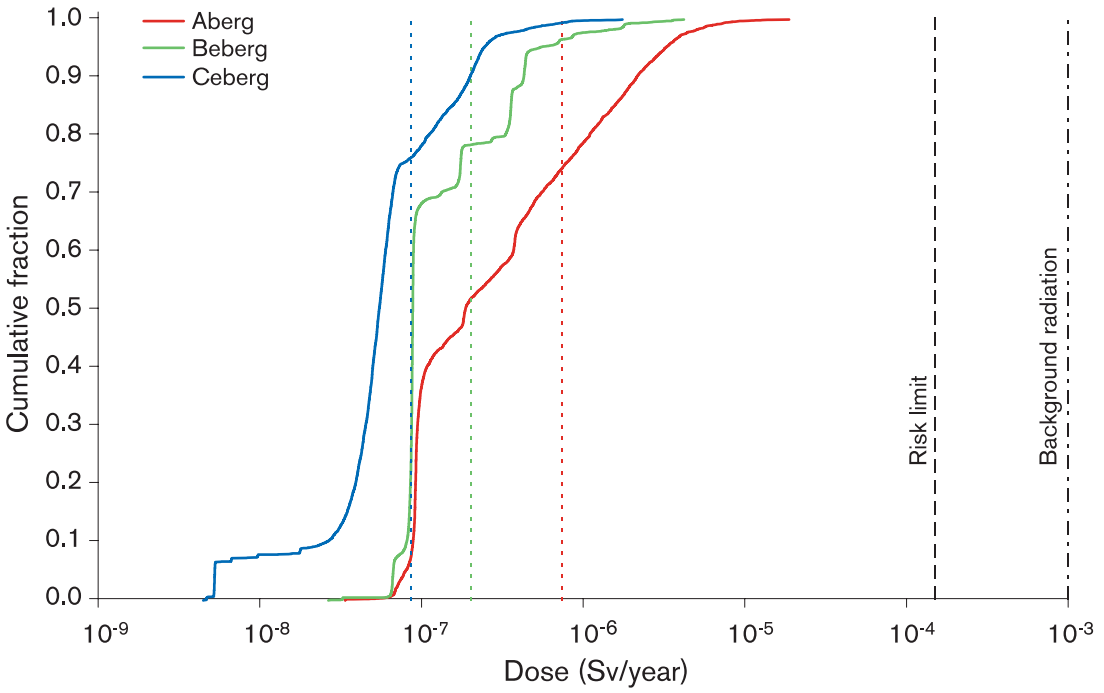

Figure 9-44. *Probabilistic results for site-specific wells. The coloured vertical lines show the mean values of the different distributions, i.e. the calculated risk on the three sites.*

The reasonableness of the assigned probabilities can only be judged by studying the procedure used in the selection of reasonable and pessimistic values in each individual case, which is reported in the Data Report. The probability values 0.9 and 0.1 are based on a general study of this type and are deemed to be a conservative choice.

The purpose of the calculations is to judge the risk associated with the canister defect scenario. The risk in a situation where a number of different outcomes are possible is defined as the sum of the partial risks for each outcome. The partial risk is in turn the product of probability and consequence for the outcome in question. Mathematically, the risk R is expressed as:

$$R = \sum_i p_i k_i$$

where p_i and k_i are the probability and consequence, respectively, for outcome i. The risk R is thereby by definition the mean of all consequences.

As regards the risk in the canister defect scenario, different data choices for the models give rise to the different outcomes. The consequence is chosen as the maximum annual dose that arises during a million years. The risk is thereby the mean of the maximum doses in all realizations. The mean values for Aberg, Beberg and Ceberg are therefore plotted in Figures 9-43 and 9-44.

The mean values should be compared with the risk limit in the figures. The risk limit applies to the most exposed individuals in a regional group, which is also true of the EDFs used for well and peat. The mean values for all sites lie well below the risk limit, in both the well and peat cases. It is also apparent that the safety margin differs between the sites: it is largest in Ceberg and smallest in Aberg.

It is also worth noting for the well case that **all** realizations for all sites are less than one-tenth of the dose that corresponds to the risk limit in these calculations, i.e. the distributions in Figure 9-44 never come close to the risk limit.

Nearly all realizations that give significant maximum doses in the risk calculations are dominated either by I-129 or, if geosphere retention is weak, by Ra-226. A large canister defect is created after 20,000 years (pessimistic value in all realizations). The maximum dose of I-129 comes shortly thereafter.

The maximum dose of Ra-226 never arises until after more than 100,000 years, however, for fundamental reasons: Ra-226 is not present in the fuel initially, but is formed by chain decay of the initial content of U-238 and U-234. The nature of the decay chain is such that the rate of formation of Ra-226 does not become significant until after around 100,000 years.

In order to shed light on the importance of Ra-226, the result of the risk calculation can also be evaluated with Ra-226 excluded. The results are shown in Figure 9-45 and Table 9-5. The results are influenced greatly for the peat ecosystem at Aberg and Beberg, in other cases more marginally.

Table 9-5. Relative risks for peat ecosystem and well with and without Ra-226. The risks are expressed as fractions of the acceptance criterion for the most exposed individuals, i.e. 0.15 mSv/y.

	Peat ecosystem		**Well**	
	with Ra-226	without Ra-226	with Ra-226	without Ra-226
Aberg	0.11	0.003	0.005	0.001
Beberg	0.006	0.0006	0.001	0.001
Ceberg	0.0002	0.0002	0.0006	0.0006

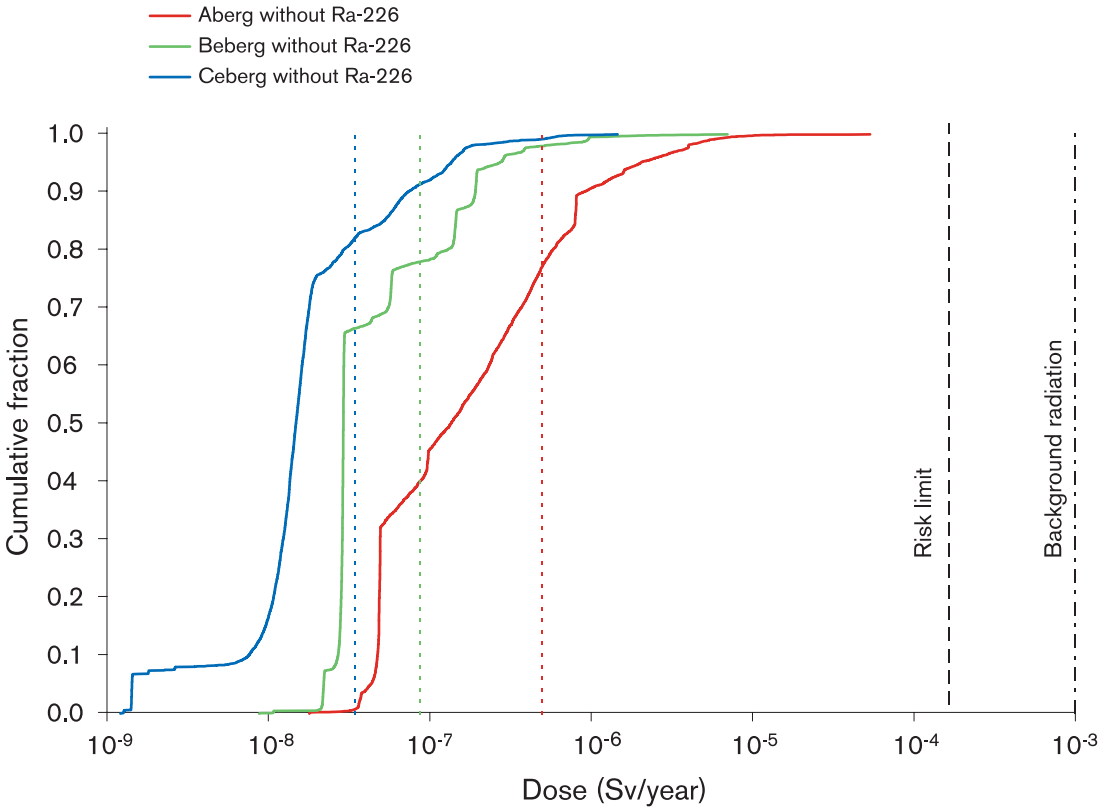

Figure 9-45. *Risk calculation for peat bog without Ra-226. The coloured vertical lines show the mean values of the different distributions, i.e. the calculated risk on the three sites.*

The effect would have been roughly the same if the risk calculation had been done for a period of 100,000 years instead of a million years, since significant doses from Ra-226 come after roughly 100,000 years and for other nuclides that dominate the dose picture shortly after the canister breach has become large, i.e. 20,000 years.

In summary, the three sites are relatively equivalent during the initial 100,000 years. The differences between the sites are roughly a factor of ten and the risks are always less than one percent of the risk limit, for both well and peat ecosystem. The same conclusion applies to the well case for the period between 100,000 and one million years. With a peat ecosystem, the risk increases at Aberg and Beberg by a factor of 10 and 20, respectively, but is always well below the risk limit. An important reason why this outcome is obtained for the peat ecosystem is accumulation of Ra-226 in peat, a process which is included in the biosphere model. To put the result in perspective, it can be noted that certain peat bogs in Sweden exhibit sharply elevated concentrations of Ra-226, which comes naturally from the bedrock /Ek et al, 1982/.

The results should also be viewed in the light of the fact that extensive glaciations are to be expected in Sweden within a period of a hundred thousand years, which is the subject of the climate scenario in Chapter 10. A glaciation leads to erosion of virtually the entire soil layer. Aberg can be expected to be under the sea for a large part of the next hundred thousand years. These aspects are weighed together in the overall discussion of the results of the entire assessment in the last chapter of the report.

Robustness

The shape of the distributions in the risk calculations also illustrates differences in the repository's "insensitivity" to variations in parameters: Regard the distribution for Ceberg in Figure 9-43. It has a nearly vertical section around a dose of 10^{-8} Sv/y where the cumulative fraction of realizations goes from 0.1 to over 0.7, i.e. over 60 percent of the realizations give rise to doses of around 10^{-8} Sv/y. These realizations include a large number of parameter combinations that all give equivalent results of around 10^{-8} Sv/y, which is also the maximum dose for the case where all parameters are chosen as reasonable, Figure 9-28.

The dose is lower in about ten percent of the realizations. These realizations have advective travel times that are longer than those chosen as reasonable. If pessimistic data had been compensated with "favourable" data, the fraction with lower doses would be greater.

The other barely 30 percent have results over 10^{-8} Sv/y. Only for these realizations are the parameter combinations sufficiently disadvantageous to affect the result significantly in an unfavourable direction.

The corresponding "vertical" range at Beberg lies around $3 \cdot 10^{-8}$ Sv/y (around the maximum dose for the reasonable case) and includes around 60 percent of the realizations. Approximately 40 percent of the realizations have less favourable results. These also span a considerably larger dose range than the equivalent realizations for Ceberg.

The "vertical" part of the curve for Aberg lies around $5 \cdot 10^{-8}$ Sv/y (around the maximum dose for the reasonable case) and includes only 20 percent of the realizations. In 80 percent of the realizations, the parameter combinations are less favourable in Aberg.

The above exposition illustrates two points:

- Aberg is most and Ceberg least sensitive to parameter variations. The "height" of the nearly vertical section can be said to be a measure of the repository's robustness on the site in question.
- The distributions also illustrate the fact that data that are more favourable than the reasonable data have not been included (except for travel times and groundwater fluxes): A very small fraction of the realizations have a more favourable result than the case with thoroughly reasonable values, i.e. a very small fraction lie to the left of the "vertical" part of the respective distribution.

Similar observations can be made for the well case, Figure 9-44. Note that the distributions have a different shape, despite the fact that they are the result of the same realizations as for the peat case. The releases from the geosphere are exactly the same, but other nuclides dominate the doses for the well. This means that the geosphere releases undergo a different turnover in the biosphere, and the effects of different parameter combinations in fuel, buffer and geosphere are different than in the peat case.

As regards robustness as well, differences between the sites mainly show up in a very long time perspective, for the same reasons as in the above risk discussion.

9.11.10 Special cases

To shed light on the roles of different barriers in the canister defect scenario, a number of special cases have been calculated:

- The fuel is completely dissolved when a continuous water pathway is created.
- No solubility limitations.
- Big initial canister defect.
- Diffusion resistance in the buffer is neglected.
- Retention in the geosphere is neglected.

None of the cases is realistic. They are included to illustrate the function of the barrier system. The changes that have been made in the models pertain only to radionuclide transport. The system's evolution in other respects, for example the hydromechanical consequences of a large initial canister defect, are not dealt with. The point of departure in all calculation cases is reasonable data for Aberg.

Immediate fuel dissolution

Figure 9-46 shows the effect of assuming that the fuel dissolves immediately when it comes into contact with water. Otherwise, reasonable data are used for Aberg. The doses for several non-sorbing nuclides have increased compared with the thoroughly reasonable case, since the entire inventory of these nuclides is now immediately accessible for transport.

The effect is otherwise relatively limited, especially since low solubilities limit the releases for many nuclides. The release of Ra-226 from the near field is sufficiently large to make a contribution to the dose after retention in the geosphere for this case. The concentration of Ra-226 in the canister has reached the solubility limit. Other nuclides that give rise to markedly increased doses are Cs-135 and Se-79.

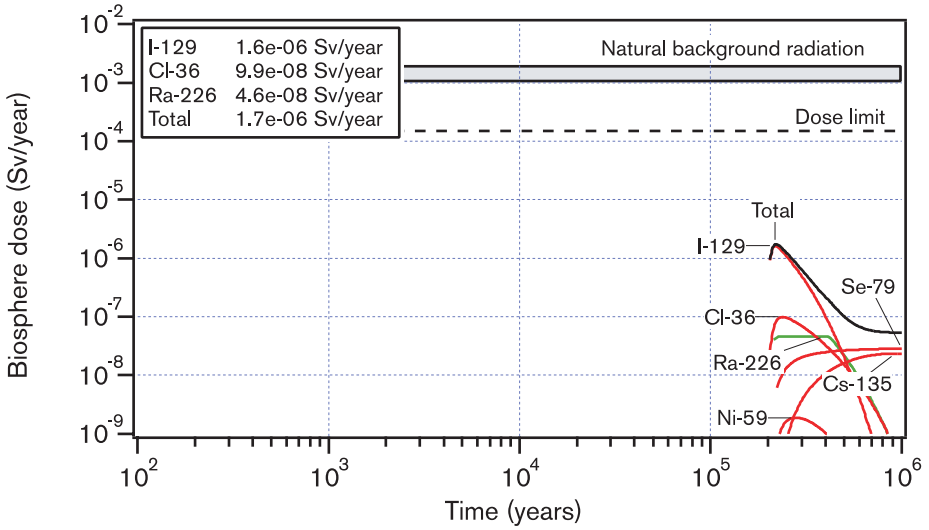

Figure 9-46. *Immediate fuel dissolution.*

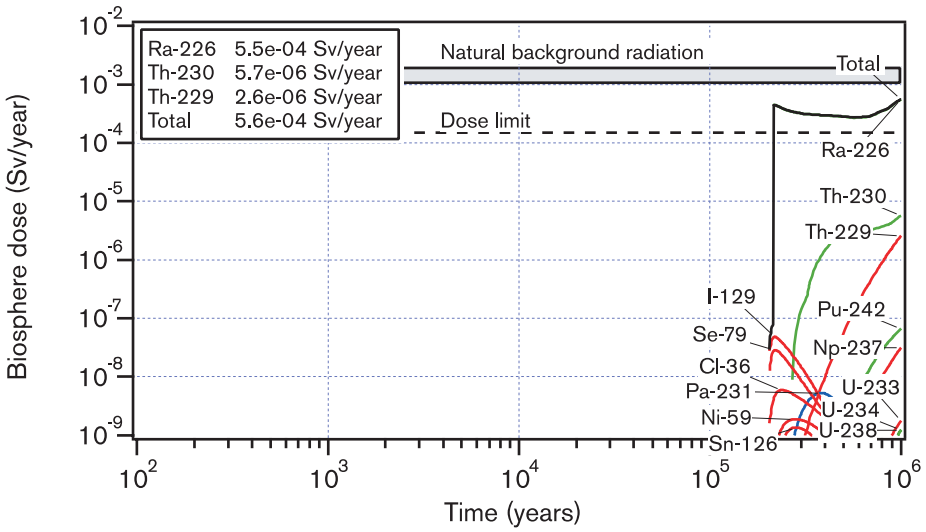

Figure 9-47. *No solubility limitations.*

The most important conclusion of this variation case is that the fuel dissolution rate, which is difficult to estimate, is of limited importance for the integrated performance of the barrier system.

No solubility limitations

Figure 9-47 shows the effect of disregarding all solubility limitations for radionuclides in the water in the canister cavity.

Several long-lived isotopes of uranium, plutonium, neptunium and thorium appear in the figure. Doses from Ra-226 exceed the dose limit. In this case, formation of Ra-226 from parent nuclides in buffer and geosphere also contribute. The dose contributions from nuclides that are not assumed to have any solubility limit in the reasonable case either, such as I-129 and Cl-36, are unchanged. The calculation case illustrates the large contribution made by the solubilities to the performance of the barrier system. The values for the solubilities of e.g. uranium, plutonium and thorium may vary, as illustrated by the span between reasonable and pessimistic values. The very existence of solubility limits and the fact that they can be assigned pessimistic upper limits rests, however, on a fundamental thermodynamic foundation.

Large initial canister defect

Figure 9-48 shows the effect of an initial canister defect with a size of 1 dm^2.

The case can be compared with the one where pessimistic values are assumed for canister damages, Figure 9-32. In that case, the biosphere doses will be around 10^{-3} mSv/y after 20,000 years; in the case with large initial canister defect, Sr-90 and I-129 together give doses of that size after only 100 years.

The rest of the barrier system thus provides good protection even with a completely unreasonable initial defect. The hydromechanical consequences as regards corrosion of the insert with accompanying gas generation etc. are not dealt with in this case.

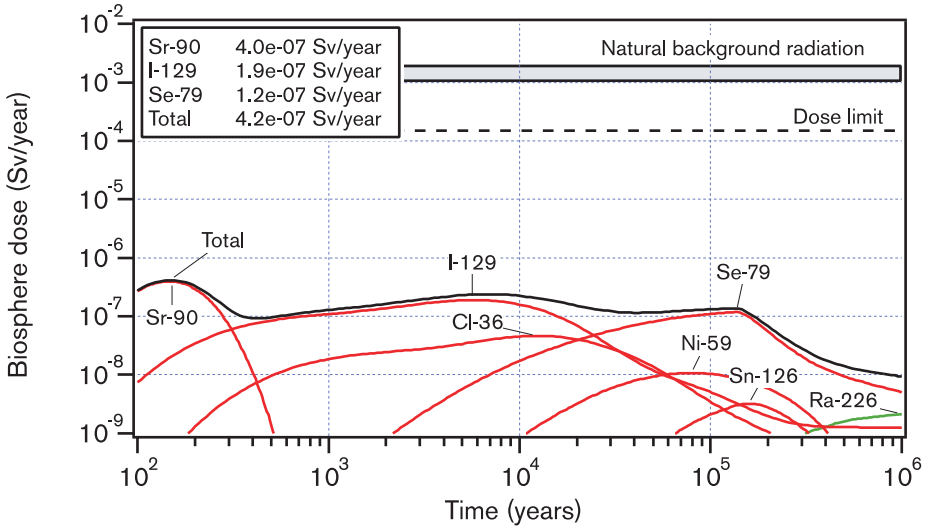

Figure 9-48. *Large initial canister defect.*

No diffusion resistance in the buffer

Figure 9-49 shows the consequences of neglecting the diffusion resistance associated with radionuclide transport in the buffer.

The buffer material has been replaced with water. The effects are very limited, since other transport resistances, above all that from the boundary layer between buffer and rock, still dominate for many nuclides. Compared with Figure 9-34, which shows the effects of assuming pessimistic sorption data for the buffer, the maximum, relatively short-duration releases of I-129, Cl-36 and Se-79 are around ten times higher.

Once again, the conclusion is that in this case the buffer's function as far as radionuclide transport is concerned is well covered by other barriers.

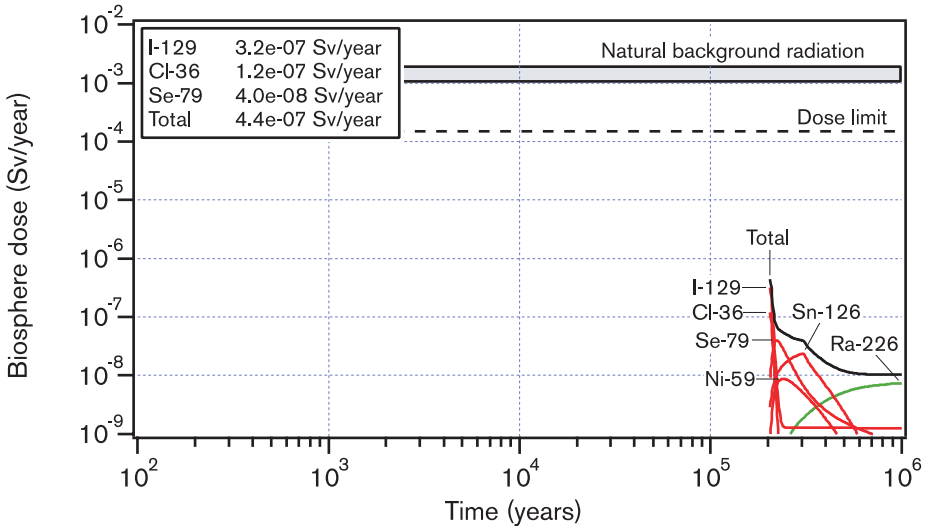

Figure 9-49. *No diffusion resistance in the buffer.*

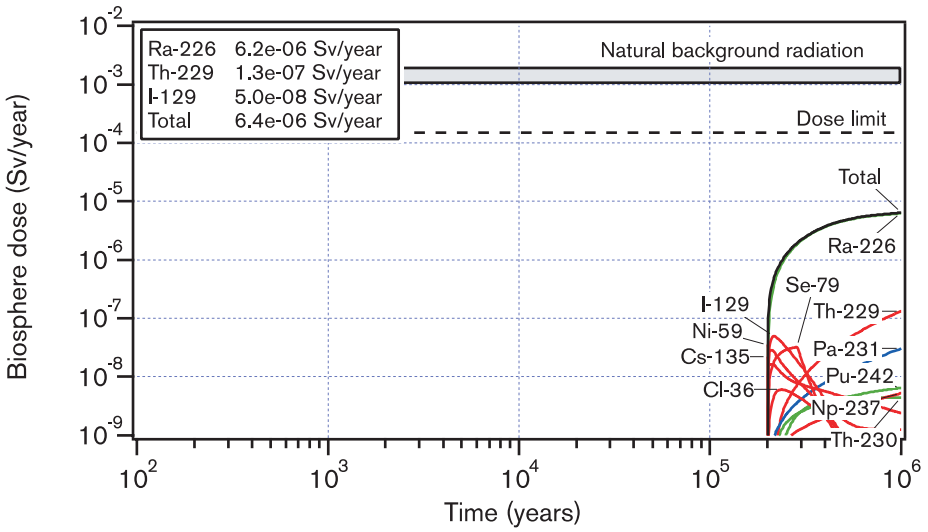

Figure 9-50. No retention in the geosphere.

No geosphere retention

Figure 9-50 shows the consequence of completely disregarding retention in the geosphere at Aberg. The releases from the near field have been assumed to reach the biosphere immediately. The only geosphere function that has been retained is that a reasonable value for the transport resistance between buffer and geosphere has been used.

The result is virtually identical with that shown in Figure 9-37, where pessimistic values have been assumed for flow-related transport data for the geosphere at Aberg. This mainly illustrates the great variability of the geosphere. The effect of going from reasonable to pessimistic data is roughly the same as completely neglecting geosphere retention.

Conclusions

The above variation cases illustrate the multi-barrier principle as far as radionuclide transport is concerned. Not even extreme and completely unrealistic assumptions concerning a single barrier function have unacceptable consequences.

9.11.11 Analytical calculations

Near field

In Hedin /1999/, a simple analytical model is derived for release and transport of radionuclides in canister and buffer. The model handles:

- radioactive decay in the entire near field, including chain decay in the fuel matrix,
- fuel dissolution,
- release of instant release fraction (IRF) of radionuclides in the canister,
- solubility limitations,
- diffusive transport through a damaged canister,

- transient and steady-state transport, diffusion and sorption through the buffer,
- release to the surrounding rock via the two most important release pathways, Q1 and Q2, which are dealt with in COMP23.

Figure 9-51 shows the results of a calculation of near-field release at Aberg. Pessimistic values have been used for data related to canister damages and to the boundary layer between buffer and rock.

The results should be compared with Figure 9-52, which is calculated with COMP23 with the same data. The discrepancies as regards maximum calculated release are less than a factor of ten for all nuclides in this case. The greatest difference for many nuclides is in the long-term situation after the maximum dose. The reason is the simplified modelling of radionuclide migration in the buffer.

A simplified model such as this one can never completely take the place of a numerical model like COMP23, especially not when it comes to modelling of complex geometries. The analytical model, on the other hand, is useful for:

- demonstrating an understanding of how the results are quantitatively dependent on input data,
- facilitating an evaluation of the reasonableness of the model-calculated releases from the near field,
- assuring quality in data management for the numerical model.

With the analytical expressions, it is for example simple to show that the transport resistance in the near field is greatly dominated by the small hole in the canister up to the time when the defect is enlarged due to internal pressure from corrosion products (after 20,000 years in this example). The analytical model is a first version, which can be refined for future safety assessments.

Geosphere

The essential transport properties of the geosphere can also be described with relatively simple analytical expressions. From a pulse release from the repository, after decay during transport through the geosphere, the fraction T will eventually reach the biosphere, where

$$T = e^{-\lambda t_w - t_w a_w \sqrt{\lambda D_e [\varepsilon_p + (1-\varepsilon_p) K_d \rho]}}$$

Here, λ is the nuclide's decay constant, t_w is the advective travel time, a_w is the flow-wetted surface area per volume of flowing water, ε_p is the matrix porosity and D_e, K_d and ρ are the rock's diffusivity, sorption coefficient and density, respectively /see e.g. Carslaw and Jaeger, 1959/. The product $t_w \cdot a_w$ is equal to the F factor.

T is called transmission and thus designates how large a fraction of a release of a given radionuclide passes through the geosphere without decaying. The expression applies not only to a pulse release, but to an arbitrarily time-dependent release, since such a release can always be described as a series of pulse releases.

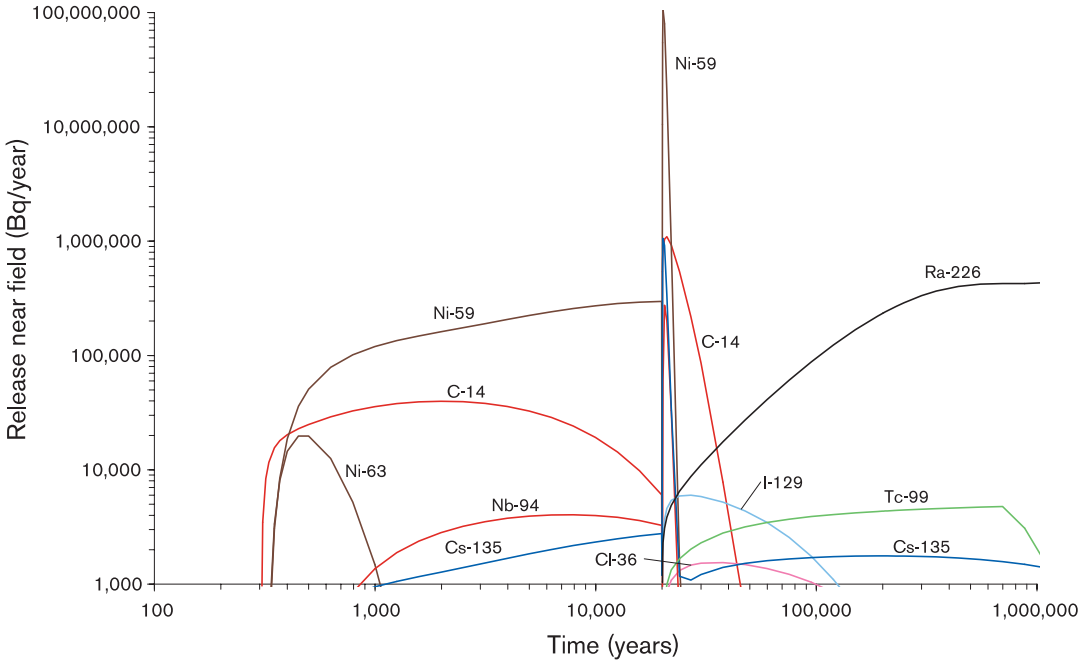

Figure 9-51. *Releases from the near field for pessimistic values for data related to canister damages and the boundary layer between buffer and rock at Aberg. Analytical calculation.*

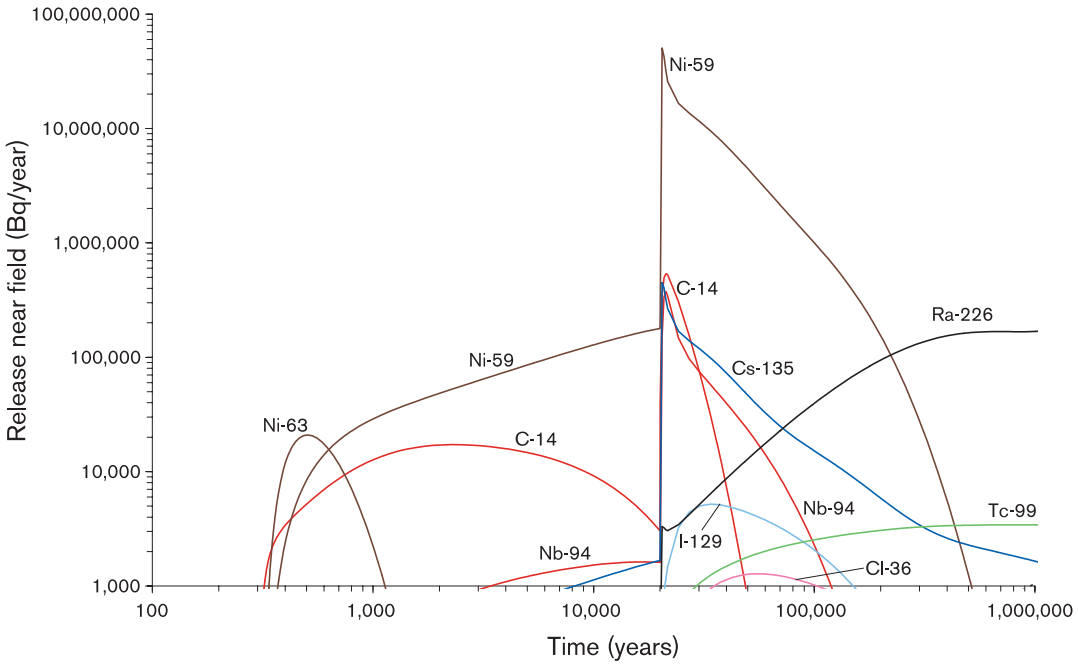

Figure 9-52. *Numerical calculation with COMP23 of the same case as in Figure 9-51.*

The same processes and assumptions about fracture geometries etc. as in the far-field model FARF31 have been used in deriving the expression, except that dispersion has been disregarded and the rock matrix has been assumed to have an infinite penetration depth. The effect of both these assumptions is limited.

To discuss the performance of the geosphere with regard to radionuclide transport, it is illustrative to calculate transmission for a number of nuclides with different combinations of reasonable and pessimistic data. Table 9-6 shows the results of such a calculation for Aberg.

The table shows the following for Aberg:

- Certain nuclides pass through the geosphere even with thoroughly reasonable data. These include long-lived non-sorbing nuclides such as I-129 and Cl-36. C-14, Cs-135 and Sn-126 also have relatively high transmission values for reasonable data.
- If only one parameter is chosen pessimistically, retention capacity is very limited at Aberg for the nuclides in the point above and in many cases also for Ra-226, Ni-59, Sr-90 and Tc-99.
- The single parameter with the greatest influence on the results is the advective travel time t_w. With a pessimistic t_w and otherwise reasonable values, retention is very limited for most of the tabulated nuclides.
- With thoroughly pessimistic data, the geosphere at Aberg has very poor retention capacity for all tabulated nuclides.

Table 9-6. Transmission for a number of nuclides at Aberg. Transmission is given in percent. R and P stand for reasonable and pessimistic data for the parameter in question. < means less than 0.001 percent.

t_w	R	P	R	R	R	P	P	P	P	R
a_w	R	R	P	R	R	P	R	R	P	R
K_d	R	R	R	P	R	R	P	R	P	P
D_e	R	R	R	R	P	R	R	P	P	P
C-14	14	86	82	25	82	98	90	98	100	87
Cl-36	99	100	100	99	100	100	100	100	100	100
Ni-59	17	87	84	28	57	99	90	96	100	67
Ni-63	<	2	1	<	<	67	6	29	91	0.002
Sr-90	0.004	44	29	0.1	4	91	56	77	96	9
Nb-94	<	10	5	<	0.01	79	19	48	95	0.1
Tc-99	0.01	49	41	1	6	93	67	80	99	21
Sn-126	66	97	96	98	88	100	100	99	100	99
I-129	100	100	100	100	100	100	100	100	100	100
Cs-135	38	93	91	65	73	99	97	98	100	87
Cs-137	<	<	<	<	<	13	0.01	0.2	74	<
Ra-226	<	33	24	0.005	1	89	45	70	97	4
Pa-231	<	16	10	<	0.1	83	28	56	96	1
U-234	<	23	16	0.02	0.3	86	51	62	98	7
Pu-239	<	1	0.3	<	<	62	12	22	93	0.02

Table 9-7. Transmission for a number of nuclides at Beberg. Transmission is given in percent. R and P stand for reasonable and pessimistic data for the parameter in question. < means less than 0.001 percent.

t_w	R	P	R	R	R	P	P	P	P	R
a_w	R	R	P	R	R	P	R	R	P	R
K_d	R	R	R	P	R	R	P	R	P	P
D_e	R	R	R	R	P	R	R	P	P	P
C-14	3	82	69	7	31	98	87	94	100	44
Cl-36	99	100	100	99	100	100	100	100	100	100
Ni-59	<	27	9	<	0.1	88	39	66	97	0.5
Ni-63	<	<	<	<	<	3	<	0.001	44	<
Sr-90	<	<	<	<	<	0.1	<	0.1	56	<
Nb-94	<	0.01	<	<	<	38	0.1	5	81	<
Tc-99	<	5	0.4	<	<	74	20	39	95	0.01
Sn-126	8	87	78	90	46	99	99	96	100	97
I-129	100	100	100	100	100	100	100	100	100	100
Cs-135	<	4	0.3	<	0.3	72	24	72	99	7
Cs-137	<	<	<	<	<	<	<	<	2	<
Ra-226	<	0.003	<	<	<	35	0.1	4	79	<
Pa-231	<	0.05	<	<	<	47	0.5	9	85	<
U-234	<	0.2	0.001	<	<	54	6	14	92	<
Pu-239	<	<	<	<	<	14	0.02	0.2	76	<

Table 9-7 shows the equivalent calculation for Beberg. The table shows that:

- Long-lived non-sorbing nuclides such as I-129 pass through the geosphere even with thoroughly reasonable data.
- The single parameter with the greatest influence on the results is the advective travel time t_w, but the effect is less than at Aberg.
- If both t_w and a_w are chosen pessimistically, i.e. with an extremely pessimistic F factor, retention at Beberg is very limited.
- Pessimistic values for chemical transport data (diffusivities and sorption coefficients) do not change retention appreciably at Beberg.

Table 9-8 shows the equivalent calculation for Ceberg. The table shows that:

- Long-lived non-sorbing nuclides such as I-129 pass through the geosphere even with thoroughly reasonable data.
- The single parameter with the greatest influence on the results is the advective travel time t_w, but the effect is limited.
- Even if all parameters are chosen pessimistically, the reduction of retention at Ceberg is very moderate.

Table 9-8. Transmission for a number of nuclides at Ceberg. Transmission is given in percent. R and P stand for reasonable and pessimistic data for the parameter in question. < means less than 0.001 percent.

t_w	R	P	R	R	R	P	P	P	P	R
a_w	R	R	P	R	R	P	R	R	P	R
K_d	R	R	R	P	R	R	P	R	P	P
D_e	R	R	R	R	P	R	R	P	P	P
C-14	<	8	<	0.01	2	8	17	44	55	5
Cl-36	97	99	97	97	99	99	99	100	100	99
Ni-59	<	<	<	<	<	<	0.001	1	3	<
Ni-63	<	<	<	<	<	<	<	<	<	<
Sr-90	<	<	<	<	<	<	<	<	<	<
Nb-94	<	<	<	<	<	<	<	<	<	<
Tc-99	<	<	<	<	<	<	<	0.001	0.2	<
Sn-126	0.03	19	0.03	69	7	19	93	59	98	88
I-129	100	100	100	100	100	100	100	100	100	100
Cs-135	<	<	<	<	<	<	<	2	17	0.02
Cs-137	<	<	<	<	<	<	<	<	<	<
Ra-226	<	<	<	<	<	<	<	<	<	<
Pa-231	<	<	<	<	<	<	<	<	<	<
U-234	<	<	<	<	<	<	<	<	0.003	<
Pu-239	<	<	<	<	<	<	<	<	<	<

9.11.12 Gas-phase transport

A defective canister is expected to contain hydrogen gas for a very long time, see section 9.6. Radionuclides could thereby be transported to the surface in the gas phase if hydrogen were released. Carbon-14 and radon-222 are the only remaining radionuclides that could conceivably be transported in the gas phase at the times such transport is possible according to section 9.6.

Release of carbon-14

C-14 could occur as carbon dioxide or methane, which means that it could be transported in the gas phase. A large portion of the gas in a canister is expected to be released as a pulse. The transport resistances in both the near and far field are small for gas transport. In SR 95 /SKB, 1995/, the importance of gas-phase transport was illustrated with an extreme case:

- 2.5 percent of the inventory of C-14 was released at the time of deposition.
- The gas was released directly to the biosphere without retardation.
- The dose was calculated in the same way as for gas releases from reprocessing plants.

With these premises, the collective dose was 480 μmanSv for C-14 locally and regionally.

Release of radon-222

After several hundred thousand years, the total quantity of Rn-222 in a canister has grown to approximately 10^{11} Bq, after which it remains fairly constant. With the same premises as above, as an extreme upper-limit case, this entire quantity could be released to the atmosphere. However, due to the nuclide's short half-life (3.8 days), together with the large dilution of an atmospheric release, the dose consequence of such a gas release is negligible.

Conclusion

Based on the above, gas-phase transport is judged in SR 97 not to be of any safety-related importance for the deep repository.

9.11.13 Discussion of results

Risk analyses

The repositories at Aberg, Beberg and Ceberg meet the Swedish Radiation Protection Institute's acceptance criteria for a deep repository for spent nuclear fuel.

The conclusion is based on calculations with the conservative estimate that the probability that the pessimistic values will become reality is 0.1 throughout. An exhaustive discussion of the probabilities of reasonable versus pessimistic values is beyond the scope of this report. All data choices are thoroughly justified in the Data Report, and probability assessments must be based on the choices of data in the individual cases. The choice of a probability of 0.1 for pessimistic data is based on a general such evaluation.

If the release takes place to a well, the risk at Aberg is less than one hundredth of the acceptance criterion if the calculation is performed for a timespan of one million years. The risk at Beberg is approximately one-fifth, and at Ceberg one-tenth, of the risk at Aberg.

In the case of release to a peat ecosystem, the sites differ in roughly the same way for times up to around 100,000 years. For a million years, the risk at Aberg then increases by approximately a factor of 40, at Beberg by a factor of ten and at Ceberg only marginally. The natural radionuclide Ra-226 dominates the consequences for the peat ecosystem for times over 100,000 years.

The calculated retention capacity is equivalent at the three sites for long-lived non-sorbing nuclides. For sorbing nuclides, retention is strongest at Ceberg and weakest at Aberg.

The risk calculations pertain to the maximum dose that arises in 100,000 or one million years. The maximum dose always arises at times after 20,000 years. For times up to 20,000 years, even an initially defective canister provides considerable protection, even with the most pessimistic assessment of the course of events.

How do the sites differ?

Geosphere: The retention capacity of the rock is of importance for the repository's retarding function in the event of a canister defect. The capacity is nuclide-specific and is determined by the nuclide's half-life, nuclide-specific chemical factors and the rock's flow properties. The latter are expressed by the F factor, i.e. the product of the advective travel time and the flow-wetted surface area.

From the discussion of uncertainties in the hydraulic modelling, it is also worth recapitulating the assessment that calculated differences in travel times and groundwater fluxes between the sites are probably to a large extent physically based and can be traced to site-specific hydrogeological conditions. The rock mass in Aberg and Beberg is, for example, approximately 100 times more permeable than the one in Ceberg, although some of the difference might be caused by differences in investigation methodology between the sites.

However, non-sorbing nuclides such as I-129 often dominate in the dose and risk calculations. They always penetrate through the rock, regardless of the F factor, so that the effect of differences in F factors between sites is evened out to some extent in a total risk analysis.

Biosphere: The biosphere conditions have a great influence on the calculated dose. The doses will be several orders of magnitude lower if the release takes place to watercourses, lakes or the sea, compared with if it takes place to land (peat, agricultural land, well). For Ra-226, which dominates the dose in many unfavourable realizations, the EDF for peatland is moreover more than two orders of magnitude higher than the well value.

Despite the great differences in EDFs, it is unreasonable to attach great importance to today's biosphere conditions in site discussions. The biosphere types peat, agricultural land and well exist or will probably exist on every conceivable deep repository site. The role of the biosphere in the analysis must also be regarded in the light of the extensive impact on the biosphere that follows from the expected climate changes, see Chapter 10.

Uncertainty analysis

The effect of substituting pessimistic for reasonable data is studied systematically in the uncertainty analyses. It is first observed that for the well case, the dose does not exceed the value equivalent to the risk limit in a single realization of the risk calculation at any site. The same applies to the peat module at Ceberg, whereas the dose has been exceeded in a few of the most unfavourable realizations at Aberg and Beberg if Ra-226 is included.

This is also a form of illustration of the multiple barrier principle: Reduced performance (pessimistic values) of one barrier does not lead to unacceptable performance of the system as a whole. The margins are greatest here for Ceberg and smallest for Aberg.

Canister: The difficult-to-assess uncertainties in the number of damaged canisters (reasonable value 1, pessimistic 5) directly affect the result. It is not apparent how these uncertainties can be reduced in the future.

The analysis of the canister's hydromechanical evolution after being damaged is surrounded by great uncertainties. Although reasonable and pessimistic estimations can be made today of the few factors that are used in the calculation of radionuclide transport, it is urgent to improve our understanding of the hydromechanical evolution.

Fuel: Another uncertain factor is fuel dissolution. The influence of uncertainties in fuel dissolution rate is limited for most nuclides.

Even a completely unrealistic assumption of immediate fuel dissolution has limited effects with otherwise reasonable data. The solubilities of the individual nuclides limit the release. The most important exception is Ra-226, for which the effect only becomes noticeable after more than 100,000 years.

It is urgent to improve our theoretical and experimental understanding of the fuel dissolution process.

Buffer: The effects of uncertainties surrounding the properties of the buffer as regards radionuclide transport are small. Provided that the buffer's long-term evolution is as in the base scenario, our understanding of the buffer's role in radionuclide transport is good.

Backfill: Uncertainties surrounding the influence of the backfill material on the total release of radionuclides from the near field are small. This conclusion must be verified against the results of more detailed analyses of the long-term evolution and general performance of the backfill material. The need for such analyses is pointed out in the discussion of results for the base scenario.

Geosphere: The simplified uncertainty analyses show that the natural variability in the F factor in the geosphere has the greatest effects on the calculation result (maximum dose over 1 million years). Uncertainty in sorption and matrix diffusion properties are also important for retention, but are of less importance than the flow properties. The results point towards important conditions in the bedrock to determine in a site investigation.

The methods for determining the F factor can be improved. Experiments within e.g. the TRUE projects /Winberg ed, 1999/ and simulations with alternative descriptions of the rock can improve the means available for assessing this crucial parameter. This work will most probably show that the pessimistic values currently proposed are much too low.

The fracture structure and hydraulic properties around individual deposition holes are handled pessimistically in SR 97. Among other things, a small fracture has been assumed to intersect each deposition hole directly opposite the breach in the canister's copper shell. No deposition holes have been deselected as a result of the hydraulic calculations. On a real repository site with bored deposition holes, active choices based on observations in the deposition hole and calculations could improve the result of the analysis. By means of active choices on a small scale, large-scale differences between different sites could also be evened out. This would require a selection method that has been shown to work under realistic field conditions.

Biosphere: An important improvement of the data for the analysis ought to be able to be accomplished with an improved biosphere modelling. The conclusion is not really based on the factor of 10 that separates the reasonable values from the pessimistic ones, such differences are probably unavoidable. The assessment is rather that even the reasonable values are probably often greatly overestimated, justifying further work on the biosphere models.

The highest EDFs for many radionuclides are obtained for peatland and agricultural land, which is not in agreement with previous safety assessments such as SITE-94 /SKI, 1996/ and TILA-99 /Vieno and Nordman, 1999/, where the migration pathway via well has been considered to make the dominant dose contribution. The capacities of peat and agricultural land to accumulate radionuclides are the basis of the high EDFs. The modelling of the EDFs in SR 97 is, however, simplified and probably overly pessimistic. It is also questionable whether it is meaningful to calculate dose consequences hundreds of thousands of years into the future. Alternative safety indicators, such as activity releases, may be more meaningful since they make it possible to determine whether the repository will pose a general environmental problem or not.

The risk analysis is carried out using a method that permits probabilistic calculations, despite a limited body of statistics. It is urgent that the method be evaluated for coming assessments.

Environmental protection

According to the Swedish Radiation Protection Institute's regulations, the impact of the repository on surrounding ecosystems shall also be described. No specific methods for this are available today.

In most calculations cases in the canister defect scenario, the doses are many orders of magnitude below the natural background radiation. Based on this, the general assessment is made that the ecosystems at Aberg, Beberg and Ceberg are not adversely affected by the radionuclide migration in the canister defect scenario.

9.12 References

Ahlbom K, Andersson J-E, Andersson P, Ittner T, Ljunggren C, Tirén S, 1992. Finnsjön Study Site. Scope of activities and main results.
SKB TR-91-08. Svensk Kärnbränslehantering AB.

Agrenius L, 1999. Kriticitetsförhållandena i kapslar för slutförvaring av använt kärnbränsle.
SKB R-99-52. Svensk Kärnbränslehantering AB.

Allard B, Karlsson F, Neretnieks I, 1991. Concentrations of particulate matter and humic substances in deep groundwaters and estimated effects on the adsorption and transport of radionuclides.
SKB TR-91-50. Svensk Kärnbränslehantering AB.

Amaya T, Chiba T, Suzuki K, Oda C, Yoshikawa H, Yui M, 1997. Solubility of Sn(IV) oxide in dilute NaClO4 solution at ambient temperature. Mat. Res. Soc. Symp. Proc. Vol 465. pp 751–758.

Andersson J, Elert M, Hermansson J, Moreno L, Gylling B, Selroos J O, 1998. Derivation and treatment of the flow wetted surface and other geosphere parameters in the transport models FARF31 and COMP32 for use in safety assessment. SKB R-98-60. Svensk Kärnbränslehantering AB.

Andersson J, Riggare P, Skagius K, 1998a. Project SAFE – Update of the SFR-1 safety assessment Phase 1.
SKB R-98-43. Svensk Kärnbränslehantering AB.

Andersson J, Riggare P, Skagius K, 1998b. Project SAFE – Update of the SFR-1 safety assessment Phase 1 Appendices.
SKB R-98-44. Svensk Kärnbränslehantering AB.

Antilla, 1992. Spent fuel characateristics for TVO-92 safety analysis. Report YJT-92-03. Nuclear Waste Commission of Finnish Power Companies, Helsinki, Finland (in Finnish).

Bergman B, Walker D, 1998. The relationship between stochastic anisotropy and hydraulic anisotropy: Numerical experiments using HYDRASTAR 1.7.2.
SKB U-98-12. Svensk Kärnbränslehantering AB.

Bergström U, Edlund O, Evans S, Röjder B, 1982. BIOPATH – A computer code for calculation of the turnover of nuclides in the biosphere and the resulting doses to man.
STUDSVIK/NW-82/261, Studsvik AB, Sverige.

Bergström U, Nordlinder S, Aggeryd I, 1999. Models for dose assessments – Modules for various biosphere types.
SKB TR-99-14. Svensk Kärnbränslehantering AB.

Berner U, 1994. Kristallin-I: Estimates of solubility limits for safety relevant radionuclides. NAGRA Technischer Bericht NTB 94-08. NAGRA, Switzerland.

BIOMOVS, 1993. Final report. BIOMOVS Technical report 15, SSI, Stockholm.

BIOMOVS II, 1996. An overview of the BIOMOVS II study and its findings, TR17. Swedish Radiation Protection Institute (SSI), Stockholm.

Birgersson L, Neretnieks I, 1988. Diffusion in the Matrix of Granitic Rock. Field Test in the Stripa Mine. Final Report.
SKB TR-88-08. Svensk Kärnbränslehantering AB.

Blackwood D J, Hoch A R, Naish C C, Rance A A, Sharland S M, 1994. Research on corrosion aspects of the Advanced Cold Process Canister.
SKB TR-94-12. Svensk Kärnbränslehantering AB.

Bond A E, Hoch A R, Jones G D, Tomczyk A, Jiggin R M, Worraker W J, 1997. Assessment of a spent fuel disposal canister. Assessment studies for a copper canister with cast steel inner component.
SKB TR-97-19. Svensk Kärnbränslehantering AB.

Bruno J, Cera E, de Pablo J, Duro L, Jordana S, Savage D, 1997. Determination of radionuclide solubility limits to be used in SR 97. Uncertainties associated to calculated solubilities.
SKB TR-97-33. Svensk Kärnbränslehantering AB,.

Bruno J, Cera E, Duro L, Pon, J, de Pablo J, Eriksen T, 1998. Development of a kinetic model for the dissolution of the UO2 spent nuclear fuel. Application of the model to the minor radionuclides.
SKB TR-98-22. Svensk Kärnbränslehantering AB.

Carbol P, Engkvist I, 1995. Sorption och sorptionsmodeller – Tillämpningar och begränsningar i säkerhetsanalys.
SKB AR-95-26. Svensk Kärnbränslehantering AB.

Carbol P, Engkvist I, 1997. Compilation of radionuclide sorption coefficients for performance assessment.
SKB R-97-13. Svensk Kärnbränslehantering AB.

Carslaw H S, Jaeger J C, 1959. Conduction of heat in solids. New York, Oxford University Press, pp 336.

Carver M B, Hanley D V, Chaplin K R, 1979. ”Macksima-Chemist”. A program for mass action kinetics simulation by automatic chemical equation manipulation and integration using stiff techniques, AECL 6413.

Dershowitz B, Follin S, Andersson J, Eiben T, 1999. SR 97 Alternative Models Project: Discrete fracture network modeling for performance assessment of Aberg. SKB R-99-43. Svensk Kärnbränslehantering AB.

Draganic Z D m fl, 1991. Radiat. Phys: Chem, Vol 38, No 2, 1991, 317–21.

Ek J, Evans S, Ljungqvist L, 1982. Variation in radioactivity, uranium and radium-226 contents in three radioactive springs and along their out-flows in northern Sweden.. SKBF/KBS TR-82-13. Svensk Kärnbränsleförsörjning AB.

Elert M, Neretnieks I, Kjellbert N, Ström A, 1992. Description of the transport mechanisms and pathways in the far field of a KBS-3 type repository. SKB TR-92-09. Svensk Kärnbränslehantering AB.

Elert M, 1997. Retention mechanisms and the flow wetted surface – implications for safety analysis. SKB TR-97-01. Svensk Kärnbränslehantering AB.

Elert M, 1999. The Äspö Task Force on Modelling of Groundwater Flow and Transport of Solutes. Evaluation of modelling of radially converging and dipole tests with conservative tracers (TRUE-1 Tasks 4C and 4D). SKB TR-99-04. Svensk Kärnbränslehantering AB.

Eriksen T, 1996. Radiolysis of water within a ruptured fuel element. SKB PR U-96-29. Svensk Kärnbränslehantering AB.

Eriksen T, 1999. Radiolysis of water within a ruptured fuel element. SKB TR-99-XX (in preparation). Svensk Kärnbränslehantering AB.

Follin S, 1999. Hydrogeological boundary settings in SR 97. Uncertainties in regional boundary settings and transfer of boundary conditions to site-scale models. SKB R-99-45. Svensk Kärnbränslehantering AB.

Gardner R H, Röjder B, Bergström I, 1983. PRISM – A systematic method for determining the effect of parameter uncertainities on model predictions. STUDSVIK/NW-83/555, Studsvik AB.

Gimenez L, 1996. Dissertation, Universitat de Barcelona.

Gnirk P, 1993. OECD/NEA International Stripa Project. Overview volume II. Natural barriers. Svensk Kärnbränslehantering AB.

Gustafson G, Ström A, 1995. The Äspö Task Force on Modelling of Groundwater Flow and Transport of Solutes. Evaluation report on Task No 1, the LPT2 large scale field experiments. SKB ICR 95-05. Svensk Kärnbränslehantering AB.

Gylling B, Walker D, Hartley L, 1999a. Site-scale groundwater flow modelling of Beberg. SKB TR-99-18. Svensk Kärnbränslehantering AB.

Gylling B, Moreno L, Neretnieks I, 1999b. SR 97 Alternative Models Project: Performance assessment using CHAN3D.
SKB R-99-44. Svensk Kärnbränslehantering AB.

Hartley L, Boghammar A, Grundfelt B, 1998. Investigation of the large scale regional hydrogeological situation at Beberg.
SKB TR-98-24. Svensk Kärnbränslehantering AB.

Hedin A, 1997. Spent nuclear fuel – how dangerous is it? A report from the project "Description of risk".
SKB TR-97-13. Svensk Kärnbränslehantering AB.

Hedin A, 1999. An analytic model for radionuclide releases in the near-field.
SKB Internal PM 1999. Svensk Kärnbränslehantering AB.

Hicks T W, Green T H, 1999. A Review of the treatment of Criticality in Post-Closure Safety Assessment of Radioactive Waste Disposal.
Environment Agency R&D Technical Report P222.

Hofmann B A, 1989. Geochemical analogue study in the Krunkelbach mine, Menzenschwand, Southern Germany: geology and water-rock interaction.
Materials Research Society, Proceedings 127, XII, pp 921–926.

Horseman, S T, Harrington J F, Sellin P, 1997. Gas migration in MX80 buffer bentonite.
Mat. Res. Soc. Symp. Proc. Vol 465. pp 1003–1010.

Johansson H, Byegård J, Skarnemark G, Skålberg M, 1996. Matrix diffusion of some alkali- and alkaline earth-metals in granitic rock. Proceedings Materials Research Society, Scientific Basis for Nuclear Waste Management, 1996 Fall Meeting, Boston, Massachusetts.

Johnson L H, Tait J C, 1997. Release of segregated nuclides from spent fuel.
SKB TR-97-18. Svensk Kärnbränslehantering AB.

Kersting A B, Efurd D W, Finnegan D L, Rokop D K, Thompson J L, 1999. Migration of plutonium in groundwater at the Nevada Test Site. Nature, Vol 397, pp 56–59.

Laaksoharju M, Degueldre C, 1995. Studies of colloids and their importance for repository performance assessment.
SKB TR-95-24. Svensk Kärnbränslehantering AB.

Lindgren M, Widén H, 1998. Discretization in COMP23 for SR 97.
SKB R-98-03. Svensk Kärnbränslehantering AB.

Lindgren M, Lindström F, 1999. SR 97 – Radionuclide transport calculations.
SKB TR-99-23. Svensk Kärnbränslehantering.

Lusczynski N J, 1961. Head and flow of ground water of variable density.
Journal of Geophysical Research, 66(12), 4247–4256.

Marsic N, Hartley L, 1999. Modelling of the site scale hydrogeological situation at Beberg using NAMMU.
SKB R-99-XX (in preparation). Svensk Kärnbränslehantering AB.

Miekeley N, Couthino de Jesus H, Porto da Silveira, Degueldre C, 1992. Chemical and physical characterisation of suspended particles and colloids in waters from Osamu Utsumi mine and Morro do Ferro analogue study sites, Poços de Caldas, Brazil. Journal of Geochemical Exploration, Vol 45, pp 409–437.

Miller W, Alexander R, Chapman N, McKinley I, Smellie J, 1994. Natural analogue studies in the geological disposal of radioactive wastes, Elsevier, Amsterdam.

Moreno L, Gylling B, Neretnieks I, 1995. Solute Transport in Fractured Media. The Important Mechanisms for Performance Assessment.
SKB TR-95-11. Svensk Kärnbränslehantering AB.

Moreno L, Gylling B, 1998. Equivalent flow rate concept in near field transport model COMP23.
SKB R-98-53. Svensk Kärnbränslehantering AB.

Moreno L, 1999. Impact of the water flow rate in the tunnel on the release of radionuclides.
SKB R-99-XX (in preparation). Svensk Kärnbränslehantering AB.

Morris S T, Cliffe K A, 1994. Verification of HYDRASTAR: Analysis of hydraulic conductivity fields and dispersion.
SKB TR-94-21. Svensk Kärnbränslehantering AB.

Munier R, Sandstedt H, Niland L, 1997. Förslag till principiella utformningar av förvar enligt KBS-3 för Aberg, Beberg and Ceberg.
SKB R-97-09. Svensk Kärnbränslehantering AB.

NEA/SKI, 1996. Developing groundwater flow and transport models for radioactive waste disposal. Six years of experience from the INTRAVAL project, OECD Nuclear Energy Agency, Statens kärnkraftinspektion, Stockholm.

NEA, 1999. Confidence in the long-term safety of deep geological repositories. Its development and communication. Nuclear Energy Agency of the Organisation for Economic Cooperation and Development (OECD/NEA).

Neretnieks I, 1979. Transport Mechanism and Rates of Transport of Radionuclides in the Geosphere as Related to the Swedish KBS-Concept, Proc. Symp. Underground Disposal of Radioactive Wastes, Otaniemi, Finland, July 2–6, 1979, Vol II. p 108, International Atomic Energy Agency.

Neretnieks I, 1980. Diffusion in the rock matrix: An important factor in radionuclide retardation?
J Geophysical Research, vol 85, no B8, pp 4379–4397.

Neretnieks I, 1993. Solute transport in fractured rock – Applications to radionuclide waste repositories, in ed Bear J, Tsang C-F, de Marsily G, Flow and Contaminant Transport in Fractured Rock, Academic Press, Inc.

Nordlinder S, Bergström U, Mathiasson L, 1999. Ecosystem specific dose conversion factors for Aberg, Beberg and Ceberg.
SKB TR-99-15. Svensk Kärnbränslehantering AB.

Norman S, Kjellbert N, 1990. FARF31 – A far field radionuclide migration code for use with the PROPER package.
SKB TR-90-01. Svensk Kärnbränslehantering AB.

Norman S, 1991. Verification of HYDRASTAR – A code for stochastic continuum simulation of groundwater flow.
SKB TR-91-27. Svensk Kärnbränslehantering AB.

NRC/SKI, 1999. Regulatory perspectives on model validation in high-level radioactive waste management programs: A joint NRC/SKI White Paper, NUREG-1636, US Nuclear Regulatory Commission.

Ochs M, 1997. Review of a report on diffusion and sorption properties of radionuclides in compact bentonite.
SKB R-97-15. Svensk Kärnbränslehantering AB.

Ohlsson Y, Neretnieks I, 1997. Diffusion data in granite. Recommended values.
SKB TR-97-20. Svensk Kärnbränslehantering AB.

Olin M, Lehikoinen J, 1997. Application of surface complexation modelling: Nickel sorption on quartz, manganese oxide, kaolinite and goethite, and thorium on silica, POSIVA 97-10, Helsinki.

Olsson O, Neretnieks I, Cvetkovic V, 1995. Deliberations on radionuclide transport and rationale for tracer transport experiments to be performed at Äspö. A selection of papers.
SKB HRL PR 25-95-01. Svensk Kärnbränslehantering AB.

Olsson O, Gale J E, 1995. Site assessment and characterization for high-level nuclear waste disposal: results from the Stripa Project, Sweden, Quarterly Journal of Engineering Geology, vol 28, suppl 1, pp S17–S30.

Puigdomenech I, Bruno J, 1991. Plutonium solubilities.
SKB TR-91-04. Svensk Kärnbränslehantering AB.

Punshon C S, 1997. EB welding of thick section copper for nuclear waste encapsulation – Definition of imperfection types and formation mechanisms. 220279/1197, TWI, Abington Hall, Abington, United Kingdom.

Pusch R, Ranhagen L, Nilden K, 1985. Gas migration through MX80 bentonite. NAGRA Technischer Bericht. NTB-85-36. NAGRA, Switzerland.

Rhén I, Gustafson G, Stanfors R, Wikberg P, 1997. Äspö Hard Rock Laboratory – Geoscientific Evaluation 1997/5. Models based on site characterisation 1986–1995.
SKB TR-97-06. Svensk Kärnbränslehantering AB.

Rodwell W, Harris A, Horseman S Lalieux P, Müller W, Ortiz Amaya L, Preuss K, 1999. Gas Migration and Two-Phase Flow through Engineered and Geological Barriers for a Deep Repository for Radioactive Waste. EC/NEA Status Report.

Romero L, 1995. The near-field transport in a repository for high-level nuclear waste, PhD Thesis, TRITA-KET R21, The Royal Institute of Technology, Stockholm, Sweden.

Romero L, Thompson A, Moreno L, Neretnieks I, Widén H, Boghammar A, Thompson A, 1999. COMP23, Nuctran user's guide. PROPER Version 1.1.6.
SKB R-99-XX (in preparation). Svensk Kärnbränslehantering AB.

Ross A B m fl, 1992. NDRL-NIST Solution Kinetics Database Ver. 1.

Saksa P, Nummela J, 1998. Geological-structural models used in SR 97: Uncertainty analysis.
SKB TR-98-12. Svensk Kärnbränslehantering AB.

Shoesmith D, Sunder S, 1992. The prediction of nuclear fuel dissolution rates under waste disposal conditions. J. Nucl. Mater. 190, 20–35.

Skagius K, Neretnieks I, 1985. Porosities and diffusivities of some non-sorbing species in crystalline rocks.
SKB TR-85-03. Svensk Kärnbränslehantering AB.

Skagius K, 1986. Diffusion of dissolved species in the matrix of some Swedish crystalline rocks, PhD Thesis, Department of Chemical Engineering, Royal Institute of Technology, Stockholm, Sweden.

SKB, 1983. Final storage of spent nuclear fuel – KBS-3, IV Safety, SKBF/KBS, Stockholm, Sweden.

SKB, 1992. SKB 91 – Final disposal of spent nuclear fuel. Importance of the bedrock for safety.
Svensk Kärnbränslehantering AB, Stockholm.

SKB, 1995. SR 95 – Template for safety reports with descriptive examples.
Svensk Kärnbränslehantering AB, Stockholm.

SKI, 1996. SKI SITE-94, Deep repository performance assessment project.
SKI Report 96:36. Statens kärnkraftinspektion.

Svensson U, 1997a. A regional analysis of groundwater flow and salinity distribution in the Äspö area.
SKB TR-97-09. Svensk Kärnbränslehantering AB.

Svensson U, 1997b. A site scale analysis of groundwater flow and salinity distribution in the Äspö area.
SKB TR-97-17. Svensk Kärnbränslehantering AB.

Svensson U, 1999. A numerical simulation of the origin and composition of the groundwater below Äspö.
SKB R-99-39. Svensk Kärnbränslehantering AB.

Takase H, Benbow, S, Grindrod P, 1999. Mechanical failure of SKB Spent fuel disposal canisters – mathematical modelling and scoping calculations.
SKB TR-99-XX (in preparation). Svensk Kärnbränslehantering AB.

Tanai K, Kanno T, Gallé C, 1997. Experimental study of gas permeabilities and breakthrough pressures in clays. Mat. Res. Soc. Symp. Proc. Vol 465. pp 995–1002.

Torrero L, 1995. Study of the UO_2 dissolution as a chemical analogue to the spent fuel matrix. Dissertation; Universitat Politeenica de Catalunya, Barcelona.

Vieno T, Hautojärvi A, Koskinen L, Nordman H, 1992. TVO-92 Safety analysis of spent fuel disposal.
YJT-92-33. Technical Research Centre of Finland.

Vieno T, Nordman H, 1999. Safety assessment of spent fuel disposal in Hästholmen, Kivetty, Olkiluoto and Romuvaara, TILA-99. POSIVA 99-07, Posiva Oy, Helsinki, Finland.

Walker D (ed), Eriksson L, Lovius L, 1996. Analysis of the Äspö LPT2 pumping test via simulation and inverse modelling with HYDRASTAR.
SKB TR-96-23. Svensk Kärnbränslehantering AB.

Walker D, Rhén I, Gurban I, 1997. Summary of Hydrogeologic Conditions at Aberg, Beberg and Ceberg.
SKB TR-97-23. Svensk Kärnbränslehantering AB.

Walker D, Gylling B, 1998. Site-scale groundwater flow modelling of Aberg.
SKB TR-98-23. Svensk Kärnbränslehantering AB.

Walker D, Gylling B, 1999. Site-scale groundwater flow modelling of Ceberg.
SKB TR-99-13. Svensk Kärnbränslehantering AB.

VAMP, 1996. Validation of models using Chernobyl fallout data from southern Finland. Scenario S. Second report of the VAMP Multiple Pathways Assessment Working Group.
IAEA-TECDOC-904, International Atomic Energy Agency (IAEA), Vienna.

Werme L, Sellin P, Forsyth R, 1990. Radiolytically induced oxidative dissolution of spent nuclear fuel.
SKB TR-90-08. Svensk Kärnbränslehantering AB.

Werme L O, 1998. Design premises for canister for spent nuclear fuel.
SKB TR-98-08. Svensk Kärnbränslehantering AB.

Widén H, Walker D, 1999. SR 97 Alternative Modelling Project: Stochastic continuum modelling of Aberg.
SKB R-99-42. Svensk Kärnbränslehantering AB.

Wikramaratna R S, Goodfield M, Rodwell W R, Nash P J, Agg P J, 1993.
A preliminary assessment of gas migration from the Copper/Steel Canister.
SKB TR-93-31. Svensk Kärnbränslehantering AB.

Winberg A (ed), 1999. Final report of the first stage of the tracer retention understanding experiments. Äspölaboratoriet.
SKB ICR 99-XX (in preparation). Svensk Kärnbränslehantering AB.

Yu J-W, Neretnieks I, 1997. Diffusion and sorption properties of radionuclides in compacted bentonite.
SKB TR-97-12. Svensk Kärnbränslehantering AB.

10 Climate scenario

10.1 Introduction

The safety assessment covers long periods of time, up to 100,000 years and longer. During these time spans major climate changes are expected. In Scandinavia, long-term climate change has previously led to the extension of permafrost and ice sheets. Changes similar to those in the past are also expected to occur in the future.

The climate scenario includes a brief description of the earth's climate system, and the scope of the climate changes we can expect in a hundred-thousand-year perspective. The outlined future picture is based on a number of relatively simple models.

The description of climatic conditions is based on three so-called climate-driven process domains:

- Temperate/boreal domain.
- Permafrost domain.
- Glacial domain.

Characteristic conditions and how they affect the repository are described within each domain. To give a more detailed picture, the domains are divided into regimes. This subdivision has been done in consideration of those conditions that have the greatest impact on the deep repository. The evolution of the climate is regarded as a variation of the extent of the domains and the regimes in time and space. The climate-driven process domains and the regimes are intended to give a general picture of the conditions. No strict boundaries have been defined between the different domains, in reality the transition between different domains and regimes is gradual.

The influence of climate on repository evolution is primarilydescribed in relation to the base scenario. The purpose is to show how the substantial changes on the surface affect the environment at repository depth. The climate changes will affect radionuclide transport, particularly in the biosphere but also in the geosphere. To investigate the importance of this, a comparison is made with the canister defect scenario.

10.2 Initial state

To analyze how climate changes influence the repository's capacity to isolate the spent fuel, the same initial state is assumed as in the base scenario, i.e. the repository is built according to specifications and all canisters are intact.

For analysis of the influence on radionuclide transport through the repository, the same initial state is assumed as in the canister defect scenario, i.e. a few canisters have fabrication defects and the repository is otherwise built according to specifications.

10.3 Boundary conditions

10.3.1 The earth's climate system

The climate is a description of the meteorological conditions within an area limited in time and/or space. The climate is described via the statistical properties of different climatic parameters such as mean, maximum and minimum values of temperature, humidity, air pressure, wind speed and precipitation.

The earth's climate is dependent on the radiation balance, i.e. the relationship between incoming short-wave solar radiation and outgoing long-wave radiation, and by heat transport via circulation in the atmosphere and the oceans. The predominant reasons why the climate varies over the surface of the earth is that the intensity of insolation (solar irradiance) varies with the latitude, and that continents and seas are heated in different ways by insolation. The climate is a result of this uneven heating and the heat transfer mechanisms to which it gives rise.

The atmosphere, the oceans, continental ice sheets and glaciers, the biosphere and the surface of the lithosphere – all are components in the earth's climate system. The components in the climate system interact with each other and there are numerous feedbacks and dependencies. Externally, insolation and energy from the interior of the earth affect the climate system.

The climate system is very complex and also contains a chaotic element. Its own internal dynamics influence the climate. The state and dynamics of the climate system also determine how the climate will change in response to an external change. The feedback mechanisms within the climate system can reinforce or weaken the effect of an external change. A general description of the climate system and its components is provided in Figure 10-1.

Knowledge of the earth's climate and climate system has increased considerably over the past 20–30 years. Development of sampling and measurement technology has enabled us to access geological and biological proxy records[1] that bear traces of climates in the past. Development of computer technology has made it possible to simulate the climate system. Collection and analysis of climate data has been both expanded and improved. But in spite of this we are still unable to fully describe the earth's climate system and the causes of climate change.

[1] For example loess, stalactites, deep-sea and lake sediments, ice cores and trees contain different types of data that bear witness to the climates of the past. Examples of data are the thickness of deposits and annual rings, and the content and composition of different radioactive and stable isotopes, pollen and trapped gases. A proxy record such as an ice core can contain different types of data.

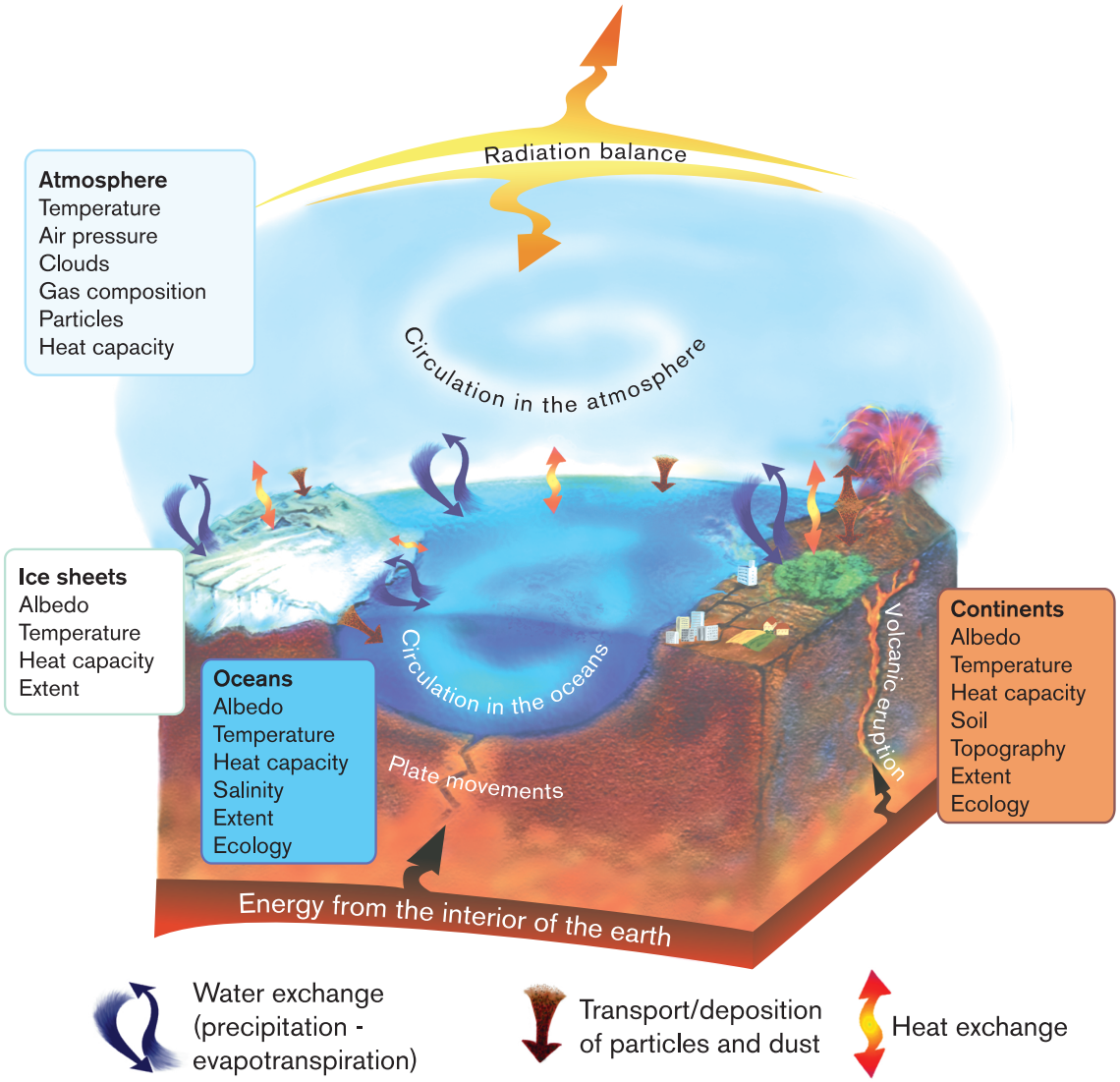

Figure 10-1. *The components of the earth's climate system and some of their properties. The climate is determined by the properties of the components and how they are changed by internal processes and interaction between the parts. Externally the climate system is affected by insolation and energy from the interior of the earth.*

10.3.2 Climate change

Historical climate change has been cyclical, where cycles of different frequency and amplitude have been superimposed. Different geological and biological records show that both large and fast climate changes have occurred in the past. The scope of global temperature changes on different timescales is shown in Figure 10-2.

The climate can change if one of the components in the climate system changes, or due to external causes such as changes in insolation or the impact of energy from the interior of the earth via volcanic eruptions and plate-tectonic movements. Different external and internal changes act over different timespans and can reinforce or counteract each other.

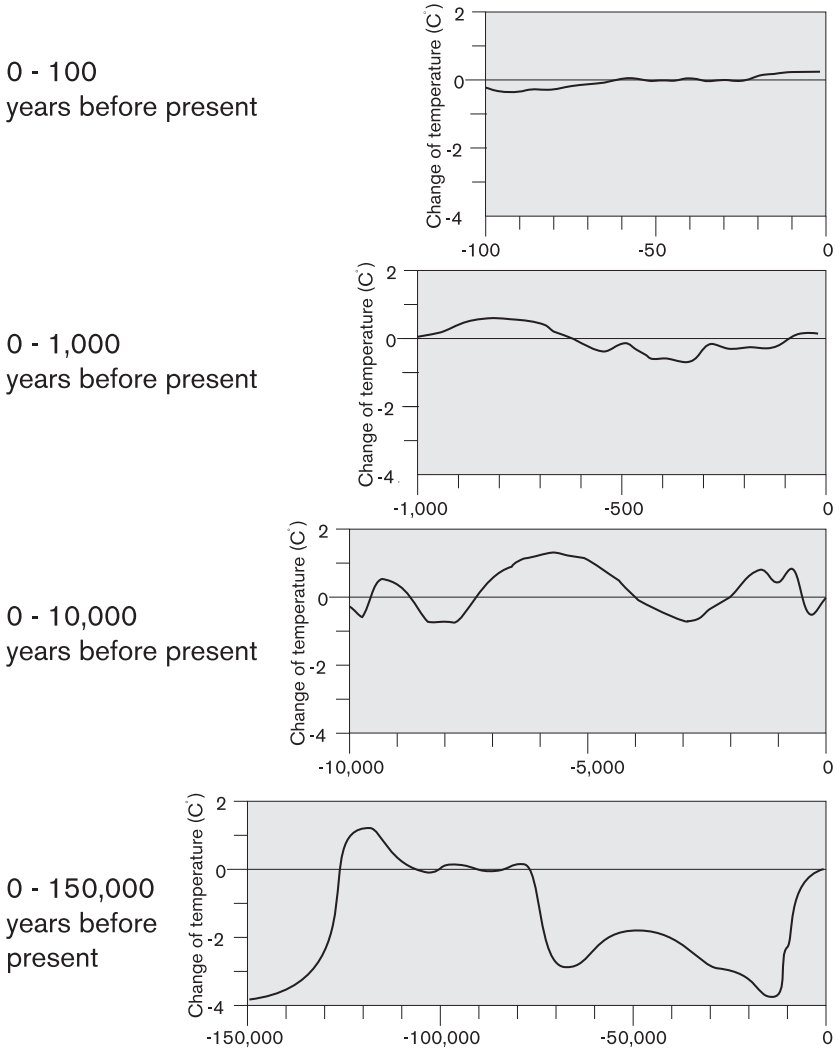

Figure 10-2. *Changes in the global mean temperature on different time scales /revised from Houghton et al, 1990/.*

Insolation varies with the activity of the sun and the earth's orbital parameters. The orbital parameters are orbital eccentricity, i.e. the shape of the earth's orbit around the sun; axial obliquity, i.e. the tilt of the earth's axis; and precession, i.e. the motion of the spinning earth that makes it wobble so that the axis of rotation sweeps out a cone around the vertical /Larsson-Leander, 1977/. Precession affects the season in which the earth makes its closest approach to the sun. The orbital parameters vary cyclically with periods of tens to hundreds of thousands of years /Berger and Loutre, 1991/. The astronomer Milankovitch calculated the variation in the orbital parameters and how they influence insolation. Milankovitch said that the variation in insolation drives climate change on earth /Milankovitch, 1941 (1969) in Berger, 1988/.

Since the 1940s when Milankovitch published his theory of climate change, several geological records that cover long timespans have become available. An important category of records is the collection and analysis of deep-sea sediments that was done in SPECMAP (Spectral Mapping Project) /Imbrie et al, 1984/. The ratio between the stable oxygen isotopes O-18 and O-16 in the fossil plankton remains present in deep-sea sediments reflects the volume of water that has been bound in ice sheets all over the world. Variations in the ratio between the oxygen isotopes are called $\delta^{18}O$. High $\delta^{18}O$

values reflect a cold climate and low values indicate a warm climate[2]. Signal analysis of the variation of the $\delta^{18}O$ values reveals the same dominant periodicities as the orbital parameters. A linear relationship exists between the $\delta^{18}O$ variation and the effects of precession and axial obliquity. The variations are periodic with dominant periodicities of around 20,000 and 40,000 years, respectively. These two periodicities dominate the variation of insolation. The $\delta^{18}O$ spectrum, on the other hand, is dominated by periodicities of around a hundred thousand years. Orbital eccentricity has a similar periodicity, but with very little importance for insolation. The ratio between $\delta^{18}O$ and eccentricity is non-linear /Hays et al, 1976/. The variation of $\delta^{18}O$ and insolation during the past 700,000 years is shown in Figure 10-3.

Today most climate researchers are of the opinion that it is variations in insolation due to variations in orbital parameters that cause the quaternary fluctuations between global warm and cold periods. Variations in insolation cannot, however, completely explain the climate changes revealed by the geological records; some kind of internal reinforcement mechanism must exist in the climate system. This is particularly true with regard to the hundred-thousand-year cycle that has dominated the past 400,000–900,000 years /Holmgren and Karlén, 1998/.

The internal dynamics and response times of the components influence the response of the climate system to an external change. The variations of insolation tell us roughly when we can expect major climate changes. To describe the scope of the climate changes, we also need a description of the climate system's response to the external change. The variation of insolation can be calculated with high precision, but lack of knowledge of the climatic system makes simulations of the corresponding climate changes very uncertain.

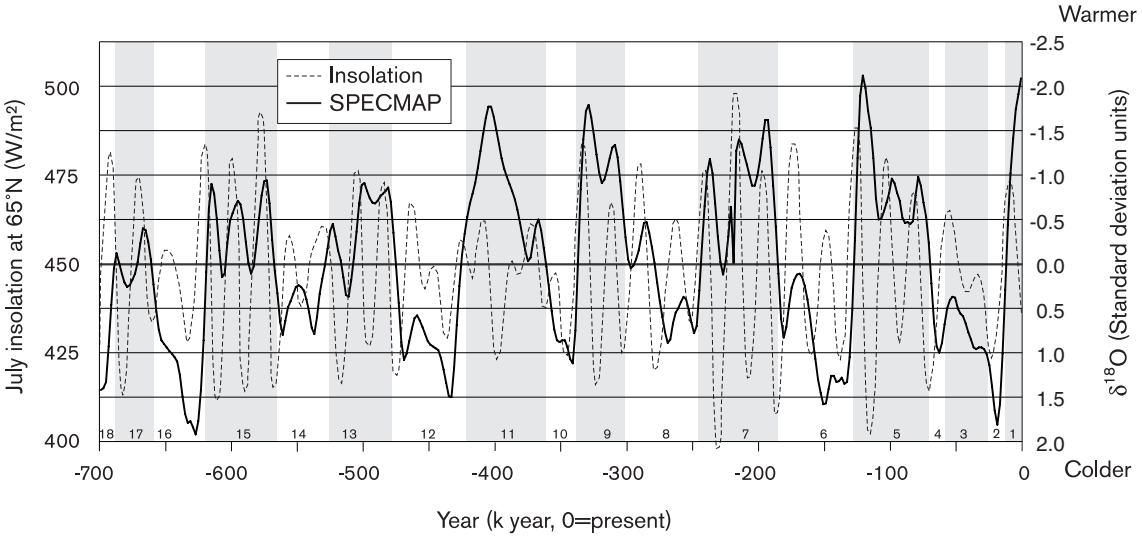

Figure 10-3. *$\delta^{18}O$ variations from 5 drill cores of deep-sea sediment expressed as number of standard deviations /from Imbrie et al, 1984/ and variation of insolation in July at 65°N /from Berger and Loutre, 1991/. The grey and white fields and the figures at the bottom edge indicate cold and warm periods, called isotopic stages /according to Imbrie et al, 1984/.*

[2] In a cold climate, the fraction of the heavier oxygen isotope, O-18, in the oceans increases. The lighter isotope, O-16, evaporates more easily and is bound in snow and ice in the ice sheets. The ratio between the oxygen isotopes is expressed in parts per mil, normally in accordance with a standard (SMOW) as $\delta^{18}O = (R_{sample}/R_{ref} - 1)*1000$ where R_{sample}= O-18/O-16 in the sediment and R_{ref} is a reference value for the same ratio.

10.3.3 A climate scenario for the next 150,000 years

In order to evaluate the influence of climatic conditions on the deep repository, a climate scenario has been formulated /Morén and Påsse, 1999/. The climate scenario is based on descriptions of past climatic evolution, and on model calculations of future conditions. It is primarily intended to describe the evolution during the next 150,000 years, but in essence describes climatic evolution during even longer time.

During the Quaternary Period, the past 2 million years, the earth's climate has been characterized by global cold periods when continental ice sheets and glaciers have extended. The cold periods have been interrupted by shorter warm periods with a climate similar to the current. The cold periods are termed glacials and the warm periods are termed interglacials. The glacials contain colder and warmer stages called stadials and interstadials, respectively. The palaeoclimatological subdivision into cold and warm periods is based on analysis of $\delta^{18}O$ in deep-sea sediments (Figure 10-3) /Imbrie et al, 1984; Martinson et al, 1987/. The subdivision reflects breakpoints in these data series, which reflect the global ice volume. The result, a division into isotopic stages, can be seen as a timescale of global climate change. A transition between a glacial (cold period) and an interglacial (warm period) is thus not the same as a transition between ice-covered and ice-free conditions in Scandinavia. At the transition to the current interglacial period for example, which has been dated to 12,000 years ago, large parts of Sweden were still covered by ice. During a period termed interglacial (warm period), it is thus possible that the glacial domain may prevail in parts of Sweden. Similarly, conditions in parts of the country may be temperate/boreal during stadials (cold periods).

During the past 900,000 years or so, a cyclic pattern with approximately 100,000-year-long glacials, abruptly terminated by a transition to a warm interglacial climate, is repeated. The stadials towards the end of the glacials tend to be the coldest. They end suddenly in a rapid transition to interglacial conditions. This "sawtooth pattern" with a gradually increasingly colder climate followed by a rapid transition to warm conditions is especially pronounced during the past 400,000 years, see Figure 10-3.

During glacial periods the extent of the Scandinavian ice sheet has varied. During warmer periods, interstadials, the extent of the ice cover may have been limited to the Caledonian mountains. Southeast of the ice sheet, conditions may have gradually changed from permafrost to temperate/boreal. During cold stages, stadials, the ice may have covered large parts of Sweden and Finland, and during the extremes of cold the ice sheet has advance as far as Russia in the east and Germany and Poland in the south.

Man influence climate by land use and by emissions of greenhouse gases. Analysis of an ice core from Antarctica shows that the present-day atmospheric concentrations of the greenhouse gases carbon dioxide and methane are the highest at any time during the past 420,000 years. The present-day concentrations are extremely high and seem to have been unprecedented during the analysed period /Petit et al, 1999/. Neither the importance of human activities for the high levels of greenhouse gases nor their impact on earth climate have however been determined.

The intention of the SR 97 climate scenario /Morén and Påsse, 1999/ is to describe the course of events during a glacial-interglacial cycle. The characteristic changes that can be seen during such a cycle can be expected to be repeated very far into the future, even though dominant periodicity and scope may vary. A process that could break the cyclic pattern of the Quaternary glacials is plate-tectonic movements, which may change the continents and their positions so that the heat transfer mechanisms in the atmosphere and oceans are radically affected. This evolution takes place over a time span of several hundred thousand to millions of years.

The scenario of the future ice sheet extent is based on simulations with three models and reconstructions of the conditions during the most recent glacial period, the Weichsel /Mangerud, 1991/. The models are in this report referred to as the ACLIN model, the Imbrie & Imbrie model and the LLN model. The ACLIN (Astronomical Climate Index) model /Kukla et al, 1981/ calculates a global climate index. It is a simple model that directly correlates variations in insolation to climatic conditions. The Imbrie & Imbrie model /Imbrie and Imbrie, 1980/ calculates the global ice volume. It contains a simple model of the ice sheet dynamics, and simulates the ice volume variations corresponding to changes in insolation. Finally, in the LLN model (Lowain-la-Neuve two-dimensional northern hemisphere climate model) /Gallée et al, 1991; Gallée et al, 1992/, a two-dimensional simulation of the northern hemisphere climate is carried through. Calculated climate data are used as input data to an ice sheet model that is coupled to the climate model. The extent of the ice sheets in the northern hemisphere is calculated. This provides new boundary conditions for a simulation of the climate system, which in turn provides new climate data for the ice sheet model, and so on.

During the next 50,000 years the variations in insolation will be small, the smallest during the past three million years /Berger et al, 1996/. This is reflected in the results from the LLN model, which provides a simple but relatively comprehensive description of the climate system, by a weak response in the northern hemisphere ice volume /Berger et al, 1996; Berger and Loutre, 1997/. The two other – older and simpler – models indicate a colder climate during this period. All models reconstruct conditions during the last glacial period, the Weichsel, relatively well. The scenario presented here is a subjective weighing-together of results from the models and the evolution during the Weichsel /according to Mangerud, 1991/. Three warm and three cold periods are predicted. During the last of the warm periods interglacial conditions are assumed. Between the warm periods, the ice is presumed to expand over Scandinavia, and during the last and most sever cold period it is assumed to reach as far as to northern Germany and Poland.

To provide a geographic picture of the evolution, the assumed ice sheet extent has been used as input to a model that calculates the shoreline displacement. The model is based on empirical data and simulates the isostatic (crustal subsidence and uplift) as well as the eustatic (change in sea level) component of shoreline displacement /Påsse, 1996; Påsse, 1997; Morén and Påsse, 1999/. Furthermore, a model that simulates the Scandinavian ice sheet has been used to estimate the extent of the different climate-driven process domains /Boulton and Payne, 1992/. A subjective assessment of the extent of permafrost has been made based on results from this model, and the current conditions in North America /French, 1996/.

The conditions that prevail in the biosphere during a given period are influenced by the preceding evolution. The soil is affected by previous glaciations, by permafrost and by whether the site has been covered with water. The vegetation is both influenced by and influences the soil /Fredén, 1994/. A schematic drawing of the change in the vegetation with the distance from the ice – in both time and space – is shown in Figure 10-4.

A schematic illustration of the assumed evolution during the next glacial-interglacial cycle is shown in Figure 10-5. The upper part of the figure shows how the radioactivity in the spent fuel declines during the same period. At the outset of the next interglacial, the activity has declined to a level that corresponds to the activity in the quantity of natural uranium that was once used to fabricate the fuel. A general description of the scenario is given in Table 10-1. Finally, Figure 10-6 shows the assumed ice sheet extent and the calculated shoreline for the glacial's three warm and cold maxima.

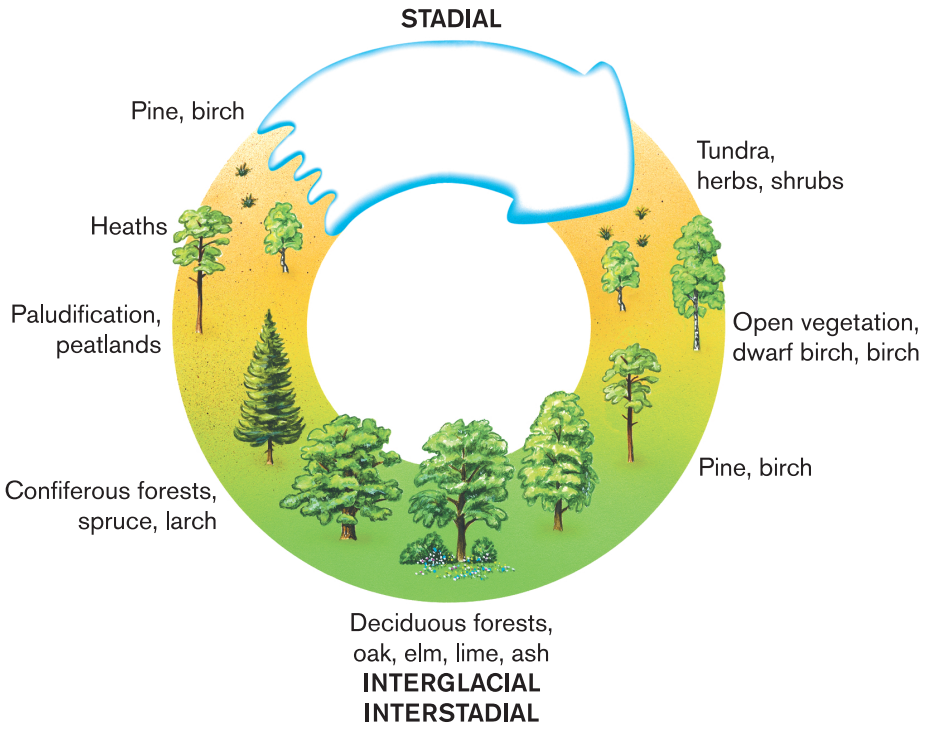

Figure 10-4. *The vegetation changes with the distance from the ice in both time and space. The vegetation stages succeed one another. Their length can vary between a hundred and more than ten thousand years, and the extent can vary from limited areas to virtually the entire surface of the country.*

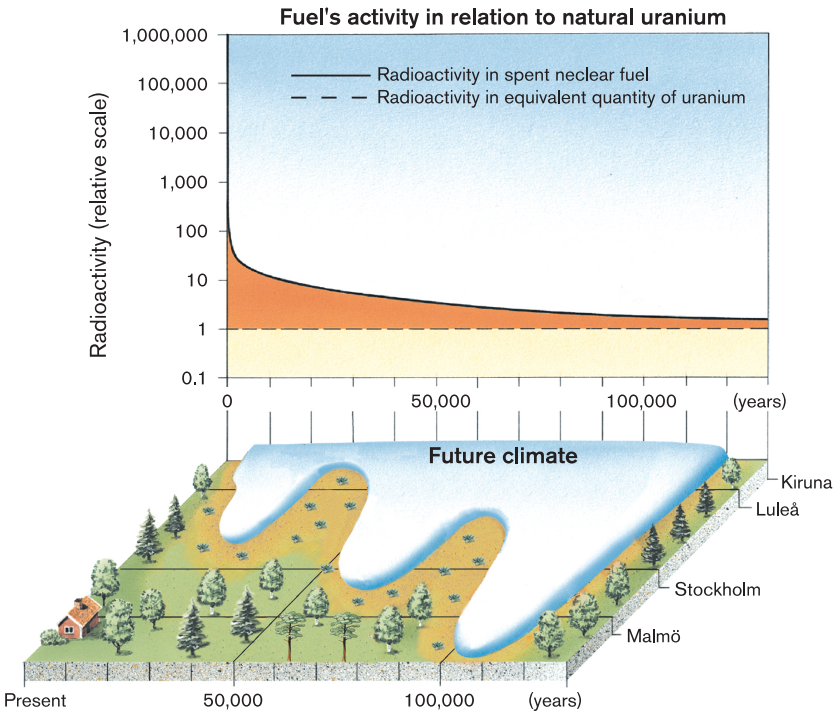

Figure 10-5. *Top part: The radioactivity of the spent fuel as a function of time. The activity is shown in relation to the radioactivity in the quantity of uranium that is needed to fabricate the fuel. Bottom part: Schematic illustration of ice sheet extent and vegetation up to and including the next interglacial period.*

Table 10-1. A scenario for climate-related conditions during the next 150,000 years (0 = present) /Morén and Påsse, 1999/.

Period (thousand years)	Climate-related conditions
0–5	– Conditions similar to today's.
5–20	– Cold period, it gets gradually colder, towards the end of the period about 8°C colder than today. – The relative shoreline (see section 10.3.4) falls first, but then rises when the ice sheet starts to grow. – The ice sheet starts to grow in the mountains in about 5,000 years. – Permafrost can occur in front of the advancing ice sheet.
20–30	– The period's glacial maximum is reached. – The ice sheet reaches the present-day Baltic Sea coast and the southern parts of Dalarna. – Permafrost exists down towards the Baltic coast in the north and on parts of the Småland highland. – The earth's crust is depressed, the Lake Mälaren Valley and large parts of the present-day Baltic coast are under water.
30–40	– Warm period, the climate grows rapidly warmer but is still slightly colder than today, with temperatures a degree or so lower than today's. – The permafrost thaws. – The ice sheet melts, with the exception of some residues in the Caledonides. – The relative shoreline falls, but large areas along the Baltic coast are still beneath the sea.
40–60	– A new cold period begins, towards the end of the period it is about 10°C colder than today. – The ice sheet advances towards the southeast. – The relative shoreline rises, and a connection may be opened between the Lake Mälaren Valley and the Kattegat. – Permafrost may occur in front of the ice sheet. Towards the end of the period, only the west coast and the southern Baltic coast are free of permafrost.
60–70	– The cold period reaches its maximum, the ice sheet covers Finland and reaches the area south of present-day Lake Vättern. – The land is depressed, only currently high-lying parts of the ice-free areas lie above the surface of the sea. – Permafrost prevails in parts of the country not covered by ice or sea.
70–80	– Warm period, it gets milder but is still around 5°C colder than today. – The ice retreats relatively rapidly to an extent slightly less than during the period 20,000–30,000 years. – The relative shoreline falls but large parts of the Lake Mälaren Valley and the present-day Baltic Sea coast are still under water. – The permafrost thaws.
80–100	– New cold period, towards the end of the period around 12°C colder than today. – The ice sheet advances. – As the ice sheet grows, the relative shoreline rises. – Permafrost occurs in front of the advancing ice sheet.
100–110	– The cold period's and the cycle's glacial maximum is reached. – The ice sheet covers the entire country and extends into Russia and down into northern Poland and Germany.
110–130	– Interglacial, it grows rapidly warmer. – The ice sheet retreats to its present-day extent. – The permafrost thaws. – The shoreline is still slightly higher than today. – The warmest period occurs around 120,000 years with temperatures like today's or slightly higher.
130–150	– A new glacial cycle begins. – Ice sheet and permafrost once again expand from the Caledonides. – Towards the end of the period, the ice sheet has roughly the same extent as at its maximum during the period 60,000–70,000 years.

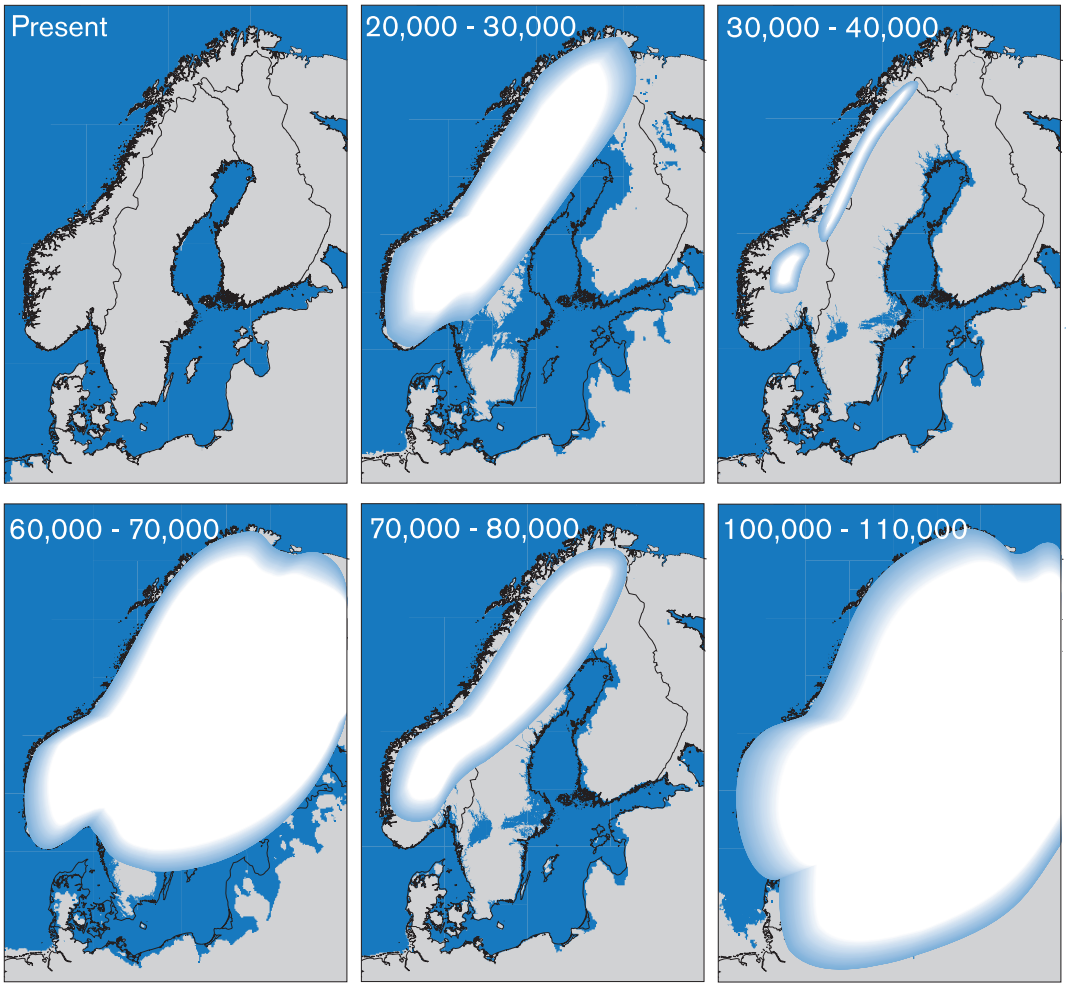

Figure 10-6. *Assumed ice sheet extent and shoreline in conjunction with the glacial's warm and cold maxima.*

10.3.4 Temperate/boreal domain

The temperate/boreal climate-driven process domain is characteristic of interglacials (warm periods). At present, temperate conditions in principle prevail from Skåne in the south of Sweden to the Dalälven River in the north. Boreal – cold temperate – conditions prevail north of the Dalälven. During interstadials (mild periods during a glacial), temperate/boreal conditions exist in the southern parts of the country and – if the climate is warm enough – in the eastern parts as well. Areas with boreal conditions can also occur during less harsh stadials (cold periods during a glacial).

The temperate climate is humid, i.e. precipitation is greater than evapotranspiration. The temperature during the warmest month is higher than 10ºC. In warm temperate areas the temperature in the coldest month is higher than –3ºC, while in cold temperate – boreal – areas it is below –3ºC /Liljequist, 1975/. The humid climate gives rise to high groundwater levels, and the groundwater table follows the topography.

The moist climate provides good conditions for vegetation and fauna. Plants are established quickly and prevent erosion. The natural vegetation is dominated by coniferous forests in cold temperate areas and deciduous forests in warm temperate

areas. Wetlands are widespread; today, 21 percent of Sweden's surface consists of wetlands. The rich vegetation and the good supply of water ensure a rich but seasonally varying fauna with insects, rodents, birds and large mammals. It also provides good conditions for agriculture, especially in areas where the soil strata have been deposited beneath a sea or lake. The productivity of agriculture is limited by the cold seasons. In coastal areas, the biosphere is influenced by shoreline displacement as well as by the salinity of the surrounding sea or lake.

Even under temperate/boreal conditions, the land is influenced by previous glaciations. The ice load depresses the earth's crust, which then strives to resume its original shape during ice-free periods. The process is slow in relation to the advance and retreat of the ice sheet, which means that the earth's crust is in constant motion. This is apparent above all in coastal areas, where the shoreline is displaced when the land rises and subsides (crustal upwarping/downwarping). Shoreline displacement is also affected by changes in sea level. Upon transition to a colder climate, the sea level falls due to the fact that water is bound in continental ice sheets. The opposite occurs when the climate gets warmer. The level of the sea is also affected by the fact that the density of the water is temperature-dependent /Boulton et al, 1999a/.

Climate-related factors that can influence the conditions at a repository are:

- Temperature and precipitation.
- Direction and rate of land uplift and shoreline displacement.
- Salinity of the Baltic Sea.

The long-term change of temperature within the temperate/boreal domain is covered by the variations we can see today between different parts of the country /Frenzel et al, 1992; Raab and Vedin, 1995/. When the ice retreats or advances over an area, both crustal upwarping and downwarping and raising/lowering of the sea level will take place much faster than today and will cause a rapid shoreline displacement. To shed light on this, the temperate/boreal domain is divided into a preglacial, an interglacial and a postglacial regime.

Conditions during the interglacial regime are described in the base and canister defect scenarios. Shoreline displacement during the preglacial regime differs from the interglacial, and the climate is colder than today. The postglacial regime is characterized by a rapid lowering of the shoreline, while the climate may be like today or colder/warmer than today. The shoreline displacement influences the Baltic Sea's connections with Kattegat/Skagerrak and thereby its salinity. As long as the Baltic Sea is a semi-enclosed sea, however, its salinity is affected more by variations in precipitation than by the depth of Öresund and the Belts /Westman et al, 1999/.

When an ice sheet grows, it depresses the earth's crust. At the same time, water is bound in the ice, lowering the sea level. In Sweden, the depression or downwarping of the earth's crust is generally greater than the lowering of the sea level. The sea level relative to a fixed point on the earth's crust – the relative sea level or relative shoreline – thus rises during a glaciation as the earth's crust is depressed. Far from the central parts of the ice sheet, downwarping is less and sea level lowering – the eustatic component of shoreline displacement – is of greater importance. Near the central parts of the ice, downwarping – the isostatic component – dominates /Boulton, 1990 in Boulton et al, 1999a/. A generalized picture of the displacement of relative sea level before and after the last glacial maximum is shown in Figure 10-7.

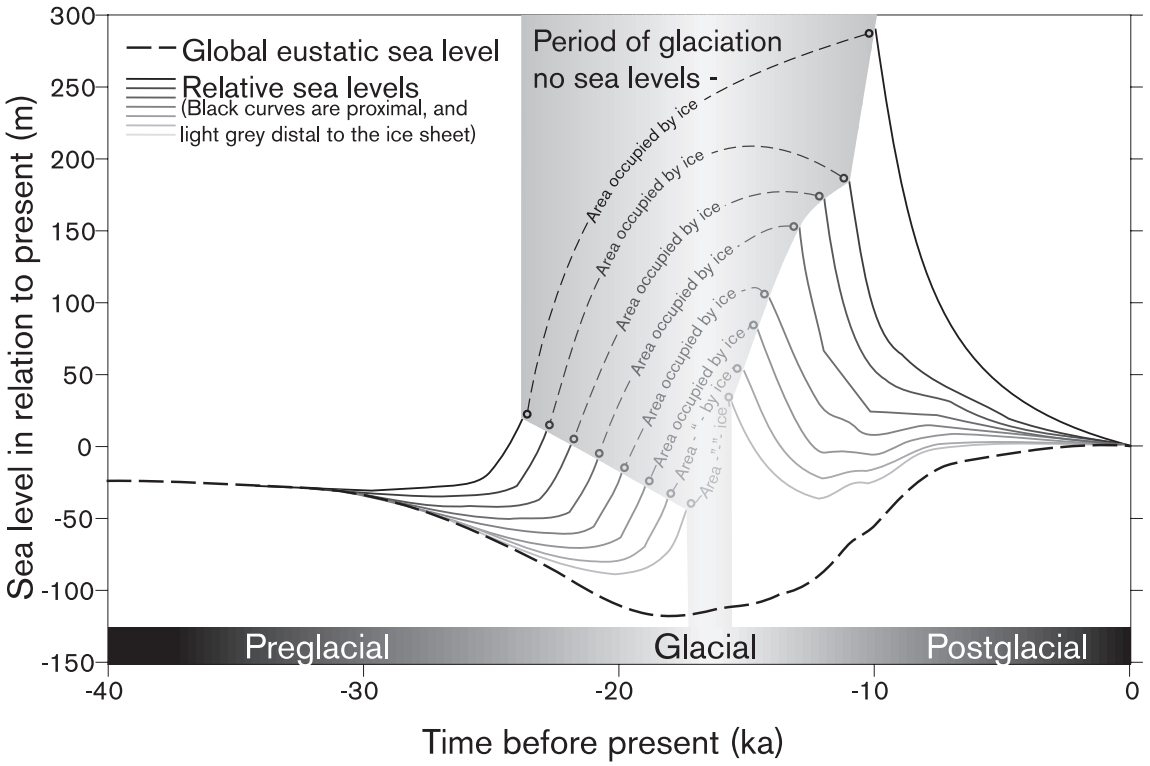

Figure 10-7. *Generalized picture of the change of the relative shoreline in the vicinity of the Scandinavian ice sheet before and after the last glacial maximum. The grey area, where the curves are linked together by dashed lines, represents the period when the area is covered with ice /from Boulton et al, 1999a/.*

The evolution during the preglacial regime is described in the left-hand portion of Figure 10-7, and in Figure 10-8. Initially regression takes place, i.e. a lowering of the relative shoreline. This is due to the fact that the sea level falls when the continental ice sheets grow all over the world, and because the density of the water increases as the temperature falls. As the Scandinavian ice sheet grows, the earth's crust is depressed and the regression becomes a transgression, i.e. the relative shoreline rises. The transgression is greatest in areas near the central parts of the ice sheet and decreases with distance from the ice sheet. During periods of regression, erosion may be considerable since the climate is cold and it may take time for the vegetation to become established /Boulton et al, 1999a/.

The evolution during the postglacial regime is described schematically in the right part of Figure 10-7, and in Figure 10-9. In the initial stage of the postglacial regime, the relative shoreline reaches its highest levels – the earth's crust is still depressed and the sea level rises. The crust rises rapidly, more rapidly than the sea level rises, and the relative shoreline falls. When the ice sheets melt, the sea level rise ceases while the earth's crust keeps rising, although at a declining rate.

The schematic pictures drawn above are complicated by the fact that the Baltic Sea is semi-enclosed sea. Periodically it may be cut off from the global oceans when sounds are closed off due to regression. During other periods, transgression may transform sounds or land areas into open connections with the global oceans. The ice sheet itself can cut off the connection to the oceans and so-called ice-dammed lakes are formed.

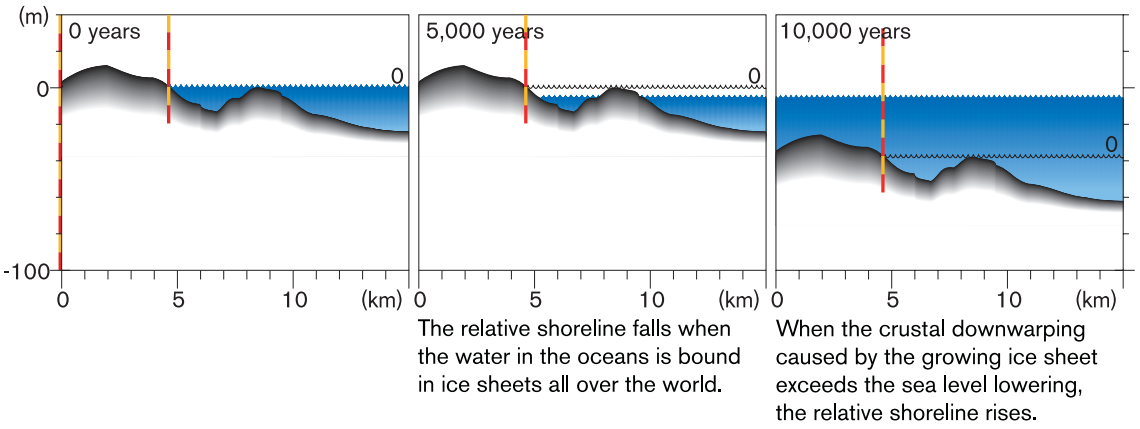

Figure 10-8. *Evolution during the preglacial regime.*

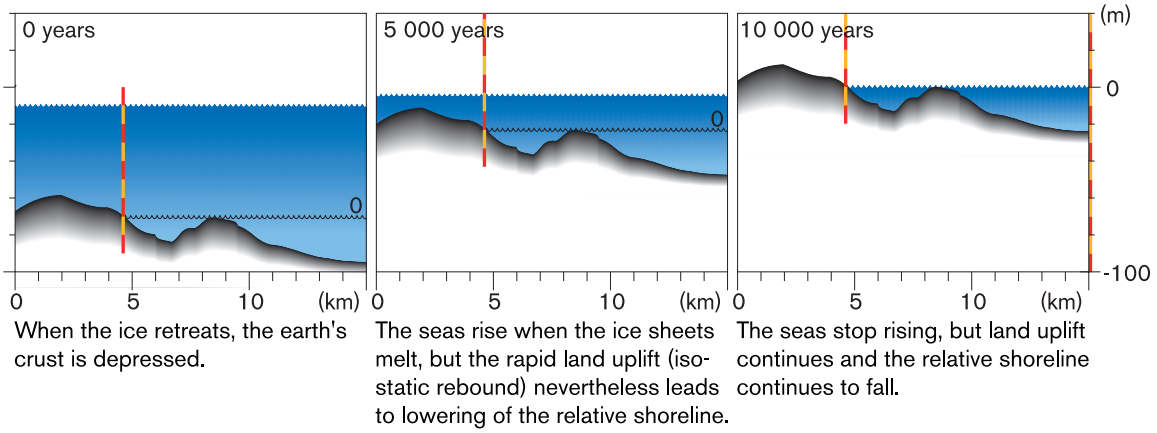

Figure 10-9. *Evolution during the postglacial regime.*

10.3.5 Permafrost domain

The permafrost domain comprises areas of permafrost where the groundwater flow is not affected by the presence of the ice sheet. During interglacials, permafrost occurs in the Caledonian Mountains. During interstadials, permafrost may exist in the northern parts of Sweden. During colder periods and when the ice sheet is expanding, the permafrost domain may also prevail in the central and southern parts of the country.

Permafrost is defined on the basis of temperature. Permafrost exists in areas where the ground temperature is below 0ºC for at least two consecutive years, i.e. at the start of the second year's cold period there are sectors where the temperature has been below 0ºC since the preceding cold period. A temperature of 0ºC does not necessarily mean that the ground is frozen, since the freezing point for water in soil and rock may be lower. At the surface of the permafrost there is a layer with a thickness of between 10 cm and a couple of meters that freezes and thaws annually. It is called the active layer. If the freezing point is below 0ºC, the active layer comprises the uppermost level of the permafrost /French, 1996/.

Today, permafrost exists at high altitudes and latitudes. Since it can take thousands of years for permafrost to thaw, residues of permafrost from previous cold periods may remain during periods of warmer climate. Such so-called relict permafrost can be found in Russia and Canada today.

The climate during the permafrost regime is cold and relatively dry. Precipitation may be 50 percent of the current /Boulton et al, 1999a/. Seasonal variations are considerable. The monthly mean temperature is below or far below 0ºC for most of the year. The temperature only rises above the freezing point during two-three months per year /French, 1996/.

The permafrost domain has two regimes that coincide with the classification that is normally made of permafrost, a continuous and a discontinuous one. In areas with continuous permafrost the ground is frozen everywhere, apart from beneath large lakes, rivers and arms of the sea. In areas with discontinuous permafrost, areas of unfrozen ground separate bodies of frozen ground. In the transition towards boreal conditions, the occurrence of permafrost becomes increasingly sporadic /French, 1996/.

In areas with continuous permafrost the tundra ecosystem is characteristic /French, 1996/. The vegetation has adapted to the very short growing season and consists of herbs, shrubs and bushes. On dry sites lichens can be found and on wet ground there are mosses. Owing to the low plant productivity, small quantities of peat form despite large areas of wetland. In the summertime there are lots of birds that thrive on mosquitoes. Reindeer and lemmings are examples of mammals that occur in areas of continuous permafrost. The birds fly south in the winter, the reindeer head for the forests, while the lemmings can overwinter beneath the insulating snow cover /Boulton et al, 1999a/.

Where permafrost changes from continuous to discontinuous, the vegetation and animal life grow increasingly similar to that in cold temperate (boreal) areas. The treeline may coincide with the limit between continuous and discontinuous permafrost. This is how it is in large parts of North America today.

There is a general relation between the annual mean temperature in air and the temperature in the ground. The ground temperature increases with depth due to heat input from the interior of the earth. At the surface heat exchange with the atmosphere takes place. The development of permafrost reflects a negative heat balance at the surface. At a certain depth, the ground temperature does not vary during the year. In temperate areas, the temperature at this depth is approximately equal to the annual mean temperature in the atmosphere. In areas with permafrost, the energy exchange at the surface is more complex and the temperature at an equivalent depth is usually several degrees warmer than the annual mean temperature in the air. The complex heat exchange has among other things to do with freezing/thawing and the fact that the thermal conductivity of the ground is affected by its water content and by whether it is frozen or not. Another important factor is the albedo of the ground surface, i.e. the fraction of incoming solar radiation that is reflected by the surface. Examples of factors that influence the heat exchange are /French, 1996/:

- Precipitation – both form (snow, rain) and the season during which the precipitation falls are of importance, affecting both water content and albedo.
- Wind – moves snow and soil and affects evaporation.

- Vegetation – affects albedo, the quantity of snow that reaches the ground, how much the wind can move snow and soil, and evaporation.
- Topography – occurrence of heights and hollows and their compass orientation.
- Properties of soil and rock – water content, albedo, thermal conductivity and heat capacity.
- Sea, lakes and watercourses – distance to (and occurrence of) major bodies of water.

In areas with continuous permafrost, where it is very cold, the thermal properties of the soil and rock mass are as a whole of the greatest importance for the development of permafrost. Where the climate is slightly warmer and the permafrost is discontinuous, factors such as topography, vegetation and occurrence of snow are of greater importance for the development of permafrost. There are examples from Canada of areas where the snow cover prevents the development of permafrost, despite annual mean temperatures of around –4.5ºC. There are also examples of areas where sporadic permafrost occurs in connection with peat-rich areas, despite the fact that the annual mean temperature is higher than 0ºC /French, 1996/.

In present-day Canada and Alaska, the permafrost line coincides for the most part with the –1ºC isotherm for annual mean temperature in the atmosphere. In areas with an annual mean temperature of between –1 and –4ºC, the permafrost is limited to exposed areas, e.g. north slopes. Where the annual mean temperature is below –4ºC, the permafrost becomes increasingly widespread. The limit to continuous permafrost runs where the annual mean temperature is between –6 and –8ºC. Temperature just below the depth where no annual variations occur is here –5ºC. The equivalent ground temperature has been measured in the borderline between continuous and discontinuous permafrost in Russia /French, 1996/.

The development of permafrost is a complex process in which the above factors are involved. The palaeoclimatological history of the site is also of importance, for example whether the site has been covered with ice. Even though conditions in present-day Canada and Alaska as a whole differ from those in Scandinavia, there are areas where the conditions can be assumed to be similar to those we can expect in a cold Scandinavia. However, more detailed studies of climatic conditions and other factors that influence the development of permafrost are required to describe the future evolution in Scandinavia. Such studies have not been carried out to date.

The permafrost and the annually frozen active layer restrict infiltration and groundwater recharge. Most of the annual precipitation contributes to surface runoff, and stream flow rates vary widely over the year. During the winter, the limited runoff is supplied by groundwater discharge from unfrozen ground. The snow and ice melt takes place during the span of a few weeks in the spring, causing peak runoff and stream flow rates. The active layer thaws. Due to the low temperature, evaporation is low. Meltwater cannot infiltrate through the frozen ground, and despite the low precipitation, large areas are waterlogged during the short summer /Boulton et al, 1999a; French, 1996/.

In areas with limited vegetation the ground surface is exposed to wind action. Higher elevations are blown free of snow. Soil is carried off and forms dunes. Wind action, together with the repeated freezing and thawing and the spring flood, contributes to severe erosion on the surface /Boulton et al, 1999a; French, 1996/.

10.3.6 Glacial domain

The glacial domain is characteristic for stadials (cold periods). When the climate gets colder, the ice sheet originates in the Caledonian Mountains along the Norwegian-Swedish border and advances towards the east and south. During the severest stadials, the ice sheet covers all of Scandinavia and reaches in over Russia in the east and as far as northern Germany and Poland in the south. This ice sheet extent has occurred on the order of every hundred thousand years. During the interstadials (warmer stages of a glacial), the glacial domain is limited to the Caledonian mountains. During less severe stadials, the area along the Norwegian border and down towards the central parts of Sweden in the south and the present-day Bothnian Sea coast in the north may be ice-covered.

The climate is cold. In order to make the ice sheet expand the precipitation cannot be too small. Simulations of the Scandinavian ice sheet show that a more maritime climate promotes ice growth /Boulton and Payne, 1992; Boulton et al, 1995/.

Algae and microbes can be found on the surface of the ice. Mountaintops, called nunataks, may stick up out of the ice cover. Here lichens and possibly herbs may occur. Birds and mammals can live at the ice margin. Where the ice sheet terminus lies in the sea, a productive marine ecosystem that can sustain a fish population may exist. Here there may also be seabirds and mammals such as polar bears, seals and whales.

In the central parts of the ice sheet – the ice divide zone – the ground is frozen. Beyond the ice divide zone, closer to the ice sheet margin, lies a broad zone – the melting zone – where the pressure melting point is reached and melting occurs in the ice/bed interface. In the terminal zone close to the ice margin the ground may once again be frozen. The frozen area may, especially during phases of ice sheet advance, extend several kilometres from the ice margin. Snow and ice accumulate on the upper parts of the ice sheet, within the so-called accumulation area. At the lower parts and at the ice margin, ice is lost by melting and calving, called ablation. At a given altitude – the equilibrium line altitude (ELA) – equilibrium exists between accumulation and ablation. During periods of ice advance, the ELA is lowered, and the opposite occurs during ice decay. The glacier ice is plastic and flows under its own weight from higher to lower levels /Boulton and Payne, 1992/. A schematic illustration of the ice sheet is shown in Figure 10-10.

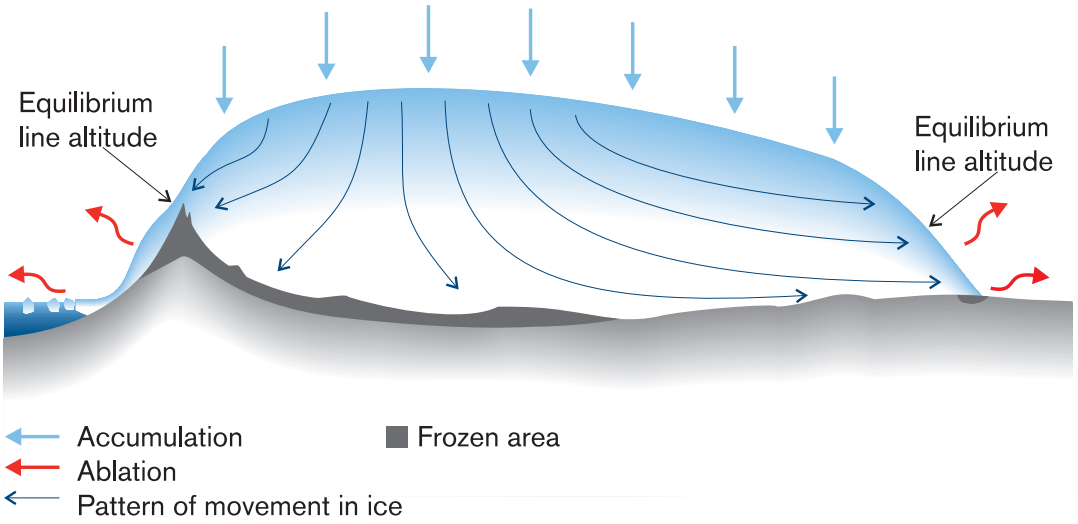

Figure 10-10. *Schematic drawing of a continental ice sheet.*

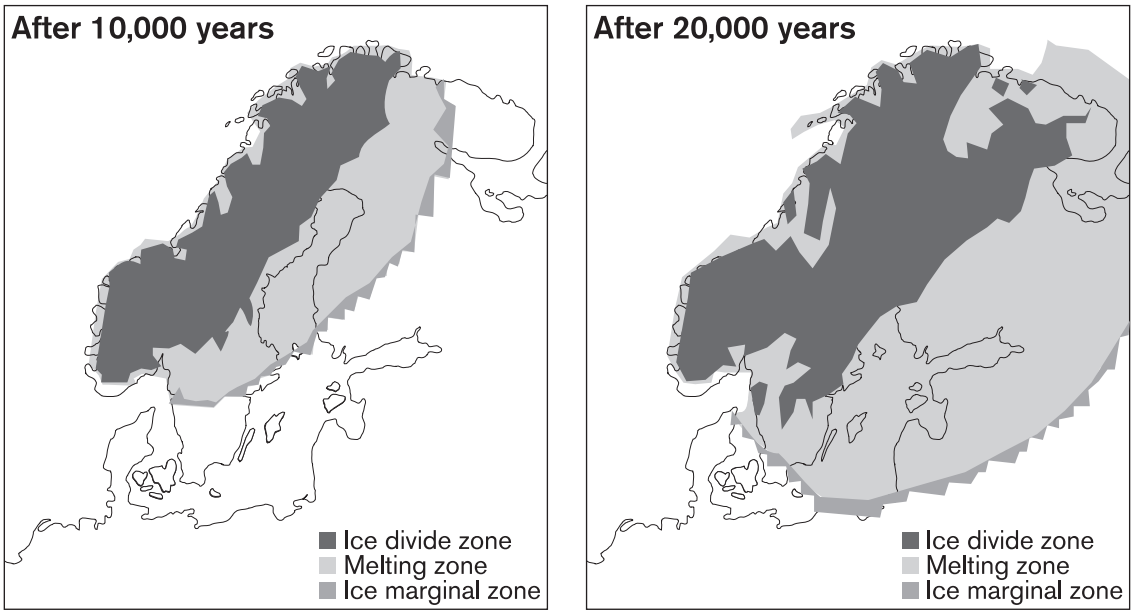

Figure 10-11. *Extent of ice sheet and ice divide zone after 10,000 and 20,000 years of ice growth /from Boulton et al, 1996/.*

Simulations of the Scandinavian ice sheet show that as the ice sheet advances from the Caledonian Mountains, the ice divide zone moves towards the east. However, it never reaches farther than to the central parts of Sweden in the south and the present-day Bothnian Sea coast in the north /Lundquist, 1986 in Boulton et al, 1999a/. The extent of the zone after 10,000 and 20,000 years of ice growth is shown in Figure 10-11.

In the melting zone, melting occurs in the ice/bed interface. The seasonal contrasts are great. During the winter melt-water flow is restricted to melting at the base of the ice sheet. During summer, large quantities of meltwater and rainwater are supplied from the surface of the ice sheet.

In an analysis of the groundwater flow beneath ice sheets, Boulton et al /1999b/ conclude that the meltwater is mainly transported towards the ice margin through ice tunnels in the interface between ice and bedrock. The meltwater is transported into the tunnels through the bedrock. The water flow in the ice/ground interface can be considerable and the transmissivity of the bedrock is limited, causing the water pressures to rise. If the water pressure exceeds the ice pressure, a tunnel is formed in the ice/bed interface. The spacing between the tunnels depends on the transmissivity of the bedrock and the inflow of meltwater to the system. The minimum tunnel spacing is the distance at which the water pressure everywhere is below the ice pressure. The system of tunnels beneath the ice is determined by the winter discharges produced entirely by basal melting. At the edge of the ice divide zone, these discharges are small. Basal discharges increase towards the ice margin, only to decrease again close to the ice margin. The maximum basal melt-water discharges have been estimated to 50 mm/y /Boulton and Payne, 1992/. The much larger discharges during the summer produce the maximum tunnel discharges and are largely responsible for esker formation. During the summer when the meltwater discharges and water pressures increase, temporary channels can form, e.g. adjacent to crevasses in the glacier. In the winter, these channels are closed by the ice flow. It is not probable that they will arise in the same place next summer. A schematic drawing of tunnels and groundwater pressure is shown in Figure 10-12.

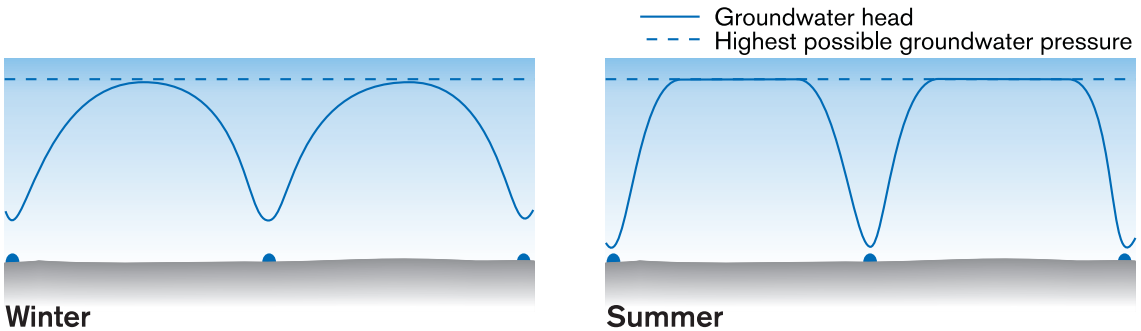

Winter

Meltwater discharges in the winter are so great that they cannot be drained off through the rock. The water pressure rises, and where it exceeds the ice pressure tunnels form.

Summer

The much larger water flux in the summer results in increased pressures and discharges and is the main cause of esker formation.

Figure 10-12. *Cross section through continental ice sheet showing groundwater pressure and ice tunnels in the melting zone. The tunnel spacing is dependent on the meltwater discharge and the transmissivity of the bedrock.*

The chemical composition of the water that infiltrates the bedrock beneath an ice sheet differs from that of the water that infiltrates under ice-free conditions. The glacial meltwater is, like meteoric water, rich in oxygen. Beneath an ice sheet only very small quantities of organic matter are expected, however. The consumption of oxygen that under ice-free conditions takes place when the meteoric water passes the uppermost soil layers thereby doesn't occur.

The ice sheet exerts a load on the earth's crust. The earth is divided into core, mantle and crust. Within plate tectonics, one also speaks about the lithosphere. The lithosphere consists of the crust and the outermost parts of the mantle. The lithosphere can be conceived as an elastic/brittle material resting on a viscous medium.

When the climate gets colder and ice sheets expand, water is moved from the oceans to the continents. The pressure exerted by the lithosphere beneath the ocean bottoms on the underlying viscous medium decreases. At the same time, an ice load is placed on parts of the continental lithosphere, which is thereby pressed down. The viscous material moves in underneath the ocean bottoms and out from the area beneath the continental ice sheets. The ocean bottoms rise and the land underneath the ice sheets sinks. When the ice sheets melt, the oceans are once again filled with water and the ice load disappears. The viscous material moves out from the area underneath the ocean bottoms and in under the areas that have been covered by continental ice sheets. The ocean bottoms sink and the lithosphere beneath the former ice sheets rises /Morén and Påsse, 1999/. The sequence of events is illustrated in Figure 10-13.

The course of events described above will affect the state of stress in the bedrock. The subsidence/uplift of the lithosphere is complicated by the fact that the thickness of the crust varies. Furthermore, the bedrock is continuously subjected to stresses by plate-tectonic movements. The mechanical state to which this gives rise in the Baltic Shield is discussed in section 11.3.2 in Chapter 11, "Tectonics – earthquake scenario".

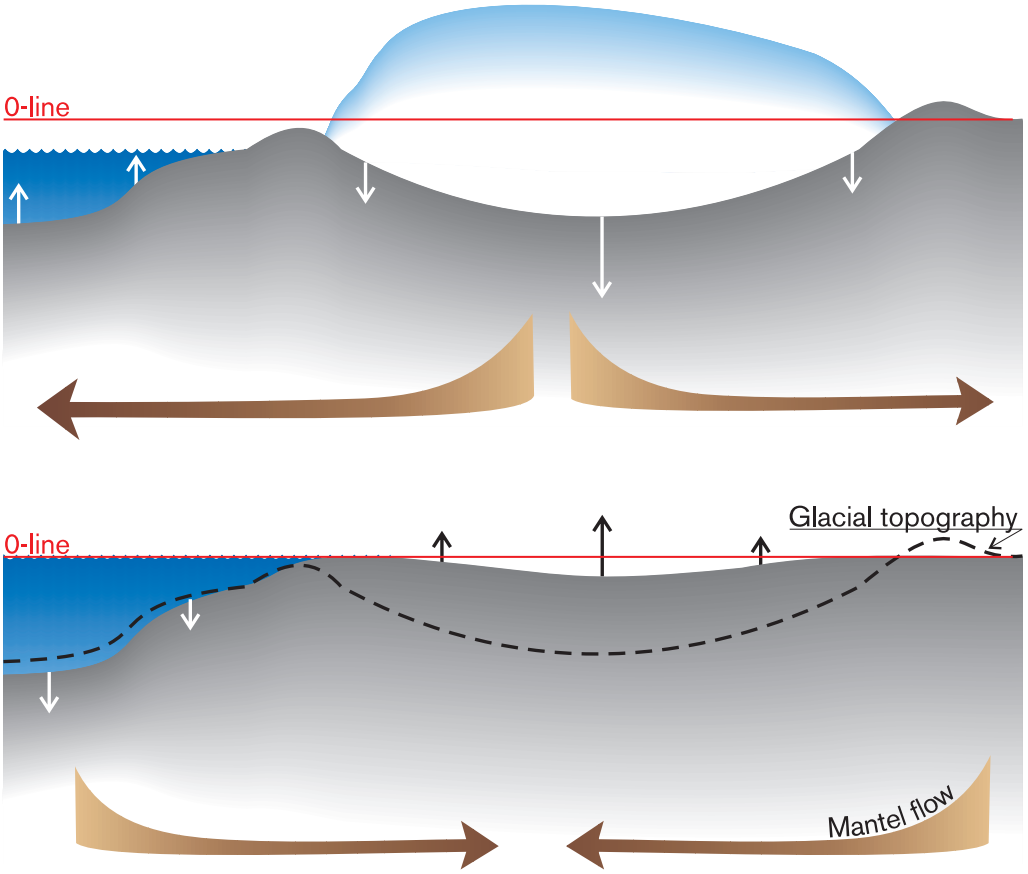

Figure 10-13. *Schematic drawing of movements of lithosphere and the viscous flow underneath the lithosphere under glacial and interglacial conditions /from Morén and Påsse, 1999/.*

The climate-related factors that affect the repository during the glacial domain are:

- temperature,
- permafrost thickness,
- ice load,
- water pressure,
- groundwater flow gradients,
- meltwater flows,
- chemical composition of meltwater.

Based on the variation of these properties, three regimes have been identified /Boulton et al, 1999a/:

- ice divide regime,
- melting zone regime,
- ice marginal regime.

10.3.7 Evolution at the three repository sites

The evolution at the three repository sites is described as time series of climate-driven process domains[3] and periods when the areas lie beneath the surface of the sea. The site-specific descriptions are based on a hypothetical extension of the climate-driven process domains in time and space. This is in turn based on the description of climatic conditions from Table 1-1, Påsse's modelling of shoreline displacement /Morén and Påsse, 1999/, and modellings and reconstructions of the dynamics and extent of the ice sheet /Boulton and Payne, 1992; Mangerud, 1991; Fredén, 1994/. Furthermore, descriptions of present-day conditions in North America have been used to make a judgement of the occurrence and extent of permafrost /French, 1996/. The evolution on the three sites is shown in Figure 10-14.

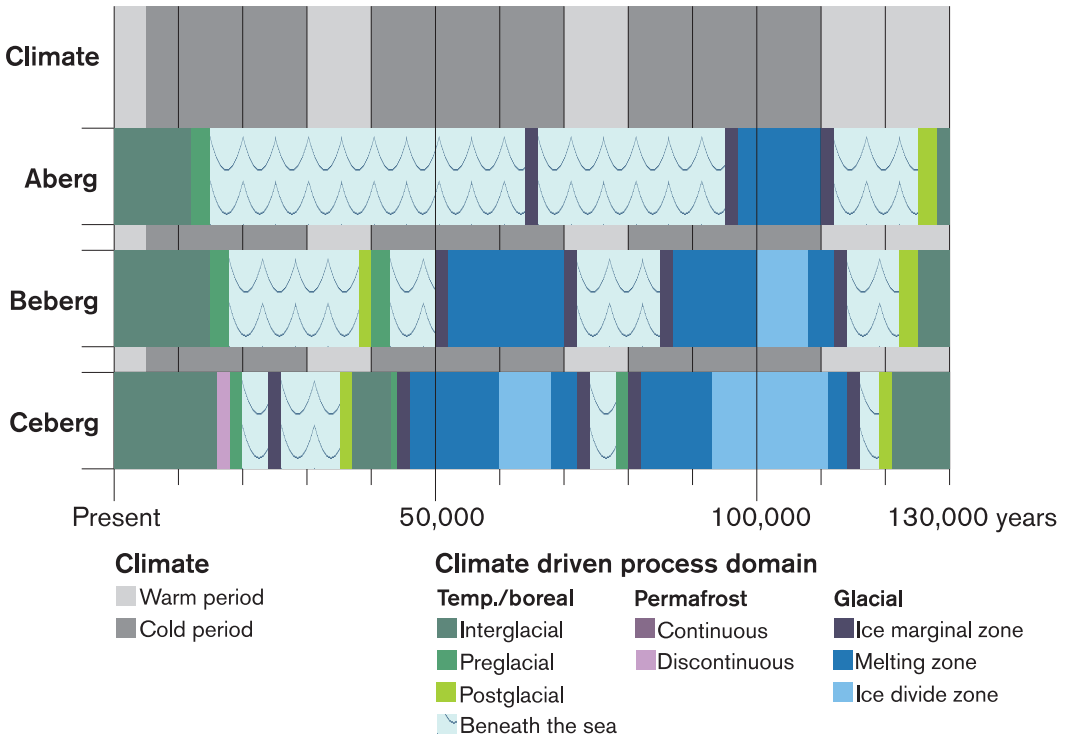

Figure 10-14. *Evolution at Aberg, Beberg and Ceberg as time series of climate domains and regimes, and the periods the sites are located beneath the surface of the sea.*

[3] Pre- and postglacial conditions are said to prevail when the sites sink/rise below/above the sea. This is not quite accurate, since the characteristic changes of the shoreline (see section 10.3.4) take place when the sites are situated far from the coast, e.g. all the sites are located far below the surface of the sea in the postglacial stage. Pre- and postglacial conditions are nevertheless said to prevail by virtue of the fact that changes that take place when a site is transformed from sea to land, and vice versa, are important for the biosphere and also affect the boundary conditions for groundwater flow.

Aberg

From today until approximately 20,000–30,000 years in the future climate gets progressively colder. When it is coldest, the annual mean temperature at Aberg may be approximately –1°C, compared with today's 7°C. Initially the relative shoreline falls. Parts of the area are though expected to remain below the sea during the whole period. The climate during this period is temperate/boreal. As the ice sheet expands from the mountains, the regression is transformed to transgression, and in about 15,000 years from now the entire Aberg area lies under water.

The area remains beneath the sea up until the next interglacial. Sea level varies as the ice sheet advances and retreats, but this is of little importance for conditions at Aberg, which remain below the sea level all the time. The conditions only change during periods when the ice sheet reaches Aberg.

The ice sheet reaches Aberg during two stages of the glacial/interglacial cycle. During the stadial, assumed to occur in 60,000–70,000 years, the ice margin may reach Aberg. The area is assumed to lie in the ice marginal zone during the period 64,000–66,000 years from now. During the severest cold period of the glacial, after about 95,000 years, the advancing ice sheet once again reaches Aberg. During the period 95,000–97,000 years, the area is assumed to lie in the ice marginal zone, and after that, between about 97,000 and 110,000 years in the future, it lies in the glacial melting zone. In about 110,000–112,000 years, it is assumed that the now retreating ice sheet passes Aberg.

In just over 125,000 years, it is assumed that the highest parts of the Aberg area rise up out of the sea. The shoreline, however, remains about 5–10 metres above the present-day shoreline throughout the interglacial.

In summary, it can be said that except for short periods during interglacials, Aberg is a site that remains beneath the surface of the sea. Aberg is only ice-covered during the coldest periods of a glacial cycle. During less severe stadials, the ice front may lie at Aberg.

Beberg

Beberg is situated farther from the coast than Aberg and will not be appreciably affected by the regression that takes place on transition to a colder climate. The lakes in the area are during this period transformed into wetlands. As the ice sheet grows, the regression turns into transgression and the sea comes closer to Beberg. In about 15,000 years, the sea begins to occupy the lowest-lying areas, and after about 18,000 years the entire area is submerged. The annual mean temperature during this stage may be –2 to –3°C, compared with the current 5.5°C. Before Beberg becomes submerged, sporadic permafrost could occur in exposed locations. Considering the fact that Beberg at this stage is situated close to the coast, the permafrost will, if it occurs at all, be very limited. Climatic conditions can be regarded as boreal.

During the warm period between 30,000 and 40,000 years, Beberg remains beneath the sea until the end. In about 38,000 years, it is assumed that the highest parts will stick up like islands in a coastal landscape. After that, land uplift is assumed to continue for another 2,000 years before the relative sea level once again begins to rise due to new ice growth, and in about 43,000 years Beberg is assumed to lie completely beneath the sea.

The advancing ice sheet may reach Beberg in about 50,000 years, when the site is located beneath the surface of the sea. During the period 50,000–52,000 years, Beberg is assumed to lie in the ice marginal zone. The area then lies in the melting zone until the

ice once again passes as it retreats. During the period 70,000–72,000 years, it is assumed that Beberg once again lies in the ice marginal zone. The site may possibly lie at the margin of the ice divide zone when the ice sheet reaches the stadial maximum in about 64,000–66,000 years.

During the subsequent brief and relatively cold interstadial, Beberg remains submerged.

In 80,000 years it gets colder again, and in about 85,000–87,000 years the growing ice sheet is assumed to once again pass Beberg, which then lies in the ice marginal zone. Then follows a long period when the site is located in the melting zone, interrupted by a shorter period in the ice divide zone in 100,000–108,000 years. During the period 112,000–114,000 years it is assumed that the ice once again passes, and Beberg lies in the ice marginal zone. The ice margin lies in the sea and Beberg is covered with water.

In about 122,000 years, it is assumed that the highest parts of the area once again rise up out of the sea. Beberg continues to rise out of the sea until the final stage of the interglacial in about 130,000 years. During the period 128,000–132,000 years, the entire area is situated above the sea. The sea level is still slightly higher than the current.

Like Aberg, Beberg will be located beneath the surface of the sea for a large portion of a glacial cycle. Its location some distance in from the present-day coast means that Beberg rises out of the sea during milder interstadials. The more northerly location entails that periods when the site is ice-covered are more frequent and longer lasting.

Ceberg

Ceberg is the northernmost of the three sites. The area is situated at some distance from the coast and is not affected by shoreline displacement until in about 18,000 years, when the rising shoreline reaches the lowest-lying parts of the area. During the initial period conditions are boreal. Successive infilling of lakes is judged to be the most significant change. In about 10,000 years, it may have become so cold that sporadic permafrost could occur in exposed locations. As the climate becomes colder, the rising shoreline approaches Ceberg. The situation close to the coast makes it unlikely that permafrost will develop to any great extent. A period of discontinuous permafrost is nevertheless assumed between 16,000 and 18,000 years. Between 18,000 and 20,000 years, preglacial conditions are assumed to prevail. In 20,000 years it is assumed that the entire area lies beneath the sea. The permafrost is assumed to thaw during the period the area is submerged.

In about 24,000 years the ice front is assumed to reach Ceberg, and during the period 24,000–26,000 years Ceberg lies in the ice marginal zone. The ice margin lies in the sea.

At the beginning of the subsequent warm period, Ceberg lies under water. In about 35,000 years, the highest parts are assumed to rise up out of the sea, and during the period 39,000–43,000 years the entire area is situated above the sea. The relative sea level then rises once again. A new cold period begins and the annual mean temperature drops, although not enough for permafrost to develop other than very sporadically.

The ice front reaches Ceberg in about 44,000 years. During this stage the area is situated on the coast and elevated parts form islands in an archipelago. During the period 44,000–46,000 years, Ceberg is assumed to lie in the ice marginal zone. Then follows a period when Ceberg lies in the melting zone. The ice divide zone reaches Ceberg in about 60,000 years. After a period in the ice divide zone, a period follows between 68,000 and 72,000 when the site is located in the melting zone. During the period

72,000–74,000 years, Ceberg is assumed to lie in the ice marginal zone once again. The ice margin lies in the sea.

The ice front is assumed to lie near Ceberg during the entire subsequent relatively cold interstadial. At the transition to the next cold period, large parts of the area nevertheless lie above the shoreline. As the ice grows, the earth's crust is depressed, the relative shoreline rises and increasingly large areas are submerged beneath the sea. Owing to the coastal location, permafrost is not expected to develop, despite the cold climate. Sporadic permafrost can occur, but not to such an extent that permafrost domain can be said to prevail. Preglacial conditions are assumed to exist during the period 78,000–80,000 years.

The ice front may reach Ceberg at the start of the subsequent cold period. During the period 80,000–82,000 years, Ceberg is assumed to lie in the ice marginal zone. This is followed by a period when the area lies in the melting zone. During the period 93,000–111,000 years, Ceberg is assumed to lie in the ice divide zone. Then the melting zone passes before the ice marginal zone reaches the site in about 114,000 years. The ice is assumed to leave Ceberg in about 116,000 years. Approximately 3,000 years later, the highest parts are assumed to stick up out of the sea. In about 122,000 years, it is assumed that the entire area lies above the shoreline, where it remains during the remainder of the interglacial.

Compared with Aberg and Beberg, Ceberg's northerly location means longer and more frequent periods when an ice sheet is present. Of the three sites, Ceberg is the one that is in the ice divide zone for the longest time.

10.4 Uncertainties in description of boundary conditions

SR 97's climate scenario is intended to describe sequence of events that may occur during the next glacial/interglacial cycle. It can also be regarded as a general description of the evolution during one of the Quaternary Period's glacial/interglacial cycles.

The current knowledge of the earth's climate system is not sufficient to estimate the probability of a given scenario. We can, however, say something about future climatic conditions. It is, for example, known that the earth is currently experiencing a period of warm climate. It is also very likely that the climate will become colder at some time in the future. It is also certain that a transition to a colder climate will mean that Scandinavia will at some time be covered with ice. It is probable that such a situation will occur at some time during the next 100,000 years. However, our knowledge of the earth's climate system is not adequate to make any exact predictions of the extent of the ice sheet during the coming glacial/interglacial cycle.

The variation of the orbital parameters and the associated variation of insolation can be more or less exactly calculated. There is a time lag between the variation in insolation and climate change on earth. It is uncertain how large this time lag is. The statements on when the climatic conditions will change can nevertheless be regarded as relatively reliable, provided that Milankovitch's theory is valid, which most researchers today agree on. The scope of the changes in climatic conditions which the varying insolation will bring about, for example temperature variations and ice sheet extent, is however highly uncertain. This uncertainty stems from inadequacies in the description of the climate system and its response to changes in insolation.

Simulations with the LLN model show that due to the weak variation of insolation in combination with anthropogenic influences, the current warm period may last for an extremely long time, up to 50,000 years. The model indicates that the importance of the climate system's internal dynamics increases during periods with small variation (low amplitude) of insolation /Berger and Loutre, 1997/.

The SR 97 scenario describes a sequence of events similar to that we know from the Weichsel period. The ice extent is greater than indicated by the simulations with the LLN model. Compared with the climate scenario in SKB's safety report SKB 91, the scenario describes a warmer climate during the initial 70,000 years /SKB, 1992; Ahlbom et al, 1991/. The scenario is a weighing-together of more recent and older calculation results and geological data. The scenario contains three cold periods and three warm periods. During the last of the cold periods, an ice extent equivalent to the largest known from geological data is assumed. During the last warm period, interglacial conditions are assumed. The intention is to cover changes of importance for the evolution of the repository in such a way that their consequences are not underestimated.

When a continental ice sheet advances, severe erosion takes place on the surface. In Scandinavia we therefore almost solely see the traces of the most recent glaciation and the following period. There are also traces from previous ice sheets. To describe other climatic conditions, we are dependent on geological and biological data from other places on earth. The descriptions of the conditions within the different climate-driven process domains are based on geological and biological data, modellings and investigations on sites that today have climatic conditions similar to those we expect in Sweden in the future. To judge how correct the descriptions are, it would be desirable to have more information on the long-term variations of the Scandinavian climatic conditions (temperature, precipitation, etc.). Such data are used e.g. in modellings of ice extent and occurrence of permafrost.

10.5 Overview of processes and dependencies

The processes and dependencies that control the evolution **within** the repository system in the climate scenario are in the main the same as in the base scenario, see Figure 10-15.

However, climate change leads to radically changed conditions in the repository's surroundings, which changes the boundary conditions for the evolution in the repository. The effects of climate change only become noticeable after many of the initial, transient processes in the base scenario have run their course. This is true of water uptake in buffer and backfill, the restoration of natural hydrogeochemical and hydraulic conditions in the geosphere, and essentially also the heating of the entire repository system that is caused by the decay heat in the fuel. All of these processes are expected to be more or less the same as in the base scenario.

As regards the radiation-related evolution, the same evolution is expected as in the base scenario in the long term as well.

Thermally, a colder climate leads to development of permafrost in parts of the geosphere. The groundwater thereby freezes and the groundwater flow is affected.

The hydraulic evolution is also greatly influenced by the changed hydraulic boundary conditions as a result of changed precipitation, shoreline displacement and ice growth in the surroundings. The groundwater pressure can increase considerably beneath an ice

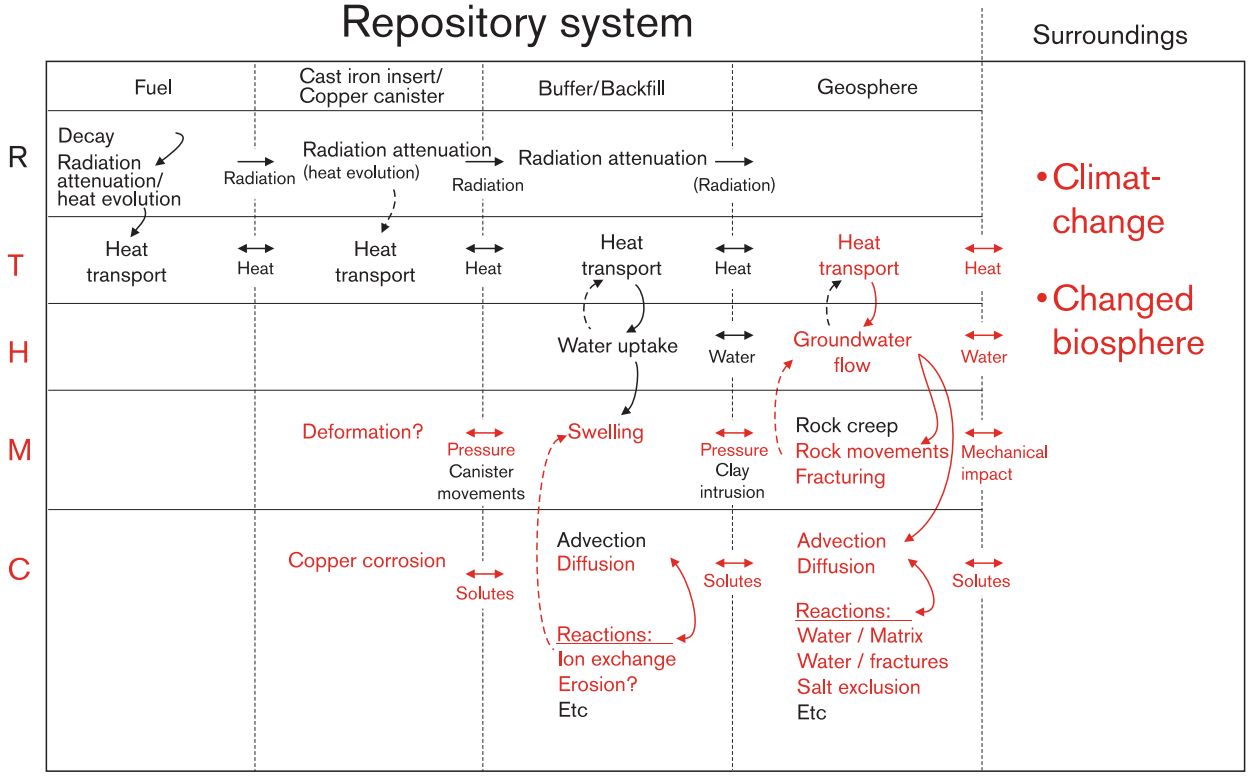

Figure 10-15. *Main features of the process system for the climate scenario. Red processes follow a different course or have a different scope than in the base scenario.*

sheet and the infiltration pattern changes. If a site becomes sea-covered, the pressure differences in the geosphere are evened out and the hydraulic conditions can become virtually stagnant.

Mechanically, the boundary conditions are changed radically by the weight of an ice sheet. Both the static load from the ice sheet and the dynamic processes when the ice sheet advances and recedes have mechanical repercussions in the repository rock. The interaction between the mechanical load and the high groundwater pressure can cause fractures to both widen – hydraulic fracturing – and close, thereby affecting the groundwater flow. In other words, feedback is obtained to the hydraulic evolution.

Chemically, the boundary conditions are changed compared with the base scenario by the fact that oxygen-rich water infiltrates down into the bedrock without the oxygen being consumed in an organic soil layer, since this layer is expected to be obliterated during large parts of a glacial cycle. The oxygen is instead consumed mainly by reactions with the minerals in the geosphere.

Climate change also causes changes in the salinity of the groundwater. In the first place, salt is excluded from the water when permafrost forms so that the still-unfrozen water has a higher salinity. In the second place, the altered flow conditions in the geosphere create new conditions for transport and mixing of water from different parts of the geosphere and infiltrating surface water. The result can be both higher and lower salinities than in the base scenario. The altered groundwater composition mainly affects the process of ion exchange and the development of swelling pressure in the buffer.

Radionuclide transport in the repository system, if any, is above all influenced by the altered hydraulic conditions.

10.6 Radiation-related evolution

The radiation-related evolution described in the base scenario is not affected by climate change.

10.7 Thermal evolution

The thermal evolution is coupled to the mechanical and the chemical evolutions. In the base scenario, the maximum temperature on the canister surface plus the temperature in the repository as a whole are calculated. The maximum temperature on the canister surface is reached after 10–15 years and is thereby not influenced by climate change. Changes of the annual mean temperature influence the temperature in the geosphere. The temperature changes in the rock decline with depth and are always less than the temperature variations at the surface.

During a glacial/interglacial cycle, the temperature variation[4] between the coldest and warmest periods at Swedish latitudes can be estimated to be about 10–15ºC /based on Boulton and Curle, 1997; Boulton et al, 1995; Guiot et al, 1989; Holmgren and Karlén, 1998/). Today the annual mean temperature varies between approximately –3 and 9ºC from north to south /Raab and Vedin, 1995/. During the warmest stage of the current interglacial, the temperature may have been 2–3ºC higher than today /Bogren et al, 1998; Holmgren and Karlén, 1998; Losjö et al, 1998/.

10.7.1 Temperate/boreal domain

The annual mean temperature within the temperate/boreal domain may be up around 5ºC higher than today. The transition to permafrost domain can take place at an annual mean temperature of around –1ºC. The variation of the annual mean temperature in the temperate/boreal domain is of the same order of magnitude as the differences in annual mean temperature between the three repository sites. Its importance for the temperature evolution is thereby dealt with in the base scenario.

10.7.2 Permafrost domain

During periods with permafrost, the temperature may be about 8–15ºC lower than today's temperature. There is no geological evidence available today of past permafrost depths. Boulton and Payne have simulated ice sheet and permafrost extent during the Weichsel /Boulton and Payne, 1992/. In the model, the temperature was assumed to vary with the topography. In a calculation case when the temperature at the sea was –10ºC at the lowest, the maximum permafrost depth in Sweden was calculated to be about 300 metres. When the minimum temperature at the sea was assumed to be –5ºC, the permafrost depth was just over 100 metres.

The heat from the spent fuel will affect the permafrost depth. Permafrost is not expected for at least several thousand years. The heat flux from the fuel will then have declined considerably, and the repository and the rock around it will have an even temperature. The reduction of the permafrost depth is expected to be relatively small. Permafrost will contribute to a lower temperature in the rock in relation to the base scenario.

[4] No account taken of the topography and its changes in conjunction with a glaciation.

The reduction of the temperature brought about by the colder climate declines with depth /Delisle, 1998/ and can never exceed the temperature reduction in the atmosphere. The freezing point is not reached at repository depth, and no direct thermal impact on the repository is judged to occur.

10.7.3 Glacial domain

In the ice divide zone the ground is frozen. The bedrock beneath the ice is also frozen. In the central parts of the ice divide zone the permafrost may reach down to 400 metres depth /Boulton and Payne, 1992/. In the melting zone the pressure melting point is reached. The temperature is below 0ºC and by definition permafrost thus prevails despite the fact that the ground is not frozen. The pressures are lower near the ice margin and the ground may be frozen. The permafrost depths are much less than in the ice divide zone. The influence on the thermal evolution is the same as in the permafrost domain.

10.7.4 Evolution in the geosphere at the three repository sites

Aberg

Beberg will also eventually wind up underneath the sea. Before the highest parts of the Beberg area are covered with water in about 18,000 years, the annual mean temperature may have fallen to –2ºC to –3ºC. However, no permafrost is expected due to the coastal location. At Beberg as well, the temperatures remain above zero with the exception of the periods when the area is ice-covered. During the period 100,000–108,000 years, Beberg lies in the ice divide zone and the temperatures fall considerably. Permafrost may prevail down to a depth of around a hundred metres. As at Aberg climate change is judged to be of marginal importance for the temperature evolution in the geosphere, and thereby also in other parts of the repository.

Beberg

Beberg will also eventually wind up underneath the sea. Before the highest parts of the Beberg area are covered with water in about 18,000 years, the annual mean temperature has fallen to –2ºC to –3ºC. However, no permafrost is expected due to the coastal location. At Beberg as well, the temperatures remain above zero with the exception of the periods when the area is ice-covered. During the period 100,000–108,000 years, Beberg lies in the ice divide zone and the temperatures fall considerably. Permafrost may prevail down to a depth of around a hundred metres. Here as well climate change is judged to be of marginal importance for the temperature evolution in the geosphere, and thereby also in other parts of the repository.

Ceberg

At Ceberg, discontinuous permafrost may occur before the sea rises and covers the entire area in about 20,000 years. The permafrost depths may be around 50 metres, and relatively large areas of unfrozen ground are assumed to exist. Ceberg lies in the ice marginal zone in about 24,000 years, then the ground temperature may be around –2ºC. Ceberg lies in the ice divide zone during two stages: 60,000–68,000 and 93,000–111,000 years. During these periods, permafrost depths of up to a couple of hundred metres may occur. Climate change is not judged to be of any significant importance for the thermal evolution at Ceberg either.

10.7.5 Evolution in the near field

Climate-driven temperature changes in the rock are of subordinate importance for the thermal evolution in the near field.

10.7.6 Conclusions

Temperature changes due to climate variations do not require any analyses of thermal evolution beyond what has been reported in the base scenario.

10.8 Hydraulic evolution

The hydraulic evolution is coupled to the mechanical and chemical evolutions. In the base scenario, the hydraulic evolution is described based on the premise that present-day conditions and trends will continue to prevail in the future. This means that the variations that can be expected within the interglacial regime of the temperate/boreal domain already have been elucidated.

10.8.1 Temperate/boreal domain

Climate variations within the temperate/boreal domain affect groundwater recharge, the depth of lakes and stream discharges in watercourses. The most significant changes are related to the rate and direction of shoreline displacement. The changes are of the greatest importance in coastal locations.

During periods of regression the relative sea level falls. Areas that were formerly seabed become land. When an area lies beneath the sea, occurring groundwater flow is driven by density differences and saline water penetrates into the bedrock. When the area rises out of the sea, the new land surface becomes accessible for infiltration of meteoric water. Owing to the humid climate, the groundwater table, and thereby the hydraulic gradient, will follow the topography. The non-saline meteoric water displaces and mixes with the more saline water. The level of the repository in relation to the sea is raised. On a site that before regression was situated near the coast, the gradients for groundwater flow increase. The evolution is illustrated schematically in Figure 10-16.

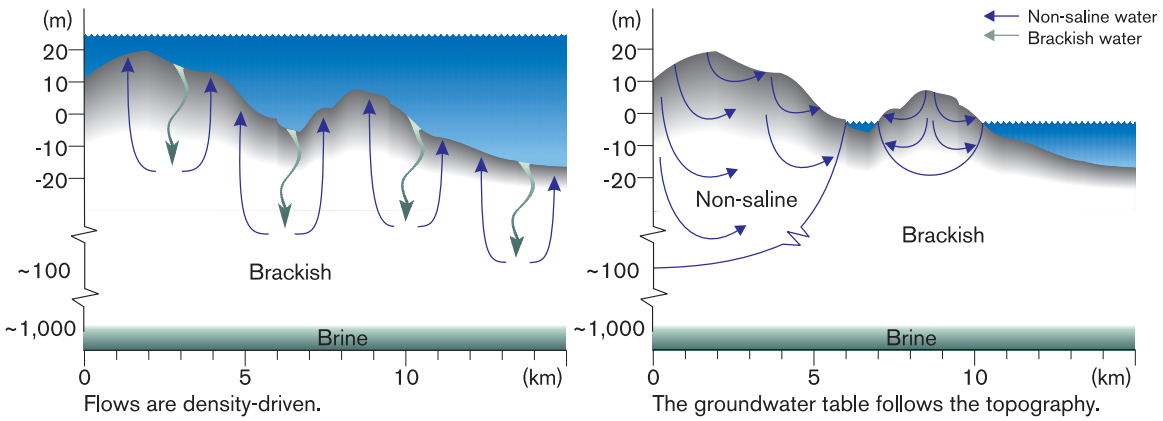

Figure 10-16. *The hydraulic evolution in conjunction with regression.*

Regression due to sea level lowering occurs at the beginning of the preglacial stage. The fastest regression takes place due to land uplift at the beginning of the postglacial stage, however. Regression is fastest in the areas that have been situated closest to the central parts of the melting ice sheet /Boulton, 1990 in Boulton et al, 1999a/.

During periods of transgression the relative sea level rises. Areas that have previously been land are transformed into seabed. Below the sea, hydraulic gradients following the topography cease to exist. Saline water penetrates down into the bedrock due to density differences. The level of the repository relative to the sea is lowered. On a site that before transgression was situated close to the coast, the gradients for groundwater flow decrease. The evolution is the opposite of the one shown in Figure 10-16.

Transgression is most intensive at the end of the preglacial regime, when the depression of the earth's crust by the growing ice sheet escalates. As for the regression, the changes are greatest in areas close to the central parts of the ice sheet.

10.8.2 Permafrost domain

Decreased precipitation and frozen ground result in very limited groundwater recharge. In areas with continuous permafrost, virtually all precipitation contributes to surface run-off /French, 1996/.

The groundwater flow is limited to unfrozen patches, called taliks. The temperature may be below 0ºC in a talik. The taliks may be open or closed. Open taliks are in contact with the active layer. Open taliks occur under large lakes and watercourses in the continuous zone. Closed taliks may occur under small lakes and watercourses, or as a remnant from a warmer period, for example in a clay lens /French, 1996/.

The impermeable frozen ground drives groundwater flow to a greater depth. Frozen impermeable areas can occupy a large portion of the surface. Even the open patches are frozen during most of the year. Water turnover and flow in the bedrock is therefore small in relation to the situation in the temperate/boreal domain. Water turnover decreases due to the limited infiltration, but also as a result of the longer path the flow is forced to travel in the rock, despite the fact that large gradients can occur locally. This is particularly true in the upper parts of the bedrock. Flows at great depth may be driven by regional gradients. Regional gradients could be sustained at taliks, for example between two lakes. A schematic drawing of the flow situation is shown in Figure 10-17.

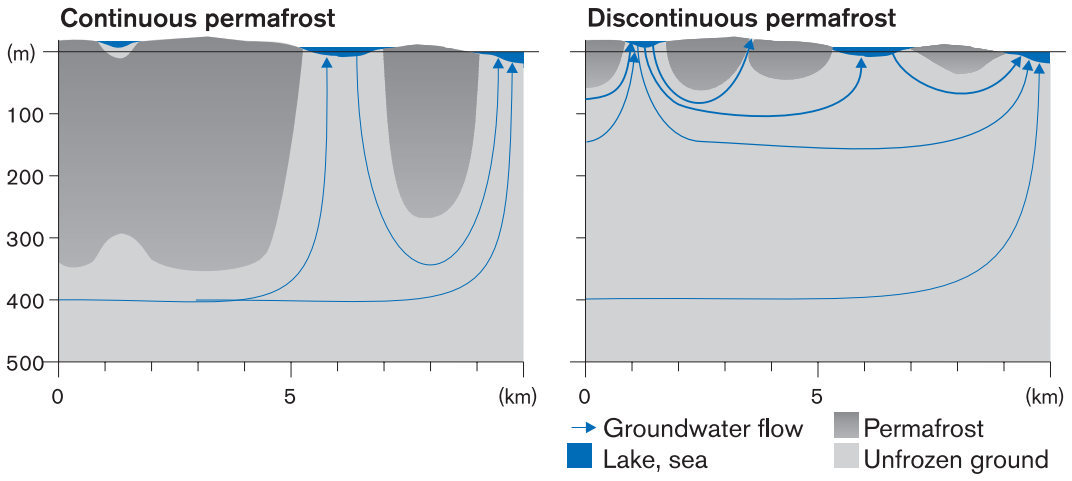

Figure 10-17. Groundwater flows in a permafrost domain.

10.8.3 Glacial domain

Two processes drive groundwater flow beneath ice sheets /Boulton et al, 1999a/:

1. Influx of meltwater.

2. Compression (consolidation) of the bedrock.

In the ice divide zone the ground and ice sheet are frozen, there is no melt-water flow, and neither groundwater flow nor pressure gradients occur. The groundwater table is horizontal and corresponds to the head at the boundary of the melting zone. The ice pressure exceeds the groundwater pressure and the effective stresses are high (see section 10.9.3). The bedrock is compressed in relation to the increasing ice thickness, and a limited groundwater flow out of the zone arises. Aside from this process, the conditions can be considered to be stagnant in the ice divide zone.

In the melting zone, the ice melts at the ice/bed interface. During the summer, there is also an influx of meltwater and rainwater from the surface. The meltwater is driven towards the ice margin by a pressure gradient that follows the slope of the ice sheet. From the ice margin, the water pressure increases progressively in relation to the ice thickness. The maximum water pressures are reached at the boundary between the melting zone and the ice divide zone. The magnitude of the pressure is dependent on the temperature and thickness of the ice. The maximum water pressures can be between 20 and 25 MPa (estimate based on Boulton and Payne /1992/). The meltwater is pressed down into the bedrock, and due to the low permeability of the bedrock the water pressure rises. Where the water pressure exceeds the ice pressure, channels form at the ice/bed interface, see section 10.3.6. The channels, or ice tunnels, give rise to local water table drawdowns, and the pressure gradients in towards the tunnels can be considerable. In the area between the ice tunnels, the distance to the tunnels and the topography of the ice controls the groundwater flow. Most of the flow towards the ice margin is expected to take place through the ice tunnels. The groundwater flow mainly takes place in towards the ice tunnels /Boulton et al, 1999b/. Due to the increasing slope of the ice sheet the gradients for groundwater flow increases towards the ice margin.

At the ice margin, and in towards the ice tunnels, the gradients for groundwater flows are high. Groundwater flow takes place both in towards the tunnels and out towards the ice margin. The rapidly decreasing ice thickness gives lower pressures, the pressure melting point is not reached and the ground is frozen. The thermal capacity of the meltwater flow in the tunnels is though enough to keep the ground unfrozen in their vicinity. As the ice advances over an area with permafrost, it carries with it its system of tunnels. In the frozen zones between the mouths of the tunnels, the groundwater is driven to greater depths and the gradients, both in towards the tunnels and out towards the ice-free area, increases. How large the gradients can become depends on the slope of the ice sheet and the extent of the permafrost, where both depth and extent from the ice margin are of importance. Where the ice terminates in the sea no permafrost occur in the ice marginal zone. The flow situation in the melting and ice divide zones is sketched in Figure 10-18.

The rate of advance of the ice front is on the order of 10 m/y (estimate based on Boulton and Payne /1992/). The maximum rate of advance may be a few tens of metres per year. The ice sheet retreats much faster than it advances. At the most recent glaciation, the ice front retreated across Sweden at a rate on the order of 100 m/y. The retreat rate in the interior of Norrland may have been up around 1,000 m/y (estimated from map in Fredén /1994/). The slope of the ice sheet may be between 1 and 10 per mil, and increases close to the ice margin /Boulton and Payne, 1992/. This means that

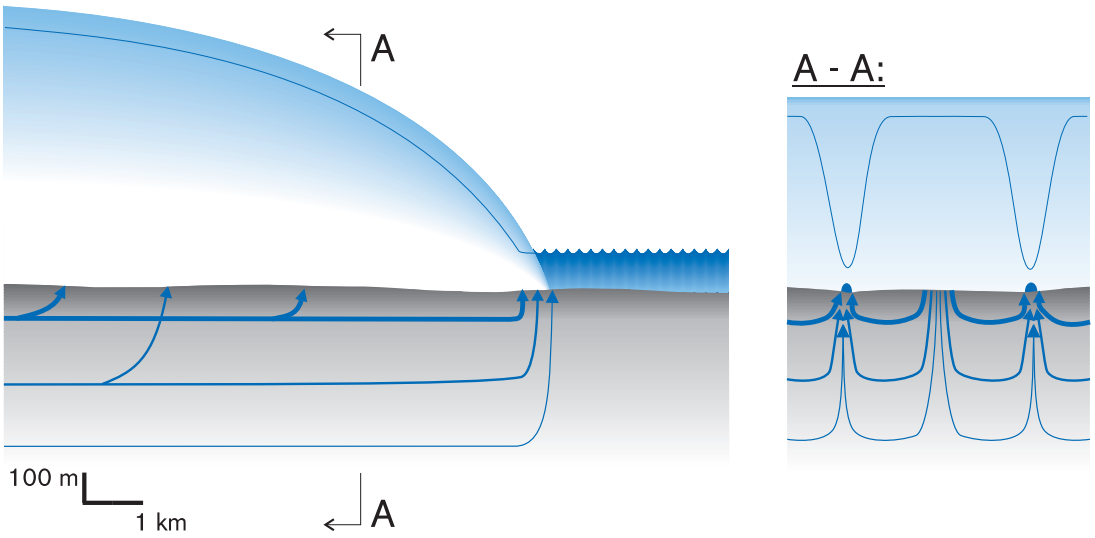

Figure 10-18. *Groundwater flow in the melting and ice marginal zones. The ice margin lies in the sea.*

the water pressure can increase by on the order of 0.1 to 1 kPa/y when the ice sheet is growing. When the ice sheet is retreating the pressure may decrease by on the order of 1 to 100 kPa/y.

10.8.4 Evolution in the geosphere at the three repository sites

Aberg

During the initial period the relative shoreline declines. The regression leads to an increase of the groundwater flow gradients. Svensson /1999b/ has simulated the evolution at Aberg during the period from 10,000 years before present up to 5,000 years after present. 7,000 years ago, Aberg was located beneath the sea. When the area lies underneath the sea, the calculated flows at repository depth are extremely small, and conditions are virtually stagnant. When the area rises up out of the sea, the flows increase, reaching a maximum in 5,000 years when the relative shoreline is at its lowest. The flows at repository depth have then been calculated to be approximately five times the present-day flows.

In approximately 5,000 years, the regression turns into an increasing transgression. As the shoreline rises, the pressure gradients for groundwater flow diminish. After about 15,000 years, the entire Aberg area is covered by water. The shoreline continues to rise. When the whole area is below the surface of the sea, the groundwater flows are driven by density differences. The more saline seawater displaces the non-saline water in the rock. Flows and water turnover decrease relative to the base scenario.

In around 64,000 years, the ice front reaches Aberg, which is then situated in the ice marginal zone. The ice margin lies in the sea. When the ice approaches, pressure gradients once again appear. The extent of the ice sheet varies during the period, and the ice front may be located at a distance of 0–10 km from the repository. During the period the maximum ice thickness may amount to several hundred metres. The maximum water pressures may amount to several hundred kPa, and appear in the area midway between two ice tunnels. Gradients and flows are controlled by the topography of the ice sheet and by the existence of ice tunnels. Very large gradients occur locally and non-saline,

oxygen-rich meltwater infiltrates the bedrock. Flows and water turnover increase in relation to the base scenario. The groundwater flows for a situation where the ice front is located directly above Äspö have been calculated by Svensson /1999a/ (see also Figure 10-21 and section 1.10.3). On the basis of these calculations and the simulations mentioned above /Svensson, 1999b/, the increase of the flows when the area is located in the ice margin zone are judged to be much greater than during regression.

When the ice retreats, Aberg lies below the surface of the sea. The pressure gradients disappear and flows are again driven by density differences. The conditions remain largely the same – even though the sea level varies – until the ice sheet once again approaches Aberg.

In about 95,000 years, the ice front once again approaches Aberg. The area is situated in the ice marginal or melting zone up until the start of the next interglacial. The maximum ice thickness can amount to about 2,000 metres, which means a maximum increase of the water pressure by nearly 20 MPa. After approximately 112,000 years, the ice sheet leaves the Aberg area, which is then once again below the surface of the sea. An approximately 17,000-year long period with increased flows is thereby interrupted.

Aberg then remains below the surface of the sea for around 13,000 years, after which the highest parts rise up out of the sea. The pressure gradients follow the topography, and as the land rises the gradients increase. The conditions more and more resemble present-day conditions. Since the interglacial is both shorter and colder than the current one, the shoreline continues to lie above today's all the way until the next cold period begins and a new glacial/interglacial cycle is initiated.

During the period from 15,000 to 125,000 years from today, Aberg is assumed to be located completely beneath the sea. This means that, with the exception of the periods when the ice passes Aberg, gradients and groundwater flows will be much less than the current ones. A comparison of future groundwater flows with today's situation is made in Figure 10-19.

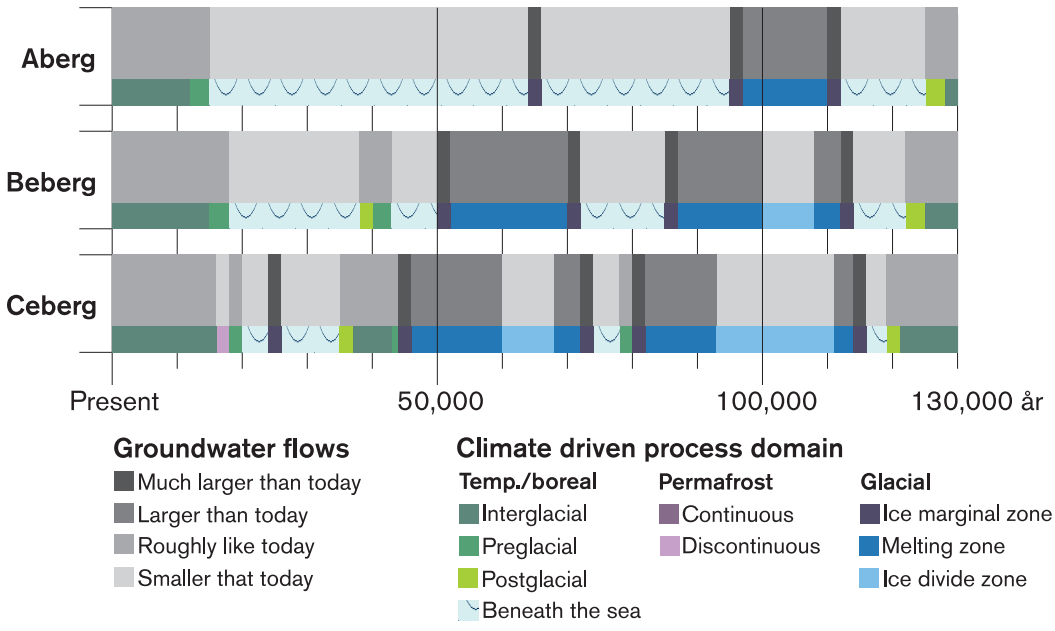

Figure 10-19. *A comparison between today's groundwater flows at Aberg, Beberg and Ceberg and the flows during the different stages of the next glacial/interglacial cycle.*

Beberg

Beberg is situated further north and further from the coast than Aberg. This means that the initial lowering of the relative shoreline will have less of an effect than at Aberg. As the ice sheet grows, Beberg becomes covered with water in a later stage. Furthermore, Beberg – unlike Aberg – rises up above the sea during the warmer of the cycle's two interstadials. Beberg is ice-covered during longer periods than Aberg, and the maximum ice thickness is greater, which means longer periods with increased groundwater flows and greater maximum groundwater pressures. The maximum increase of the groundwater pressure may reach around 25 MPa at Beberg. At the glacial maximum of the glacial/interglacial cycle, Beberg lies in the ice divide zone for approximately 8,000 years. During this period there are no gradients for groundwater flows, and conditions are virtually stagnant. A comparison of future groundwater flows with today's situation is made in Figure 10-19.

Ceberg

Ceberg is situated even further from the present-day coast and even further north than Beberg. Here the initial period of falling relative sea level will be of very little importance for the hydraulic evolution. A period of discontinuous permafrost will occur in about 16,000–18,000 years. During this period and the following 2,000 years when Ceberg gradually becomes submerged, groundwater turnover decreases.

The periods when Ceberg is ice-covered are more frequent and longer lasting than at Aberg and Beberg. The periods with increased groundwater flows are longer than at Aberg, but shorter than at Beberg. This is because Ceberg is situated in, or near, the ice divide zone for more frequent and longer periods. The maximum increase of the groundwater pressures is comparable with that at Beberg. The ice thickness is though greater at Ceberg, but when the ice thickness is at a maximum the area is situated in the ice divide zone. A comparison of future groundwater flows with today's situation is made in Figure 10-19.

10.8.5 Evolution in the near field

Climate-related changes influence groundwater pressures and groundwater flows. Substantially greater pressures and flows are expected in the glacial domain than in the base scenario. Increased flows are above all expected in the vicinity of the ice margin, but to some extent also in the melting zone. High water pressures may affect the canister mechanically, which is discussed in section 10.9.5. High groundwater flows at repository depth influence the potential inward transport of corrosive substances to the canister surface, as well as the influx of substances that can affect buffer function. These aspects are discussed in conjunction with the chemical evolution, section 10.10.5. During permafrost domains, within the ice divide zone, and when a site is transformed into seabed, the flows decrease relative to today. The potential influx of substances is affected not only by the flow, but also by the groundwater composition.

Hydraulic evolution in a defective canister

Changes in the water pressure when an ice sheet moves over an area will influence the inflow and outflow to/from a defective canister. Future pressures are discussed above. It is assumed that the maximum rate of ice sheet advance is 20 metres per year, and that the ice front retreats at a rate of 10–500 metres per year. The maximum water pressure is assumed to be 25 MPa, which corresponds to an ice thickness of 2,700 metres in the boundary between the melting zone and the ice divide zone.

When the ice sheet approaches, an initially defective canister is judged to have an internal hydrogen gas pressure from corrosion of the insert that is equal to (or greater than) the hydrostatic pressure in the rock, see section 9.1.7. The gas pressure prevents water flow into the canister. Water can only enter the canister by diffusion in the vapour phase. Corrosion of the insert is controlled by the ingress of water, which means that only a limited portion of the insert will corrode.

When an ice sheet moves over an area, the hydrostatic pressure in the repository increases. A pressure gradient is created across the buffer, which causes water to flow into the canister. Due to the increased water input, corrosion is expected to increase over the entire surface of the canister. Water influx can continue as long as the pressure gradient remains. If the whole surface of the canister is assumed to be accessible for corrosion, the corrosion rate is 0.1 μm/y and if the water supply is unlimited the pressure increase in the canister is estimated to be about 2 kPa/y. With the assumed values of ice surface slope and rate of advance of the ice front, this means that the gas pressure in the canister and the water pressure in the rock build up at the same rate. The water ingress process is not any different in principle from the initial water ingress in a defective canister, see section 9.1.7.

Gas can be transported out from a defective canister if the internal gas pressure exceeds the sum of the hydrostatic pressure in the rock and the buffer's swelling pressure (see section 9.1.7). In order for gas transport to take place, the gas overpressure in the canister must be at least equal to the buffer's swelling pressure. When the ice sheet is growing and the pressure is gradually building up, it is not likely that any gas transport will occur, although pressure reductions can occur in connection with ice tunnels.

When an ice sheet moves over the repository, the hydrostatic pressure may increase by 20–25 MPa. The gas pressure in the canister may increase to a level equivalent to the maximum water pressures. When the ice sheet reaches its maximum thickness the gas pressure inside a defective canister may be around 30 MPa, which is equivalent to 25 MPa ice pressure and 5–6 MPa from the water in the host rock. When the ice retreats, the hydrostatic pressure falls. When the pressure at repository level has fallen to a level equal to the gas pressure in the canister minus the buffer's swelling pressure, i.e. about 22 MPa, a gas channel can open in the buffer. Gas flows out from the canister. The gas channel remains open until the pressure gradient across the buffer has declined to the buffer's "shut-in pressure", see section 9.1.7. The ice sheet continues to retreat and the hydrostatic pressure continues to fall. The channel opens again when the hydrostatic pressure has fallen to a value that is lower than the gas pressure in the canister minus the buffer's swelling pressure. The safety-related importance of gas transport through the buffer is analyzed in the canister defect scenario, section 9.6.5.

10.8.6 Conclusions

During a glacial the groundwater flows change; they may both increase and decrease in relation to today's situation. On all three sites the groundwater flows will be less than or comparable with today's flows during the greater part of the coming glacial/interglacial cycle. At Aberg, this will be true about 85 percent of the time, at Beberg and Ceberg just under 70 percent. The groundwater flows can be expected to be greater than today when the areas are in the melting or ice marginal zone. The greatest increase of the flows can be expected in the ice marginal zone. Of the three sites, Beberg remains in the melting or ice marginal zone for the longest time; Ceberg, however, will lie at the ice margin for a slightly longer time.

10.9 Mechanical evolution

The mechanical evolution is coupled to the thermal and hydraulic evolutions. The mechanical evolution caused by the stresses to which the repository is exposed during the buffer's saturation stage, the thermal pulse from the spent fuel and long-term large-scale tectonic movements is described in the base scenario. Climate change is not expected to affect the saturation stage. The temperature variations that can occur due to climate change are small in relation to those generated by the spent fuel and are judged generally to be of subordinate thermomechanical importance. The development of an ice sheet is of importance for the large-scale tectonic movements.

10.9.1 Temperate/boreal domain

In addition to what is described in the base scenario, crustal upwarping/downwarping is deemed to be the only significant climate-related mechanical process that occurs in the temperate/boreal domain. The importance of the process for the repository's mechanical evolution is discussed in section 10.9.3 "Glacial domain" and in Chapter 11 "Tectonics – earthquake scenario".

10.9.2 Permafrost domain

When the water in the fractures in the rock freezes, it expands and exerts a pressure against the fracture surfaces and the fractures are widened. Since the deformation is not entirely elastic, the widening is partially permanent /Boulton et al, 1999a/. Freezing is not believed to occur at repository depth.

In the permafrost domain, the temperature at the surface is considerably lower than today. In contrast to the heat generated by the spent fuel, which gives rise to local stress concentrations in and around the heated rock volume, climate change only affects the vertical temperature gradients. The effect is uniform over large areas and is judged to be of subordinate importance for the repository's mechanical evolution.

10.9.3 Glacial domain

When an ice sheet moves over an area, the rock stresses are affected. Under ice-free conditions, the greatest principal stress is expected to be horizontal down to a depth of about 400–500 metres /Stephansson, 1993 in Boulton et al, 1999a/. The size of the horizontal stresses can presumably be coupled to tectonic movements. The vertical stresses are in principle equivalent to the weight of the overlying rock mass. When an ice sheet weighs down the bedrock, the vertical stresses in particular increase, but the horizontal stresses will also increase. The weight of the ice sheet depresses the earth's crust (the lithosphere, see Figure 10-13), which causes a flexure of the crust. The increment of the horizontal stresses caused by the downward flexure of the crust is different at different distances from the ice margin /Rehbinder and Yakubenko, 1998/. When the ice retreats the stresses decrease. Eventually the state of stress returns to that which prevailed before the ice sheet passed over the area. The horizontal stress increment persists longer than the vertical one. The stresses are affected not only by the ice load, but also by prevailing water pressures /Boulton et al, 1999a/. The changes in the stresses and the maximum water pressures are shown in Figure 10-20.

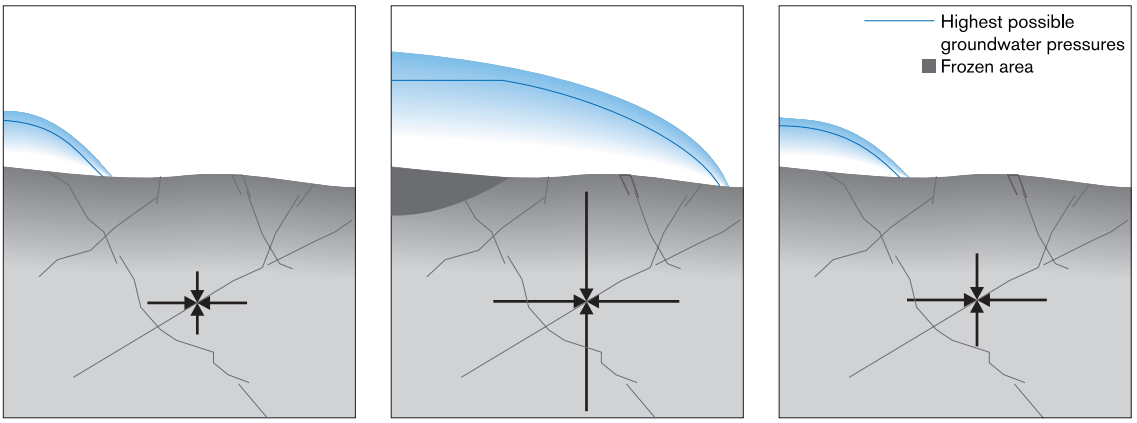

Before the ice sheet reaches the site, the horizontal stresses dominate.

When an ice sheet of great thickness overlies the site we can expect a surplus of vertical stresses.

After the ice has melted away, the vertical stresses are relieved faster than the horizontal stresses, which can cause horizontal and gently-dipping fractures to widen.

Figure 10-20. *The stresses in the rock vary when an ice sheet passes over an area.*

In the ice divide zone where the ice cover is thickest, ice thicknesses of up to 3,500 metres can occur. The total stresses, i.e. the combined effect of the unloaded rock stresses and the stresses caused by the ice load, are high. The ground is frozen, and the water pressure is equal to the pressure at the margin of the melting zone. The water pressure (groundwater head) is lower than the ice pressure (ice head). This means that the effective stresses, i.e. the total stresses reduced by the water pressure, are great. The bedrock is compressed (consolidated) and the fractures are pressed together (narrowed). Because the stress increment is anisotropic, fractures oriented in different directions are pressed together by different amounts. Permeability is altered in both magnitude and direction. The narrowing of the fractures leads to generally reduced permeability. The altered state of stress may, however, cause shear movements along certain critically oriented fractures. This shearing can lead to widening of the fractures /Rosengren and Stephansson, 1990; Israelsson et al, 1992 in Boulton et al, 1999a/.

The ice thickness is less in the melting zone. The water pressure is at most equal to the ice pressure. The water pressure is lower adjacent to the ice tunnels. The effective stresses are at a minimum in the area between two ice tunnels and increase towards the ice tunnel. In areas where the water pressure exceeds the minimum stress across a fracture, hydraulic fracturing occurs. At an ice thickness of 1,000 metres, the depth to which hydraulic fracturing can occur has been estimated to be 60 metres (ice thickness/16) /Lindblom, 1997/. When the ice retreats, the increased horizontal stresses remain. In combination with the decreased vertical stresses and high water pressures, this can lead to shearing and widening of gently-dipping fractures. Sediment can be injected into the fractures owing to the high pressures /Leijon and Ljunggren, 1992 in Boulton et al, 1999a/.

It is generally assumed that the ice load will have a stabilizing effect, which will suppress seismic activity. The strain energy that has been stored under the ice cover may be released during deglaciation. An increase in seismic activity and major earthquakes can therefore be expected when the ice retreats. This is discussed in Chapter 11, "Tectonics – earthquake scenario".

10.9.4 Evolution in the geosphere at the three repository sites

Aberg

The mechanical evolution of the repository is affected above all by the presence of the ice sheet. Aberg is situated in the ice marginal zone between 64,000 and 66,000 years in the future, when the ice cover reaches the stadial's maximum extent. The area lies beneath the sea. Where ice and sea meet, the thickness of the ice is assumed to be approximately 1.1 times the depth of the sea, i.e. the ice pressure and the water pressure are equally great. The total stresses increase with the ice thickness. If ice pressure and water pressure are equal, the effective stresses will be the same as under ice-free conditions. This is true at the ice margin. From the ice margin, the ice thickness increases at the rate of one metre every 50–150 metres; the total stresses increase accordingly. In the area between two ice tunnels, ice pressure and water pressure are roughly the same and the effective stresses are equal to those that prevail under ice-free conditions. Next to the ice tunnels the water pressures are lower and the effective stresses higher than under ice-free conditions.

During this period the ice front passes over the repository and the ice thickness may vary by on the order of 100 metres. The maximum ice thickness at Aberg is several hundred metres (sea depth + approximately 100 metres). The vertical stress increment is on the order of 1 MPa. This stress increment is judged to have a limited influence on the fracture geometry of the host rock. When the ice covers the area, however, hydraulic fracturing may occur near the surface.

After 95,000 years the ice front again reaches Aberg. The area then remains ice-covered for approximately 17,000 years. When the ice reaches Aberg the area is beneath the surface of the sea and the situation resembles that described above. Unlike before, the ice sheet continues to expand. When it reaches its maximum extent in about 105,000 years, the ice thickness at Aberg is projected to be around 2,000 metres. Ice and water pressure are thus much higher during this period. The total stresses increase. Aberg lies in the melting zone. The effective stresses between two ice tunnels are equivalent to those under ice-free conditions. The effective stresses increase in connection with the ice tunnels. Since ice and water pressure are higher, the increase of both total and effective stresses is greater than in the previous stage when Aberg was ice-covered. When the ice retreats in about 110,000 years there are considerable residual horizontal stress increments. In this stage, gently-dipping fractures may open and allow increased groundwater flows.

Viewed over the whole glacial/interglacial cycle, the bedrock has been depressed in three phases. When the ice recedes, the bedrock rises once again. This process can – possibly in combination with stresses caused by plate-tectonic movements – lead to an increase in earthquake frequency when the ice retreats. This is discussed in Chapter 11, "Tectonics – earthquake scenario".

Beberg

Like Aberg, Beberg lies under the ice sheet during two periods in the coming glacial/interglacial cycle. The evolution during the first of these periods (50,000–72,000 years) resembles the one that takes place at Aberg between 95,000 and 112,000 years. During the second of the periods, Beberg is ice-covered for a longer time, between 85,000 and 114,000 years. When the area is located in the melting zone, the conditions are similar to those described above. During this period, Beberg also lies in the ice divide zone for about 8,000 years. In this stage the effective stresses increase. The maximum ice

thickness may be just under 3,000 metres. This means that the total stresses will also be higher at Beberg than at Aberg. When the ice recedes in about 114,000 years, the residual horizontal stress increments are greater. The forces acting to widen gently-dipping fractures increase, and if this happens it allows larger groundwater flows.

Ceberg

Ceberg is located under the ice on three occasions during the glacial/interglacial cycle. On the first of these occasions (24,000–26,000 years) the situation is similar to that which arises at Aberg in 64,000 years. On the second occasion (44,000–74,000 years) the conditions resemble those at Beberg during the period 85,000–114,000 years. During the third period Ceberg is ice-covered (80,000–116,000 years), the cycle's maximum ice extent is reached. The ice thickness at Ceberg is then over 3,000 metres. The ground is frozen and both effective and total stresses are high. When the ice leaves the area in about 116,000 years, the horizontal stresses are high. This means that gently-dipping fractures may be opened.

10.9.5 Evolution in the near field

The changes during a glaciation affect the state of stress in the rock and thereby also the premises for fracture movements, fracturing and convergence of deposition holes.

Movements along a fracture intersecting a deposition hole can, if they are large enough, lead to canister damage. However, large movements can only occur along large fractures, i.e. fractures that extend far in their own plane. Fracturing, i.e. formation of new fractures or propagation of existing fractures, at a great distance from the repository's cavities could lead to amalgamation of fractures, and fractures of great extent that intersect canisters could develop. Such fractures are not desirable, since they can lead to large rock movements and water fluxes at the canisters. If the rock around the deposition holes is deformed in its entirety, the deposition hole is compressed – i.e. it converges. When the buffer material is compressed, its pressure on the canister increases. These pressure increases could damage the canister. The high water pressures that occur during a glaciation also contribute to the pressure increase. The maximum hydrostatic pressures are determined by the thickness of the ice at the transition between the melting and the ice divide zones, and by the water pressures that occur in the melting zone. (The boundary between the ice divide zone and the melting zone runs where the temperature at the ice/bed interface exceeds the pressure melting point.)

The scope of fracture movements – i.e. movements along existing fractures – has been calculated based on different ways of representing the properties of the bedrock and the interaction between ice sheet and bedrock. Both movements directly beneath the ice cover and movements in boundary areas have been studied. In the cases analyzed to date, no fracture movements large enough to damage canisters have been obtained /Hansson et al, 1995 in the Process Report/.

Fracturing and/or propagation of existing fractures can occur if the stresses and the stress anisotropy generated by the ice load are great enough. Increased principal stress differences may lead to shear failure. In the analyses performed to date, however, the stress increment from the ice load has only led to increased stress anisotropy in the vicinity of the tunnels and the deposition holes /Rosengren and Stephansson, 1996; Hansson et al, 1995 in the Process Report/. Glaciations are therefore not expected to be able to cause formation of new large fractures that intersect deposition holes or propagation and amalgamation of existing small fractures so that such fractures are formed.

Creep movements that could lead to compression of the deposition hole have been studied in general terms under very pessimistic assumptions regarding the properties and deformation of the rock /Process Report/. It was assumed in the calculations that the hypothetically possible creep movements around the deposition holes take place during the glaciation. The state of stress in the rock was assumed to be hydrostatic, i.e. the stresses are equal in all directions and are determined by the dead weight of the rock mass (approximately 14 MPa) and the ice load (approximately 30 MPa). The pressure on the canister then increased to approximately 44 MPa. If it is assumed that no creep movements occur, the convergence of the deposition holes will be negligible, which means that the bentonite buffer is not compressed and therefore retains its original swelling pressure (approximately 7 MPa). The ice load then acts instead on the canister via an elevated pore water pressure determined by the hydrostatic pressure. The maximum hydrostatic pressure is attained at the transition between the melting and ice divide zones. The maximum pressure increment has here been estimated to be about 25 MPa, which means that the hydrostatic pressure at repository depth will in this case be about 32 MPa. Thus, the total pressure on the canister will be about 39 MPa.

The canister insert in the BWR version has been calculated to withstand an external evenly distributed pressure of 80 MPa, while the insert in the PWR version can withstand 110 MPa, see section 8.8.2. This means that the canister ought to withstand the pressure increases that can arise during a glaciation. The calculations of canister strength need to be refined with more realistic inhomogeneous material properties according to section 8.9.2.

10.9.6 Conclusions

The state of stress in the rock will change during a glacial/interglacial cycle, which affects both seismic and aseismic movements in the bedrock. The influence of these changes on the state of stress and rock movements has not been fully analysed. The load situation is complex; both factors such as ice thickness, water pressure, crustal downwarping and large-scale tectonic movements, and the properties of the rock mass and the fractures influence the state of stress. The calculations presented above include several different ways of representing the interaction between bedrock and ice sheet. Based on the calculation results, it is assumed that the changes will not lead to rock movements that cause canister damage entailing a loss of integrity. The canisters are also expected to resist future hydrostatic pressures, but the canister calculations need to be refined. The conditions for groundwater flows will change when fractures are narrowed or widened. The coupling between hydraulic and mechanical conditions during glaciation has not been fully elucidated.

10.10 Chemical evolution

The chemical evolution is coupled to the thermal and hydraulic evolutions. In the base scenario, the chemical evolution in the repository is described under the assumption that today's climate situation remains unchanged and that land uplift continues. This means that the variations within the temperate/boreal domain's interglacial regime have already been elucidated. The thermal evolution influences the chemical evolution when temperatures below the freezing point occur. Otherwise the temperature variations within a glacial/interglacial cycle are of negligible importance for the chemical evolution. The hydraulic and chemical evolutions are strongly coupled; the expected changes in groundwater recharge and groundwater flows will influence the composition of the groundwater.

10.10.1 Temperate/boreal domain

The quantity of water that infiltrates the bedrock, as well as its composition, is affected by changes in temperature and precipitation as well as by shoreline displacement. Of these factors, only shoreline displacement is judged to be of any significant importance for groundwater composition. Shoreline displacement influences the salinity of the groundwater. In areas located above sea level, non-saline meteoric water infiltrates the bedrock. Near and under the sea (the Baltic Sea), salt water can, due to its higher density, penetrate down into the rock's fracture system (see section 10.8.1). The salinity of the seawater varies, partly due to changes in the Baltic Sea's connections with the ocean, and partly due to changes in runoff in the Baltic Sea basin. At the time of the most recent deglaciation, the Baltic Sea is believed to have been cut off from the ocean during several periods. During these periods the water was non-saline. There are also assumed to have been periods when the water was more saline than today's Baltic Sea. Traces of the most recent period with water more saline than today's have been confirmed /Andersson, 1998/.

How fast and how much the salinity changes depends on the direction and rate of shoreline displacement, the salinity of the rising/falling sea, the permeability of the rock and the salinity of the groundwater before the change. The permeability of the rock changes when the ice sheet passes over an area. Just after the ice sheet has retreated, water turnover may be elevated, see section 10.9.3. This may result in a more rapid exchange between non-saline and saline water. Variations in groundwater composition within the temperate/boreal domain are judged to be covered by the base scenario's undisturbed and future compositions.

10.10.2 Permafrost domain

The low temperatures mean that reaction and dissolution rates are reduced. At the same time the solubility of carbon dioxide increases, which in turn means that the solubility of calcite increases. For most chemical reactions, the temperature reduction is not of importance until the freezing point is reached. Another important process related to freezing is that solutes are frozen out and contribute to the salinity. Since freezing-induced salt exclusion takes place from the top down and water turnover thereby ceases, salt exclusion can make a significant contribution to an increase in salinity.

The magnitude of the increase in the salt concentration caused by freezing-induced salt exclusion is uncertain. There are indications of precipitated sodium sulphate mineral in study areas in Finland that suggest that high salinities caused by salt exclusion may have occurred. Under present-day conditions, and after the permafrost has thawed, these minerals go into solution and can only be traced in the water composition. At the site, sulphate-rich waters occur at depths of 100–300 metres. The interpretation that the sulphate-rich water is an indication of salt exclusion is not clear-cut, however; the sulphate may also originate from sulphide oxidation. Sulphide oxidation may have been caused by penetration of oxygen-rich water down into the bedrock, see section 10.10.3 below.

10.10.3 Glacial domain

As in the permafrost domain, the temperatures are low. The hydraulic situation differs from that in the permafrost domain. In the ice divide zone where the ground is frozen, conditions are more or less stagnant; the groundwaterpressure has a high but constant level. Freezing-induced salt exclusion occurs, and salinity can be expected to increase.

The areas in Sweden that may wind up in the ice divide zone generally have non-saline groundwater. The water can be expected to be non-saline due to the fact that the areas lie above the highest shoreline (marine limit) and/or have lain within the melting zone for an extended period before ending up in the ice divide zone. The increase in salinity due to salt exclusion can therefore be expected to be limited.

In the melting zone and at the ice margin, high water pressures occur locally, see section 10.8.3. Hydraulic fracturing, i.e. fracturing due to high water pressures, can increase permeability, and when the ice sheet withdraws gently-dipping fractures can open, see section 10.9.3. Oxygen-rich meltwater can infiltrate the bedrock. Calculations show that at the expected flow rates, the rock's redox-buffering capacity will prevent oxygen-rich water from reaching repository depth /Guimera et al, 1999/.

The transport of oxygen-rich glacial meltwater through the bedrock has been studied thoroughly /Guimera et al, 1999/. Data on pressure and flow conditions have been obtained from simulations of the conditions when the ice front is located straight above Aberg /Svensson, 1999a/, see also Figure 10-21. (In these calculations a functional relationship between hydraulic conductivity and kinematic porosity has been used, i.e. not the constant porosity value given in Figure 10-21.) The results of Guimera's calculations have been checked /Gascoyne, 1999/, and the conclusion of both studies is that the rock has the capacity to consume the oxygen before it reaches repository level. Theoretically it is possible to calculate a flow rate that is so fast that the reactions in the rock do not have time to consume all oxygen before the water reaches repository level. This happens when the advective velocity is higher than 10^{-5} m/s. The median value of the advective velocities in Svensson's calculations /1999a/ is $1.5 \cdot 10^{-7}$ m/s, two orders of magnitude lower. In zones of high permeability, however, when the pressure gradients are at a maximum, much higher calculated advective velocities occur. In the model it is assumed that the ice front stays in a position right above the repository. In reality the ice front moves at a rate of 10–100 m per year, which means that the areas with high pressure gradients are relocated. From the investigations SKB has conducted at Äspö, as well as on other sites, there are no geological indications that oxidizing water has occurred at repository depth. In the section on permafrost above, sulphate-rich water found in Finland is mentioned as a possible result of the occurrence of oxygen-rich water. The sulphate-rich water occurs at depths down to 300 metres.

The rock's redox buffering capacity is always sufficient to consume all the oxygen that will be infiltrated. If it is assumed that the water flow is so low that a redox front is formed, this front will move down to the repository in 400,000 years, i.e. at a rate of 1 mm per year /Guimera et al, 1999/. This estimation is based on flow in fractures solely. If the pyrite content in the rock matrix is also taken into account, the time will be 10 million years.

In the melting zone where high water pressures occur, glacial meltwater can penetrate deep down in the bedrock, whereby saline water from great depths is displaced by the non-saline meltwater. The saline water is conducted up to the surface at the ice tunnels and at the ice front, a phenomenon known as upconing. An outflow of saline water occurs from the area beneath the ice sheet, where the salinity decreases. The situation has been modelled under the assumption that the ice front is situated directly above Aberg /Svensson, 1999b/. The geological structural model is based on Rhén et al /1997/. Results and premises for the modelling are shown in Figure 10-21.

In general, salinities decrease in the melting zone, but adjacent to the ice margin and the ice tunnels, where saline water from great depths is transported up towards the surface, the calculated salinities increase. The salinity increase is greatest in the area in front of

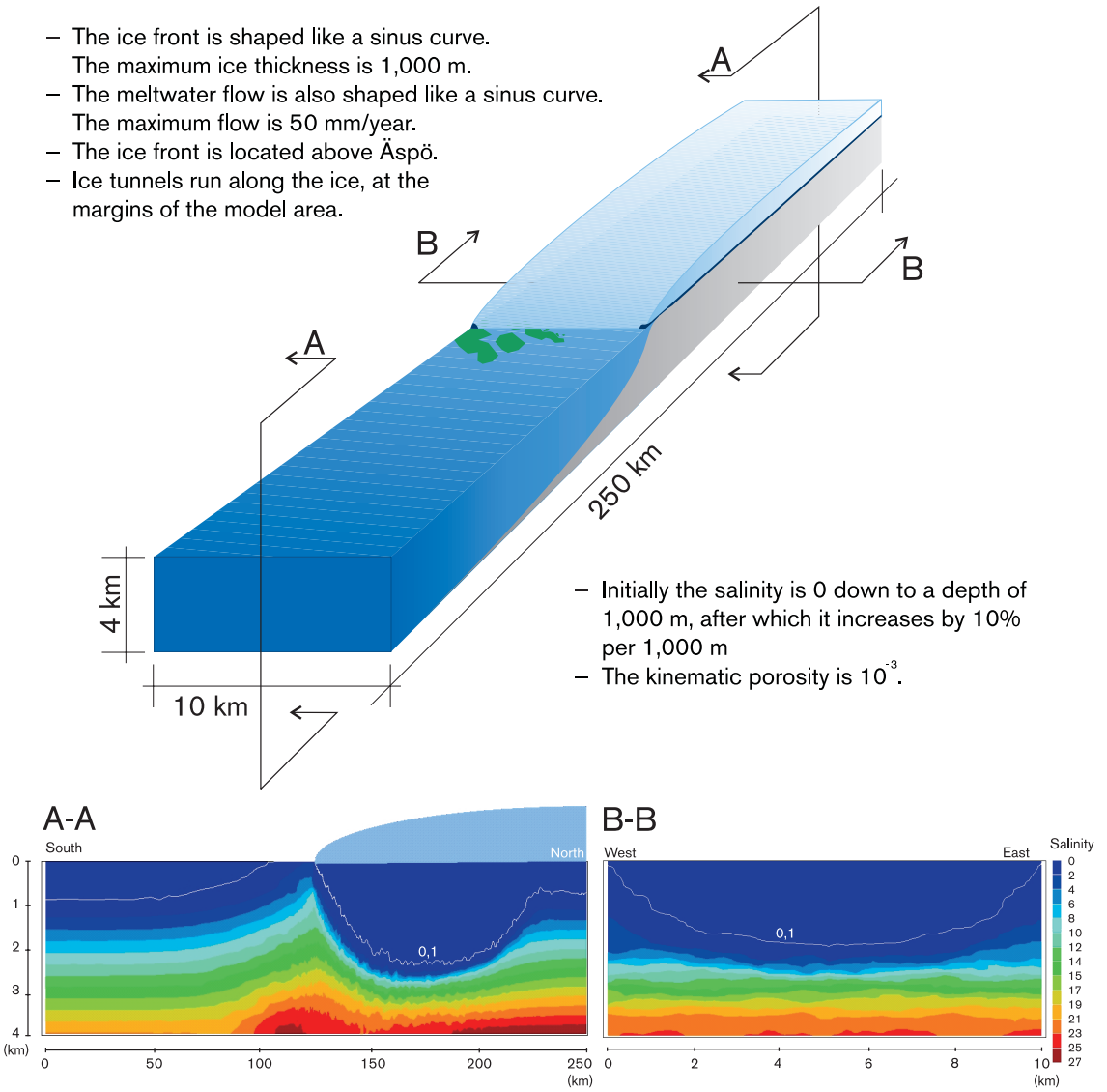

Figure 10-21. *Changes of the groundwater's salinity when the ice front is located straight above the repository /from Svensson, 1999/.*

the ice margin midway between two ice tunnels. Here salinities of 4–6 percent (40–60 g/l) have been calculated to occur at repository depth within a zone extending 5–10 km ahead of the ice front. In the modelling it is assumed that the ice is stationary. In reality the ice front moves at a velocity of tens of metres per year when the ice sheet is advancing, and hundreds of metres per year when it is retreating. The high salinities at repository depth are therefore only expected to occur during periods of at most one or two thousand years.

It is calculated that non-saline glacial meltwater can occur at repository depth for more or less the entire time the area is in the melting zone. Meltwater is forced down into the bedrock in the area between the ice tunnels. Water that was previously in the rock is conducted up towards the surface adjacent to the ice margin and into the ice tunnels. Around 5–10 km in from the ice margin and approximately 0.5 km from the ice tunnels and within the entire melting zone, the calculated salinity at repository depth is less than 0.1 percent.

Svensson's model describes the flow conditions at Aberg. The model includes a subdivision between saline and non-saline water where the initial state is non-saline water down to a depth of 1,000 metres. At greater depth the salinity increases continuously by 10 percent per 1,000 metres. This subdivision makes it possible to use the results quantitatively to assess the effects of upconing of deep (saline) groundwater. The results show that a salinity increase of up to 4–6 percent can be expected at repository depth at Aberg.

A salinity of 4–6 percent corresponds to a mean chloride concentration of about 25,000 mg/l. In order to calculate the composition of the saline groundwater at the ice front, a model was used /Laaksoharju et al, 1999/ based on the mixing of reference waters, see section 8.9.2. The present-day waters reported in the base scenario correspond to measured data from repository depth and the selected reference waters (glacial, meteoric, biogenic and marine water plus brine) /Laaksoharju et al, 1998/. In the case with saline water at the ice front, the fraction of brine in the measured groundwater samples has been proportionally increased until a chloride concentration of around 25,000 mg/l has been reached. In this way the composition of the saline water has been estimated based on the present-day water and its content of the different reference waters.

The evaluation is more complicated for infiltration of glacial meltwater. Svensson's calculation results show that glacial water can reach down to a depth of 4,000 metres, i.e. the bottom of the modelled rock volume. In some cases the calculated transit times through the rock and up to the ice margin are short, down to about 20 years. These results must be judged against the background of the model premises and established boundary conditions. The model's hydraulic conductivity is higher in the uppermost 600 metres than below that. This means that virtually all particles pass the uppermost 600 metres of rock. The conclusion is that glacial water can be expected to reach down to a depth of 600 metres in conductive fractures and fracture zones. It is, on the other hand, doubtful whether the glacial water will enter the fractures of lower conductivity that are in contact with deposition volumes in the rock. Some glacial water will probably be mixed with existing groundwater in proportions that are dependent on the conductivity. The lower the conductivity, the smaller the glacial water fraction.

Glacial meltwater has a low salinity where the most important ions are sodium, calcium, carbonate and chloride. The concentrations lie under 1 mg/l for each ion /Laaksoharju and Wallin, 1997/. The glacial meltwater resembles shallow groundwater. There is an important difference, however: shallow groundwater has a substantially higher concentration of calcium and carbonate than glacial meltwater. The reason is that infiltrating meteoric water passes through a soil layer with organic matter where biological processes emit carbon dioxide, the infiltrating water absorbs the carbon dioxide, which then becomes aggressive. These processes are not expected to occur beneath an ice sheet. In the rock the infiltrated aggressive water quickly dissolves calcite and other easily weathered minerals, while equivalent reactions take a much longer time for the glacial meltwater that penetrates down into the bedrock.

Even if glacial meltwater dissolves minerals more slowly, it is eventually affected by reactions with the minerals in the rock. In Table 10-2 below, two different water compositions have been selected as representative of waters that have undergone a similar evolution as glacial meltwater. They are:

- Grimsel – a water that has passed through the Alps for 500 metres before reaching a tunnel drilled into the rock. This water has infiltrated the rock high up in the Alps without being affected by soil layers and then migrated in the young granite fractures, where it has been affected in particular by sodium and calcium feldspar.

- Taavinunnanen – a modern water with a residence time in the rock of a few tens of years, which can be regarded as comparable with Grimsel water but under colder climatic conditions.

The composition of glacial meltwater as measured at the outlet from a glacier is also included in the table.

The Grimsel and Taavinunnanen waters are very similar to each other, but both are very different from glacial water. Reactions in the rock and mixing are the processes that cause the difference.

In Table 10-3, the base scenario's long-term compositions of the groundwater at Aberg, Beberg and Ceberg are compared with the above-presented compositions of the saline water at the ice front and the non-saline water in the melting zone. The saline water (saline ice front) can be expected during a short period when the ice front passes the site(s). The non-saline water (non-saline melting zone) can be expected during the periods an area is situated within the melting zone. The composition of the saline/non-saline water is determined above all by the presence of the ice and can be expected to be similar on the three repository sites.

Table 10-2. Composition of groundwaters that can be regarded as representing glacial meltwater that has infiltrated beneath an ice sheet and then been driven down to repository level over a period of some tens of years. The composition of a glacial meltwater is given for comparison.

Component/ variable	Grimsel	Taavinunnanen	Glacial water
pH	9.6	9.1	–
Sodium (Na^+ mg/l)	16	4.5	0.17
Calcium (Ca^{2+} mg/l)	8	7	0.18
Magnesium (Mg^{2+} mg/l)	0.2	1.2	0.1
Bicarbonate (HCO_3^- mg/l)	35	25	0.12
Chloride (Cl^- mg/l)	5	<1	0.1
Sulphate (SO_4^{2-} mg/l)	11	5	0.5

Table 10-3. The long-term water composition at the three sites in the base scenario and in the climate scenario. The data for the climate scenario pertain to the highest and lowest salinities that could conceivably occur.

Component/ variable	Base scenario Aberg	Beberg	Ceberg	Climate scenario Saline ice front	Non-saline melting zone
pH	8–9	7–9	8–10	6–8	8–10
Eh (mV)	−250 ± 50	−250 ± 50	−250 ± 50	−200 ± 100	−100 ± 100
Na^+ (mg/l)	100–2000	100–1000	50–150	4500	4.5
K^+ (mg/l)	2–10	2–10	0–5	37	4
Ca^{2+} (mg/l)	20–2000	20–1000	10–20	9900	7
Mg^{2+} (mg/l)	1–40	4–100	1–5	41	1
HCO_3^- (mg/l)	10–20	20–40	10–20	71	25
Cl^- (mg/l)	200–5000	200–5000	100–200	25000	<1
SO_4^{2-} (mg/l)	1–400	1–400	0,1–1	511	5
HS^- (mg/l)	0–1	0–1	0.1–1	0–1	<0.1
Colloids (mg/l)	< 0.5	<0.5	<0.5	<0.5	2–4
Fulvic and humic acids (mg/l)	< 0.5	<0.5	<0.5	<0.5	<0.5

10.10.4 Evolution in the geosphere at the three repository sites

Aberg

Today parts of the Aberg area lie below sea level. The height above sea level varies between –21 and 15 metres. The evolution during the initial phase of regression is described in the base scenario. After about 5,000 years the regression reverses into transgression. During the period 12,000–15,000 years, the area istransformed into seabed. Saline, or rather brackish, water (chloride content 1,000–5,000 mg/l) inundates the area. The pressure gradients for groundwater flow decline. As the transgression proceeds, the saline water infiltrates the bedrock due to density differences. The Baltic Sea is, like today, a semi-enclosed sea. Its salinity may be slightly higher than today, mainly due to reduced runoff after the transition to a colder climate.

The entire Aberg area remains below the shoreline 110,000 years into the future. Only after 125,000 years do the highest parts of Aberg once again rise up out of the sea. A saline water is expected; its composition is covered by the variations included in the base scenario. The only change that can affect the groundwater composition during this long period is occurring when the ice sheet reaches the area. This occurs during two periods: in 64,000–66,000 years, and in 95,000–112,000 years. During the first of these periods the ice front reaches the area, and the ice margin can be expected to lie close to Aberg. The ice front may stay within a distance of about 0–10 km from the deep repository. Underneath the ice, saline water is displaced by non-saline glacial meltwater. Saline water is pressed up towards the surface at the ice front and the ice tunnels. The water composition at repository depth depends on the position of the repository in relation to the ice margin and ice tunnels; both less and more saline conditions than in the base scenario are possible during this relatively short period.

The second time the ice front reaches the area is in 95,000 years. This time the ice continues to grow and the ice front passes over and past Aberg. When the ice sheet reaches its maximum extent, the ice thickness at Aberg may be over 2,000 metres. Aberg is situated in the melting zone. Non-saline glacial water displaces the brackish groundwater. Towards the end of the period, the water at repository depth can be expected to be non-saline with a composition similar to that given for the melting zone in Table 10-3. When the ice withdraws, gently-dipping fractures may be opened and permeability may increase. This may speed up penetration of non-saline meltwater, expulsion of saline water from greater depth and infiltration of seawater. At this stage the Baltic Sea is periodically a freshwater lake and periodically an semi-enclosed sea with a salinity higher than in today's Baltic Sea. The evolution resembles that which took place during the most recent deglaciation, about 14,000–8,000 years ago. Aberg is situated beneath the surface of the lake/sea all the way up until 125,000 years into the future, when the highest parts rise out of the sea. In about 128,000 years, the conditions once again resemble today's, even though the relative shoreline is still slightly higher than today.

Beberg

Beberg is situated about 10 km from the coast, 20–44 metres above sea level and further north than Aberg. The higher elevation means that the periods when the area is above sea level are more frequent and longer-lasting than at Aberg. The northerly location means that the periods when the ice reaches the area are also more frequent and longer-lasting. During the next glacial cycle, which spans 130,000 years, the entire Beberg area will lie below the shoreline for 99,000 years, during which period the area will be ice-covered for a total of 51,000 years, of which it will lie in the ice divide zone for 8,000 years. This can be compared with the Aberg area, which lies completely below the

shoreline for 110,000 years, of which it lies in the ice marginal or melting zone for 19,000 years. The entire Beberg area lies above the shoreline for a total of 17,000 years (0–15,000 years and 128,000–130,000 years). It never happens that the entire Aberg area lies above the shoreline.

Non-saline water can infiltrate the ground surface (the bedrock) when all or part of the bedrock lies above sea level or when it lies beneath the ice, i.e. when conditions are temperate/boreal or when the area lies in the ice marginal or melting zone. During a relatively short period when the ice front passes, saline water from great depths may be conducted up towards the surface. Salinity increase due to groundwater recharge takes place when the area is submerged. When an area lies above sea level, the groundwater flow is controlled by pressure gradients that follow the topography. When it lies beneath (or close to) the ice, the groundwater flow is controlled by the presence of the ice. The topography in Beberg is flat, which means that the pressure gradients for groundwater flow can be expected to increase considerably when the area lies in the ice marginal or melting zone.

All or parts of the Beberg area may thus be infiltrated by fresh water during 74,000 of the 130,000 years of the next glacial/interglacial cycle, while the area lies completely beneath the sea for 48,000 years. Beberg lies in the ice divide zone for 8,000 years and no groundwater recharge takes place. This can be compared with the Aberg area, which is accessible for infiltration by non-saline water for 39,000 years and lies completely submerged for 91,000 years. Viewed over the glacial/interglacial cycle, we can thus expect a greater presence of non-saline water at Beberg than at Aberg.

Ceberg

Ceberg is located closer to the coast than Beberg, but considerably higher: 80–130 metres above sea level. Ceberg is the most northerly of the repository sites. Its higher altitude means that the periods during which the area lies above the shoreline are more frequent and longer-lasting than at Aberg and Beberg. The northerly location means that the site is ice-covered during longer periods. Of the three sites, only Ceberg is reached by the ice sheet during all cold periods of the glacial cycle. Ceberg has the steepest topography of the three sites; the increase of the pressure gradients in the presence of the ice is therefore less at Ceberg. During the next glacial/interglacial cycle (130,000 years), the entire area is situated below the shoreline for 74,000 years, during which time it is ice-covered for 54,000 years. (Altogether the area is ice-covered for 68,000 of the cycle's 130,000 years.)

The entire Ceberg area lies above the shoreline for a total of 30,000 years (0–18,000 years, 39,000–43,000 years, and 122,000–130,000 years). Parts of the area lie above the shoreline for 12,000 ice-free years (18,000–20,000 years, 35,000–39,000 years, 43,000–44,000 years, 78,000–80,000 years, 119,000–122,000 years). The Ceberg area lies in the ice marginal or melting zone for a total of 42,000 years (24,000–26,000 years, 44,000–60,000 years, 68,000–74,000 years, 80,000–93,000 years and 111,000–116,000 years). All or parts of the Ceberg area can thus be infiltrated by fresh water during 84,000 of the 130,000 years of the next glacial/interglacial cycle, while the area lies completely beneath the sea for 20,000 years. Ceberg lies in the ice divide zone for 26,000 years and no groundwater recharge takes place. The Aberg area can be infiltrated by fresh water for 39,000 years, lies completely beneath the sea for 91,000 years, and never lies in the ice divide zone. Equivalent periods for Beberg are 74,000 years, 48,000 years and 8,000 years. Viewed over the glacial/interglacial cycle, we can thus expect a greater presence of non-saline water at Ceberg than at both Beberg and Aberg.

Figure 10-22 shows for how large a portion of the next glacial/interglacial cycle the three sites are in a climate domain where all or parts of the groundwater that is recharged within the area is non-saline. The figure also shows the periods during which the areas lie completely beneath the sea and salt water penetrates into the bedrock. Finally, the periods during which the sites lie in the ice divide zone, and when a permafrost domain can prevail, are shown. During these periods, virtually no groundwater recharge takes place, but the salinity of the water can be expected to increase as a result of salt exclusion due to freezing. Brief periods of increased salinity also occur when the ice front passes and saline water from great depth is conducted up towards the surface.

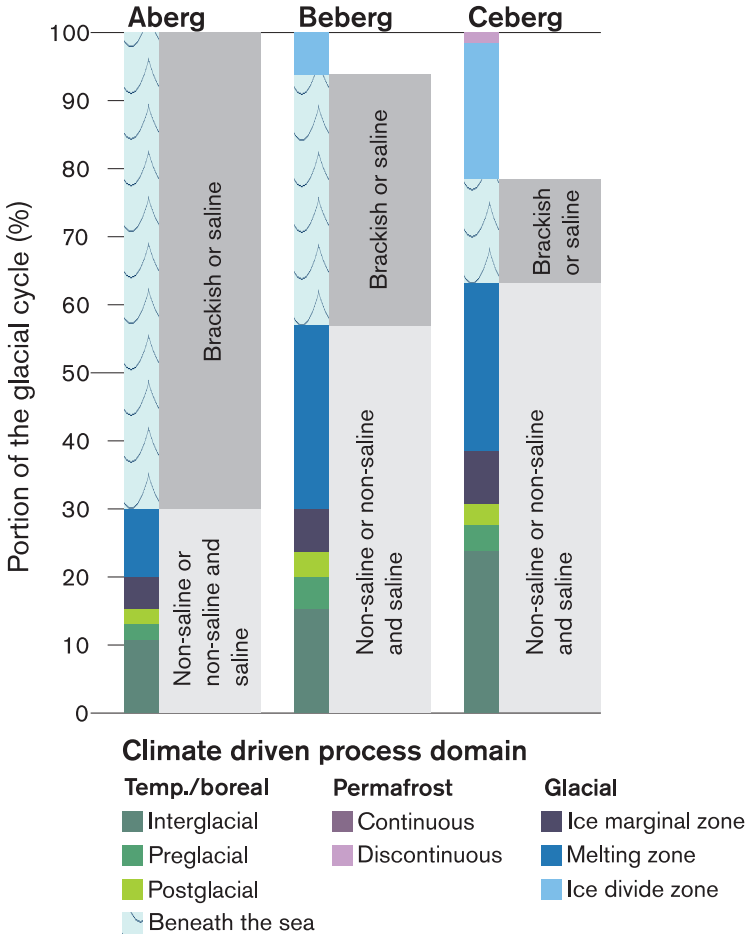

Figure 10-22. *Portion of the next glacial/interglacial cycle during which the three repository sites are in a climate domain where all or parts of the groundwater that is recharged within the area is non-saline; the periods during which the areas lie completely beneath the sea and infiltrating water is brackish or saline; and the periods during which the sites lie in the ice divide zone, or permafrost prevails, and virtually no infiltration of water from the surface takes place.*

10.10.5 Evolution in the near field

The changes during a glaciation that can have a negative influence on the chemical evolution in the near field are intrusion of oxygen-rich water, presence of very saline water, and presence of non-saline water with low content of positive ions. The following processes in the near field are affected:

- Corrosion of the copper canister.
- Ion exchange, swelling and chemical erosion of the buffer.
- In case of leaking canisters:
  - corrosion of the cast iron insert,
  - speciation of radionuclides.

In comparison with the base scenario, oxygen-rich water is expected at greater depths when an ice sheet moves over an area. The oxygenated water occurs in fracture zones with high hydraulic conductivity. It is generally not likely that oxygenated water will reach repository depth. Nevertheless, locally where groundwater flow gradients and hydraulic conductivity are high, oxygenated water could be transported down to great depth. This means that if oxygenated water should occur at repository level, its occurrence will be limited, both in time and space. In the unlikely event that oxygenated water should reach a deposition hole, the bentonite buffer has a high capacity to consume oxygen /Guimera et al, 1999/, so oxygenated water should never reach the canister.

During the temperate/boreal domain the expected salinity variations lie within the variations between non-saline and saline water that exist today at the three repository sites. When the ice front passes, high salinities can occur at repository depth. Higher salinity results in faster ion exchange and thereby faster lowering of the swelling pressure to 4–5 MPa, which is reached after completed ion exchange from Na^+ to Ca^{2+}, see the base scenario. Not even if the high salinities occurring briefly when the ice front passes were to be permanent would the function of the buffer be jeopardized, according to the analysis in the base scenario.

The low salinities that can occur at repository depth when a site lies in the melting zone lie slightly below the range reported in the base scenario. Lower salinity results in slower ion exchange. The estimated concentration of divalent cations is sufficient to prevent buffer erosion, but the margin is small.

The changes in groundwater composition that can be expected in relation to the base scenario are not judged to have any significant impact on the corrosion of the cast iron insert or the speciation of radionuclides.

10.10.6 Conclusions

The groundwater composition, particularly the salinity, will change during a glacial cycle. The variations in groundwater composition that can be expected within a glacial/interglacial cycle are reported in Table 10-3. The expected changes in relation to the base scenario are not judged to threaten the integrity of the engineered barriers.

As in the base scenario, the conclusion is drawn that the long-term effects of erosion under extreme conditions may need to be further investigated. The chemical evolution and function of the backfill in the climate scenario remain to be accounted for.

10.11 Radionuclide transport

Radionuclide transport only occurs if there are leaking canisters in the repository. The changes during a glaciation are not expected to cause any damage to canisters such that their integrity is threatened. The conditions for groundwater flow and thereby the groundwater composition changes during a glaciation. If there are initially leaking canisters, these changes will influence the transport of radionuclides from the repository and through the rock. Conditions in the biosphere are radically altered during a glacial/interglacial cycle. This greatly influences the doses to which man may be exposed. The doses are also affected by changes in the nuclide content of the spent fuel, and the fact that the radioactivity of the spent fuel declines with time. Higher and lower doses are discussed below with the intention of describing how the climate-related changes affect the doses, relative to a case with a given (arbitrary) set of canister defects.

The changes within the climate scenario can be handled with the same models as are used to describe radionuclide transport in the canister defect scenario (see 9.10). The climate scenario can primarily influence the transport processes advection, sorption and colloid transport in the rock and sorption in the buffer. The other transport processes discussed in the canister defect scenario (section 9.10) are influenced to a lesser extent.

Changes in groundwater flow will directly influence advection in the rock, partly by changing the magnitude of the groundwater flow, and partly by changing the routing of the transport pathways. The resultant changes in the form of changed groundwater fluxes and changed advective travel times can be described with the model chain, but the actual transition phase from one domain to another is not described. Theoretically, radionuclides could first be accumulated, via matrix diffusion and sorption, along a transport pathway and then be "washed out" if the groundwater flow changes direction. The importance of these transient effects is judged to be very limited, however.

Changes in groundwater composition influence sorption. In calculations with the model chain, such changes can be described by changing the sorption coefficients (K_d values) in the models. The transition between the domains is not described in the models, but neither in this case is this simplification judged to be of any great importance for the calculation results.

Water with an extremely low concentration of dissolved salts could erode the bentonite buffer, whereby colloids might be formed. As observed in section 10.10.5, this is not projected to happen in the climate scenario. Transport of radionuclides sorbed to colloids can thereby be neglected in the climate scenario as well.

10.11.1 Temperate/boreal domain

Radionuclide transport within the temperate/boreal domain's interglacial regime is investigated in the base and canister defect scenarios.

The climate-related process in the temperate/boreal domain that is of the greatest importance for radionuclide transport is shoreline displacement. The pressure gradients for groundwater flows increase during regression. When seabed becomes land, the biosphere changes so that dilution of radionuclides decreases. The reverse happens during transgression. The salinity of the groundwater also changes during regression/transgression, but the variations are not judged to have any significant bearing on radionuclide transport. Regression leads to increased doses on a coastal site, especially when the biosphere is transformed from sea or sea bay to wetland or forest. The reverse happens during transgression, leading to reduced doses.

Within the preglacial regime, regression occurs initially, which may be faster than the interglacial. In the base and canister defect scenarios, the conclusion is drawn that the transformation of seabed to land has a limited influence on the groundwater flow at repository level, since the shoreline is already downstream of the repository locations. The rate of the regression does not affect this conclusion. The expected variations of groundwater salinity also lie within the frame of the base and canister defect scenarios. The most dramatic changes occur in the biosphere. When seabed becomes land, the conditions for turnover of radionuclides in the biosphere are radically changed. Wetlands formed in the preglacial stage may have a relatively short lifetime, since the regression is interrupted by transgression when the growing ice sheet depresses the earth's crust.

During transgression, when a land area is transformed into a seabed, the groundwater flows switch from having been pressure-driven to being density-driven. Saline water displaces non-saline water that infiltrated the bedrock when it was above the shoreline. The biosphere switches to marine, which means that the doses to which humans will be exposed decrease radically.

At the start of the postglacial regime, the relative shoreline is much higher than today. A very rapid regression takes place. When the ice sheet begins to grow again, or the shoreline approaches the present-day one, the rate of regression slows. The influence on groundwater flows and biosphere is the same as described above for regression within the preglacial stage. Wetlands formed in the postglacial stage will have a much longer lifetime than those formed in the preglacial stage.

10.11.2 Permafrost domain

In the permafrost domain, water turnover in the rock diminishes. During most of the year the ground is frozen and no groundwater recharge takes place. Locally, large pressure gradients for groundwater flows may occur. Even if this is taken into account, the possible transport of radionuclides to the biosphere is projected to decrease under permafrost conditions. No studies confirming this have been conducted to date.

During the short summer when the active layer thaws, water turnover at the surface is great. Due to the plentiful supply of water and erosion when the ground thaws, radionuclides that may have been frozen fast will be greatly diluted.

In general, the rock's capacity to retard radionuclide transport is judged to be as good as or better than under present-day conditions. The same applies to dilution and dispersal in the biosphere. More in-depth analyses of the permafrost domain need to be carried out to quantify these differences, however.

10.11.3 Glacial domain

Conditions in the ice divide zone are more or less stagnant. No groundwater flows occur, and thereby no radionuclide transport.

In the melting and ice marginal zones, the groundwater table is determined by the topography of the ice, meltwater flows and the permeability of the bedrock. The maximum groundwater pressure is equivalent to the ice pressure. Where the water pressure exceeds the ice pressure, ice tunnels form, causing local drawdowns in the groundwater table. Midway between two ice tunnels, the pressure gradients correspond to the topography of the ice. In towards the ice tunnels, the gradients may be considerably greater. The gradients for groundwater flow increase with decreasing

distance to the ice margin. Close to the ice margin, and next to the ice tunnels, water turnover in the bedrock is generally greater than under ice-free conditions. A little way in from the ice margin in the area between the ice tunnels, the groundwater flow may either decrease or increase compared with today's. Whether the flow increases or decreases depends on the meltwater flow, the location of the site in relation to the ice tunnels and the topography of the site in relation to that of the ice sheet. The groundwater moves in towards the ice tunnels. Meltwater and groundwater are then transported through the ice tunnels towards the ice margin, which may be located many hundreds of kilometres from the repository site. In the areas where groundwater flows increase, water turnover at the surface is also great. This means that dilution and dispersal in the biosphere will be great, and the potential doses low.

10.11.4 Evolution in the geosphere at the three repository sites

Climatic conditions and the hydraulic evolution at the three repository sites are shown in Figure 10-19.

Aberg

Conditions during the initial period are described in the base and canister defect scenarios. After some time the relative shoreline stops falling and begins to rise instead. In about 10,000 years it is back at the present-day level, and in about 15,000 years the entire area lies under water. The changes in the hydraulic conditions during this period are not of any great importance for radionuclide transport through the rock. Dilution and turnover of radionuclides in the biosphere will increase and doses decrease when land is transformed into sea.

During the period 15,000–64,000 years, Aberg lies beneath the surface of the sea. Initially the groundwater flow is density-driven as non-saline water is displaced by saline water. When the non-saline water has been replaced by saline water, conditions are more or less stagnant. The area lies beneath the sea, which means great dispersal in the biosphere. No calculations of groundwater flows have been carried out, but it can be concluded that the transport of groundwater from great depth up to the surface will decrease in relation to present-day conditions. This, and the change of the biosphere, lead to a decrease in the dose to man.

During the period 64,000–66,000 years, the ice front is assumed to reach Aberg. Figure 10-21 shows how salinity varies next to the ice margin. The same calculation model and boundary conditions have been used to calculate groundwater fluxes, travel times and exit points for radionuclides /Svensson, 1999a/. Based on these results, a calculation case for the model chain has been set up. The groundwater flux has been set at 200 times today's median flux. The estimate is based on the relations between the maximum fluxes in the above modelling and a modelling of today's regional fluxes /Svensson, 1997/. The high fluxes give rise to such small advective travel times that the geosphere's capacity to retard radionuclide transport (see section 9.10) is negligible. The exit points are above all along the ice tunnels. In the area in the vicinity of the ice margin there are some exit points just in front of the ice margin. Furthermore, pessimistic values are assumed for canister damage, i.e. a large breach arises after 20,000 years. The results of the calculation case are shown in Figure 10-23.

The results in Figure 10-23 are relevant for the periods Aberg lies in the ice marginal zone, in other words 64,000–66,000 years, 95,000–97,000 years and 110,000–112,000 years. When the area lies in the melting zone (97,000–110,000 years), they can be

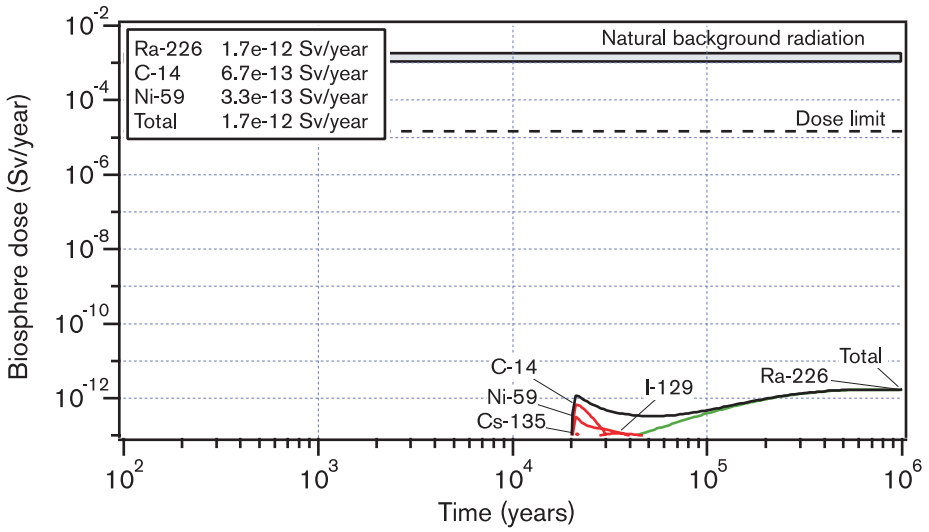

Figure 10-23. *Results of radionuclide transport calculations under the assumption that the ice front all the time lies directly above the repository at Aberg.*

regarded as an upper limit for radionuclide transport and doses. The larger groundwater flux is calculated to give rise to increased outward transport from the near field in relation to present-day conditions. The high fluxes and short travel times entail that the calculated retardation in the far field is negligible, see Figure 10-23. Since the dilution of radionuclides in the biosphere is so great, the calculated doses are nevertheless negligible and far below the dose limit, 0.014 mSv/y.

When the ice leaves Aberg, the area is far below the surface of the sea. The relative shoreline falls rapidly, and after 125,000 years the highest parts of Aberg rise up out of the sea. Conditions are once again similar to today's.

In summary, it can be said that during most of a glacial/interglacial cycle, the groundwater flows at Aberg will be smaller than today's. At the same time, the dilution of radionuclides in the biosphere will be greater than today. This is because most of the area lies beneath the sea. During the relatively short periods when the ice sheet leads to increased groundwater flows, radionuclide dilution in the biosphere increases even more. Water turnover in the ice tunnels is considerable, and when the ice front is located above Aberg the area lies beneath the surface of the sea.

A rough estimate of how groundwater flows and radionuclide dilution in the biosphere change during the next glacial/interglacial has been made in Figure 10-24. The estimate of groundwater flows is based on Svensson's simulations /1997; 1999a; 1999b/. Data on dilution in the biosphere are based on assumptions concerning what typical ecosystems (modules) are expected during the different epochs /Nordlinder et al, 1999/. Only the order of magnitude of the changes (1, 10, 100 etc.) in relation to present-day conditions is given. A notional zero value has been introduced for the groundwater flows pertaining to periods when conditions are more or less stagnant. During these periods, virtually no transport of radionuclides to the surface takes place. Moreover, the periods when the area is ice-covered are marked. The human beings that could be exposed to radionuclides during these periods are assumed to reside at the ice margin, far from the repository site.

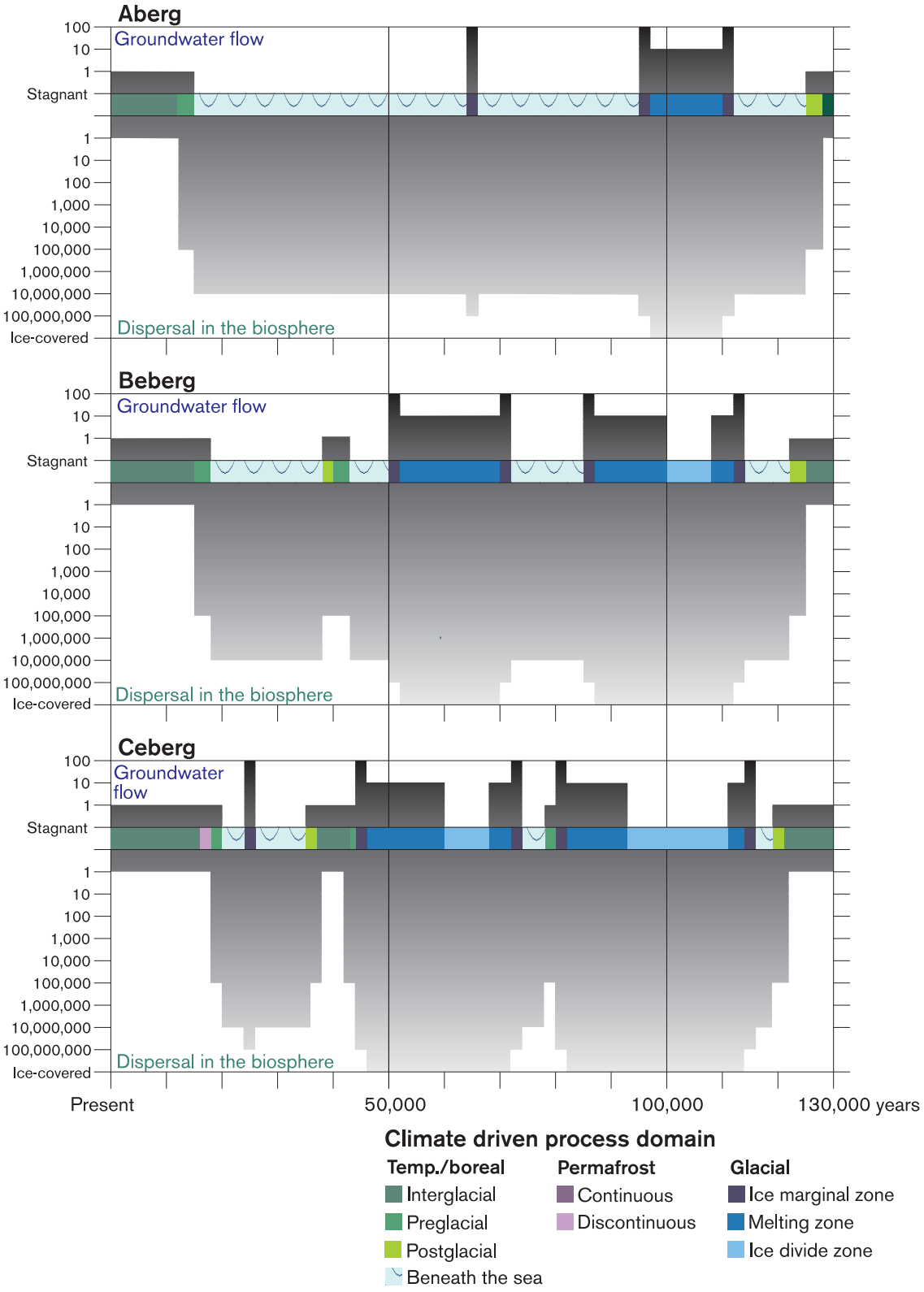

Figure 10-24. *Roughly estimated changes in groundwater flows and dilution in the biosphere at the three repository sites. Increased groundwater flows lead to greater releases of radionuclides from the near field and poorer capacity of the rock to retain and retard radionuclides. With increased dilution in the biosphere, the dose to man decreases accordingly.*

Beberg

Conditions during the initial period are described within the base and canister defect scenarios. The evolution during the initial period resembles that at Aberg. After approximately 15,000 years, the rising shoreline reaches the lowest-lying parts of Beberg, and after 18,000 years the entire area lies beneath the sea. The groundwater flows decrease, and dispersal in the biosphere increases. During a period with warmer climate between 38,000 and 43,000 years in the future, parts of the Beberg area, in contrast to Aberg, rise out of the sea,. The groundwater flows are similar to today's. The biosphere is similar to that in present-day coastal districts. During the period 43,000–50,000 years, Beberg once again lies beneath the sea.

During the cold period between 40,000 and 70,000 years, the ice sheet reaches Beberg earlier than Aberg. The ice sheet expands over the site and remains for a longer period. When the ice margin passes, Beberg lies beneath the sea. At the stadial's maximum, the ice margin is approaching the Baltic States.

When the ice has left Beberg, the area remains beneath the sea until the ice sheet once again approaches in 85,000 years. The area lies in the ice marginal and melting zone until 100,000 years. During the period 100,000–108,000 years, Beberg lies in the ice divide zone. No groundwater flows occur and thereby no radionuclide transport. Then follows another period in the melting zone before the ice margin passes the area. The groundwater flows are larger than today, but the doses are small thanks to increased dilution in the biosphere.

When the ice leaves Beberg the area lies beneath the sea. After 122,000 years the highest parts of the area rise up out of the sea, and conditions increasingly resemble today's.

As at Aberg, the groundwater flows, and thereby radionuclide transport, are less than today's for most of the time. When the flows are large, dispersal in the biosphere is also large.

Ceberg

Conditions during the initial period are described in the base and canister defect scenarios. Before subsidence of the bedrock transforms the Ceberg area into seabed, the area experiences a brief period with discontinuous permafrost. Radionuclide releases and doses are assumed to be less during this period than under present-day conditions.

Ceberg is in contact with the ice sheet for one period more than Aberg and Beberg. During this 2,000-year-long period, the area lies in the ice marginal zone, the ice margin lies in the sea. During the other two stadials, Ceberg lies beneath the ice cover for a longer time than Aberg and Beberg. For a large part of the time Ceberg is ice-covered, the area lies in the ice divide zone.

Since Ceberg is situated further from the coast than the two other sites, it rises up out of the sea during the interstadials. In connection to the interstadial between 30,000 and 40,000 years and between 39,000 and 43,000 years, the entire area lies above the sea surface. Conditions for radionuclide transport are similar to those described in the canister defect scenario. During the subsequent cold period, the ice front reaches Ceberg in 44,000 years. Ceberg then lies on the coast, and the high parts stick up like islands in an archipelago. The groundwater flows increase, as does dispersal in the biosphere. Since the area is not completely submerged, dispersal in the biosphere may be less than on the other sites, but it is projected to be large enough that the doses will be lower than in the canister defect scenario.

When the glacial period is interrupted by the next interglacial period, Ceberg lies beneath the sea. The shoreline falls rapidly, and in about 122,000 years the area lies completely above the shoreline and conditions are similar to today's.

10.11.5 Conclusions

During periods of high groundwater flows, the potential outward transport of radionuclides from a repository with leaking canisters increases. Increased groundwater flows can be expected in coastal locations during regression, but above all when an area lies in the melting or ice marginal zone. When the groundwater flows are at a maximum, water turnover at the surface is also great. This means that the dilution of radionuclides in the biosphere is expected to increase. Taken together, this means that the doses will decrease relative to present-day conditions.

A relative increase of the doses is only expected at Aberg, where the relative shoreline falls compared with the present-day level so that submerged areas become land. This only occurs during interglacials at the transition to a colder climate, in other words roughly every hundred thousand year. The increased doses are above all due to changes in the biosphere. The importance of this change is being investigated in the canister defect scenario, where the effects of land uplift are included in the reasonable case.

10.12 Summary

The climate scenario describes an assumed course of events during the next glacial/interglacial cycle. It is based partly on modellings of the evolution during this period, and partly on the historical pattern that has characterized the past 400,000–900,000 years (especially the Weichsel period). The depicted evolution can thereby be seen both as a scenario for the next 130,000 years and as a general description of the course of events during any glacial/interglacial cycle.

The description of future climatic conditions is based on three climate-driven process domains:

- Temperate/boreal domain.
- Permafrost domain.
- Glacial domain.

The changes in the repository's surroundings and how they may influence the evolution of the repository are discussed within each domain.

In relation to the base scenario, the transitions between colder climate, with permafrost and ice growth, and warmer climate, with conditions similar to today's, have the following consequences:

- Conditions in the biosphere are radically altered.
- The temperature in the rock is affected.
- The conditions for groundwater flow are changed – groundwater flow may both decrease and increase during different periods.
- Changed load conditions in the rock during glaciation. The load conditions influence the properties of the fractures, and thereby have feedback to the conditions for groundwater flow.
- The ice sheet also causes subsidence/uplift of the earth's crust. In coastal districts, this influences the conditions for groundwater flow. Subsidence/uplift also influences the large-scale tectonic conditions.
- Changed groundwater composition, in particular the water's salinity will vary.

The most striking climate-related changes take place in the biosphere. During a glacial/interglacial cycle, the biosphere is altered radically in several respects, for example when land is transformed into seabed and vice versa, or when an ice sheet covers an area. The load from an ice sheet influences the mechanical evolution of the repository. The composition of the water that is conducted down into the rock, the boundary conditions for the groundwater flow through the rock, and thereby the groundwater composition will be altered during a glacial/interglacial cycle. The expected changes are not projected to jeopardize the integrity of the engineered barriers. Climate-related changes are, for example, not expected to cause a loss of integrity in the canisters.

The repository's capacity to retard radionuclide transport will be altered during a glacial/interglacial cycle. At the same time, conditions for dilution of radionuclides in the biosphere change. The situation on the three repository sites will be more favourable than today during most of a glacial/interglacial cycle, above all due to an increased dilution in the biosphere. The greatest changes take place when the ice moves over an area. In the event there are leaking canisters, the repository's capacity to retard radionuclide transport is expected to be degraded during portions of the periods when the area is ice-covered. During these periods, a large turnover is also expected in the biosphere. This is natural, since increased water turnover in the rock presumes high turnover on the surface.

In summary, it can be said that the changes that are expected during a glaciation will not threaten the integrity of the engineered barriers. In the event of leaking canisters, periods with reduced capacity of the repository to retard radionuclide transport are combined with a radically increased dilution in the biosphere, so that calculated doses to man decrease. However, it should be borne in mind that radionuclide transport from the repository has been discussed for each climate domain independently. In the event of a rapid increase of groundwater flows, radionuclides that have accumulated in rock and/or biosphere may be released and give rise to a temporary increase in the possible doses.

10.12.1 Coming work

This review of the course of events during a glacial/interglacial cycle shows that climate-related changes should not affect the safety of the repository. However, several areas require further study:

- Possible variations of the Scandinavian climate – for the purpose of improving the biosphere descriptions, and as a basis for studies of permafrost and ice development.
- Development of permafrost in Scandinavia, and the hydrological conditions associated with permafrost.
- The relationship between ice load and stresses/movements in the bedrock. Both the coupling between hydraulic and mechanical evolution, and the large-scale tectonic changes.
- Mixing of waters of different origins in the rock's system of fractures and pores.
- Canister strength, where calculations need to be refined by the use of more realistic material properties.
- Buffer erosion with extremely ion-poor groundwater compositions.
- Evolution and performance of the backfill in conjunction with climate change.

It is also important to monitor research on the earth's climate system and the causes of climate change.

10.13 References

Ahlbom K, Äikäs T, Ericsson L O, 1991. SKB/TVO ice age scenario.
SKB TR 91-32. Svensk Kärnbränslehantering AB.

Andersson C, 1998. Compilation of information on the climate and evaluation of the hydrochemical and isotopic composition during Late Pleistocene and Holocene.
SKB R-98-02. Svensk Kärnbränslehantering AB.

Berger A, 1988. Milankovitch theory and climate. Reviews of Geophysics, Vol 26, No 4, 624–657.

Berger A, Loutre M F, 1991. Insolation values for the climate of the last 10 million years. Quaternary Science Reviews, Vol 10, 297–317.

Berger A, Loutre M F, Gallee H, 1996. Sensitivity of the LLN 2-D climate model to the astronomical and CO_2 forcings (from 200 kyr BP to 130 kyr AP). Scientific Report 1996/1. Institut d'Astronomie et de Géophysique Georges Lemaître. Université Catholique de Louvain.

Berger A, Loutre M F, 1997. Palaeoclimate Sensitivity to CO_2 and Insolation Ambio Vol 26, No 1, 32–37.

Bogren J, Gustavsson T, Loman G, 1998. Klimatförändringar – Naturliga och anropogena orsaker. Studentlitteratur, Art.nr 6452, ISBN 91-44-00320.

Boulton G S, 1990. Sedimentary and sea level changes during glacial cycles and their control on glacimarine facies architecture. In: Dowdeswell J A and Scourse J D (eds) 1990. Glaciomarine Environments: Processes and Sediments. Geological Society Special Publication No 53, 15–52.

Boulton G S, Payne A, 1992. Simulation of the European ice sheet through the last glacial cycle and prediction of future glaciation.
SKB TR 93-14. Svensk Kärnbränslehantering AB.

Boulton G S, Hulton N, Vautravers M, 1995. Ice-sheet models as tools for palaeoclimatic analysis: the example of the European ice sheet through the last glacial cycle. Annals of Glaciology 21, 103–110.

Boulton G S, Caban P E, 1995. Groundwater flow beneath ice sheets. Part II – Its impact on glacier tectonic structures and moraine formation. Quaternary Science Reviews.

Boulton G S, Hulton N, Wallroth T, 1996. Impacts of long-term climate change on subsurface conditions: Time sequences, scenarios and boundary conditions for safety assessments.
SKB PR U-96-19. Svensk Kärnbränslehantering AB.

Boulton G S, Curle F eds, 1997. Simulation of the effects of long-term climatic change on groundwater flow and the safety of geological disposal sites.
Report EUR 17793 EN. Luxembourg: Office for Official Publications of the European Communities. IBSN 92-828-0789-4.

Boulton G S, Wallroth T, Morén L, Kautsky U, 1999a. Impact of long-term climate change on a deep geological repository for spent nuclear fuel.
SKB TR-99-05. Svensk Kärnbränslehantering AB.

Boulton G S, Zatsepin S, Maillot B, 1999b. Analysis of groundwater flow beneath ice sheets.
SKB TR-99-XX (in preparation). Svensk Kärnbränslehantering AB.

Delisle G, 1998. Numerical simulation of permafrost growth and decay. Journal of Quaternary Science Vol 13 (4), pp 325–333. ISSN 0267-8179.

Fredén C (ed), 1994. National Atlas of Sweden – Geology. Almqvist & Wiksell International, Stockholm. ISBN 91-87760-28-2.

French H M, 1996. The periglacial environment. Second edition. Addison Wesley Longman Limited. ISBN 0-582-30536-5.

Frenzel B, Pesci M, Velichko A A (eds), 1992. Atlas of palaeoclimates and palaeoenvironments of the northern hemisphere. Gustav Fischer Verlag, Stuttgart.

Gallée H, van Ypersele J P, Fichefet Th, Tricot Ch, Berger A, 1991. Simulation of the Last Glacial Cycle by a Coupled, Sectorially Averaged Climate-Ice Sheet Model. 1. The Climate Model. Journal of Geophysical Research, vol. 96, NO D7, 13,139–13,161.

Gallée H, van Ypersele J P, Fichefet Th, Tricot Ch, Berger A, 1992. Simulation of the Last Glacial Cycle by a Coupled, Sectorially Averaged Climate-Ice Sheet Model. 2. Response to Insolation and CO_2 Variations. Journal of Geophysical Research, vol 97, NO D14, 15,713–15,740.

Gascoyne M, 1999. Long-term maintenance of reducing conditions in a spent nuclear fuel repository: A re-examination of critical factors.
SKB R-99-41. Svensk Kärnbränslehantering AB.

Guimera J, Duro L, Jordana S, Bruno J, 1999. Effects of ice melting and redox front migration in fractured rocks of low permeability.
SKB TR-99-19. Svensk Kärnbränslehantering AB.

Guiot J, Pons J, de Beaulieu L, Reille M, 1989. A 140,000-year continental climate reconstruction from two European pollen records. Nature, 338(6213), 309–331.

Hansson H, Stephansson O, Shen B, 1995. SITE-94. Far-field rock mechanics modelling for nuclear waste disposal.
SKI Report 95:40. Statens kärnkraftinspektion.

Hays J D, Imbrie J, Shackleton N J, 1976. Variations in the Earth's Orbit: Pacemaker of the Ice Ages. Science, vol 194 (4270), 1121–1132.

Holmgren K, Karlén W, 1998. Late Quarternary changes in climate.
SKB TR-98-13. Svensk Kärnbränslehantering AB.

Imbrie J, Hays J D, Martinson D G, McIntyre A, Mix A C, Morley J J, Pisias N G, Prell W L, Shackleton N J, 1984. The orbital theory of Pleistocene climate: Support from a revised chronology of the marine $d^{18}O$ record. Berger A L et al Eds, Milankovitch and Climate, Part 1, 269-305. Reidel Publishing Company.

Imbrie J, Imbrie J Z, 1980. Modelling the Climatic Response to Orbital Variations. Science, Vol 207, 943–953.

Israelsson J, Rosengren L, Stephansson O, 1992. Sensitivity study of rock mass response to glaciation at Finnsjön, central Sweden.
SKB TR 92-34. Svensk Kärnbränslehantering AB.

Kukla G, Berger A, Lotti R, Brown J P, 1981. Orbital signatures of interglacials. Nature, 290(5804), 295–300.

Laaksoharju M, Wallin B, 1997. Evolution of the groundwater chemistry at the Äspö Hard Rock Laboratory. Proceedings of the second Äspö International Geochemistry Workshop, June 6–7, 1995.
SKB HRL ICR 97-04. Svensk Kärnbränslehantering AB.

Laaksoharju M, Gurban I, Andersson C, 1999. Summary of hydrochemical conditions at Aberg, Beberg and Ceberg. Intera KB, Sollentuna, Sweden.

Laaksoharju M, Gurban I, Andersson C, 1999. Indications of the origin and evolution of the groundwater at Palmottu. The EU Palmottu natural analogue project.
SKB TR-99-XX (in preparation). Svensk Kärnbränslehantering AB.

Larsson-Leander G, 1977. Astronomi och astrofysik. 2:a reviderade upplagan. Liber Läromedel, ISBN 91-23-71074-8.

Leijon B, Ljunggren C, 1992. A rock mechanics study of fracture zone 2 at the Finnsjön site.
SKB TR 92-28. Svensk Kärnbränslehantering AB.

Liljequist G H, 1975. Jordens klimat. Generalstabens Litografiska Anstalt.

Lindblom U, 1997. Hydromechanical instability of a crystalline rock mass below a glaciation front.
SKB PR U-97-13. Svensk Kärnbränslehantering AB.

Losjö K, Johansson B, Bringfelt B, Oleskog I, Bergström S, 1998. Groundwater recharge – climatic and vegetation induced variations. Simulations in the Emån and Äspö areas in southern Sweden.
SKB TR-99-01. Svensk Kärnbränslehantering AB.

Lundquist J, 1986. Late Weichselian glaciation and deglaciation in Scandinavia. In: Sibrava V, Bowen D Q and Richmond G M. Quaternary glaciations in the northern hemisphere. Quaternary Science Reviews, 5, 269–293.

Mangerud J, 1991. The Scandinavian ice sheet through the last interglacial/glacial cycle. In Frenzel B ed Klimatgeschichtliche Probleme der letzen 130,000 Jahre. Stuttgart, Fisher Verlag, 307–330.

Martinson D G, Pisias N G, Hays J D, Imbrie J, Moore T C, Shackleton N J, 1987. Age dating and orbital theory of the ice ages: Development of a high resolution 0 to 300,000 year chronostratigraphy. Quaternary Research 27, 1–29.

Milankovitch M, 1941 (1969). Kanon der Erdbesttrahlung. R Serbian Acad Spec Publ 132, Sect Math Nat Sci. (Canon of insolation and the ice-age problem. English translation by Israel Program for Scientific Translations, Jerusalem).

Morén L, Påsse T, 1999. Climate and shoreline in Sweden during the Weichsel and the next 150,000 years.
SKB TR-99-XX (in preparation). Svensk Kärnbränslehantering AB.

Nordlinder S, Bergström U, Mathiasson L, 1999. Ecosystem specific dose conversion factors for Aberg, Beberg and Ceberg.
SKB TR-99-15. Svensk Kärnbränslehantering AB.

Petit J R, Jouzel J, Raynaud D, Barkov N I, Barnola J M, Basile I, Bender M, Chappellaz J, Davis M, Delaygue G, Delmotte M, Kotlyakov V M, Legrand M, Lipenkov V Y, Lorius C, Pépin L, Ritz C, Saltzman E, Stievenard M, 1999. Climate and atmospheric history of the past 420,000 years from the Vostok ice core, Antarctica. Nature 399, 429-436, 1999.

Påsse T, 1996. A mathematical model of the shore level displacement in Fennoscandia.
SKB TR 96-24. Svensk Kärnbränslehantering AB.

Påsse T, 1997. A mathematical model of past, present and future shore level displacement in Fennsoscandia.
SKB TR 97-28. Svensk Kärnbränslehantering AB.

Raab B, Vedin H (eds), 1995. Sveriges Nationalatlas – Klimat, sjöar och vattendrag. Bra Böcker, Höganäs. ISBN 91-87760-31-2.

Rehbinder G, Yakubenko P A, 1998. Displacements and fluxural stresses of a loaded elastic plate on viscous liquid.
SKB PR U-98-04. Svensk Kärnbränslehantering AB.

Rhén I (ed), Gustafson G, Stanfors R, Wikberg P, 1997. Äspö HRL-Geoscientific evaluation 1997/5. Models based on site characterization 1986–1995.
SKB TR 97-06. Svensk Kärnbränslehantering AB.

Rosengren L, Stephansson O, 1990. Distinct element modelling of the rock mass response to glaciation at Finnsjön, central Sweden.
SKB TR 90-40. Svensk Kärnbränslehantering AB.

SKB, 1992. SKB 91. Slutlig förvaring av använt kärnbränsle. Berggrundens betydelse för säkerheten.
Svensk Kärnbränslehantering AB.

Stephansson O, 1993. Rock stress in the Fennoscandian Shield. In: Hudson J A (ed) Comprehensive Rock Engineering, Vol 3, Rock Testing and Site Characterisation, pp 445–459, Pergamon Press.

Svensson U, 1999a. Subglacial groundwater flow at Äspö as governed by basal melting and ice tunnels.
SKB R-99-38. Svensk Kärnbränslehantering AB.

Svensson U, 1999b. A numerical simulation of the origin and composition of the groundwater below Äspö.
SKB R-99-39. Svensk Kärnbränslehantering AB.

Svensson U, 1997. A regional analysis of groundwater flow and salinity distribution in the Äspö area.
SKB TR 97-09. Svensk Kärnbränslehantering AB.

Westman P, Gustafsson B, Wastegård S, Omstedt A, Schoning K, 1999. Salinity change in the Baltic Sea during the last 8500 years: evidence, causes and models.
SKB TR-99-XX (in preparation). Svensk Kärnbränslehantering AB.

11 Tectonics – earthquake scenario

11.1 Introduction

The earthquake scenario examines how earthquakes can affect repository safety. The analysis is centred on the question of whether earthquakes can lead to a breach in isolation in one or more canisters. The premises for the scenario are the same as for the base scenario, except that earthquakes are also assumed to occur in the surrounding area. Otherwise, as in the base scenario, the repository is built according to specifications, and present-day conditions in the surroundings are projected to persist.

The account begins with a description of the initial and boundary conditions that apply for the scenario. The emphasis here is on the large-scale tectonic evolution and its importance for the occurrence of earthquakes.

Thereafter an overview is provided of the processes and dependencies that control the evolution of the repository system in the event of an earthquake. The focus is on the mechanical processes in the geosphere, the mechanical interaction between geosphere and canister via the buffer, and how the canister reacts to the mechanical stresses to which it is subjected.

Subsequently a more detailed account is provided of how a canister is affected by movements in the rock around the deposition hole. The section concludes with a criterion for which rock movements are acceptable without the isolation of the canister being jeopardized.

Most of the chapter is devoted to an account of simulations of earthquakes on the three repository sites. The simulations are aimed at calculating the probability of the criterion for canister damage being exceeded.

The chapter ends up with the conclusions that can be drawn today about how earthquakes can influence the safety of a deep repository.

11.2 Initial state

The initial state of the repository is thus assumed to be the same as in the base scenario, see Chapter 8.

11.3 Boundary conditions

The external conditions in the earthquake scenario are assumed to be the same as those in the base scenario, with the important exception that seismic processes are also included. In short they entail that:

- Today's climatic conditions are assumed to prevail in the future as well.
- Land uplift and its influence on groundwater flows, the biosphere etc are included in the base scenario.
- Today's site-specific biospheres are assumed to persist, in addition to the effects land uplift has on the biosphere.
- Rock-mechanical changes take place only as a consequence of aseismic processes, i.e. earthquakes are not included in the base scenario.
- There are no human intrusions.

All boundary conditions, except the mechanical ones, are described in detail in the base scenario in Chapter 8. In the following, a description is provided of the large-scale tectonic conditions existing around Sweden and the premises they create for the occurrence of earthquakes.

11.3.1 Introduction

The earth's crust and the outermost, or uppermost, layers of the underlying mantle together comprise the lithosphere. The surface of the earth is covered by six large and a number of smaller lithospheric plates that move in different ways in relation to each other, see Figure 11-1. The surface areas of the individual plates can be roughly divided into areas with a thick continental crust and areas with a significantly thinner oceanic

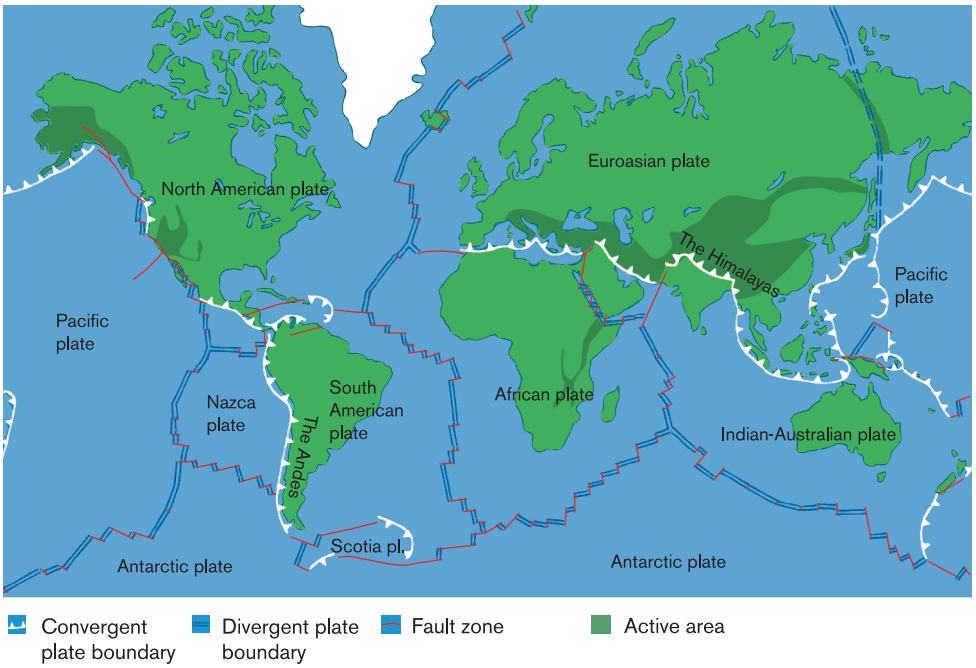

Figure 11-1. *The lithosphere is divided into a number of plates that are separated by different types of plate boundaries.*

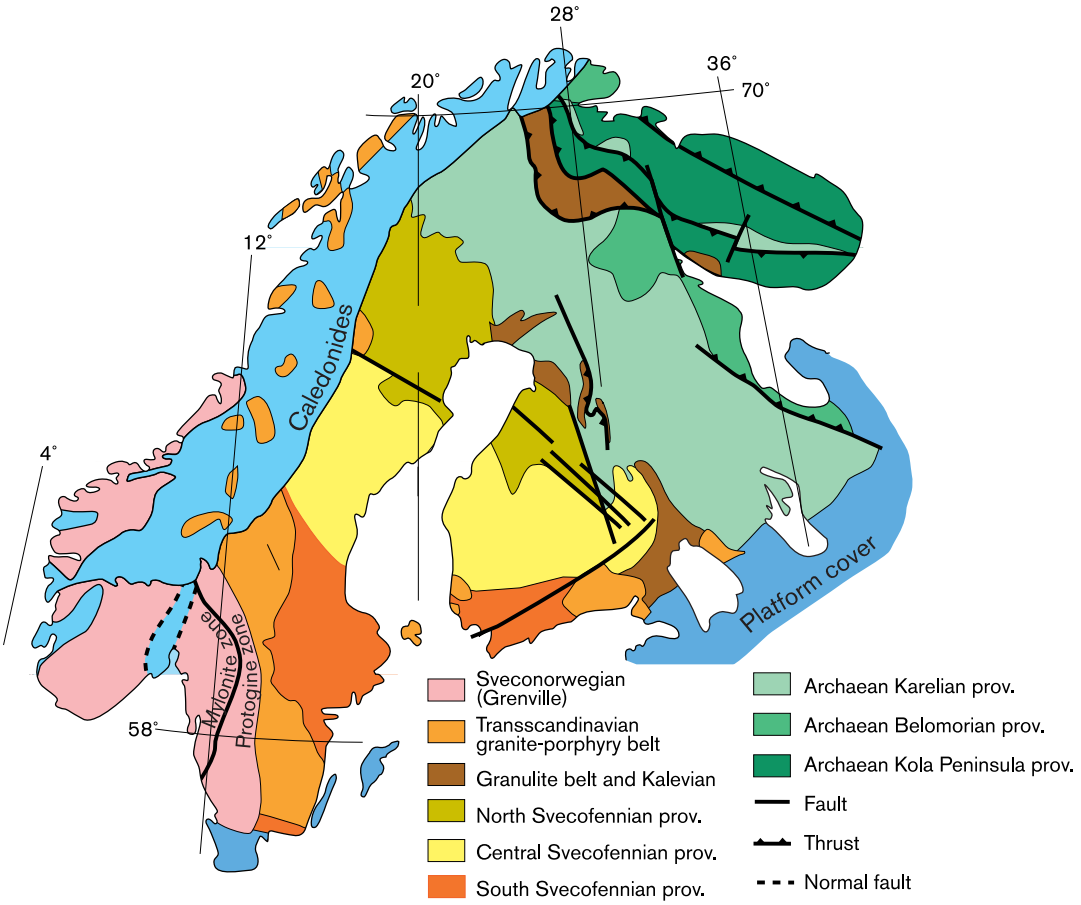

Figure 11-2. *Different parts of the Baltic Shield /from Weihed et al, 1992/.*

crust. Oceanic crust can be generated through supply of material from the mantle (seafloor spreading) or destroyed when the crust (the seafloor) is forced down beneath the margin of a colliding plate (subduction). At other plate boundaries the two plates slide along each other's margins.

The continental crust is made up of lighter materials and cannot, like the oceanic crust, be subducted beneath a colliding plate. Instead, the parts of the continental crust that comprise boundary areas of colliding lithospheric plates are compressed, deformed and folded, leading to formation of mountain chains (orogeny), volcanic activity, upwelling of magma and rock alteration. Today's continents have been formed and reworked in a sequence of such orogenies. While the oceanic crust is continuously being generated and recycled and is therefore relatively young, the continents are much older. This is particularly true of the shield areas, such as the Canadian Shield on the North American plate and the Baltic and Ukrainian Shields on the Euroasian plate. The shields can be defined as large areas of exposed Precambrian crystalline rock surrounded by areas covered with sedimentary rocks /Juhlin et al, 1998/.

The Baltic or Fennoscandian Shield, which comprises a portion of the continental crust on the Euroasian lithospheric plate, is composed of a number of provinces formed in a sequence of early orogenies mainly between 1.5 and 3.5 billion years ago /Muir Wood, 1993; Juhlin et al, 1998/, see Figure 11-2. The latest phase was the Caledonian orogeny, which culminated approximately 0.4 billion years ago when the North American and European continents collided and amalgamated to form part of the supercontinent Pangea /Juhlin et al, 1998/.

11.3.2 Mechanical structure of the Baltic Shield

In simplified terms, the Shield can be described mechanically as an approximately 60–80 km thick plate of elastic/brittle material resting on a viscous medium. The crusts consist of the uppermost 45 kilometres or so down to the Moho depth. In actuality, the strength conditions in the Shield are complex. In the first place the thickness of the crust varies, so that it is up around 60 km in central Finland and down around 30 km in southwestern Sweden /Muir Wood, 1993; Juhlin et al 1998/, in the second place the relationship between strength and depth may be dependent on the geothermal heat flow and the horizontal strain rate /Milnes et al, 1998/. At small horizontal strain rates a strength reduction may be obtained in the lower parts of the crust, and at large geothermal heat flows a strength reduction may be obtained in the upper parts of the mantle. The strength profile, or the rheological profile, therefore looks different for cross-sections through the Shield in northern Sweden with small geothermal flows than in southeastern Sweden, where the geothermal heat flow is greater /Sundberg, 1995/. The deformation of the Shield under load is further affected by the fact that it is crossed by a number of deformation zones that enable the different parts of the Shield to move in relation to each other, for example the Protogine Zone, which constitutes the boundary of the Sveconorwegian province in the southwest (Figure 11-2).

11.3.3 Mechanical state and evolution of the shield

The Baltic Shield is continuously subjected to a horizontal compression or "ridge push" due to seafloor spreading from the Mid-Atlantic Ridge at the western tectonic plate boundary /Muir Wood, 1993/. The compression is probably an important factor for the development of the state of stress currently prevailing in the Swedish bedrock (see the Process Report), where the maximum principal stress tends to be horizontal and oriented NW-SE, i.e. in the compression direction. This is true in the southern and central parts of Sweden, while the picture is more fragmented in the northernmost parts of the country, where a possible tendency towards N-S orientation of the maximum principal stress can be observed /Juhlin et al, 1998/.

In general the vertical stress is also a principal stress. In magnitude it is often considerably smaller than the largest horizontal principal stress and can be assumed to be determined by the rock overburden. This means that the state of stress is deviatoric, i.e. with direction-dependent stresses. The rock therefore contains inherent shear stresses, so that the rock can be in a state of unstable equilibrium, where small stress changes can give rise to shear failure along discontinuities with low strength. Theories positing that the mechanical equilibrium in the bedrock is in actual fact determined by a balance between rock stresses and frictional forces in large fracture zones have been proposed and entail that the rock mass adapts continuously by means of friction-controlled movements in the major fracture zones /Scholz, 1990; Leijon, 1993/.

Current tectonic conditions can be judged to have been constant for the past two million years, while the state of stress may have persisted for the most part during the past 25 million years /Muir Wood, 1995/.

The Shield has also been subjected to loadings due to glaciations and will probably be subjected to new such loadings /Wallroth, 1997/. The timescale for a glaciation cycle, approximately a hundred thousand years, is short in a tectonic time perspective, and it can be assumed that the state of stress is largely restored between glaciations /Muir Wood, 1993/. There are, however, uncertainties with regard to what state of stress will prevail under the ice cap and at the margin of the ice cap, and what timescale applies to the recovery of the stress field.

For the state of stress under the ice sheet, the simplest hypothesis is to assume that the vertical stresses increase by an amount that is equal to the ice load, and that the increase of the horizontal stresses can be calculated with simple expressions from elasticity theory, which gives a stress increase that is approximately one-third of the vertical stress increment. This model entails that the state of stress is less deviatoric and the rock therefore more stable with less tendency towards shear movements /Muir Wood, 1993/. This model is the one that is normally assumed to apply. Other models entail that the horizontal stresses will be influenced by the extent of the ice load, by the flexural stiffness of the crust and the uppermost part of the mantle, and by the rheological properties of the viscous medium underneath the elastic plate. Such models give a complex distribution of horizontal stress increment in the upper parts of the crust /Stephansson, 1987; Rehbinder and Yakubenko, 1998/, with some flexural stresses above all in the vicinity of the area around the ice margin. Under the ice, the effect on the stability of the rock in the upper part of the crust is in principle the same as for the simpler model, i.e. the horizontal stress increment is less than the vertical stress increment, which results in reduced shear stresses and greater stability. The picture around the marginal areas of the ice is less clear.

The timescale for the downwarping of the crust during the growth of the ice sheet, as well as the timescale for land uplift after melting of the ice sheet, is dependent on the rheological properties of the viscous material underneath the elastic/brittle plate. Land uplift following the most recent glaciation (glacial rebound) is still proceeding, at different rates in different parts of the Shield, which means that the bedrock is still being deformed. Of a vertical subsidence of approximately 900 metres in the most depressed portion of the Shield, approximately 140 metres is now estimated to remain /Kakkuri, 1986/.

The land uplift rate is at most approximately 90 cm in a hundred years /Wallroth, 1997/. The deformations that take place in conjunction with the successive differential uplift result in horizontal strains of the crust in the Shield. Calculations show that these strains may be 10^{-9}/year /Muir Wood, 1993/, which in one hundred years can give a relative movement of 1 cm for points at a distance of 100 km from each other.

There are different opinions as to how great the compressive strain is due to ridge push. Muir Wood /1995/ argues that most of the seafloor movements are absorbed in the Shield's marginal areas, so that the strain that is transferred to the interior of the Shield is not greater than 10^{-11}/year, i.e. a hundredth of the strain due to glacial rebound. Slunga /1991/ claims that at least a hundred times greater strains are transferred to interior of the Shield and that the main part are absorbed in the form of aseismic movements in large deformation zones. According to the model, the clear difference in seismicity between the provinces separated by the Protogine Zone in southern Sweden may indicate that this zone, without exhibiting seismic activity of its own, is of importance for the tectonic movements.

The results that are now available from geodetic measurements are not sufficiently accurate to provide a clear and systematic picture of the horizontal strains currently occurring in the Shield, and indicate both regions with compression and regions with expansion. Which viewpoint best describes reality, i.e. whether tectonics or glacial rebound is the primary driving force, can therefore presumably not be determined without comprehensive and careful geodetic measurements being made over a long period of time. To determine the strain rates with sufficient accuracy, data will probably have to be gathered from satellite-based measurement systems during a period of at least ten years /Scherneck et al, 1996/.

The large-scale movements that take place in the Shield determine the boundary conditions for the long-term mechanical evolution in the repository's host rock. If no adjustment occurs by means of friction movements, stress changes in the earth's crust and changes of the loads that act on the host rock will be obtained. A strain rate on the order of 10^{-9}/year then gives a horizontal stress change of 5 MPa in a hundred thousand years, counting on the high side. If the bedrock is generally in a state where the stresses in the bedrock are continuously balanced by frictional forces in large fracture zones, the influence of large-scale movements in the Shield on the load conditions in the host rock will probably be less. A third possibility is that the energy input is released seismically, i.e. via earthquakes, which means that the host rock may be affected by dynamic effects.

11.3.4 Earthquakes

The Swedish bedrock is of ancient origin and exhibits, like other Shield areas, a seismic activity that is small in relation to areas where orogeny is currently taking place. Quakes in the Swedish part of the Shield mainly occur in the southwest in the Lake Vänern area and along the Norrland coast, Figure 11-3. The magnitude of the earthquake has rarely exceeded 4.0 /Slunga, 1991/. The earthquakes in the Kattegat in 1985 and in Skövde in 1986 were, for example, of magnitudes 4.6 and 4.5, respectively /Muir Wood, 1993/. Earthquakes that occur in conjunction with one of the earth's tectonically active areas, e.g. Japan, Caucasus or California, can have a magnitude of around 8, which means that nearly 1 million times more energy is released than by an earthquake of magnitude 4.

An earthquake occurs when strain energy that has accumulated over a slow process of deformation is suddenly released by shear movements along a major or minor discontinuity. The released energy is given by the seismic moment, which is the product of the area of the displaced surface, the magnitude of the average displacement and the elastic shear modulus of the rock. In terms of seismic moment, i.e. released energy, one step on the magnitude scale corresponds to a factor of about 30 /Hanks and Kanamori, 1979/. It follows from the above that earthquakes of great magnitude can only occur on very large fractures, partly because the seismic moment is directly proportional to the area of the

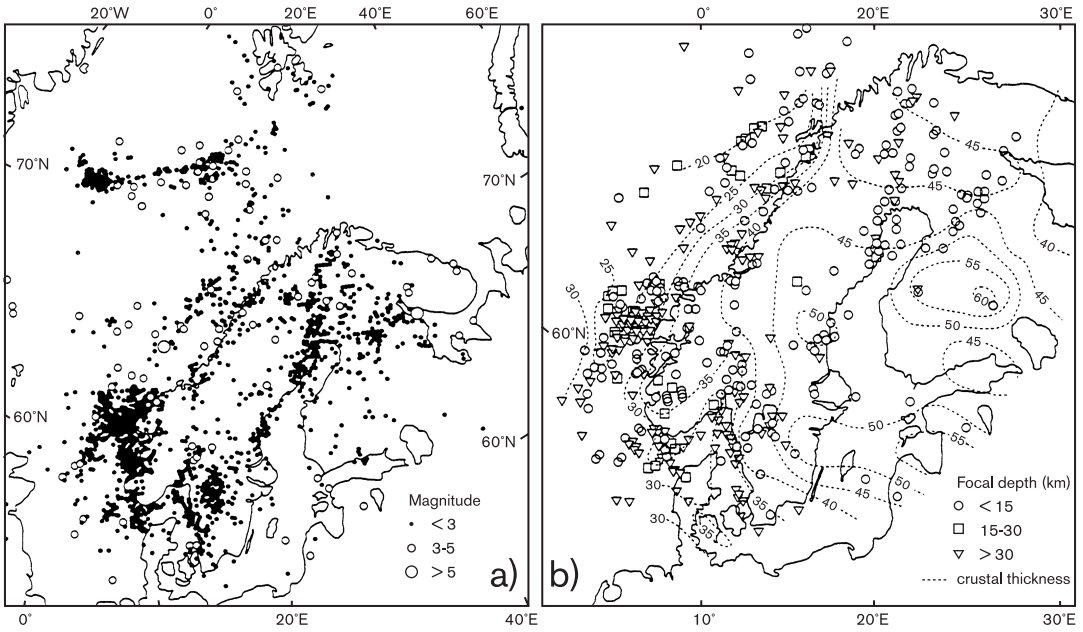

Figure 11-3. Earthquakes in northern Europe during the period 1965–1989. Distribution according to magnitude and depth /Blundell et al, 1992/.

displaced surface, and partly because the maximum possible average displacement cannot amount to more than a fraction of the fracture's extent in its own plane.

An earthquake can be perceived as a sudden local rupture at an asperity (roughness) that is loaded increasingly due to aseismic creep movement, i.e. stable time-continuous movement, along surrounding, smoother portions of the fracture plane /Slunga, 1991/. The earthquake is triggered when the stress concentration around the asperity or asperities that lock the movement has become sufficient to cause rupture. The altered stress picture around the fracture zone may lead to new stress concentrations around other asperities, either in the fracture zone where the earthquake occurred or in a nearby zone. If enough strain energy has not been released to restore stability in the region, then new ruptures can take place in a sequence of aftershocks. An earthquake has both static effects in the form of a permanent deformation and an altered stress field in the area around the fracture zone in which the earthquake took place, and dynamic effects in the form of mechanical oscillations that can be propagated long distances in the earth's crust.

All the mechanical energy input to the Shield does not necessarily have to be released in detectable earthquakes. The seismically released strain energy may be only a small fraction of the strain energy that is continuously cycled due to deformations in different parts of the Shield /Slunga, 1991/. Conversely, frequent earthquakes do not necessarily entail the continuous input of equivalent quantities of strain energy due to ongoing large-scale deformations. Small deformations may be sufficient to trigger large earthquakes so that energy accumulated during some earlier epoch is released /Muir Wood, 1993/.

There are two different views regarding which type of large-scale deformation is the principal cause of the current seismic activity in Scandinavia:

1. Deformations due to tectonic movements, "ridge push".
2. Deformations due to the differential land uplift that is still in progress since the most recent ice age, "glacial rebound".

Furthermore, there is evidence that intensive seismic activity, postglacial faulting, took place in Lapland in direct conjunction with the melting of the most recent ice cap (the Lansjärv Fault, the Parvie Fault, etc.). The seismic activity in the area may at some time have been on a level with that which currently exists in highly tectonically active areas, such as Iran /Muir Wood, 1993/. The magnitude of the Lansjärv earthquake is calculated to have been 7.8.

There are two basic views concerning the mechanism behind the postglacial faults:

1. Tectonically generated stresses accumulated during the glaciation and were released in the form of earthquakes when the vertical stresses were reduced in response to retreat of the ice sheet. The reason why postglacial fault movements took place in this part of the Shield and not at other places is that the glaciation had a longer and unbroken duration here, so that larger amounts of energy could accumulate.
2. Deglaciation proceeded more rapidly in the area southeast of the remaining ice cap, while it proceeded much more slowly in the northwest. This led to a highly asymmetrical unloading where the two deglaciation zones approached one another. Furthermore, during the glaciation the area lay beneath the northwestern flank of the ice cap, which meant that the stress contribution from the radial mantle movements were added to the pre-existing NW-SE oriented stresses. When the vertical load rapidly diminished, the large shear stresses this created triggered the earthquake.

Both views accord with the direction of the fault zones. The question has received a great deal of attention from the geological community, and the prevailing view is that both mechanisms were involved /Stanfors and Ericsson, 1993/. There is also agreement that the fault movements took place as a reactivation of existing fracture zones rather than new fracturing.

11.4 Overview of processes and dependencies

The processes within the repository system are the same as in the base scenario. In the tectonics scenario, attention is first focused on the mechanical evolution of the geosphere (rock movements and possibly fracturing) as a consequence of earthquakes and on the mechanical consequences this has for other parts of the repository, see Figure 11-4.

The radiological, thermal, hydraulic and chemical evolutions in the tectonics scenario are expected to be essentially the same as in the base scenario.

11.4.1 Mechanical evolution for the canister

The base scenario gives an account of calculations of canister strength in the event of a postulated displacement of 0.1 metre lasting 30 days along a horizontal fracture intersecting the deposition hole, see section 8.8.2. The canister was of a weaker previous design and the calculations can therefore be regarded as pessimistic in this respect.

Based on the calculation results, the following earthquake analysis employs the pessimistic criterion that rock movements with a magnitude of 0.1 metre or more around a deposition hole could lead to canister damage.

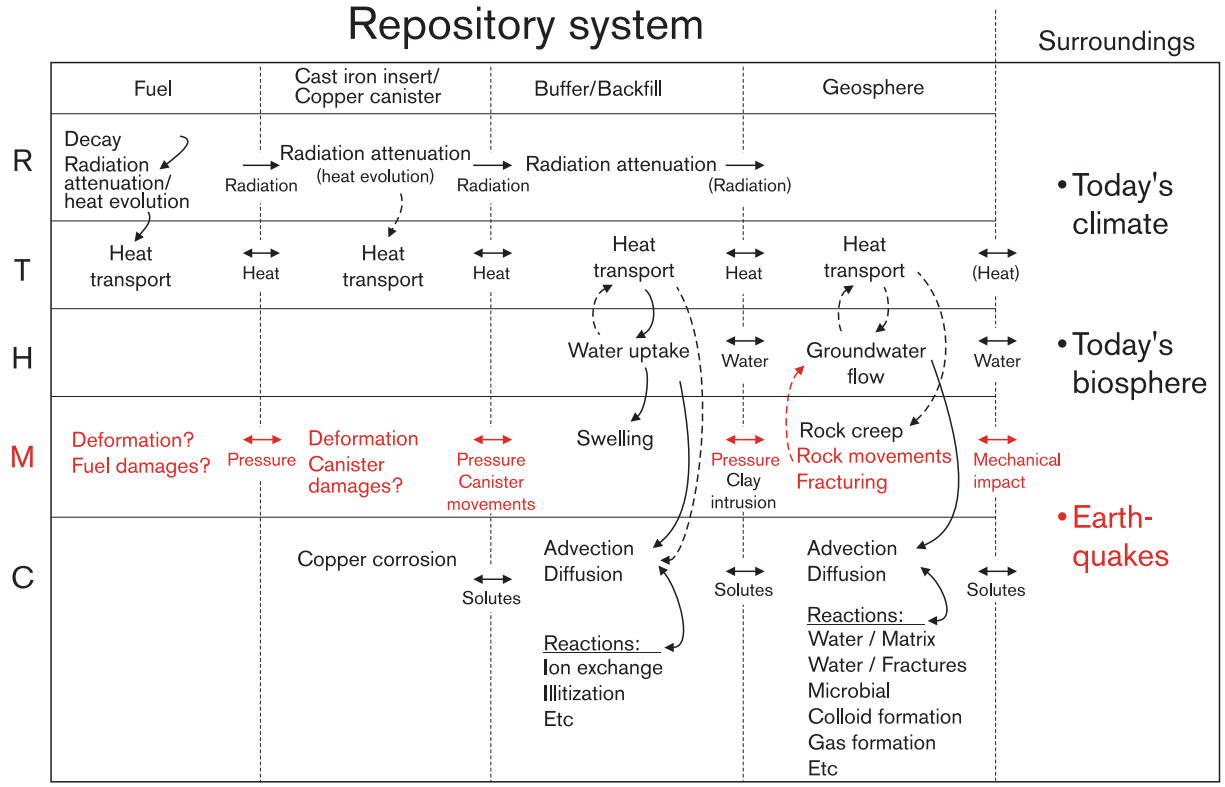

Figure 11-4. *Main features of the process system for the climate scenario. Red processes follow a different course or have a different scope than in the base scenario.*

11.5 Mechanical evolution in the geosphere

The slow movements that may take place in the Swedish bedrock during the next hundred thousand years, either due to tectonic movements or due to glaciation effects, may entail slow changes in the load conditions in the host rock, or gradual adaptation of the bedrock by means of aseismic movements in major fracture zones so that the load conditions in the rock only change to a small extent. The safety aspects of such time-continuous effects are dealt with in the base scenario.

The seismic activity that currently exists in the Swedish bedrock shows that some of the strain energy that is continuously accumulated or that has been accumulated during some previous epoch is released by earthquakes. The risks to repository safety that can arise due to the propagation of the mechanical effects of earthquakes into the repository area must therefore be analyzed and evaluated.

11.5.1 Analysis of earthquake risks

The mechanical structure of the rock mass, with stiff intact rock of high strength and discontinuities of lower strength and lower stiffness, is such that significant deformations mainly take place along the discontinuities, see the Process Report. The most important mechanical process from a safety viewpoint is shear movements along fractures that intersect one or more canister hole positions. The criterion that is applied entails that shear displacements exceeding 0.1 metre at a canister hole could cause canister damage, section 8.8.3. This criterion applies regardless of whether the displacement takes place time-continuously or instantaneously, e.g. due to earthquake, and regardless of whether it takes place in one large or several smaller episodes.

To estimate the number of canisters that could be damaged due to earthquakes within the next hundred thousand years at the three repository sites, it must therefore be possible to calculate or estimate at how many canister hole positions single or accumulated shear displacements along fractures may exceed 0.1 metre during the time period. Such calculations have been carried out by LaPointe et al /1999/ for the three repository sites Aberg, Beberg and Ceberg. To carry out the analysis it is necessary to:

1. Be able to simulate the mechanical effect of single earthquakes of a given magnitude and at a given distance from the repository. A method for this has been developed by LaPointe et al /1997/, and then refined and expanded in the application work /LaPointe et al, 1999/.

2. Make a prediction of how the frequency of earthquakes of different magnitudes varies in time and space during the next hundred thousand years. Such a prediction has been made by LaPointe et al /1999/. The prediction is based on the assumption that currently available magnitude/frequency statistics, which only include small and medium-sized earthquakes, can be extrapolated both in time and beyond the observation interval, i.e. for large quakes as well.

3. Carry out simulations of single earthquakes according to the magnitude/frequency statistics that apply in a given area with the conditions regarding occurrence of fractures and fracture zones that apply specifically on the three repository sites. A sufficient number of simulations must be performed per site in order to obtain statistically significant results.

Effect of single earthquakes

LaPointe et al /1997/ show that the most important parameters that control a secondary fracture movement, for example at a deposition hole, are the magnitude of the earthquake, the distance from the fracture zone where the earthquake takes place to the fracture intersecting the canister hole, and the length of the fracture, i.e. its extent in its own plane. In a generic example, it is shown that fracture movements of 0.1 metre can be reached if an earthquake of magnitude 7.5 occurs within a distance of 100 metres from the repository. Similarly, fracture movements of 0.1 metre can be reached if an earthquake of magnitude 8.2 occurs within a distance of about 1 km from the repository. These results have also been cited in the most recently conducted safety assessment in Finland, TILA-99 /Vieno and Nordman, 1999/. The study is based on simulating a single earthquake of given magnitude as an instantaneous shear displacement along a fracture plane, "primary fracture", in a semi-infinite elastic medium, which thereby obtains a static stress increment. The simulation is performed with the 3-dimensional code POLY3D. For earthquakes of a given magnitude, the earthquake parameters, i.e. the primary displacement and the dimensions of the primary fracture, are chosen according to regression relationships that have been found to apply globally between registered earthquake magnitudes and these parameters. The regression relationships are also found to agree well with expressions that have been proposed for the relationship between magnitude and seismic moment /Hanks and Kanamori, 1979/.

The static stress increment gives a shear stress increment and secondary shear displacements in fracture planes in the repository area. The size of the displacement is dependent on the individual fracture's size, orientation and distance to the primary fracture. Secondary displacements along many thousand fractures can be calculated simultaneously in POLY3D, but the different fractures do not interact mechanically with each other. To evaluate the effects in a repository, the fractures in the host rock are distributed in accordance with the discrete fracture network model (DFN model) that applies for the repository site and distributes the canister hole positions in accordance with the layout that has been proposed for that site. Only fractures that intersect canister hole positions are taken into account. The result of the simulation of a single earthquake is obtained as maximum secondary displacements in all fractures in the model. The maximum displacement takes place in the centre of the fracture and the result is converted to pertain to the displacement where the fracture actually intersects the canister hole or holes.

Prediction of earthquake frequency

The strategy is to use existing earthquake statistics and extrapolate them a hundred thousand years into the future. Statistics on the magnitude and frequency for earthquakes that have occurred within four regions (southern Sweden, the Lake Vänern region, the Gulf of Bothnia and northern Sweden) have been used. The Lake Vänern region and the Gulf of Bothnia are subregions in southern and northern Sweden that have been singled out due to special seismic conditions, see Figure 11-5a. When these statistics are standardized to an area with a radius of 100 km and a timeframe of a hundred thousand years, it turns out that the Lake Vänern region has the largest number of earthquakes for all magnitudes greater than 3. It is followed by southern Sweden, the Gulf of Bothnia and northern Sweden, which indicates that the most large earthquakes can be expected at Aberg, while Ceberg gets the smallest number. This may be slightly misleading, since the statistics for southern Sweden are dominated by the Lake Vänern region. A corrected statistical distribution for the eastern part of southern Sweden has therefore also been drawn up. However, the number of earthquakes in southeastern Sweden is so small that the correction, and thereby also the extrapolations for the region, is of limited value.

Frequency/magnitude relationships are usually characterized by two parameters: a, which has to do with the total earthquake frequency, and b, which has to do with the distribution between small and large earthquakes so that large values of b entail a small portion of large earthquakes. The statistics on Swedish earthquakes only include earthquakes with magnitudes < 5. Both a and b are determined for the different earthquake regions by fitting the frequency/magnitude relationships to existing statistics and extrapolating to earthquakes with magnitudes up to and including 8.5. Both a and b are assumed to be constant. Figure 11-5b shows the results. The earthquakes are assumed to be Poisson-distributed over time.

Application

For each of the three repository sites, trace data obtained during mapping on different scales are analyzed and parameters for stochastic fracture network models are determined (Figure 11-6a). The statistical parameters are determined by means of a fractal approach, so that fractures on scales that are often suppressed in mapping are also included.

A hundred realizations of the fracture network model are generated for each site. The realizations are combined with the layout that has been proposed for the particular site /Munier et al, 1997/. The realizations are performed with the FracMan code. A sufficiently large number of randomly chosen canister positions are included to obtain a statistically representative selection of canister-intersecting fractures, see Figure 11-6b. Each of the hundred realizations is represented in the following earthquake simulations by these selections, which consist of between 300 and 600 fractures.

The earthquake statistics established for the three repository sites are used to randomly distribute earthquakes within areas with a 100 km radius around the sites (see Figure 11-6c). Large and medium-sized earthquakes are distributed randomly on mapped fracture zones with the only restriction that the fracture zone must have an extent in the ground surface that is sufficient according to the regression relationships to accommodate the earthquake. Small earthquakes are located randomly without respect to mapping data. Earthquake parameters (primary displacement, depth) are then chosen stochastically within the intervals given by the regression relationships.

For each of the hundred realizations per repository site, 50 earthquake simulations are performed with the POLY3D code with magnitudes according to relevant frequency/magnitude statistics. The results are obtained as statistical distributions of displacements along canister-intersecting fractures, see Figure 11-6d. To examine the importance of the earthquake statistics in relation to the importance of the site-specific fracture network models, simulations are done for Ceberg with earthquake statistics from two subregions: Northern Sweden and the Gulf of Bothnia. The Beberg simulations are performed with statistics from southern Sweden, the Gulf of Bothnia and northern Sweden, and with the corrected statistics for the eastern part of southern Sweden. The Aberg simulations are performed with statistics for southern Sweden and with the corrected statistics. Altogether, this means that 40,000 earthquake simulations are done, each including effects on between 300 and 600 canister-intersecting fractures.

Results

The results of the analysis are expressed as the percentage of canister holes that are subjected to fracture movements greater than 0.1 metre during a hundred thousand years. All such events are registered as canister failures, even if the fracture doesn't intersect the part of the eight-metre-deep canister hole actually occupied by the five-

a)

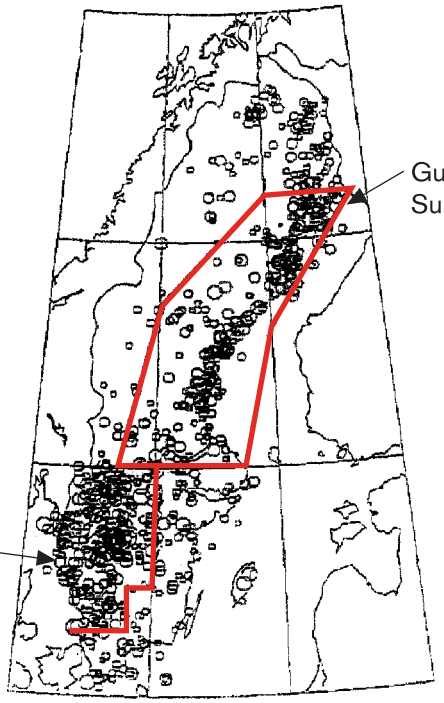

b)

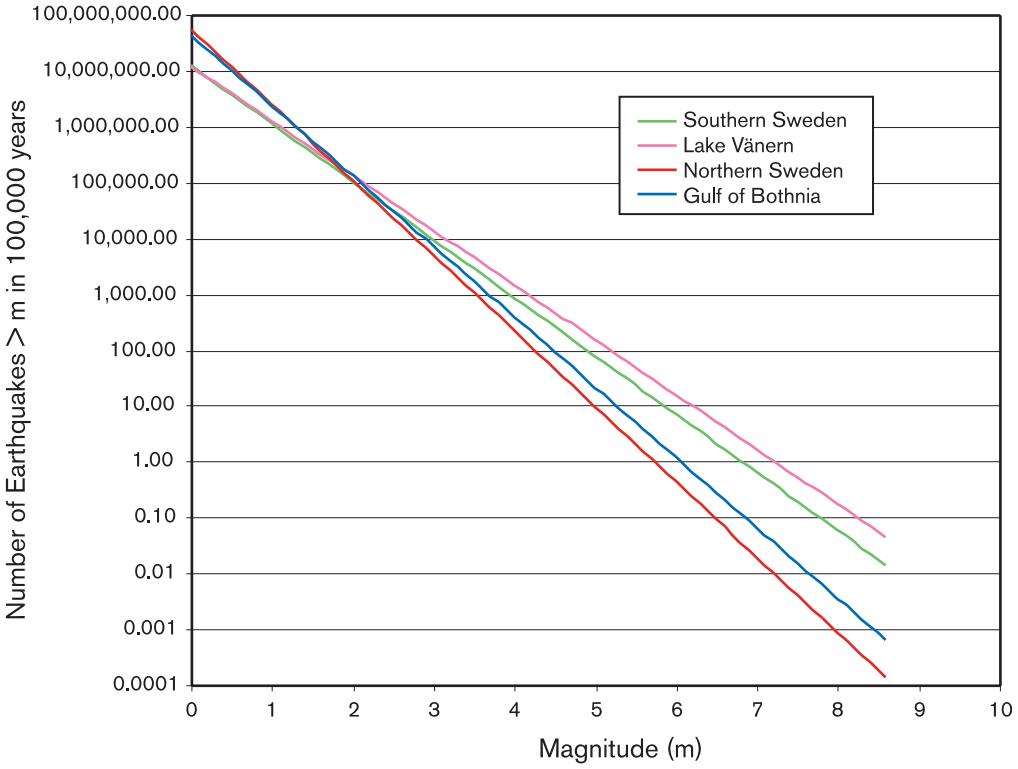

Figure 11-5.
a: Geographic distribution of earthquakes in Sweden.
b: Prediction of number of earthquakes within the next 100,000 years. The numbers are standardized to an area corresponding to a circle with a radius of 100 km.

metre-high canister. In the results, canister failures that have occurred due to single earthquakes and failures that have occurred due to the cumulative effect of multiple earthquakes can be distinguished. Since a stochastic approach is used, the percentages are expressed statistically via their distributions and are then characterized with mean and median values.

The analysis shows that Aberg has the greatest percentage of canister failures (mean 0.65 percent for single and multiple earthquakes together, which means 32 damaged canisters for a repository with a total of 5,000 canisters), followed by Beberg (0.12–0.15 percent or 6–7 canisters, depending on which earthquake region Beberg is assumed to belong to) and Ceberg (0.04 percent or two canisters). The reason Aberg has the highest canister failure rate is the larger proportion of large earthquakes at Aberg and the higher fracture intensity with more subhorizontal fractures. The figures for Aberg are, however, affected by the fact that the earthquake statistics from the Lake Vänern subregion have been included in the random distribution of earthquakes. If the corrected statistics are instead used, the mean rates for Aberg come down on a level with Beberg and Ceberg.

The canister failure distributions are highly asymmetrical. The median rates for all sites are zero percent canister failure, despite the fact that the median rates are on the order of tenths of a percent (Figure 11-7). This is also evident from the rest of the results, which show that no canister failures at all occur in about 90 percent of the simulations for most combinations of sites and earthquake statistics. In the other ten percent it is usually single earthquakes ("damaging earthquakes") that cause the failures; the cumulative effects are thus small. Despite the fact that the probability that single earthquakes of sufficient magnitude will occur sufficiently close to the repository to cause canister failure is small, the canister damage statistics are dominated by such earthquakes due to the fact that they often affect several canisters. The statistics show that a damaging earthquake damages an average of 90 canisters for Aberg, 34 for Beberg and 23 for Ceberg.

The analysis also shows that damaging earthquakes usually occur within a couple of kilometres from the repository. This conveys a picture much like that reported in LaPointe et al /1997/. If the repository can be located so that fracture zones big enough to accommodate appreciable earthquakes can be avoided with a margin of a couple of kilometres, the probability of canister failure is very small. The probability that an earthquake big enough to cause canister failure will occur directly in a canister that intersects the canister (primary earthquake) is negligible.

11.5.2 Uncertainties

Uncertainties that are dealt with pessimistically

- **Mechanical properties of the fractures.** The fractures are assumed to be without friction and cohesion. This is pessimistic; if the fractures had a shear strength, all secondary displacements would be smaller. A friction angle of 30 degrees would reduce the cumulative displacements by perhaps a factor of 5, see the Process Report. To take credit for the margin, it must be ensured that the fracture surfaces are not separated when the displacement takes place. Dynamic calculations with models that contain a single fracture or a few single fractures could be carried out to shed light on the role of friction. If it can be shown in a reasonably credible manner that friction is active in typical dynamic processes, credit can be taken for the margin, which would mean that only displacements that exceed 0.5 metre in the analysis performed would exceed the threshold value of 0.1 metre. The implication for the result is that no canister damages at all would occur.

a)

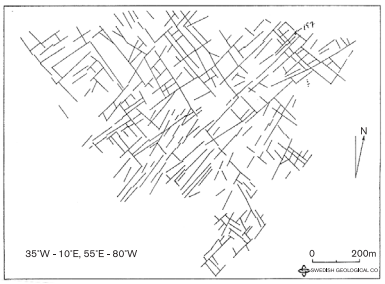

Trace data from the three repository sites are analyzed and used to devise fracture network models. The fracture network models have a deterministic portion and a stochastic portion.

b)

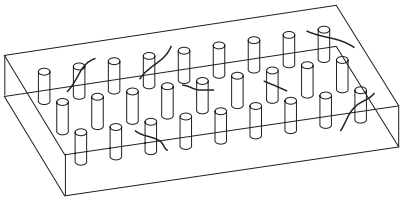

For each repository site, 100 realizations of the fracture network model are generated with the aid of the FracMan code. For each realization, a statistically representative selection of canister-intersecting fractures is kept for the subsequent earthquake analysis.

c)

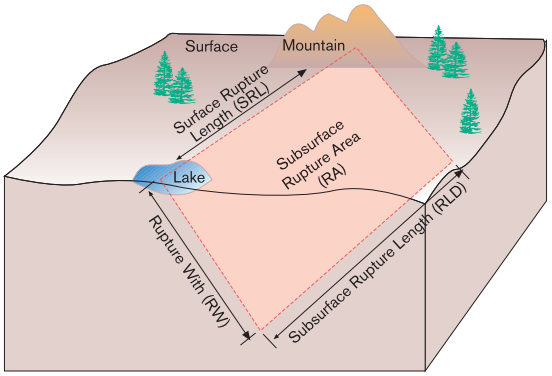

For each repository site, earthquakes are randomly distributed among zones situated within a distance of 100 km from the repository site in accordance with the earthquake statistics that are assumed to apply to the region.
Global regression relationships are used to determine the minimum surface rupture length required to accommodate the earthquake. The earthquake is represented as an instantaneous shear displacement. The maximum displacement, as well as the depth, is obtained stochastically from globally applicable regression relationships.

d)

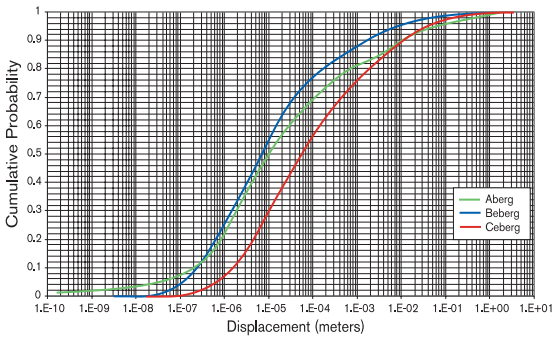

The earthquake's effect on a statistically representative selection of canister-intersecting fractures is analyzed with the POLY3D code.

Figure 11-6. *The different steps in applying the method.*

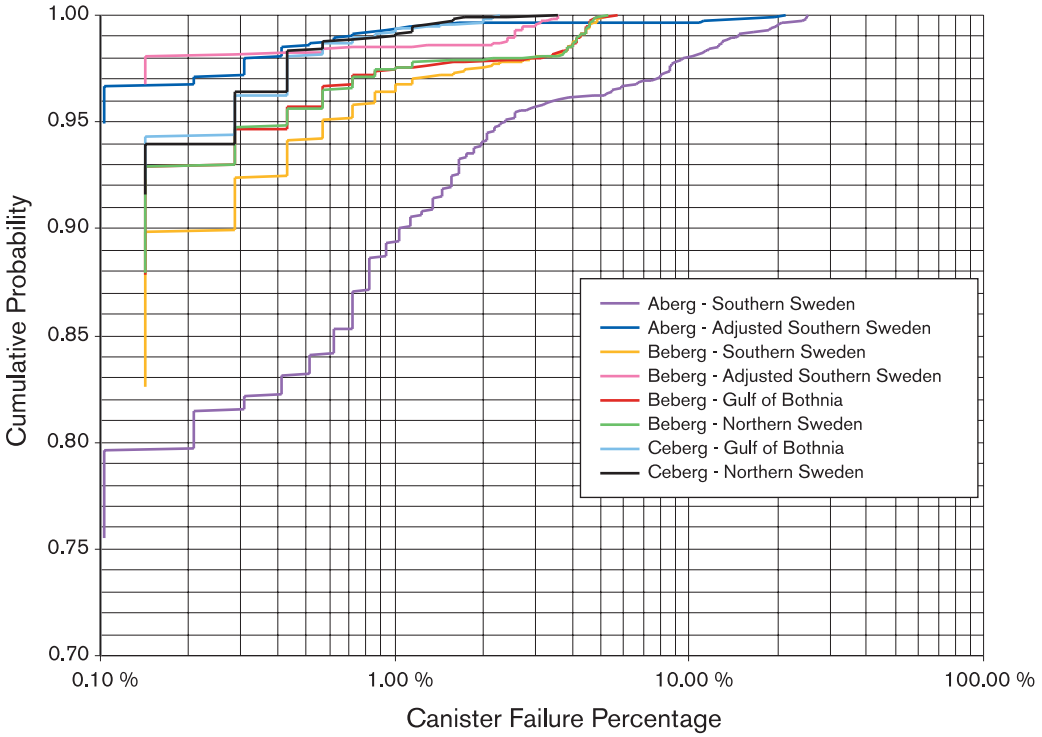

Figure 11-7. *Cumulative probability of canister failure due to single or multiple earthquakes. The figure shows that nearly 90 percent of the simulations did not give any canister failure.*

- **Mechanical properties of the rock mass.** The fractures' secondary displacements are not affected in the simulations performed by other fractures or by the repository cavities. The rock is assumed to behave linear-elastically. This is also pessimistic. If fractures located between the primary fracture where the earthquake occurs and the secondary fractures in the repository had been active, for example by undergoing plastic deformation, this would entail a loss of energy on the way and the secondary displacements in the repository would have been smaller. Dynamic calculations with models containing a few fractures could be carried out to illustrate the size of the effect of such friction damping.
- **Magnitude/displacement relationships.** Different relationships apply for different types of faults. Since it cannot be predicted whether a given zone will be reactivated as a strike-slip fault, a thrust fault or a normal fault, a worst-case scenario has been posited. Earthquakes along zones with a surface length of less than 40 km have been assumed to take place by thrusting, and earthquakes along longer zones as strike-slip faults.
- **Cumulative effects.** Most of the canister damages that occur due to cumulative effects of multiple earthquakes are presumably overestimates, regardless of all other assumptions. The cumulative effect is obtained by superimposing a consequence of statically calculated displacements. The secondary fracture displacements that are calculated should, however, be regarded as deflections in an oscillating motion, not as permanent displacements, even though a static calculation method is used to represent the dynamic effect. The actual static effects of an earthquake are small, since an earthquake doesn't increase the static load on the fractures in the surroundings, but on the contrary reduces the load that previously existed.

- **Canister positions.** There is uncertainty as to how successful actual efforts will be to avoid depositing canisters in holes intersected by large fractures. In the analysis, no credit has been taken for the fact that it will be possible to reject unsuitable canister positions.

Other uncertainties

- **Extrapolation of earthquake statistics.** The greatest uncertainty in the risk analysis is probably related to the extrapolation of the earthquake statistics, in part because existing statistics do not cover earthquakes of a magnitude greater than 5, and in part because there is no clear-cut answer to the question of the causes of past and current seismic activities or the possible scope and duration of future glaciations.

  If present-day seismic activity is exclusively due to tectonic forces (ridge push), strain energy will continue to be accumulated in the bedrock at the present-day rate. The rate at which energy is released, aseismically or seismically, will also be constant, but only until the bedrock is eventually stabilized beneath a future ice cap. Owing to the smaller deviatoric stress state that will then prevail, the bedrock will be able to accumulate the strain energy generated by ridge push, and seismic activity will decrease. The risk analysis thus applies up until the beginning of the next glaciation, while the risks are overestimated during the glaciation itself. During deglaciation, the accumulated energy will be able to be released and seismic activity will increase. If the same distribution between seismically and aseismically released energy exists as now, as well as the same distribution between small and large earthquakes, this merely means that earthquakes are redistributed over time, so that the canister damage estimate applies, calculated as a mean value over a complete glaciation cycle. It is, however, possible that, due to the rapid stress change connected with deglaciation, the proportions between seismically and aseismically released energy will change towards a higher proportion of seismic movements and that the distribution between earthquakes of different magnitudes will shift towards large earthquakes. If this is true, the number of earthquakes in general will be underestimated in the analysis, and above all the proportion of large earthquakes. The postglacial fault movements that have been documented in e.g. Lansjärv suggest that this is the case, at least in the far north of Sweden. The intensive seismic activity with large earthquakes that has taken place in the region may possibly be due to the fact that the glaciation has lasted for such a long time that exceptionally large quantities of strain energy have been accumulated.

  If present-day seismic activity is exclusive due to the still-ongoing glacial rebound and not to ridge push, the risk analysis entails an overestimate, since the land uplift rate is now diminishing and will continue to diminish. This is, however, only true until after the next glaciation. After that the land uplift rate increases, meaning that the performed risk analysis then underestimates the earthquake frequency. It is not possible to determine whether the earthquake statistics that have been used in the risk analysis generally entail an underestimate or an overestimate, counted as a mean value over a glaciation cycle. However, the large earthquakes with magnitudes greater than 8 that took place in northernmost Sweden in connection with the most recent deglaciation clearly show that the earthquake statistics used underestimate the future earthquake frequency in northernmost Sweden if a deglaciation similar to the most recent one takes place within the next hundred thousand years.

The frequency assumptions in the risk analysis are thus not pessimistic if a glaciation with subsequent deglaciation should occur within the next hundred thousand years. This is true regardless of which mechanism is assumed to be the cause of today's seismic activity. The underestimation of the earthquake frequency pertains only to the deglaciation phase, and possibly only in the region in northernmost Sweden where clear signs have been found of postglacial fault movements. In that region, an estimated seven earthquakes of magnitude 7 or more may have taken place during the most recent glaciation cycle /Muir Wood, 1993/. In the earthquake statistics that have been applied for northern Sweden, it is assumed that 0.23 such earthquakes occur within the next hundred thousand years, i.e. 1/30th as many. If the factor of 30 is applied to earthquakes of all magnitudes, this would entail a 30-fold underestimation of canister damages, provided the repository were located in the fault region. If the next glaciation follows a pattern similar to the previous one, however, all the repository sites are situated far enough away, with good margin, for the underestimation to be considerably less.

- **Fracture network models.** There is probably an uncertainty when it comes to the fracture networks at the three repository sites as well. It can, for example, be seen that the fracture intensity is greater in Aberg than in Beberg and Ceberg, which is either an actual circumstance or an effect of the much more comprehensive mapping work that has been done in Aberg. The interpretation of the mapping and determination of the DFN parameters has furthermore been done in different contexts for Aberg compared with Beberg and Ceberg. The difference between the fracture network models for Aberg and Beberg/Ceberg may perhaps therefore be regarded as a rough and pessimistic measure of the uncertainty associated with the DFN models. In the results it can be seen that the expected number of damaged canisters for the same earthquake region can vary by a factor of between 2 and 4 depending on which DFN model is used.

11.5.3 Improvements of the analysis

The biggest uncertainty lies in the prediction of the frequency of future earthquakes. It may be possible, by means of systematic and careful geodetic measurements carried out over a long period of time, to obtain a more accurate description of the movements that cause today's seismic activity. This will also make it possible to better determine what roles ridge push, glacial rebound and postglacial fault movements have now and have had in the past. It may also be possible to better understand what factors will control seismic activity during and after a future glaciation. Uncertainty regarding the scope and duration of a future glaciation will nevertheless persist, which will presumably make it impossible to improve the prediction of future earthquakes to any significant degree. Improvements of the analysis can instead be achieved by taking into account and utilizing the margins that are inherent in the pessimistically handled uncertainties.

One big margin is inherent in the assumption that the secondary fractures are without friction and cohesion. If it is assumed, for example, that the fractures have a 30 degree friction angle, it is possible to estimate that the displacements will be considerably smaller, perhaps by a factor of 5, see the Process Report. This means that only such earthquakes that give displacements on the order of 0.5 metre in the friction-free analysis that has now been performed would have given displacements exceeding the threshold value of 0.1 metre if the analysis had been done with the assumption of a 30 degree

friction angle. Only ten percent of the simulations that have now been done gave canister damages, i.e. shear displacements in excess of 0.1 metre across one or more canister holes. If the criterion of 0.5 metre had instead been applied with the same calculation data, it is highly likely that no canister damage at all would have been obtained. This is true regardless of the earthquake frequency: In order to obtain a 0.5 metre displacement, an earthquake of magnitude 8.2 would have had to occur at a distance of less than a hundred metres from the repository /LaPointe et al, 1997/. According to the regression relationships between magnitude and earthquake parameters that have been found to apply globally and are also assumed to apply for seismic activity in Sweden, an earthquake of this size would have required a primary fracture zone with a surface length of more than 100 km /LaPointe et al, 1999/. The interpretation of the fault zones in northernmost Sweden is that the earthquakes occurred as reactivation of existing zones, rather than as new fracturing /Stanfors and Ericsson, 1993/, which means that if it is possible to avoid siting the repository within a distance of 100 metres from an existing 100 km long zone, then it will also be possible to completely avoid canister damages caused by earthquakes.

A possible improvement of the analysis would be to verify, by comparison with the results of dynamic calculations, that the effects of friction and cohesion on the secondary displacements are of the order of magnitude described above. The estimated effect, a reduction of the secondary displacements by a factor of 5, is based on analytical expressions (see the Process Report) that can easily be verified by static calculations. It is not realistic today to carry out dynamic analyses of models with a large number of fractures, but the verification can be done in principle in models with a few fractures or just one fracture.

In summary, the pessimistic assumptions that are made in the risk analysis are judged to be able with good margin to compensate for the uncertainties associated with the prediction of future earthquakes and with the description of the fracture systems on the three repository sites. Just making more realistic assumptions about the mechanical properties of the fractures, for example, leads to such a great reduction of the movements that the number of damaged canisters will be zero, provided that the repository is not sited closer than 100 metres to zones, i.e. potential primary fractures, that are more than 100 kilometres in length. Added to this are the effects of other pessimistic assumptions and pessimistically handled uncertainties, where presumably above all the assumption that the rock mass is a linear-elastic medium without damping properties entails considerable margins.

All conclusions apply under the provision that the static representation of the dynamic effects is adequate and preferably pessimistic. The physical processes around actual earthquakes are complicated and may, for example, include sequences of aftershocks. The employed code, POLY3D, has been verified against analytical solutions of static problems /LaPointe et al, 1997/. The results should also be verified by comparing with results obtained from dynamic treatment of simple cases and attempting to analyze the importance of aftershock sequences.

Finally, it must be observed that the evaluation of the performed calculations is based on the assumption that a 0.1 metre shear movements causes canister damage. The criterion is pessimistic and is based on early calculations that showed a moderate plastic strain in the copper canister in connection with this deformation /Börgesson, 1992/. The relevance of the criterion ought to be re-evaluated by means of new calculations with the present-day canister design.

11.6 Conclusions for the safety assessment

The analysis methodology presented here is under development and comprises a first step in a procedure for quantitative analysis of earthquake scenarios.

Certain conclusions for the safety assessment can, however, be drawn now. The median risk for canister damage is zero percent for all combinations of sites and earthquake parameters. In approximately 90 percent of the realizations for the various combinations, no canisters are damaged. The analysis also shows that most damages result from a single earthquake. The number of such earthquakes expected during a hundred thousand years is lower than 0.35 for all combinations of sites and earthquake parameters. These observations provide an upper limit for the probability of canister damages.

From a strict risk perspective, however, it is the mean value (expected value) of the risk that is interesting. Here the analysis shows that the expected risk of canister damage on the different sites varies between 0.04 percent for Ceberg to 0.65 percent for Aberg. These risks can be compared with the risk of an initial canister defect, which is 0.1 percent. The order of magnitude is the same for these two risk types.

The methodology leads to overestimates of the risk, and the number of expected damaged canisters should in reality be much lower. For one thing, the effect of including friction in the calculations can be roughly estimated to lead to a prediction of zero damaged canisters. Furthermore, earthquakes that may cause canister damage require primary fracture zones of such an extent that they can with great certainty be avoided in connection with the positioning of a future repository, which means that the risk of canister damages caused by earthquakes can be considered negligible.

Consequently, earthquakes are not expected to lead to any canister damages. For this reason, no calculations of radionuclide transport are performed in the tectonics-earthquake scenario in SR 97. The methodology for earthquake analyses will be further refined for future safety assessments.

11.7 References

Börgesson L, 1992. Interaction between rock, bentonite, buffer and canister. FEM calculations of some mechanical effects on the canister in different disposal concepts. SKB TR 92-30. Svensk Kärnbränslehantering AB.

Hanks T C, Kanamori H, 1979. A moment-magnitude scale. Journal of Geophysical Research, Vol 84, 2348–2350.

Juhlin C, Wallroth T, Smellie J, Eliasson T, Ljunggren C, Leijon B, Beswick J, 1998. The very deep hole concept – geoscientific appraisal of conditions at great depth. SKB TR 98-05. Svensk Kärnbränslehantering AB.

Kakkuri J, 1986. Newest results obtained in studying the Fennoscandian uplift phenomenon. Tectonophysics Vol 130, 327–331.

LaPointe P, Wallman P, Thomas A, Follin S, 1997. A methodology to estimate earthquake effects on fractures intersecting canister holes.
SKB TR 97-07. Svensk Kärnbränslehantering AB.

LaPointe P, Cladohous T, Follin S, 1999. Calculation of displacements on fractures intersecting canisters induced by earthquakes: Aberg, Beberg and Ceberg examples.
SKB TR-99-03. Svensk Kärnbränslehantering AB.

Leijon B, 1993. Mechanical properties of fracture zones.
SKB TR 93-19. Svensk Kärnbränslehantering AB.

Milnes A G, Gee D G, Lund C-E, 1998. Crustal structure and regional tectonics of SE Sweden and the Baltic Sea.
SKB TR-98-21. Svensk Kärnbränslehantering AB.

Muir Wood R, 1993. A review of the seismotectonics of Sweden.
SKB TR 93-13. Svensk Kärnbränslehantering AB.

Muir Wood R, 1995. Reconstructing the tectonic history of Fennoscandia from its margins: The past 100 million years.
SKB TR 95-36. Svensk Kärnbränslehantering AB.

Munier R, Sandstedt H, Niland L, 1997. Förslag till principiell utformning av förvar enligt KBS-3 för Aberg, Beberg och Ceberg.
SKB R-97-09. Svensk Kärnbränslehantering AB.

Rehbinder G, Yakubenko P A, 1998. Displacement and flexural stresses of a loaded elastic plate on a viscous liquid.
SKB PR U-98-04. Svensk Kärnbränslehantering AB.

Scherneck H-G, Johansson J M, Elgerud G, 1996. Application of space geodetic techniques for the determination of intraplate deformations and movements in relation with the postglacial rebound of Fennoscandia.
SKB TR 96-19. Svensk Kärnbränslehantering AB.

Scholz C H, 1990. The mechanics of earthquakes and faulting. Cambridge University Press, Cambridge.

Slunga R, 1991. The Baltic Shield earthquakes. Tectonphysics, Vol 189, 323–331.

Stanfors R, Ericsson L O (eds), 1993. Post-glacial faulting in the Lansjärv area, Northern Sweden. Comments from the expert group on a field visit at the Molberget post-glacial fault areas.
SKB TR 93-11. Svensk Kärnbränslehantering AB.

Stephansson O, 1987. Modelling of crustal rock mechanics for radioactive waste storage in Fennoscandia – Problem definition.
SKB TR 87-11. Svensk Kärnbränslehantering AB.

Sundberg J, 1995. Termiska egenskaper för kristallint berg i Sverige. Kartor över värmekonduktivitet, värmeflöde och temperatur på 500 m djup.
SKB PR D-95-018. Svensk Kärnbränslehantering AB.

Wallroth T, 1997. Vad betyder en istid för djupförvaret. En delrapport från projektet ”Beskrivning av risk”.
SKB R-97-11. Svensk Kärnbränslehantering AB.

Vieno T, Nordman H, 1999. Safety assessment of spent fuel disposal in Hästholmen, Kivetty, Olkiluoto and Romuvaara, TILA-99.
Posiva 99-07. Posiva Oy, Finland.

12 Scenarios based on human actions

12.1 Introduction

In principle, three different options are conceivable for managing hazardous waste:

- Dilute it to harmless concentrations and disperse it in the environment.
- Convert it to a harmless form.
- Collect it and keep it isolated from man environment.

The last principle is applied to the spent nuclear fuel, as well as to the major part of the radioactive waste generated by society. The spent nuclear fuel is planned to be encapsulated and placed in a repository deep down in the bedrock. This means that the radioactive substances will be collected in one place. If humans disable the repository's barriers, they may be exposed to large quantities of the radiotoxic material. This potential risk is a direct consequence of the chosen disposal principle.

Man is dependent on, and influences, the environment in which he lives. Human actions affect the biosphere and thereby migration pathways for possibly occurring toxic substances. Human actions – such as irrigation, land drainage, construction of dams and canals – can affect the hydrological boundary conditions for a deep repository. By drilling and building in the rock, or constructing dumps and landfillings or carrying out weapons testing on the surface above the repository, humans can affect the mechanical conditions in the rock. The thermal conditions can be affected by extraction/storage of heat from/in the rock.

The list of human actions that influence the conditions on a repository site can be made very long. Since the future development of human society is basically unpredictable, it can never be made complete. The safety assessment covers only actions:

- that influence the performance and safety of the repository system and that can lead to radiological consequences, and
- that are performed without knowledge of the repository and/or its function and purpose, i.e. inadvertent actions.

The idea of only taking inadvertent actions into account has been discussed and affirmed within the OECD/NEA (Organisation for Economic Co-operation and Development/ Nuclear Energy Agency). They support the principle that the society that produces the radioactive waste should also bear responsibility for developing a safety disposal system. In developing such a system, as much consideration as possible should be given to future generations. However, society today cannot protect future societies from their own actions if the latter are aware of the consequences /OECD NEA, 1995/.

12.2 Method

Human actions can affect the repository in different ways. Many factors of differing character such as settlement pattern, type of society, and level of knowledge and technology are of importance for human actions on the repository site. For the purpose of providing as comprehensive a picture as possible of different human actions that may impact the deep repository as well as their background and purpose, the following systematics has been used /OECD NEA, 1995; Morén et al, 1998/:

A. Technical analysis:
Use the repository's system description and identify human actions that could influence the performance of the repository; describe and justify the actions in technical terms.

B. Analysis of societal factors:
Describe societal factors and conditions of importance for whether human actions that influence the safety of the repository will take place.

C. Choice of representative scenarios:
Put together the results of the technical and socio-economic analyses and choose a number of scenarios that illustrate how some future human actions may affect the repository.

D. Analysis of the chosen scenarios:
Describe the chosen actions in detail, and investigate their consequences and the probability of their happening.

Future human actions that may influence the safety of a repository include, besides technical aspects, questions relating to the evolution of society and human behaviour. Examples of such questions are:

- How will technology and science develop?
- What will the future society look like?
- What will human living conditions be?

Answers to these types of questions cannot be found by means of conventional scientific methods. It is, for example, not possible to predict knowledge that doesn't exist today, and knowledge is deemed to be a key factor in this context. To formulate scenarios based on human actions, we have to rely on current knowledge, gathered from people who are alive and active today. An ambition has been to incorporate experience from people with expert knowledge within a wide spectrum of relevant fields. To achieve this, steps A and B above – technical analysis and analysis of societal factors – have been dealt with at work sessions to which experts with different backgrounds and knowledge have been invited /Morén et al, 1998/.

12.3 Technical analysis

To carry out step A – Technical analysis – a group of engineers with good knowledge in the fields of geotechnics, geology, geohydrology, chemistry, systems analysis and risk analysis were selected. The technical aspects of human actions on the repository site were dealt with at a work session /Morén et al, 1998/. The purpose of the session was to:

- based on current technical knowledge, draw up a list of human actions that could impact the repository system.
- describe and explain the actions in technical terms.

The human actions in question were supposed to be ones that influence repository performance and are feasible and credible from a technical viewpoint. In order to obtain a systematically structured and relatively complete list of actions, they were identified with the support of the system description in the form of THMC diagrams (see section 4.2 and Chapter 5).

An inventory of conceivable actions within each category was carried out. The actions are presented in Table 12-1. It should be mentioned that most human actions that fit the above description lead to influences within several of the categories T, H, M and C.

Table 12-1. Human actions that can affect a deep repository classified into the categories T, H, M and C /Morén et al, 1998/.

Category	No.	Action
Thermal influence (T)	T1	Build heat store-age plant*
	T2	Build heat pump plant*
	T3	Extract geothermal energy (geothermy)*
	T4	Build plant that generates heat/cold on the surface above the repository
Hydrological influence (H)	H1	Drill well*
	H2	Build dam
	H3	Change surface water body's (watercourse, lake, sea) course, size and connections with other water bodies
	H4	Build hydropower plant*
	H5	Build drainage system
	H6	Build infiltration system
	H7	Build irrigation system*
	H8	Change conditions for groundwater recharge by change in land use
Mechanical influence (M)	M1	Drill in the rock*
	M2	Build rock cavern, tunnel, shaft, etc.*
	M3	Excavate open-cast mine or quarry*
	M4	Construct dump or landfilling
	M5	Bomb or blast on the surface above the repository
Chemical influence (C)	C1	Dispose of hazardous waste in the rock*
	C2	Construct sanitary landfill (refuse tip)
	C3	Acidify air and land
	C4	Sterilize land
	C5	Cause accident leading to chemical contamination

*) Includes, or may include, drilling and/or construction of rock cavern.

The system description in the form of THMC diagrams was also used as a tool for judging which of the identified actions has the greatest influence on the performance and safety of the repository. It was found that actions that include drilling and/or construction in rock are those with the greatest potential influence on the repository system.

A technical assessment of the suitability of the repository site for the actions in Table 12-1 is that it is more favourable for building a heat store or heat pump plant than other places, due to the heat generated by the spent fuel. For the other actions, the repository site is equivalent to or less favourable than other places with similar bedrock.

Some other technical aspects of human actions on the repository site are:

- The possibility of future human actions that might impact the repository has been considered in the repository design and site selection processes.
- In order for an action to be carried out, someone must be willing to pay for it, or it must be expected to yield a profit that covers the costs of carrying it out.
- Both costs and potential profits are coupled to technological progress and overall societal evolution.
- The utilization time for man-made facilities that involve some kind of continuous operation may be from tens to hundreds of years.

12.4 Analysis of societal factors

In order to be able to judge the consequences of a disruptive action on the repository site, it is important to investigate why the disruptive action is being carried out and the societal conditions prevailing at the time of the disruption. This is primarily a humanistic, socio-economic problem.

In order to shed light on humanistic and socio-economic aspects and to implement step B (Analysis of societal factors) in the strategy, another work session was held with experts in the fields of cultural geography, history of science and technology, and systems analysis. Framework scenarios that describe plausible societal contexts for future human actions with an influence on the radiological safety of the deep repository were formulated /Morén et al, 1998/.

The framework scenarios were developed by means of morphological field analysis /Morén et al, 1998; Ritchey, 1997/, a group- and process-oriented interactive method for structuring and analyzing complex problem fields that are non-quantifiable, contain non-determinable uncertainties and require a judgmental approach. For this a morphological field is employed, which is a matrix that describes the dimensions and outcome spaces of the problem complex. The headings of the columns identify the essential parameters (factors or variables) on which the problem is to be based. The alternative values or conditions which each parameter can have are given in the rows.

The following essential parameters and their "values" were identified for human actions at the repository site:

- **Settlement pattern:** geo-demographic pattern on or near the repository.
  - Megalopolis – Most people live in very big "modern" cities (of the type New York, Tokyo, Los Angeles).
  - X-city – Most people live in cities and towns that are distributed with a linearly diminishing relationship between size and number (roughly like Sweden today).
  - Sparse – The population is spread out over a large area. "Sparse modern" (such as Iceland or Canada today) or "sparse degenerate".

- **General scientific and knowledge level:** relative to the western world today.
  - Very high, but only among an elite.
  - Very high among the general public.
  - Roughly like today.
  - Considerably lower.

- **Transportation system:** relative to the western world today.
  - Considerably higher capacity (faster, more efficient, more reliable, more accessible, cheaper, cleaner).
  - Like today or slightly higher capacity.
  - Lower capacity.
  - Degenerate – means that something is happening that is causing a downward or decadent trend. It may be war, pollution and/or natural disasters that are destroying resources so that they cannot be restored, much less continue to develop. This may occur more or less dramatically, over a long or short period of time.

- **Information system:** relative to the western world today.
  - Considerably higher capacity.
  - Like today or slightly higher capacity.
  - Lower capacity.
  - Degenerate (see above).

- **Knowledge of the repository:** existence, properties and location.
  - Generally known.
  - Known only by an elite.
  - Only locally known. (Example: The "rumour" or "myth" of the repository is a part of the culture of the local populace.)
  - Lost.

- **Type of society:** legitimacy of form of government and relative governability of society. Legitimacy describes to what extent the population give the government their approval and support. Governability describes to what extent the population obey the laws and rules laid down by the government.
  - High legitimacy and governable society.
  - High legitimacy and poorly governable society.
  - Low legitimacy and governable society.
  - Low legitimacy and poorly governable society.

- **Purpose:** of the action that impacts the repository.
  - To retrieve another resource than the radioactive waste or to build something in the rock (repository unknown).
  - To retrieve the waste as a resource or to relocate it.
  - To check the repository and its safety.
  - To map and explore the area (repository unknown).
  - To sabotage the repository, practise extortion etc., i.e. evil intent.

The morphological field used by the group is shown in Figure 12-1.

Settlement pattern (geo-demo)	General scientific and knowledge level	Transportation system	Information system	Knowledge of the repository	Type of society	Purpose of disruption
Megapolis	Very high among elite	Unknown capacity	Higher capacity	Generally known	Legitimate Hard to govern	Retrieve other resource or build
X-city	Generally high (much higher than today)	Like today	Like today	Known to elite	Legitimate Hard to govern	Retrieve as resource
Sparse	Like today	Lower capacity	Lower capacity	Locally known (only)	Illegitimate Governable	Check the repository
	Lower than today	Degenerate	Degenerate	Lost	Illegitimate Hard to govern	Mapping/ exploration
						Sabotage

Figure 12-1. *Morphological field for societal context of human actions that might influence the repository's performance and safety.*

In the analysis of the morphological field, the group makes pair-wise comparisons of the parameters. Each pair of "parameter values" is ranked on a 3- or 5-point scale. The extreme values on the scale indicate that the two "parameter values" depend on or contradict each other, the middle value indicates that they are neutral. That the values depend on each other means that if one is valid then the other must also be valid. The middle value indicates that the two values neither depend on nor contradict each other, but that the conditions described can co-exist. The 5-point scale has two additional positions, which indicate that the two "parameter values" either depend on or contradict each other to some degree. The 5-point scale was used.

When all combinations have been discussed, the morphological field is investigated for the purpose of finding internal relationships, patterns and consistent configurations. In the first step, all contradictory combinations are eliminated. The configurations that are left are studied against the background of the purpose of the analysis. This analysis showed that of the total number of internally consistent configurations, the so-called solution space, three parameters dominated:

1. general scientific and knowledge level,
2. knowledge of the repository's existence, and
3. intentionality in disrupting the repository.

These three parameters are thus decisive for all conceivable future human actions on the repository site. Furthermore there is one additional parameter, which describes the socio-technical development process as continuous or discontinuous. Discontinuous development means that the development of society and technology contains a sudden, large change. After the analysis, it was thus possible to reduce the morphological field to the form described in Figure 12-2.

General scientific and knowledge level	**Knowledge of the repository**	**Purpose of disruption**	**Societal development process**
Very high among elite	Generally known	Retrieve other resource or build	Continuous
Generally high (much higher than today)	Known to elite	Retrieve as resource	Dis-continuous
Like today	Locally known (only)	Check the repository	
Lower than today	Lost	Mapping/ exploration	
		Sabotage	

Figure 12-2. *The morphological field after the analysis.*

Four framework scenarios for inadvertent human impact on the deep repository were identified within this solution space. The scenarios were given the names "The Inclined Plane" (Figure 12-3), "The Collapse" (Figure 12-4), "The Recovery" (Figure 12-5) and "Selective Forgetfulness" (Figure 12-6).

The Inclined Plane

General scientific and knowledge level	Knowledge of the repository	Purpose of disruption	Social development process
Very high among elite	Generally known	Retrieve other resource or build	Continuous
Generally high (much higher than today)	Known to elite	Retrieve as resource	Dis-continuous
Like today	Locally known (only)	Check the repository	
Lower than today	Lost	Mapping/ exploration	
		Sabotage	

Society is progressively degenerating. The general scientific and knowledge level is lower than in the western world today.

Knowledge of the repository is gone. The repository may be disrupted inadvertently in this society. Something is built in the rock near the repository, for example for the purpose of retrieving a resource.

Another purpose may be drilling in the rock to map or explore the area.

Figure 12-3. *The framework scenario "The Inclined Plane".*

The Collapse

General scientific and knowledge level	Knowledge of the repository	Purpose of disruption	Social development process
Very high among elite	Generally known	Retrieve other resource or build	Continuous
Generally high (much higher than today)	Known to elite	Retrieve as resource	Dis-continuous
Like today	Locally known (only)	Check the repository	
Lower than today	Lost	Mapping/ exploration	
		Sabotage	

A dramatic course of events has occurred and we are in a period following a (possibly global) breakdown of society.

The general knowledge level is lower than today and knowledge of the repository is either gone or exists only locally in the form of a local culture based on myths and rumours.

In this society (as in The Inclined Plane), the repository may be disrupted inadvertently. As above, something is built in the rock near the repository, for example for the purpose of retrieving a resource, or holes are drilled in the rock for the purpose of mapping or exploring the area.

Figure 12-4. *The framework scenario "The Collapse".*

The Recovery

General scientific and knowledge level	Knowledge of the repository	Purpose of disruption	Social development process
Very high among elite	Generally known	Retrieve other resource or build	Continuous
Generally high (much higher than today)	Known to elite	Retrieve as resource	Discontinuous
Like today	Locally known (only)	Check the repository	
Lower than today	Lost	Mapping/ exploration	
		Sabotage	

Figure 12-5. *The framework scenario "The Recovery".*

A dramatic course of events has occurred and we are in a period after the breakdown (discontinuity in societal evolution).

In contrast to The Collapse, society has been rebuilt. The general knowledge level is higher than in the western world today. Knowledge of the repository has been lost, however.

The purpose of the disruption is as above, but the consequences may be different.

Selective Forgetfulness

General scientific and knowledge level	Knowledge of the repository	Purpose of disruption	Social development process
Very high among elite	Generally known	Retrieve other resource or build	Continuous
Generally high (much higher than today)	Known to elite	Retrieve as resource	Discontinuous
Like today	Locally known (only)	Check the repository	
Lower than today	Lost	Mapping/ exploration	
		Sabotage	

Figure 12-6. *The framework scenario "Selective Forgetfulness".*

Some knowledge has been lost, even though the knowledge level in general has increased.

Due to new (at present unknown or "unspecified") knowledge, other specific fields of knowledge may have become dormant.

Nuclear fission, and thereby present-day nuclear power technology, may be obsolete by radically new energy technologies (e.g. fusion energy, photosynthesis, vacuum energy).

Nuclear waste is no longer an important and debated issue. The repository site is abandoned and the repository is eventually forgotten.

One conclusion from the study of societal aspects was that it is difficult to imagine inadvertent intrusion, given a continuous development of society and knowledge. Owing to the long time horizon, however, it is not possible to rule out the possibility that the repository and its purpose is forgotten, even if both society and knowledge make gradual progress. Nor is it possible to guarantee that institutional control over the repository site will be retained in a long time perspective. With a discontinuous development of society, it is reasonable that knowledge will be lost and institutions will break down.

12.5 Choice of representative scenarios

It is probable that the repository site will be used by people in the future. Human actions that influence radiological safety and are carried through without knowledge of the repository and/or its purpose are taken into account in the safety assessment. Actions that influence the isolation of the spent fuel are of the greatest importance for safety, followed by actions that influence the repository's capacity to retain and retard radionuclides if the isolation for some other reason has been breached. Changes in the biosphere influence the doses to which human beings may be exposed if the repository contains leaking canisters.

The deep repository will be situated 400–700 metres deep in the rock. The reason for this is the wish to locate the repository in an environment where the isolation of the fuel will be retained even in the event of extensive changes on the surface. Changes that have been considered are natural changes and changes caused by man. Examples of natural changes are change of the repository's location in relation to the sea, and the presence of permafrost and ice sheets. Natural changes influence man's opportunities to use the repository site.

Large uncertainties are associated with the development of technology and society. It is not possible to say that any of the actions in Table 12-1 is more representative or plausible than any other. For the same reason, it is not possible to provide detailed technical descriptions of future installations, or to describe the society and living conditions of the future. The choice of scenarios is therefore based on present-day knowledge and experience.

All actions in Table 12-1 influence the migration of radionuclides in the biosphere. However, actions that are performed on or near the surface, down to a depth of a few tens of metres, are judged not to be able to affect the technical barriers and the isolation of the fuel. This applies to the actions T4, H2, H3, H4, H5, H6, H7, H8, H9, M3, M4, C2, C3, C4 and C5. Activities near the surface that belong to categories M and H are deemed to have less influence on the repository than natural changes in conjunction with future climate change (see Chapter 10). Of the actions that entail a chemical influence (C2–C5), acidification of air and land (C3) has been studied more closely. In realistic cases of acidification by atmospheric sulphur and carbon dioxide, the environment at repository depth is not affected /Nebot and Jordi, 1991; Wersin et al, 1994/. Soil layers and bedrock are judged to work efficiently as both filter and buffer against other chemical compounds as well.

Bombing or blasting on the ground surface above the repository (M5) cannot affect the isolation of the waste, except if blasting is done with a powerful nuclear weapon. Such an event is in itself deemed to be highly improbable; moreover the consequence of the blast itself is much greater than the consequence of leakage from the repository.

Some of the actions in Table 12-1 can – besides influencing radionuclide transport – indirectly influence the isolation of the waste if they render the environment at repository depth unstable. Such actions are performed directly above or near the deep repository and include drilling and/or construction in the rock (M1, M2). These categories include actions that have to do with heat extraction (T1, T2, T3), well drilling (H1) and disposal of hazardous waste in the rock (C1). Hydropower plants (H5) and open-cast mines and quarries (M3) may also involve drilling or rock works at great depth. Before a rock facility is built, drilling is carried out to investigate the rock. What all of these cases share is therefore that – if present day technology is applied – they involve drilling in the rock.

Large rock facilities adjacent to the repository are deemed to be completely out of the question in a short time perspective, i.e. within a few hundred years, for several reasons. For example, the deep repository is itself a large rock facility – the only one of its kind in Sweden – that is very unlikely to be forgotten over such a short timespan. Institutional control can be expected to endure on this timescale. The enumerated actions that encompass major rock works are less likely, based on current technology and economics. In a slightly longer time perspective, i.e. a few or several hundred years or more, it is difficult to predict how knowledge, technology and society will develop, and thereby how and why rock facilities will be built. If construction of deep rock facilities should become commonplace, however, it can be assumed that both construction and investigation methods will have improved compared with current technology. Expanded construction of deep rock facilities would thereby also lead to an increased probability that the repository will be discovered during construction.

Changes of radionuclide transport through the repository's barriers and the time when waste isolation is breached are dealt with in the canister defect scenario (Chapter 9). The consequences of most cases with rock facilities thereby fall within the frames of the uncertainty analyses in the canister defect scenario. Far-reaching assumptions regarding the design and purpose of the facilities are required in order to perform detailed consequence analyses of the enumerated actions. In view of the great uncertainties surrounding the future development of technology and society, such assumptions are not regarded as meaningful.

Of the actions in Table 12-1, "Drill in the rock" is judged to be the only one that can directly lead to penetration of the copper canister and breach of waste isolation, while at the same time being inadvertent, technically possible, practically feasible and plausible. "Drill in the rock" is furthermore a conceivable action in the light of the framework scenarios in section 12.4. Even if it is possible to build a rock cavern, tunnel or shaft or to excavate an open-cast mine which leads to penetration of the copper canister, doing so without having investigated the rock so the repository is discovered, i.e. without knowledge of the repository, is not deemed to be technically plausible. The scenario "Canister penetration by drilling" has therefore been selected as the only human-caused scenario whose consequences are further explored. Besides the reasons given above, this choice is warranted by the fact that the consequences of canister penetration by drilling fall outside the analyses performed in the canister defect scenario.

12.6 Analysis of the scenario – drilling of deep boreholes

The analysis is performed as a risk analysis where risk is the product of the probability of an undesirable event occurring and its consequences. The acceptance criterion specified by SSI is an annual risk of 10^{-6} for persons exposed to radiation from the repository. The risk applies to cancer or genetic injuries. For a hypothetical situation where exposure occurs with certainty, this is equivalent to an annual radiation dose of $1.5 \cdot 10^{-5}$ Sv/y. In the following the importance of the presence of the deep repository for risks associated with drilling of deep boreholes is analyzed. The following issues are dealt with in the analysis:

- execution and purpose of drilling,
- probability of penetrating a canister,
- radiological consequences and risk of the event.

The consequence – i.e. the effect on the repository system and the release of radionuclides to which it leads – cannot be quantified without descriptions of how drilling has been carried out. Furthermore, assumptions must be made regarding human behaviour in connection with the event. The assumptions made are based on today's technology and premises; speculations about future conditions have been avoided wherever possible.

12.6.1 Execution and purpose of drilling

The drilling technique used is dependent on the purpose of the drilling. Today drilling is done to sink wells, for the extraction of heat from the ground, and for exploratory purposes. Rock wells are normally drilled to a depth of between 50 and 100 metres, occasionally wells are drilled down to 130–150 metres. Deeper wells are very uncommon. The reason is that it is expensive to drill and the probability of finding potable water in sufficient quantity declines with depth. The deeper wells are usually used to extract heat. Well drilling is generally done by percussion drilling. Today's standard drill rigs are capable of drilling to a maximum depth of 200–250 metres. Drilling to greater depth is done for exploratory purposes, generally prospecting. It is therefore assumed that drilling through the repository is done for exploratory purposes.

A special percussion drilling technique may be used for oil prospecting, but diamond (core) drilling is normally employed for exploratory drilling. The drill core is then retrieved in a core barrel with a maximum length of six metres. The core is inspected and placed in boxes with one-metre long compartments. Now and then the cores are inspected by a geologist. The cuttings (the pulverized rock mixed with the drill's cooling water) are normally removed with water, which also cools the drill. The water with cuttings is usually spread on the ground around the borehole.

When drilling is finished, the boxes with cores are sent to core mapping and the borehole is abandoned. If the hole has passed a zone with a high water flow, so that a great deal of water is brought up to the surface, the borehole may be filled in. This is generally only done if the flow entails a nuisance to local residents.

The diameter of the hole conforms to standards: 46 mm, 56 mm, 66 mm, etc. A diameter of 46 mm is generally used for prospecting, since it is adequate and least expensive. SKB uses 56 and 76 mm in order to provide room for the desired measuring equipment. The direction of the borehole varies depending on the purpose and what is known about the rock volume to be investigated. In general the drill is slightly inclined; the angle with the ground plane is usually 70–85 degrees. If the drill reaches the buffer and the canister, these may be penetrated without this being noticed until the drill core is inspected.

12.6.2 Probability that the scenario will occur

Only drilling done without knowledge of the location and purpose of the repository is taken into account. Different countermeasures are planned to prevent inadvertent intrusion in the repository, such as conservation of information on the repository in archives, marking the site and various types of institutional control of the site. Examples of control measures are physical surveillance, ownership restrictions and restrictions on land use. These types of measures ought to contribute towards reducing the probability of inadvertent penetration by drilling. It is, however, not possible to guarantee that knowledge and control will be conserved.

Here it is assumed that knowledge of the location and purpose of the repository will be conserved for a hundred years after repository closure. The probability of inadvertent intrusion during this time is zero. This assumption is based on the assessment that it takes at least three generations for knowledge to be forgotten. How knowledge of the repository will be altered over a long period of time is highly uncertain. Here it is assumed that all knowledge of the repository is lost after 300 years, i.e. the probability that the repository will have been forgotten in 300 years is 1. The probability that the purpose and location of the repository will be forgotten is assumed to increase linearly during the period between 100 and 300 years.

The probability that one (1) deep borehole will be drilled on the repository site can be estimated, provided that:

- Only drilling in Sweden is taken into account.
- Drilling on the repository site is just as likely as on other sites with similar bedrock.

If these premises apply, the probability of drilling through a canister can be estimated as the product of the following two probabilities:

1. the probability of drilling within the repository area,
2. the probability of drilling through a canister, provided that drilling is done within the repository area.

The first probability is approximately $5 \cdot 10^{-6}$ and has been calculated as the ratio of the repository's area to the total area in Sweden with similar bedrock (1 km^2/200,000 km^2). The second probability has been estimated by means of a geometric analysis of the repository layout to be approximately one percent. The probability of drilling through a canister is thus $5 \cdot 10^{-8}$ per deep borehole drilled. This means that if 200 deep boreholes are drilled per year in Sweden's crystalline basement, every year during a hundred-thousand-year period, the probability of drilling through a canister at some time is 1. The estimated probabilities are compiled in Table 12-2.

Table 12-2. The estimated probabilities of inadvertently drilling through a canister.

Event	Probability
Knowledge of the repository and its contents has been lost	0 during 100 years 1 after 300 years Linear increase from 0 to 1 in the period 100–300 years
Borehole is drilled in repository areas	10^{-5}
Borehole penetrates a canister	10^{-2}

Trying to estimate the number of boreholes that will be drilled annually for exploratory purposes far in the future is not judged to be meaningful. Today a length of approximately 200,000–230,000 metres per year is drilled (diamond drilling with core retrieval). The mean depth is estimated to be about 400 metres, which means 500–600 deep boreholes per year. The purpose of the drillings is generally prospecting, and approximately 60 percent are done near existing mines. The majority of drillings are done in Upper Norrland /Berglund, 1995/. The repository will be located within an area that today is of no interest for prospecting. Since the area is suitable for the excavation of rock caverns, however, drilling for construction-related geological purposes is conceivable. SKB is carrying out such drilling today.

12.6.3 Radiological consequences and risk

In the scenario it is assumed that the repository and its purpose have been forgotten. The rock is investigated by drilling and a drill core is retrieved that contains pieces of pure copper, cast iron and small bits of tube with cracked uranium dioxide. The drill core is taken away for examination. One suspect mischiet and drilling is stopped. The site and the boreholes are abandoned without further measures. Some time later a family moves to the site and operates a based on domestic production farm there. Two exposure situations are investigated:

- Dose and risk to drilling personnel if they are exposed to radiation from the radionuclides in the drill cuttings and drill core.
- Dose and risk to individuals in the family if they are exposed to radionuclides brought up from the repository, assuming that the capacity of the rock and canister to prevent radionuclide transport has been lost, but the buffer's function is preserved.

Radiation dose and risk to drilling personnel

The dose to which the drilling personnel are exposed depends partly on the quantity of waste and its radionuclide content, and partly on how they are exposed to the waste /Bergström et al, 1995; Wuschke, 1996/. The drillers are assumed to have employed diamond drilling with core retrieval (see section 12.6.1). The diameter of the core is assumed to be 46 mm, the outer diameter of the borehole 52 mm and its inclination in relation to the ground plane 70 degrees. The cuttings are removed by water and spread on a circular area assumed to have a diameter of three metres centred on the borehole. The retrieved cores are assumed to be divided into 1 m long pieces and placed just outside the area with cuttings. The personnel are exposed to external irradiation from the drill core and the ground area contaminated with the drill cuttings, as well as from drilling dust that has adhered to clothing /Bergström et al, 1995/. They are also assumed to inhale contaminated dust /Wuschke, 1996/. The dust concentration in the air has been set at 100 mg/m^3, which can be compared with the Swedish Environmental Protection Agency's guideline value for urban air quality, where the 24-hour mean is 115 mg/m^3 and the 6-month mean 50 mg/m^3. The dust is a mixture of soil and contaminated drill cuttings. The inventory in the cuttings is assumed to be evenly distributed in the top 10 centimetres of soil. Geometric assumptions are shown in Figure 12-7.

The external radiation dose from the drill core depends on the thickness and length of the core and the distance between the exposed person and the core. Most important is the distance to the core. The dose from the cuttings-contaminated area depends on the size of the area and where the person is located in relation to the area. The dose from the dust-contaminated clothing depends on the thickness and size of the dust layer and where on the body the dust lands. The uncertainty in the calculation of the external dose

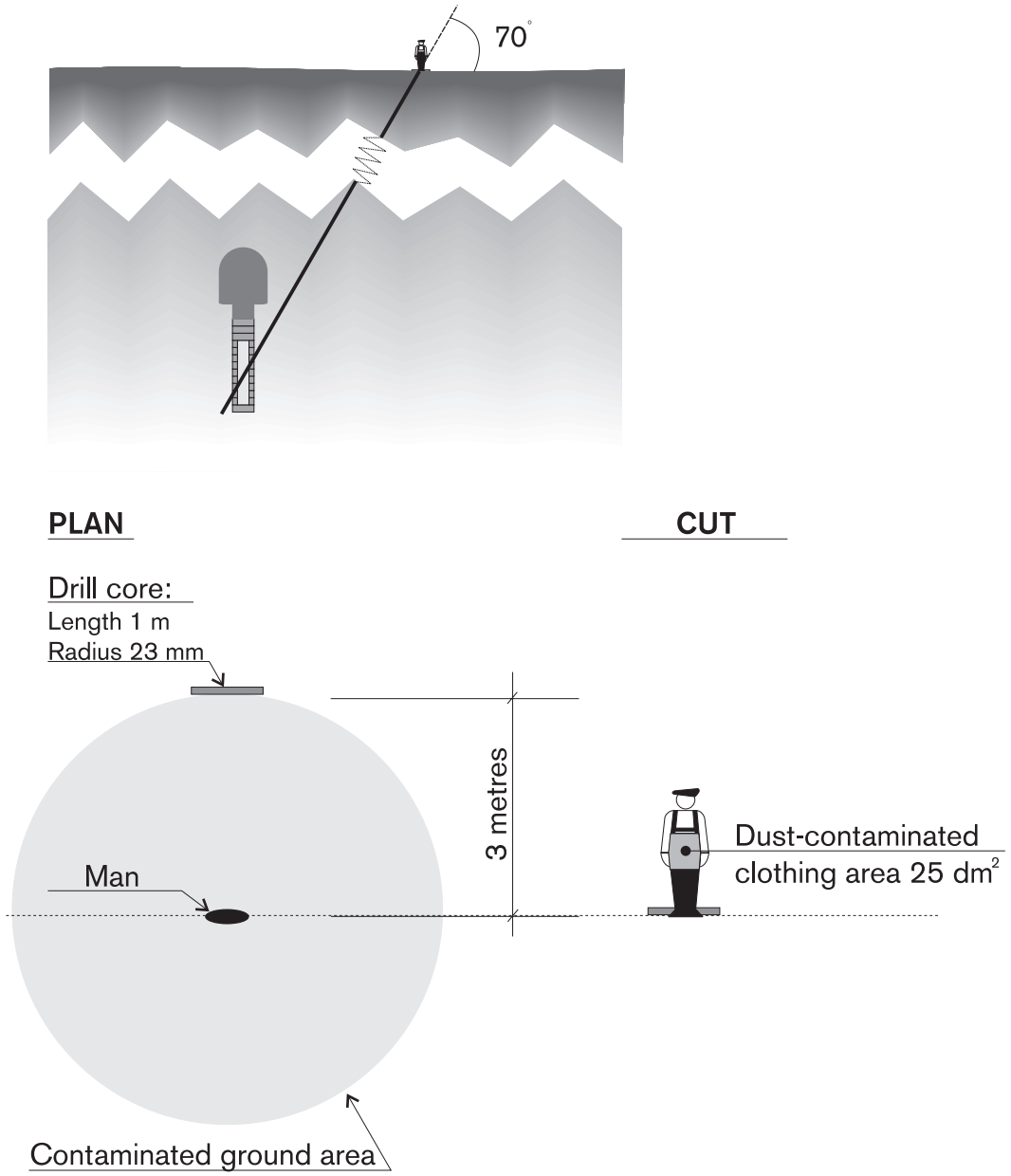

Figure 12-7. *Top: Execution of drilling. Bottom: The position of the exposed individual in relation to the radiation sources.*

has been estimated to be a factor of 10, but both lower and higher doses are possible /SKB, 1995/. The dose from inhalation of dust depends on the dust's content of radionuclides and is directly proportional to the assumed dust concentration in the air. Since the cuttings are removed via water, the dust quantity in the air is probably less than that assumed.

The radiation dose to a person who inhales contaminated dust for one hour and is exposed to external irradiation from a drill core, drill cuttings and dust-contaminated clothing is shown in Figure 12-8. As the radiotoxicity of the spent fuel declines, the potential dose diminishes. The natural background level is also shown as a comparison. The maximum dose per hour of exposure is approximately 20 mSv, i.e. of the same size as the annual dose allowed today for persons in radiological occupations.

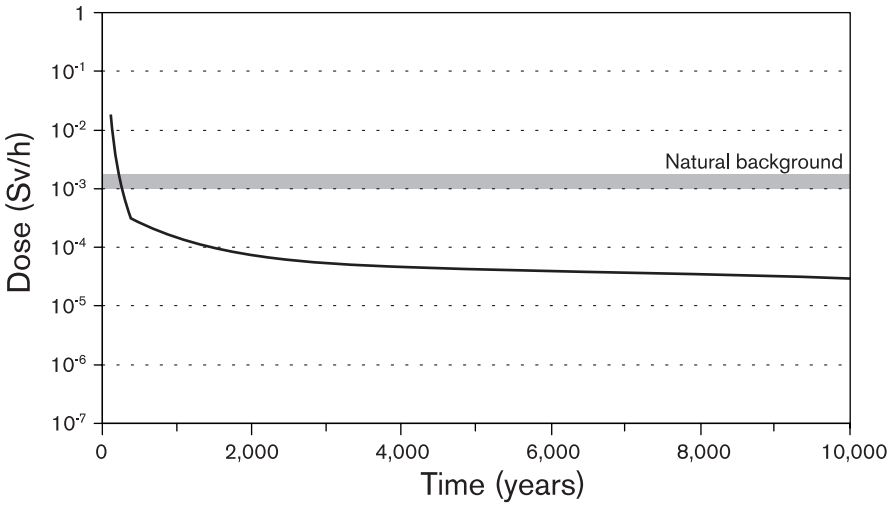

Figure 12-8. *Dose to drilling personnel as a function of time after repository closure. The exposure time is one hour. The personnel inhale contaminated dust and are exposed to external irradiation. The radiation sources and the position of the exposed individual in relation to them are shown in Figure 12-7.*

The risk to which future drilling personnel are exposed due to the fact that the deep repository has been built is a product of the probability of inadvertently drilling through a canister and the consequences of this event. Based on the assumption that the drilling personnel are exposed to a dose that is five times the calculated dose per hour when they have drilled through a canister, the risk per borehole can be estimated. This risk is the product of the following factors:

- the probability that the repository has been forgotten,
- the probability of drilling through a canister,
- the consequence expressed as the radiation dose to which the drilling personnel have been exposed.

The risk to persons who have inadvertently drilled through a canister of spent nuclear fuel is shown in Figure 12-9. The risk applies per borehole and at the exposure described.

The maximum risk per borehole is reached about 200 years after repository closure and is approximately $5 \cdot 10^{-10}$. The acceptance criterion is stipulated as an annual risk and a dose that is related to this risk. In order to be able to compare the calculated risk with the acceptance criterion, knowledge is thus needed on how many boreholes are drilled per year, a figure that is not known. During the period the risk is greatest, approximately 30,000 boreholes per year are needed to get up to an annual risk equivalent to a dose of $1.5 \cdot 10^{-5}$ Sv for exposed persons. One person alone could hardly drill that many boreholes during a year, and it is unlikely that there are so many people drilling boreholes that they could drill that many holes together. The risk to which future drilling personnel are exposed due to existence of the deep repository is therefore in all probability lower than the accepted risk.

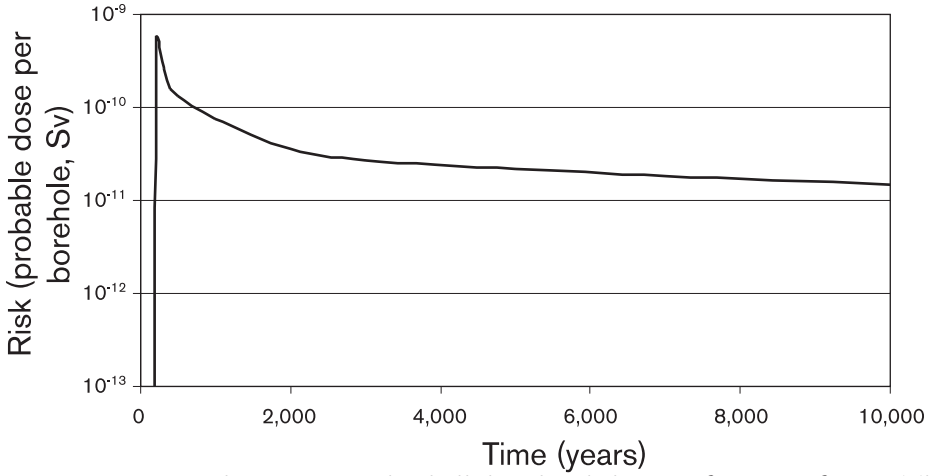

Figure 12-9. *Risk to persons who drill deep boreholes as a function of time. The risk is given per borehole.*

Radiation dose and risk to the family

The dose to which the family who settles down on the site is exposed depends on how much radionuclides can be transported up to the surface through the abandoned borehole, where the family lives or is located in relation to the borehole, and what they eat. How much radionuclides can be transported up to the surface depends on the amount of water flowing past the penetrated canister and the speed at which the contaminated water can be transported up to the surface. The borehole can, if it passes through water-bearing zones, cause an increase of the groundwater flux at repository depth in relation to undisturbed conditions. Here the groundwater flux at repository depth has been set equal to 10^{-1} m/s. This is a high flux, and is equivalent to the Data Report's value for the maximum groundwater flux (Darcy velocity) at Aberg. The canister has completely lost its isolating capacity. The buffer is assumed to swell shut after penetration. It has lost a portion of its volume and thereby has a lower swelling pressure than before, but its capacity to retard radionuclide transport is preserved. The radionuclides that can be transported out through the damaged canister and the buffer with the stipulated flux are assumed to be carried directly up to the surface. When the family arrives at the site, it is assumed that the traces in the landscape left by drilling have been eradicated, and the borehole is not discovered. The family is assumed to operate a farm based on domastic production on the site.

The typical ecosystem that has been used in the calculation of the potential dose to individuals in the family is the peat bog, see section 9.9.2. In this ecosystem, nuclides are assumed to have accumulated in peat for such a long time that there is a constant level in the peat. If the constant level has not yet been reached when the family settles on the site, the dose from certain radionuclides will be overestimated. The family is assumed to make use of the contaminated land in its farming. The dose to individuals in the family is reported in Figure 12-10. The dose does not reach the natural background level.

The accepted risk of 10^{-6} corresponds to an annual dose of $1.5 \cdot 10^{-5}$ Sv/y, provided that the probability of exposure is 1. As noted above, this dose may be exceeded during the period between 100 and about 400 years after repository closure. After 400 years, the estimated annual dose to individuals in the family is less than the accepted dose. How

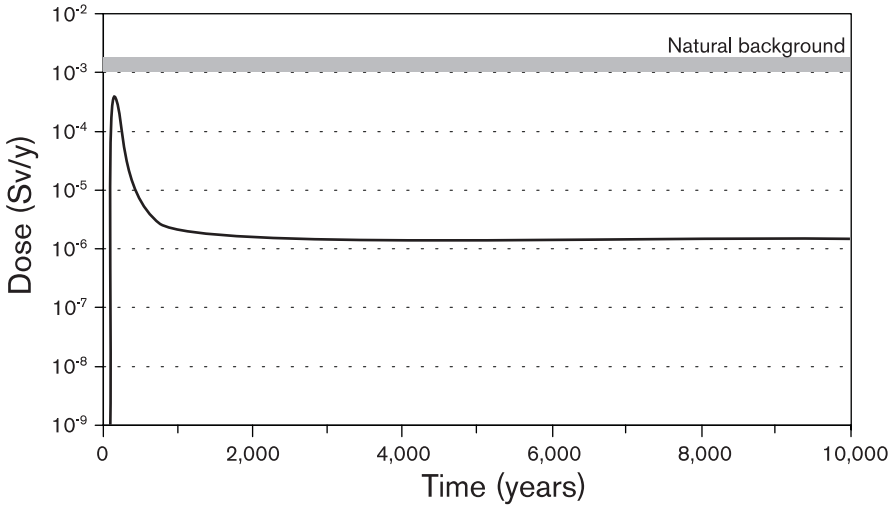

Figure 12-10. *Dose to individuals in a family that settles next to a borehole that has been drilled through a canister and then abandoned, as a function of time.*

large then is the probability that the family will be exposed, i.e. that there really is a borehole on the site when the family settles there? The probability of drilling one (1) borehole that penetrates a canister has been estimated to be 10^{-7}, the probability that someone will drill through a canister at some time is directly proportional to the number of holes drilled, i.e. if two holes are drilled the probability is $2 \cdot 10^{-7}$, if a hundred holes are drilled it is $1 \cdot 10^{-5}$, etc. This means that ten million boreholes must be drilled to a depth of at least 500 metres before the family settles on the site. This has to happen before or during the period when the acceptable dose can be exceeded, i.e. within 400 years after repository closure. This adds up to an unreasonably large number of boreholes (by today's standards), at least 25,000 per year in Sweden (approximately 33,000 allowing for the fact that the probability the repository will be forgotten is zero for the first hundred years). The risk to individuals in the family should therefore reasonably be much less than 10^{-6} per year, regardless of when they settle on the site.

12.7 Summary

Concentration and isolation of the spent nuclear fuel on a site entails that this site contains more hazardous material than other sites with similar natural conditions. As far as future use of the site is concerned, this inevitably means that certain restrictions will apply to people in the future as well. There is nothing unique about this in our society. There are many examples of sites of human activity – cities, mines, harbours, water sources, refuse tips, arable fields, rock tunnels, etc. – that have a shorter or longer impact on possible/permissible/suitable use of the original natural site. The restrictions on a deep repository site should be minimal in view of the long timescale. In principle, it should be possible to use the site for anything.

The principle of collecting hazardous waste in one place poses a risk that people will be exposed to a large quantity of the waste. If future generations forget the repository and its purpose, they may inadvertently impact it. At worst, this human impact can lead to a breach in the isolation of the waste.

Human impact has been taken into consideration in the design of the repository and in the site selection process. The depth of the repository should allow human activity on and in ground close to the surface at the repository site, as well as construction of some of the kinds of rock facilities that exist today. The site is free of what might be regarded as natural resources today.

However, due to uncertainties regarding the future development of human society, it is not possible either to guarantee that there will be no human impact on the repository or to describe what the nature of such impact will be. The construction large rock facilities close to the repository may, in combination with natural processes, affect the performance of the engineered barriers. If a borehole is drilled through a canister, the isolation will be breached immediately.

As an illustration, the consequences of inadvertent penetration of a canister by drilling have been analyzed. Dose and risk to the drilling personnel, as well as to a family that settles on the site at a later point in time, have been investigated. The drilling personnel are exposed to the highest doses. If the hole is drilled within about 300 years after repository closure, the dose to the drilling personnel may significantly exceed the background radiation and reach the levels that are permitted today for people in radiological occupations. Since the probability of drilling through a canister is low – it is estimated at 10^{-7} – the risk that future drilling personnel may be exposed to because of the existence of the deep repository will nevertheless be very small, even if the repository should be forgotten. The dose to the family will be lower than to the drilling personnel, it will never exceed the natural background radiation. If it is assumed that there is an abandoned borehole through a canister on the site when a family moves there, the dose to the family may exceed the acceptance criterion of $1.5 \cdot 10^{-5}$ Sv per year up to 400 years after repository closure. Based on the estimated probability of drilling through a canister, at least 25,000 boreholes per year to a depth of 500 metres would be needed for the risk to amount to 10^{-6} per year. This is an unreasonably large number of boreholes.

The review of human activities that could affect repository performance shows that drilling of deep holes, and construction of large rock facilities, is not suitable at the repository site. It is possible that the restrictions on such use of the site will at some time be forgotten or violated. The question is then what consequences can be allowed. In the analyzed scenario, the rock investigators proceed carelessly – more carelessly than can be expected of people today with access to present-day technology. However, they do bear some responsibility for their actions.

In a long time perspective, the repository site may be utilized in such a way that the repository is impacted. The possibilities of assessing the radiological consequences of this are limited, due to uncertainties associated with the development of human society. In the analyzed scenario, the most exposed individuals are exposed to a radiation dose equivalent to about 0.1–10 times the natural background radiation. The probability of such exposure is judged to be very small, making the risk to individuals (both drillers and those who may settle on the site after drilling) much less than 10^{-6} per year.

12.8 References

Berglund L, 1999. Hagby Asahai, personal communication.

Bergström U, Edlund O, Nordlinder S, 1995. Human activities affecting the integrity of a deep geological repository for nuclear waste – Radiological risks from intrusion. SKB PR U-96-06. Svensk Kärnbränslehantering AB.

Morén L, Ritchey T, Stenström M, 1998. Scenarier baserade på mänskliga handlingar. Tre arbetsmöten om metod- och säkerhetsanalysfrågor.
SKB R-98-54. Svensk Kärnbränslehantering AB.

OECD NEA, 1995. Future human actions at disposal sites. A report from the NEA Working Group on Assessment of Future Human Actions at Radioactive Waste Disposal Sites.
OECD/NEA, France.

Ritchey T, 1997. Scenario Development and Risk Management using Morphological Field Analysis. Proceedings of the 5th European Conference on Information Systems. Cork.

SKB, 1995. SR 95 – Template for safety reports with descriptive examples.
Svensk Kärnbränslehantering AB.

Wuschke D M, 1996. Assessment of the Long-Term Risks of Inadvertent Human Intrusion into a Proposed Canadian Nuclear Fuel Waste Disposal Vault in Deep Plutonic Rock – Revision 1. AECL-10279 Rev 1, COG-92-151 Rev 1.

Nebot J, Jordi B, 1991. The implications of soil acidification on a future HLW repository. Part I: The effects of increased weathering, erosion and deforestation.
SKB TR 91-45. Svensk Kärnbränslehantering AB.

Wersin P, Jordi B, Laaksoharju M, 1994. The implications of soil acidification on a future HLW repository. Part II: Influence on deep granitic groundwater. The Klipperås study site as test case.
SKB TR 94-31. Svensk Kärnbränslehantering AB.

13 Discussion and conclusions

The purpose of SR 97 is formulated in the introduction in four points:

1. SR 97 shall furnish supporting data to demonstrate the feasibility of finding a site in Swedish bedrock where the KBS-3 method for deep disposal of spent nuclear fuel meets the requirements on long-term safety and radiation protection that are defined in SSI's and SKI's regulations.
2. SR 97 shall demonstrate a methodology for safety assessment.
3. SR 97 shall furnish supporting data to specify the factors that serve as a basis for the selection of areas for site investigations and derive which parameters need to be determined and which other requirements ought to be made on a site investigation.
4. SR 97 shall furnish supporting data to derive preliminary functional requirements on the canister and the other barriers.

Each of the points is discussed in this chapter, followed by an account of how experience gained from SR 97 can be used to prioritize research efforts. The chapter is concluded with a few short words that put SR 97 in its context within SKB's siting programme.

13.1 Safety of KBS-3 method in Swedish bedrock

The point of departure of the safety assessment is the post-closure state of the repository system, and the assessment analyzes how the repository changes with time. Three fictitious repositories based on data from three actual sites are analyzed to shed light on various conditions in Swedish granitic bedrock. Long-term changes are analyzed by a classification into internal processes in the repository system and external forces exerted by the environment. Different conditions initially and in the surroundings yield a set of scenarios for which the evolution of the repository is analyzed quantitatively. An assessment of the results of the analysis embraces both qualitative and quantitative questions:

- Are all internal processes and external events of importance identified?
- What are the results of the different scenario analyses and what confidence can be attached to the results?
- How should the results of the scenario analyses be weighed together into a total risk assessment?
- How do different conditions in Swedish bedrock affect the feasibility of building a safe repository?

The first three questions emerge from the methodology for the safety assessment, the last concerns a specific purpose of SR 97.

13.1.1 Are all internal processes and external events of importance identified?

Identification of internal processes and external events of importance for the long-term evolution and safety of the repository has proceeded for several decades, in Sweden and in other countries. The work is documented in numerous reports and databases. SKB has its own database, which is constantly maintained and updated with international results. Very few new processes of importance have been identified in the past decade. The structure of the repository with multiple barriers with partially redundant functions also reduces its vulnerability to a possible unidentified process.

The choice of scenarios in SR 97 is an expert judgement, based on experience from previous assessments, available databases, etc. A comparison with safety assessments in other countries shows that the set of scenarios that is analyzed in SR 97 agrees very well with other assessments.

Confidence that all important points have been included must be judged on the basis of the efforts that have been made to achieve completeness and expert knowledge of the repository system and its natural surroundings.

SKB judges that the internal processes and the set of scenarios that are analyzed in SR 97 are sufficient to provide good confidence in the results of the safety assessment.

13.1.2 What are the results of the different scenario analyses and what confidence can be attached to the results?

The following scenarios are analyzed in SR 97:

- A base scenario where the repository is conceived to be built according to specifications, where no canisters have initial defects and where present-day conditions in the surroundings are assumed to persist.
- A canister defect scenario which differs from the base scenario in that a few canisters are assumed to have initial defects.
- A climate scenario that deals with future climate change.
- An earthquake scenario.
- A scenario that deals with future human actions that could conceivably affect the deep repository.

Base scenario

In the base scenario, the evolution of the repository's isolating function is analyzed under the assumption that the present-day climate persists. The overall conclusion is that the canister retains its isolating capacity, even in a million-year perspective. This means that no releases of radioactive substances occur from the repository. The long-term function of the buffer and the long-term stability of the bedrock are important questions in the base scenario. The consequences of all known thermal, hydraulic, mechanical and chemical processes of importance are analyzed for both. Model studies and pessimistic rough calculations show that the buffer can be expected to retain its function in a million-year perspective. In the same way, it is shown that the geosphere, and particularly the rock volume used for deposition, can be expected to remain stable over a very long time.

The evolution of the buffer and geosphere provide premises for quantifying the canister's thermal, hydraulic, mechanical and chemical environment. Based on this, canister isolation is projected to be retained for a very long time. The calculated safety margins against both mechanical and chemical stresses in the base scenario are large even in a million-year perspective.

The analysis assumes that the temperature on the canister surface does not exceed 100ºC and that the water at repository depth is oxygen-free. The former premise can always be ensured by a suitable deployment of deposition holes. Extensive sampling indicates oxygen-free conditions in the groundwater at depths greater than a hundred metres. The fact that oxygen-free conditions prevail at repository depth is as a rule ensured by biological processes in the soil layer in connection with groundwater recharge; furthermore, there is a very great potential for oxygen consumption in the minerals in the geosphere.

Our fundamental understanding of the processes involved and confidence in models and data are discussed systematically in the Process Report and in conjunction with the specific analyses in the base scenario. Process understanding and confidence can generally be said to be good. Most of the processes are well-known and have been studied by scientists for many decades. Models and data are sufficiently reliable for the often rough estimates that are required to set pessimistic bounds on the evolution in the base scenario.

The results of the base scenario are in part a consequence of the safety principles that have served as a basis for repository design. Copper is stable in the repository's oxygen-free environment. The buffer consists of a natural clay taken from a geological setting where it has been stable for millions of years. The Swedish bedrock has been stable for an even longer time.

Canister defect scenario

In the canister defect scenario, the course of events in an initially defective canister and the radionuclide migration in buffer, geosphere and biosphere that can result are analyzed.

The overall conclusion is that the repositories at Aberg, Beberg and Ceberg meet the acceptance criteria for a deep repository. The risk calculations are designed to ensure that the risk is not underestimated.

The risk calculations for the three sites are discussed in greater detail in section 13.1.4 below.

Confidence in data: Uncertainties in input data to calculations of radionuclide transport have been handled rigorously and as far as possible in a uniform manner for all data. The information on the uncertainties is used to formulate risk calculations, but also to evaluate the importance of different factors for the calculation results. The evaluation serves as a basis for an assessment of areas where further research could yield improved knowledge of value for the safety assessment:

- radionuclide turnover in the biosphere,
- fuel dissolution,
- hydraulic description on deposition hole scale.

Confidence in models: The quantification of radionuclide transport provides the risk measure that is directly compared with the Swedish Radiation Protection Institute's acceptance criteria. An evaluation of confidence in the models for radionuclide transport is therefore important.

The requirement on confidence in a model must be formulated in relation to the purpose of its use. For a safety assessment, it is above all important to demonstrate confidence that the models do not underestimate the consequences.

There are several different model concepts for groundwater flow, and three different concepts are compared in SR 97. The conclusion of the comparison is that the natural variability of input data to the models influences the result more than the choice of model.

Confidence in the models for radionuclide transport in canister, buffer and geosphere is judged to be adequate. Many fundamental processes such as diffusion and advection can be given reliable mathematical treatments in the models. The consequences of other processes, such as corrosion of cladding tubes, are simplified by means of pessimistic assumptions. Still others, such as surface diffusion, are handled in a simplified manner by means of pessimistic choices of data. The biosphere model contains rough pessimistic simplifications, especially for the peat ecosystem, which has the greatest consequences.

Climate scenario

The consequence of future climate change is analyzed in the climate scenario. A colder climate can be expected with high probability, but when the changes will occur and how great they will be are difficult to predict. The situation is handled in SR 97 by projecting a future climatic evolution whose main features are governed by astronomical events, but where the quantitative impact on the repository system during different periods is surrounded by greater uncertainties. The sketched evolution embraces a wide span of different climatic conditions. Even though the details of the changes will never be able to be foreseen, confidence is good that the analyzed conditions together cover possible climate changes in a hundred-thousand-year perspective.

The analysis is greatly simplified by the fact that large climate-related changes on the surface at the three repository sites only lead to limited changes at repository depth. This also justifies the format of the analysis of the consequences of climate change, namely as a comparison with repository conditions in the base scenario where the present-day climate is assumed to persist.

The overall conclusion of the climate scenario is that the climatic evolution does not lead to failure of intact canisters. Furthermore, the aggregate effect of the changes in the climate scenario on radionuclide transport processes is such that the consequences in the form of doses are expected to be less than in the canister defect scenario.

Isolation: The conclusion that the canister remains intact is essentially reached by setting bounds on the changes in temperature and rock stresses as well as in the composition, pressure and flow of the groundwater caused by the climate changes at repository depth. The groundwater pressure can be bounded by estimating the maximum ice thickness above the repository. As far as groundwater composition is concerned, there is reason to expect changes in salinity, while oxygen-containing water is not expected to infiltrate down to repository depth other than possibly during very limited periods. Changes in rock stresses can also be bounded based on the weight of the ice cover. The rock stresses do not cause deformations that damage the canisters.

Confidence that future changes in the repository system with regard to isolation will lie within the estimated bounds is good.

Retardation: Climate change also causes changes in transport conditions for radionuclides in buffer and above all geosphere. The changes in transport data almost always lie within the frame of the data used in the canister defect scenario.

Biosphere: The most important change lies in a sharp reduction of the consequences in the biosphere, since the repository sites are covered by ice or water during most of the period with a colder climate. The consequences of initially damaged canisters are thereby **less** than in the canister defect scenario.

Compared with the extreme consequences a northern European glaciation will have on living conditions for human beings, the effects of a deep repository on man and nature appear negligible.

Earthquake/tectonics scenario

A new method for analyzing the consequences of earthquakes with site-specific data on both the geosphere's fracture system and the frequencies and magnitudes of earthquakes is introduced in SR 97. The method represents the first step in the development of a future procedure for quantitative analysis of earthquake scenarios and contains several more highly pessimistic simplifications. Nevertheless, calculations with even this simplified model show that the probability of canister damages during the next 100,000 years is of the same order of magnitude as that assumed for initial canister damages, i.e. a fraction of a percent of the canisters is affected.

The pessimistic assumptions that are made in the risk analysis are judged with good margin to be able to compensate for the uncertainties that are associated with the prediction of future earthquakes. The risk of canister damages caused by earthquakes is therefore negligible.

Intrusion scenarios

The list of human actions that could influence the conditions on a repository site can be made long. Since the future development of human society is basically unpredictable, it can never be made complete. In view of each generation's right to choose how to act under different conditions and their obligation to assume full responsibility for their own actions, a practice has been established that the safety assessment should only deal with inadvertent future actions that can disturb the repository.

Possibilities for quantifying the risks that human beings will intrude into the repository in the future are greatly limited. Nor is it fully clarified how such risks should be taken into account in the total assessment of the acceptance for a deep repository.

In order to reduce the probability that human actions will inadvertently affect the safety of the repository, the site selection process takes account of the fact that different sites may have different potentials for alternative uses, e.g. for mining of ores or unusual minerals. Moreover, the depth of the repository is a way to avoid both natural disturbances on the surface and the effects of human activities.

The probability that inadvertent actions will disturb the repository can also be influenced by the length of the period of institutional controls at the repository site and by how knowledge of the repository can be preserved for the future. However, all analyses of

such factors spanning more than a few hundred years run into the difficulty of predicting how society will develop. A specific question concerns the risk of the collapse of society with resultant loss of knowledge and technical competencies.

The question of how possible effects of human actions are to be evaluated, and what responsibility we bear today for guarding against a collapse of society, is strongly influenced by ethical values. A fundamental principle is that safety is best ensured by keeping the radioactive waste contained in isolated and demarcated repositories.

How possible evolutions of society and future human actions that somehow affect the repository can be categorized and expressed as different scenarios is discussed in SR 97.

In an illustrative example, a situation is analyzed where a canister in the repository is inadvertently penetrated by rock drillers. Dose and risk are calculated for the drilling personnel and for a family that settles on the site at a later point in time. The drilling personnel may be exposed to the highest doses, but the risk to both drilling personnel and family are judged to be far below the acceptance criterion, 10^{-6}/year, since the probability of the analyzed events is estimated to be very small.

13.1.3 Weighing-together of scenario analyses

Total risk assessment

The total risk from a deep repository is a summation of the risks associated with all the different future evolutions a repository might undergo.

In a strictly executed risk calculation, the probability of each conceivable evolutionary pathway is estimated and multiplied by the calculated consequence. The sum of all such partial risks is the total risk, which is compared with the Swedish Radiation Protection Institute's acceptance criterion.

Such strict probability estimates cannot be done for a complex system such as a deep repository, whose evolution must be analyzed hundreds of thousands of years into the future. The customary method, which is the one applied in SR 97, is instead to collect a number of possible evolutionary pathways with common main features in a set of scenarios. The probability of each scenario can then be estimated or bounded upward.

With the scenario definitions that apply in SR 97, it would be reasonable to add the consequences of the canister defect and earthquake scenarios to those of the base scenario without weight factors. The canister defect and earthquake scenarios contain in themselves probability factors in the form of frequency of initial and earthquake-induced canister damages, respectively. Both of these factors have been excluded from the base scenario by definition.

In the climate scenario, the effects of initial canister damage are discussed, and to this scenario should also be added the probability of earthquake-induced damage.

The situation is complicated by the fact that it is not possible with present-day knowledge to determine what share of the earthquake statistics in the earthquake scenario is caused by residual effects of previous climate changes and what share has other causes. For this reason, all consequences of the earthquake scenario are added to both the base and climate scenarios.

The result is two "superscenarios" where different effects are added. One describes the course of events when today's climatic conditions persist, and includes both initial canister defects and earthquakes. The other describes what happens when the climate changes, with initial canister defects and earthquakes. The latter must be regarded as a much more probable alternative than the former, since climate change is highly probable.

In SR 97, consequences have only been calculated in the canister defect and climate scenarios. No radiological consequences arise in the base scenario. Nor is the earthquake scenario, where the analysis is preliminary, expected with refined analyses and/or suitable repository layout to have any consequences. The aggregate risk associated with the repository is thereby a weighing-together of the risks in the canister defect and climate scenarios. The risk in the canister defect scenario is calculated for most epochs to be much greater than the risk in the climate scenario, where the biosphere conditions often provide high dilution.

The aggregate risk associated with the repository is therefore estimated pessimistically in SR 97 to be equal to the calculated risk in the canister defect scenario.

According to the Swedish Radiation Protection Institute, consequences associated with intrusion scenarios can be assessed separately from other scenarios, and the intrusion scenarios have therefore not been included in the above line of reasoning.

General assessment of the safety of the KBS-3 method

An in-depth analysis and integrated accounting of the long-term safety of the KBS-3 method for deep geological disposal of spent nuclear fuel has been carried out in SR 97. The results confirm the previous picture that a well-designed repository located in rock with properties that do not differ essentially from normal Swedish rock has good prospects of meeting the regulatory authorities' safety requirements with ample margin.

The KBS-3 system has a flexibility as regards repository depth and layout which allows adaptation to site-specific conditions and to the information on rock conditions which is continuously collected during site investigations and repository excavation.

SKB believes that the repository design that is analyzed in SR 97 has achieved sufficient maturity, that our general understanding of the repository's long-term performance is sufficiently good, and that its potential for high safety has sufficient margins to constitute a satisfactory basis for carrying out site investigations.

13.1.4 How do different conditions in Swedish bedrock affect the feasibility of building a safe repository?

In SR 97, three sites are analyzed to shed light on different conditions in Swedish granitic bedrock as regards geology, groundwater flux, water chemistry, nearness to coast, northerly or southerly siting, surrounding biosphere, etc.

Much information can be obtained from the results of the various scenario analyses to illustrate the importance of varying conditions.

Long-term safety, isolation

Base scenario: The safety margins in the base scenario as far as isolation is concerned are very great for all sites. This applies to both mechanical and chemical stresses on the canister. Groundwater composition varies slightly between the sites, but the differences are unimportant as far as e.g. copper corrosion is concerned. Site-specific rockmechanical analyses have not been carried out; instead, the consequences of the mechanical evolution on the stability of the geosphere around the repository have been bounded by general and very pessimistic approximations.

Climate scenario: The uncertainties regarding the detailed climatic evolutions of the sites are great, but more definite statements can be made about differences between the sites. An important factor for isolation is above all the thickness of an ice cover during a glaciation. The thickest ice cover is expected at Ceberg, where the ice also remains the longest. This means that the mechanical stresses on the canister, as a result of both increased groundwater pressure and mechanical load on the bedrock, are greatest at Ceberg and smallest at Aberg. Changes in the groundwater composition in the climate scenario are not deemed to result in any site-specific differences of importance for isolation.

Earthquakes: As far as the probabilities of earthquake-induced canister damages are concerned, calculations give values that are small and equivalent at the three sites. The calculations in SR 97 have been carried out with pessimistic assumptions that greatly influence the result. It is therefore difficult to draw any conclusions about the relatively suitability of the sites as regards earthquakes. Furthermore, the earthquake risk can be reduced by utilizing a larger part of the rock for the repository. Any difference in terms of earthquake risks would thereby have economic rather than safety-related consequences. Differences between the sites stem from differences in the local fracture structure in combination with the chosen repository placement, as well as from differences in regional earthquake statistics. The earthquake statistics represent one of the greatest uncertainties in the analysis of earthquakes.

Summary, isolation: Conditions at all three sites offer very great safety margins for the repository's isolating capacity in the base scenario.

The evolution in the climate scenario as well is judged to lead to a retention of isolation at all analyzed sites. The safety margin to mechanical canister failure is deemed to be smallest at Ceberg and greatest at Aberg.

A preliminary assessment is that a safe repository in terms of earthquakes can be built at the three sites with optimized site-specific repository layouts. It is not possible today to make any comparisons between the sites in this respect.

Long-term safety, release consequences

Canister defect scenario: The calculations in the canister defect scenario (present-day climatic conditions) show that the Swedish Radiation Protection Institute's acceptance criterion for a deep repository is satisfied with ample margin on all sites. The margin is smallest for Aberg and greatest for Ceberg. The difference pertains above all to the time after 100,000 years. The risk calculations have many pessimistic assumptions to ensure the risk is not underestimated.

If the release takes place to a well, the risk at Aberg is less than one hundredth of the acceptance criterion if the calculation is performed for a timespan of one million years. The risk at Beberg is approximately one-fifth, and at Ceberg one-tenth, of the risk at Aberg.

In the case of release to a peat ecosystem, the sites differ in roughly the same way for times up to around 100,000 years. For a million years, the risk at Aberg then increases by approximately a factor of 40, at Beberg by a factor of 10 and at Ceberg only marginally. The natural radionuclide Ra-226 dominates the consequences for the peat ecosystem for times over 100,000 years.

The calculated retention capacity is equivalent at the three sites for long-lived, non-sorbing nuclides. Retention for sorbing nuclides is strongest at Ceberg and weakest at Aberg.

The differences are primarily due to different hydraulic permeabilities. The rock mass in Aberg and Beberg is, for example, approximately 100 times more permeable than that in Ceberg, with reservation for the fact that the investigation methodology differs between the sites.

Climate scenario: The big difference between the canister defect scenario and the climate scenario as regards the consequences of radionuclide releases lies in the altered and more favourable biosphere conditions. All repository sites are expected to be covered by ice or sea for much of the coming hundred thousand years. Biosphere conditions are deemed to be most favourable at Aberg, which is expected to be sea-covered during most of the period. Ceberg is most positively affected by the climate changes, but here as well the consequences of a radionuclide release will be much less than in the canister defect scenario.

Earthquakes: The evaluation of the analysis of the earthquake scenario indicates that the probability of earthquake-induced canister damages is very small. The release consequences for this scenario are therefore not analyzed.

Summary, release consequences: From this aspect as well, it is deemed possible to build a repository with large safety margins at all sites. The poorer retention at Aberg is compensated for by the more favourable biosphere evolution on the site. It is not meaningful to rank the sites with regard to the consequences of radionuclide release.

Thermal conditions

Thermal conditions differ slightly between the sites as regards temperature at repository depth and thermal conductivity of the rock. The site-specific thermal conditions, together with the fracture structure, determine how large a portion of the host rock must be exploited to accommodate a given quantity of fuel. The governing criterion is that the temperature on the surface of the copper canister may not exceed 100ºC.

The thermal conditions at Aberg, in combination with a relatively limited study site, have led to the proposal of a two-level repository layout, while a single-level repository is proposed in Beberg and Ceberg.

The differences in thermal conditions are primarily of economic importance, since the thermal criterion can always be met if a sufficiently large rock volume is used.

Conclusions

In summary, it is judged that a safe deep repository for spent nuclear fuel in accordance with the KBS-3 method can be built on a site where the conditions resemble those at either Aberg, Beberg or Ceberg.

The safety margins are calculated to be large on all sites. SR 97 has not revealed any differences in long-term safety between the three sites that have any crucial bearing on a weighing-together of all the factors that influence the siting of a deep repository. Such factors include e.g. technology, economics aspects, land use, environmental impact and societal consequences.

13.2 Methodology for safety assessment

According to the methodology description in Chapter 4, the assessment can be said to consist of five tasks:

- system description,
- description of initial state,
- choice of scenarios,
- analysis of scenarios,
- evaluation.

Several new approaches have been tried in the methodology in SR 97. The methodology for the four first tasks, as well as handling of uncertainties, is discussed below.

13.2.1 System description

The system description provides a structure for describing the state of the repository system in time and space and the processes that can change this state over time. SR 97 introduces the THMC structure for the system description.

The format for the description provides a more accurate picture of the processes that govern the evolution of the system than previous descriptions using interaction matrices.

Another important advantage is that the same format can be used in the subsequent scenario analyses where the evolution of the system is described in terms of partially coupled thermal, hydraulic, mechanical and chemical evolutions. With previous descriptions it has been difficult to show how the information in the system description has been transferred to the scenario analyses.

The methodology in SR 97 is process-oriented, which is underscored by the fact that the Process Report constitutes a cornerstone in the system description and thereby also in the basis for the subsequent analyses. In the Process Report, all processes are described according to the same format. Experience from the first version of the Process Report used in SR 97 is good. The approach has necessitated a clearer presentation of the knowledge base and permitted a quantification of different processes. The Process Report will need to be revised before each future assessment.

A number of variables that indicate the state of the repository system with time are also established in the system description. This provides a structure for describing the initial state of the system, which is the point of departure of the analysis. Uncertainties in the initial state can thereby be studied systematically and contribute to the basis for scenario selection.

The classification of variables should also be able to be used to provide a stricter description of the evolution of the repository system in future safety assessments.

The work of identifying internal processes and external conditions of importance to repository evolution also belongs to the system description. Conclusions pertaining to this are found in section 13.1.1 above.

13.2.2 Choice of scenarios

The choice of scenarios in SR 97 is an expert assessment based on previous experience, the content of available databases, choice of scenarios in the safety assessments of sister organizations, etc. The choice needs to be revised for future assessments, but this is not expected to lead to any essential changes in the set of scenarios. A clearer coupling between system description, choice of scenarios and information databases should also be made. The choice of scenarios will necessarily involve some expert judgements in future safety assessments as well.

The point of reference in SR 97 is a base scenario where present-day conditions in the surroundings are postulated to persist, despite the fact that climate change is most likely to be expected, at least in a ten-thousand-year perspective. The reason for this choice of base scenario is above all to make a clear distinction between changes caused by internal processes in the repository and those caused by interaction with a changing environment. Furthermore, the Swedish Radiation Protection Institute's regulations expressly require that a case where today's conditions persist be analyzed. The choice of base scenario in SR 97 will also be commented on under the next heading.

The basis for the assessment of probabilities that different scenarios will be realized is weak. Rough, pessimistic estimates similar to those in section 13.1.3 are deemed to be necessary in future assessments as well.

13.2.3 Analysis of chosen scenarios

The frames for the scenario assessments in SR 97 are given by the initial state and the conditions in the surroundings that are defined in each scenario. Based on these premises, the evolution of the repository as a consequence of the internal processes and interaction with the surrounding environment is analyzed. The THMC format has made it possible to show how the complex system of processes can be broken down into a thermal, a hydraulic, a mechanical and a chemical evolution with some essential couplings between them. The format of the system description also makes it possible to show how processes are systematically handled in the analyses.

The point of departure for the scenario analyses is a base scenario. The course of events in other scenarios is then compared with that in the base scenario. This method has been valuable, particularly in the analysis of the canister defect and climate scenarios. Effects and uncertainties caused by internal processes can be distinguished from those caused by external changes. This method is also natural, since the repository system is designed to be robust: Repository performance should not be seriously affected by the changes that can be expected in the surroundings.

The scenario analyses are largely done by means of model calculations. SKB has access to a large set of modelling tools for, among other things, thermal calculations, calculations of groundwater flow, chemical evolution in groundwater and buffer, and radionuclide migration in the near field, geosphere and biosphere. The models are refined continuously as needed. Probabilistic calculations have been utilized in several ways for the analyses in SR 97.

13.2.4 Handling of uncertainties

How qualitative and quantitative uncertainties are handled is an important question that concerns all aspects of a safety assessment. Table 4-1 in section 4.6 shows how uncertainties are handled in SR 97.

Completeness

The question of completeness in process identification and choice of scenarios is commented on in section 13.1.1.

Conceptual uncertainty; process understanding and model uncertainty

What is often termed conceptual uncertainty, with varying implications in different contexts, has in SR 97 been divided into the concepts "fundamental process understanding" and "model uncertainty". The former refers to the scientific understanding of a process, the latter to uncertainties that enter when a process is analyzed with a mathematical model in a safety assessment.

Uncertainties surrounding the fundamental understanding of different processes are discussed in the Process Report. The standard format for the process descriptions has been valuable for the accounting of uncertainties, and the descriptions can be further refined in coming versions of the Process Report.

Model uncertainties are discussed where modellings occur in the scenario analyses. This can also generally be carried out more systematically for future assessments. The handling of uncertainties is more sophisticated for the important models used for quantification of radionuclide transport. Three different conceptual models for groundwater flow are used with the important result that the differences in the predictions are small compared with, above all, the natural variability in the bedrock. Confidence in the models for groundwater flow and for radionuclide transport in the near field and geosphere is discussed in greater detail. Confidence that the models do not underestimate the consequences is deemed to be good.

Input data

Uncertainties in input data are discussed in connection with modellings. Here as well, the methodology is most refined for data for radionuclide transport calculations. All these data are compiled in a separate Data Report. The method of choosing reasonable and pessimistic values for all data and then using them in both probabilistic and non-probabilistic analyses has worked well. Among other things, it has been possible to study the influence of different parameters on the repository's retarding function systematically. The method for probabilistic calculations shows a practicable way for carrying out probabilistic analyses where statistical data are lacking. The method is new and needs to be evaluated for use in future assessments.

Summary

The methods that have been tested for the handling of uncertainties in SR 97 have proved to be practical in actual use. The application of the method can be refined in future assessments. The new methods that have been introduced for accounting and handling of data uncertainties for the quantification of radionuclide transport are judged to be able to serve as a basis for future safety reports as well.

13.2.5 Assessment of available methodology

SKB finds, with the support of the above account, that the methodology used in SR 97 constitutes a sufficient basis for future safety assessments based on data from site investigations.

13.3 Basis for site selection and site investigations

SR 97 constitutes an important basis for the ongoing work aimed at formulating and quantifying requirements and preferences regarding the host-rock from the perspective of long-term repository safety. Experience from SR 97 is also used in the work of formulating an integrated programme for investigation and evaluation of sites.

13.3.1 What requirements does the deep repository make on the host-rock?

SKB has pursued the work of formulating and quantifying requirements and preferences regarding the rock in parallel with SR 97. The results will be reported in 2000, and a progress report was made in conjunction with the publication of RD&D-Programme 98. The project identifies so-called geoscientific suitability indicators based on an analysis of what requirements and preferences can be formulated regarding conditions in the rock and properties of the rock. The requirements can be made both with a view towards long-term safety and so that it will be technically possible to build the repository. The judgements of what is essential from the viewpoint of long-term safety are based on previous knowledge and experience and on the analyses that have been carried out within the framework of SR 97.

A first step in the work involved determining what geoscientific information is used in safety assessment and construction analysis. Such an inventory was reported in 1996 and has now been checked against the more comprehensive analysis that was done in SR 97. In a safety assessment, it is primarily the information on the initial state that must be taken from site-specific investigations.

Since the integrated performance of the deep repository in different time periods is dependent on a large number of interacting processes, it is difficult to specify more detailed requirements on individual initial conditions. On the other hand, there is a need for a structure for the siting work and guidance as to what is essential to measure in a site investigation. For this reason, all the site-specific properties of a host rock have been reviewed and the question has been asked for each one as to whether there are value ranges that would seriously degrade any of the deep repository's isolating or retarding functions.

If it becomes apparent that there are value ranges where the deep repository's isolation may be seriously threatened, the requirement is made that these parameter values may *not* occur. This knowledge is obtained above all from the analysis of the base scenario. Conditions that could threaten e.g. canister integrity, for example the presence of dissolved oxygen, are not accepted and thereby become the subject of requirement formulations. The requirements are not absolute in the sense that the deep repository would definitely be unsafe if the requirements were not met, but are nevertheless made as a precaution. The requirements can only be reconsidered in the light of new knowledge or after a change in the repository's design.

Even if it is not possible to find grounds for requirements, it is often possible to formulate firm preferences regarding value ranges that contribute to good isolation or good retardation. The preferences stipulate value ranges that are conducive to the desired function, but do not have to specify the limit to unacceptable function. Such a limit is influenced in many cases by other conditions, is relative, is unknown or can be influenced by repository layout.

Formulation of preferences has been based on the value ranges analyzed in SR 97, along with consideration of whether other value ranges might lead to better function. The knowledge is taken from the detailed analyses of especially the base scenario and the canister scenario. In a similar manner, preferences regarding the rock are formulated from the perspective of constructability/technology.

The requirements and preferences have been formulated to provide guidance in the siting work and to permit selection of investigation methods used in site investigations. They do not take the place of integrated and comprehensive safety assessments.

13.3.2 Programme for site investigations

The identification of geoscientific suitability indicators is in turn one of the most important points of departure for SKB's programme for investigation and evaluation of sites, which will be presented in 2000. The investigation will provide a basis for judging value ranges for essential geoscientific factors on candidate sites. Criteria for site evaluation are also used to prioritize the scope of the investigations and permit more rapid feedback to the safety assessment when investigation results become available. The biosphere on the site is also surveyed.

The site investigation programme includes more than the information sought by the safety assessment, however. The investigations are supposed to provide a basis for a general geoscientific understanding, and many investigations do not in themselves furnish direct data for analyses, but are used when data are to be interpreted. These questions are also dealt with and discussed when the site investigation programme is formulated.

13.4 Basis for functional requirements

According to SKI's requirements on SR 97, the safety assessment should also serve as a basis for "deriving preliminary functional requirements on the canister and the other barriers."

The safety assessment can do this in a general sense. In analyzing the different scenarios, it describes what external stresses the repository system may be exposed to. The repository must be designed to function under these stresses, which is a very general formulation of functional requirements. The requirement applies to the system as a whole. It is only possible in certain cases to directly derive requirements for individual barriers from conditions in the surroundings. An example where this is possible:

The canister has to withstand the hydrostatic pressures and swelling pressure that occur in the base scenario, as well as the maximum hydrostatic pressures that can result from a glaciation. Both of these pressures are quantified in SR 97. The assessment thereby provides a basis for formulating functional requirements on the canister, which must retain its isolating function at these pressures.

It is more difficult to formulate functional requirements for tectonic changes. The effect of an earthquake can be controlled via the repository layout, and even if the layout has been established the effects of an earthquake are dependent on the design of the canister-buffer combination. The mechanical effects on the canister are determined by e.g. buffer thickness, and it is the combination of the two barriers that determine their performance.

Functional requirements for the buffer can be derived from the groundwater composition in the different scenarios: The buffer should retain its intended function when the groundwater has the compositions that may be encountered on the repository site during different time periods in both the base and canister defect scenarios. SR 97 provides a quantitative basis for this in the form of estimates of the different groundwater compositions that may be encountered in Swedish bedrock.

Functional requirements for the canister are not as simple to derive from the groundwater composition: Buffer and canister together determine how well the canister's isolating function withstands the chemical stresses. Functional requirements for the canister cannot be derived directly from the results of the assessment; however, the function of the canister-buffer system must be such that canister isolation is not jeopardized in a long time perspective.

The safety assessment quantifies the conditions in the surroundings and then talks about whether the chosen system design works under these conditions. However, the analysis methodology is not in general aimed at analyzing which detailed properties the barriers must possess in order to "withstand" the stresses. This inverse problem does not even have a straightforward solution.

SR 97 thus furnishes quantitative material in the form of groundwater compositions, flows and pressures, rock movements and other data that can be used as a basis for modifying the repository design if necessary, but it is only in a few cases that functional requirements can be derived directly from the analysis results.

Review of repository design

The design of the deep repository is based on the primary requirement that the repository should isolate the waste from man and the environment. If this isolation should for some reason be breached, the repository should have a secondary retarding function. Based on these fundamental functional requirements, more detailed functional requirements are established for the canister and the other barriers. Aside from the requirements on long-term safety, there are requirements aimed at facilitating fabrication, construction and operation.

The detailed repository design will be refined gradually in a long-term process, and in the meantime a number of safety assessments will be carried out. The results from each assessment will be fed back to the repository design work and may lead to modifications of functional requirements, design premises and the design/layout of different parts. Changes in design details are also initiated by experience from the development of technology for the execution of the different parts of the repository. The modified design will then serve as the point of departure for the next safety assessment.

The result of the work with SR 97 will be used as a basis for a review of the functional requirements and design premises that determine the design of the canister and the other barriers in the deep repository.

13.5 Prioritization of research

The experience gained in SR 97 also serves as a basis for refining the methodology for future safety assessments, as well as for setting priorities in the programmes of supportive research, development and technology demonstration.

Methodology for safety assessment

The programme for refinement of safety assessment methodology in RD&D-98 will be evaluated in the light of the experience from SR 97 and its review. Needs for future safety assessments that have been identified in SR 97 include:

- a revised Process Report,
- a study of the possibilities of a more systematic choice of scenarios, and
- an evaluation of probabilistic calculation methods.

Supportive research

The results of SR 97 can be used in the programme for supportive research to set priorities for R&D work on deep disposal of spent nuclear fuel. Besides annual programme reviews, a more far-reaching audit will be carried out in connection with RD&D-Programme 2001. The results of SR 97 indicate several areas that may need to be prioritized, for example:

- biosphere modelling,
- earthquake modelling,
- long-term effects of creep movements in the rock,
- the mechanical effects of tectonic rock movements on the canister, e.g. creep effects in the copper shell,
- general function of the backfill,
- erosion of buffer and backfill under different climatic conditions,
- the early hydromechanical evolution of the canister-buffer gap,
- models for hydrology and radionuclide transport on a detailed scale around deposition holes to permit optimal choices of deposition holes,
- fuel dissolution.

The needs have been identified either directly in the Process Report or when the integrated evolution resulting from several coupled processes has been studied in the safety assessment. New findings would often lead to less pessimistic treatments in the safety assessment.

Quality control

Quality control is essential in order to ensure the reliability of the assessments. Quality requirements can be made on data, models and evaluations. Traceability and the ability to reproduce results are other important aspects. A quality-controlled system for data collection and data preservation has been tested at the Äspö HRL. A version management system has been utilized for models of groundwater flow and radionuclide transport in SR 97. Premises, input data and results are archived for these calculations either digitally, with the customary security routines, or as hard copies in accordance with SKB's archive rules.

The procedures for quality control of the safety assessment need to be refined. SKB intends to have the company certified with a complete QA system in accordance with ISO 9001 when the site investigations begin. The safety assessment is covered by the certification.

13.6 Closing words

The next stage in the siting of a deep repository entails investigation of the bedrock at a number of candidate sites for a repository. The main purpose of SR 97 is, in preparation for this next stage, "to demonstrate that the KBS-3 method has good prospects of being able to meet the safety and radiation protection requirements which SKI and SSI have specified in recent years."

The radiation levels which Swedish authorities accept for individuals in the vicinity of a deep repository lie around one percent of the natural background radiation. The results of the analyses in SR 97 show maximum levels that are less than one-tenth of the official limits. The maximum levels will occur tens of thousands of years in the future and during the relatively short time intervals when candidate repository sites in Sweden are not expected to be covered by ice sheets or sea.

The results should be regarded in the light of the cautious attitude that permeates the execution of the safety assessment. Wherever knowledge in a field is not complete, a poorer outcome than is reasonable to expect is pessimistically assumed.

SR 97 shows that the prospects for building a safety deep repository for spent nuclear fuel in Swedish granitic bedrock are very good. The assessment is comprehensive and detailed by international standards when considered in the light of the next stage SKB is facing.

It is SKB's judgement that the scope of the safety assessment and confidence in its results satisfy the requirements that should be made in preparation for such a stage.

Reference Fuel

Table 1-1. Data for the reference fuel type, SVEA 96.

Area	Description	Unit	Value
	Fuel Type		SVEA 96
General Data	Fabricate		ABB ATOM
	Licensing date CLAB		1989-07-07
	Licensing date Transport Container		1989-07-07
	Reference Document 1		G6264.8
	Reference Document 2		C-264.13
	General Drawing – Assembly		AA273730
	General Drawing– Box		AA273791
	General Drawing		AA273728
	Overall Assembly Length – Without Fuel Box	mm	4042.1
	Overall Assembly Length – With Fuel Box	mm	4422.00
	Assembly Mass (Without Fuel Box)	kg	243.20
	Assembly Displacement Volume	m^3	0.03
	End Zone Bottom Length	mm	56
	End Zone Top Length	mm	273.5
	Overall Assembly Cross Section Min	mm	140.20
	Overall Assembly Cross Section Max	mm	153.00
	UO2 Mass	kg	195
	Uranium Mass	kg	171
	Initial Enrichment (Pellet Enrichment – Maximum)	%U235	
	Initial Average Enrichment (in Section with Highest Reactivity)	%U235	3.461
	Initial Uranium Enrichment (Average in Assembly)	%U235	3.27
	BA Type		Gd203
	Content of BA	%	4
	Active Fuel Length	mm	3710
	Irradiation Length Increase	mm	15
	Design Burnup	MWd/tU	43000
Assembly	Rod Array		4*(5*5)
	No of Sub-assemblies		4
	Weight of Sub-assembly	kg	60.8
	Rod Pitch – Minimum	mm	12.7
	Rod Pitch – Maximum	mm	
Rods	Number of Rods – Total		96
	Number of Fuel Rods		96
	Normal Fuel Rod Length		
	Supporting Fuel Rod Length	mm	4041
	Spacer Rod Length	mm	4004.5
	Number of Part Length Rods		
	Length of Part Length Rod	mm	
	Weight (UO2) BA Fuel Rod	kg	2
	Weight (UO2) of Fuel Rod	kg	2.03
	Rod Outside Diameter Min	mm	9.66
	Rod Outside Diameter Max	mm	9.58
	Zr Weight Supporting Rod	kg	0.49
	Zr Weight – Normal Rod	kg	0.47
	Zr Weight – Spacer Rod	kg	0.48
Pellet	UO2 Density Max	g/cc	10.62
	UO2 Density Min	g/cc	10.42
	UO2 Density BA-pellet	g/cc	10.52
	UO2 Pellet Diameter Max	mm	8.203
	UO2 Pellet Diameter Min	mm	8.177

Area	Description	Unit	Value
	Fuel Type		SVEA 96
Cladding	Clad Material/Liner		Zr2
	Clad Thickness Max	mm	0.63
	Clad Thickness Min	mm	0.58
Filling Gas	Initial Filling Gas		He
	Initial Filling Gas Pressure (abs.)	MPa	0.4
	End of Life Gas Pressure	MPa	
Water Channel	Channel Material		
Water	Water Channel Clad Thickness	mm	
	Water Channel Size Max	mm	
	Water Channel Size Min	mm	
Water Rod	No of Water Rods		
	Water Rod Cladding Thickness	mm	
	Water Rod Material		
	Water Rod Outside Diam	mm	
Water Cross	Water Cross Thickness Max	mm	0.8
	Water Cross Thickness Min	mm	
Box	Box Material		Zr2
	Weight of Box	kg	27
	Box Inner Measures	mm	137.4
	Box Wall Thickness	mm	1.1
	Box Bottom Piece Material		SS2352
	Box Zr Weight	kg	27
Handle	Handle Material		SS2352
	Handle Weight	kg	2.4
Top Plate	Top Plate Material		SS2352
	Top Plate Weight		0.13
Spacers	Number of Spacers in Active Zone		7
	Drawing (Spacers)		
	Axial partition of Spacers		568
	Spacer Thickness	mm	
	Spacer Type 1, Material 1		AMS5542
	Weight of the Above Material	kg	0.23
	Spacer Type 1, Material 2		
	Weight of the Above Material	kg	
	Spacer Type 1, Material 3		
	Weight of the Above Material	kg	
	Spacer Type 2, Material 1		
	Weight of the Above Material	kg	
	Spacer Type 2, Material 2		
	Weight of the Above Material	kg	
	Spacer Type 2, Material 3		
	Weight of the Above Material	kg	
	Spacer Type 3, Material 1		
	Weight of the Above Material	kg	
	Spacer Type 3, Material 2		
	Weight of the Above Material	kg	
	Spacer Type 3, Material 3		
	Weight of the Above Material	kg	
Bottom Plate	Bottom Plate Material		SS2352
	Bottom Plate Weight	kg	0.4

Data for radionuclide transport calculations

Contents

1.1 Inventory

Table 2-1. Inventory (Bq/tU) based on BWR element with a burn-up of 38 MWd/kg U and 40 years after discharge from reactor /based on table 9 in Håkansson, 1998/.

Nuclide	Activity (Bq/t U)	Nuclide	Activity (Bq/t U)	Nuclide	Activity (Bq/t U)
Fission products		**Actinides**		**Activation elements**	
H-3	$2.1 \cdot 10^{12}$	Ra-226	$1.4 \cdot 10^{5}$	H-3	$1.1 \cdot 10^{12}$
Se-79	$2.8 \cdot 10^{9}$	Th-229	$1.0 \cdot 10^{4}$	C-14	$5.0 \cdot 10^{10}$
Kr-85	$2.7 \cdot 10^{13}$	Th-230	$1.6 \cdot 10^{7}$	Cl-36	$5.5 \cdot 10^{8}$
Sr-90	$1.2 \cdot 10^{15}$	Th-234	$1.2 \cdot 10^{10}$	Fe-55	$9.3 \cdot 10^{9}$
Y-90	$1.2 \cdot 10^{15}$	Pa-231	$1.8 \cdot 10^{6}$	Co-60	$8.9 \cdot 10^{11}$
Zr-93	$5.0 \cdot 10^{10}$	Pa-233	$1.5 \cdot 10^{10}$	Ni-59	$8.8 \cdot 10^{10}$
Nb-93m	$4.2 \cdot 10^{10}$	Pa-234m	$1.2 \cdot 10^{10}$	Ni-63	$9.3 \cdot 10^{12}$
Tc-99	$5.7 \cdot 10^{11}$	U-233	$3.1 \cdot 10^{6}$	Sr-90	$2.6 \cdot 10^{7}$
Ru-106	$2.7 \cdot 10^{4}$	U-234	$4.6 \cdot 10^{10}$	Y-90	$2.6 \cdot 10^{7}$
Pd-107	$4.9 \cdot 10^{9}$	U-235	$4.5 \cdot 10^{8}$	Zr-93	$5.6 \cdot 10^{9}$
Cd-113m	$1.7 \cdot 10^{11}$	U-236	$1.0 \cdot 10^{10}$	Nb-93m	$2.3 \cdot 10^{10}$
Sn-121	$4.4 \cdot 10^{10}$	U-237	$1.9 \cdot 10^{10}$	Nb-94	$2.9 \cdot 10^{9}$
Sn-121m	$5.7 \cdot 10^{10}$	U-238	$1.2 \cdot 10^{10}$	Mo-93	$4.4 \cdot 10^{7}$
Sb-125	$1.1 \cdot 10^{10}$	Np-237	$1.5 \cdot 10^{10}$	Ag-108	$4.3 \cdot 10^{7}$
Te-125m	$2.7 \cdot 10^{9}$	Np-239	$1.2 \cdot 10^{12}$	Ag-108m	$5.0 \cdot 10^{8}$
Sn-126	$2.3 \cdot 10^{10}$	Pu-238	$9.5 \cdot 10^{13}$	Cd-113m	$3.4 \cdot 10^{10}$
Sb-126m	$2.3 \cdot 10^{10}$	Pu-239	$9.5 \cdot 10^{12}$	Sn-121	$1.4 \cdot 10^{10}$
I-129	$1.3 \cdot 10^{9}$	Pu-240	$1.2 \cdot 10^{13}$	Sn-121m	$1.7 \cdot 10^{10}$
Cs-134	$9.1 \cdot 10^{9}$	Pu-241	$7.7 \cdot 10^{14}$	Sb-125	$1.2 \cdot 10^{9}$
Cs-135	$2.1 \cdot 10^{10}$	Pu-242	$1.0 \cdot 10^{11}$	Te-125m	$3.0 \cdot 10^{8}$
Cs-137	$1.8 \cdot 10^{15}$	Am-241	$1.5 \cdot 10^{14}$	Eu-154	$3.2 \cdot 10^{11}$
Ba-137m	$1.7 \cdot 10^{15}$	Am-242m	$4.5 \cdot 10^{11}$	Eu-155	$1.3 \cdot 10^{10}$
Pm-146	$9.8 \cdot 10^{8}$	Am-242	$4.5 \cdot 10^{11}$	Ho-166m	$7.5 \cdot 10^{7}$
Pm-147	$1.5 \cdot 10^{11}$	Am-243	$1.2 \cdot 10^{12}$	**Total**	$1.2 \cdot 10^{13}$
Sm-151	$9.4 \cdot 10^{12}$	Cm-242	$3.7 \cdot 10^{11}$		
Eu1-52	$3.3 \cdot 10^{10}$	Cm-243	$4.4 \cdot 10^{11}$		
Eu-154	$1.8 \cdot 10^{13}$	Cm-244	$2.8 \cdot 10^{13}$		
Eu-155	$7.6 \cdot 10^{11}$	Cm245	$9.4 \cdot 10^{9}$		
Total	$6.0 \cdot 10^{15}$	Cm-246	$2.9 \cdot 10^{9}$		
		Total	$1.1 \cdot 10^{15}$		

1.2 Fuel dissolution

Table 2-2. Fuel dissolution.

Case	Description
Reasonable	Constant dissolution rate 10^{-8} $year^{-1}$

Table 2-3. Fraction of inventory assumed instantly released upon water contact (IRF) /based on table 3 in Johnson and Tait, 1997, and complemented with assumptions concerning the metal parts/.

Nuclide	IRF (%) Reasonable, fuel only	IRF (%) Reasonable, including metal parts	IRF (%) Pessimistic, including metal parts
C-14	5	15	55
Cl-36	6	6	12
Co-60	–	–	–
Ni-59	–	100	100
Ni-63	–	100	100
Se-79	3	3	6
Kr-85	2	2	4
Sr-90	0.25	0.25	1
Zr-93	–	–	–
Nb-94	–	100	100
Tc-99	0.2	0.2	1
Pd-107	0.2	0.2	1
Ag-108m	3	100	100
Cd-113m	3	3	6
Sn-126	2	2	4
I-129	3	3	6
Cs-135	3	3	6
Cs-137	3	3	6
Sm-151	–	–	–
Eu-154	–	–	–
Ho-166m	–	–	–
actinides	–	–	–

1.3 Canister defects, defect growth and delay time

Table 2-4. Canister defects, defect growth and delay time (see the Data Report).

Case	Initial defect	Growth	Delay time
Reasonable	1 canister with 1 mm^2 circular defect	Complete failure, i.e. a failure large enough (1 dm^2) not to offer any migration resistance after $2 \cdot 10^5$ years	$2 \cdot 10^5$ years
Pessimistic	5 canisters with 1 mm^2 (1 µm thin and 1 m long) defect	Complete failure, i.e. a failure large enough not to offer any migration resistance, after $2 \cdot 10^4$ years	300 years

1.4 Solubilities

Table 2-5. Solubility limiting phases, speciations and solubilities for the three sites in SR 97.

Element	Solubility-limiting phase	Dominant species	Aberg Reasonable (mol/l)	Beberg Reasonable (mol/l)	Ceberg Reasonable (mol/l)	All sites Pessimistic (mol/l)
Ag	AgCl	$AgCl_x^{y-}$	$2.96 \cdot 10^{-5}$	$9.39 \cdot 10^{-7}$	$7.12 \cdot 10^{-7}$	$3 \cdot 10^{-5}$
Am	$AmOHCO_3$	$Am(OH)_2^+$, $AmCO_2^+$, $AmOH^{2+}$	$6.87 \cdot 10^{-7}$	$9.36 \cdot 10^{-8}$	$9.34 \cdot 10^{-8}$	$7 \cdot 10^{-6}$
Cm	$CmOHCO_3$	$CmOH^{2+}$	$2.22 \cdot 10^{-7}$	$2.02 \cdot 10^{-9}$	$9.01 \cdot 10^{-10}$	$2 \cdot 10^{-6}$
Ho	$Ho_2 (CO_3)_2$	$HoCO_3^+$, $Ho(CO_3)_2^-$	$6.27 \cdot 10^{-6}$	$5.58 \cdot 10^{-6}$	$5.58 \cdot 10^{-6}$	$6 \cdot 10^{-5}$
Nb	Nb_2O_5	NbO_3^-	$1.37 \cdot 10^{-3}$	$1.37 \cdot 10^{-3}$	$1.39 \cdot 10^{-3}$	$4 \cdot 10^{-2}$
Ni	NiO	Ni^{2+}, $NiCO_3$,	high	high	high	high
Np	$Np(OH)_4$	$Np(OH)_4$, $Np(OH)_3CO_3^-$ $Np(HPO_4)_4^{6-}$	$5.87 \cdot 10^{-8}$	$1.05 \cdot 10^{-7}$	$5.87 \cdot 10^{-8}$	$2 \cdot 10^{-7}$
Pa	$Pa_2 O_5$	PaO_2OH	$3.16 \cdot 10^{-7}$	$3.16 \cdot 10^{-7}$	$3.16 \cdot 10^{-7}$	$4 \cdot 10^{-7}$
Pd	PdO	$Pd(OH)_2$	$4.21 \cdot 10^{-9}$	$4.17 \cdot 10^{-9}$	$4.18 \cdot 10^{-9}$	$8 \cdot 10^{-9}$
Pu	$Pu(OH)_4$	$Pu(OH)_4$, $PuCO_3^+$, Pu^{3+}	$6.56 \cdot 10^{-9}$	$5.35 \cdot 10^{-10}$	$1.38 \cdot 10^{-10}$	$3 \cdot 10^{-6}$
Ra	$RaSO_4$	Ra^{2+}, $RaSO_4$	$2.86 \cdot 10^{-7}$	$5.02 \cdot 10^{-7}$	$1.20 \cdot 10^{-4}$	$2 \cdot 10^{-4}$
Se	$FeSe_{(2)}$/ Selenium	HSe^-	$2.59 \cdot 10^{-9}$	$2.59 \cdot 10^{-9}$	$2.59 \cdot 10^{-9}$	high
Sm	$Sm_2 (CO_3)_2$	$SmCO_3^+$, $Sm(CO_3)_2^-$	$2.13 \cdot 10^{-6}$	$8.03 \cdot 10^{-7}$	$8.03 \cdot 10^{-7}$	$2 \cdot 10^{-5}$
Sn	SnO_2	$Sn(OH)_4$, $Sn(OH)_5^-$	$5.52 \cdot 10^{-10}$	$6.03 \cdot 10^{-10}$	$4.68 \cdot 10^{-9}$	$1 \cdot 10^{-5}$
Sr	Celestite/ Strontianite	Sr^{2+}	$6.88 \cdot 10^{-3}$	$3.09 \cdot 10^{-3}$	$1.21 \cdot 10^{-4}$	$4 \cdot 10^{-2}$
Tc	TcO_2	$TcO(OH)_2$	$7.67 \cdot 10^{-9}$	$7.92 \cdot 10^{-9}$	$7.67 \cdot 10^{-9}$	$5 \cdot 10^{-8}$
Th	$Th(OH)_4$	$Th(OH)_4$, $Th(HPO_4)_3^{2-}$	$1.22 \cdot 10^{-9}$	$1.22 \cdot 10^{-9}$	$1.22 \cdot 10^{-9}$	$2 \cdot 10^{-9}$
U	UO_2	$U(OH)_4$	$1.28 \cdot 10^{-7}$	$1.29 \cdot 10^{-7}$	$1.29 \cdot 10^{-7}$	$2 \cdot 10^{-7}$
Zr	ZrO_2	$Zr(OH)_4$	$2.48 \cdot 10^{-9}$	$2.51 \cdot 10^{-9}$	$2.51 \cdot 10^{-9}$	$3 \cdot 10^{-9}$

1.5 Sorption and diffusion in buffer

Table 2-6. K_d-values and diffusivities in buffer (ρ = 2,000 kg/m³).

Element	K_d (m³/kg) Reasonable	Pessimistic	D_e (m²/s)	Porosity
C	0	0	$3 \cdot 10^{-11}$	0.41
Cl	0	0	$1 \cdot 10^{-12}$	0.05
Ni	0.1	0.02	$1 \cdot 10^{-9}$	0.41
Se	0.003	0	$7 \cdot 10^{-11}$	0.41
Sr	0.01	0.001	$5 \cdot 10^{-10}$	0.41
Zr	2	0.05	$5 \cdot 10^{-11}$	0.41
Nb	0.2	0	$5 \cdot 10^{-10}$	0.41
Tc	0.1	0.01	$5 \cdot 10^{-10}$	0.41
Pd	0.01	0	$1 \cdot 10^{-10}$	0.41
Ag	0	0	$2 \cdot 10^{-10}$	0.41
Sn	3	0.01	$7 \cdot 10^{-11}$	0.41
I	0	0	$3 \cdot 10^{-12}$	0.05
Cs	0.05	0.005	$6 \cdot 10^{-10}$	0.41
Ce	1	0.2	$2 \cdot 10^{-10}$	0.41
Sm	1	0.2	$2 \cdot 10^{-10}$	0.41
Ho	1	0.2	$2 \cdot 10^{-10}$	0.41
Pb	0.5	0	$1 \cdot 10^{-9}$	0.41
Rn	0	0	$3 \cdot 10^{-11}$	0.41
Ra	0.01	0.001	$5 \cdot 10^{-10}$	0.41
Th	3	0.1	$7 \cdot 10^{-11}$	0.41
Pa	0.3	0.001	$7 \cdot 10^{-10}$	0.41
U	1	0.01	$5 \cdot 10^{-10}$	0.41
Np	3	0.1	$1 \cdot 10^{-9}$	0.41
Pu	3	1	$3 \cdot 10^{-10}$	0.41
Am	3	1	$7 \cdot 10^{-11}$	0.41
Cm	3	1	$7 \cdot 10^{-11}$	0.41

1.6 Sorption and diffusion in backfill

Table 2-7. Diffusivity and porosity in backfill.

Case	D_e (m^2/s)	Porosity
All cases and sites	10^{-10} m^2/s	0.30

Table 2-8. K_d-values in backfill calculated as 15 percent of bentonite values /Yu and Neretnieks, 1997/ and 85 percent sand (quarts) values /Carbol and Engkvist, 1997/.

Element	Kd (m^3/kg) Reasonable Aberg (saline)	Reasonable Beberg and Ceberg (fresh)	Pessimistic All sites (saline)
C	0.0009	0.0009	0.0004
Cl	0	0	0
Ni	0.03	0.1	0.01
Se	0.001	0.001	0.0004
Sr	0.002	0.08	0.0002
Zr	1	1	0.5
Nb	0.9	0.9	0.4
Tc	0.9	0.9	0.3
Pd	0.01	0.09	0.0009
Ag	0.05	0.5	0.009
Sn	0.5	0.5	0.002
I	0	0	0
Cs	0.05	0.5	0.009
Sm	2	2	0.9
Ho	2	2	0.9
Ra	0.02	0.2	0.009
Th	5	5	0.9
Pa	0.9	1	0.4
U	4	4	0.9
Np	5	5	0.9
Pu	5	5	1
Am	3	3	1
Cm	3	3	1

1.7 Near-field flow

Table 2-9. Groundwater flux in near-field q_0 (m/yr).

Case	Aberg	Beberg	Ceberg
Reasonable	$2 \cdot 10^{-3}$	$1 \cdot 10^{-3}$	$4 \cdot 10^{-5}$
Pessimistic	10^{-1}	$2 \cdot 10^{-2}$	$2 \cdot 10^{-4}$
Probabilistic	Base case in Walker and Gylling /1998/	Base case in Gylling et al /1999/	Base case in Walker and Gylling /1999/

Table 2-10. Non site specific parameters for input to COMP23.

Parameter	Reasonable	Pessimistic
Groundwater flux		
q_1	q_0	$5q_0$
q_2	$10q_0$	$100q_0$
q_3	$100q_0$	$1000q_0$
q_4	$100q_0$	$10000q_0$
Porosity		
ε_1	10^{-4}	10^{-3}
ε_2	$3 \cdot 10^{-4}$	10^{-3}
ε_3	10^{-3}	10^{-3}
ε_4	10^{-3}	10^{-3}

1.8 Sorption and diffusion in rock matrix

Table 2-11. Rock matrix porosity.

Element	Aberg	Beberg	Ceberg
Br, C, Cl, I	$5 \cdot 10^{-3}$	$5 \cdot 10^{-4}$	$5 \cdot 10^{-4}$
All other	$5 \cdot 10^{-3}$	$5 \cdot 10^{-3}$	$5 \cdot 10^{-3}$

Table 2-12. Rock diffusivities.

Element	$D_e \cdot 10^{13}$ (m^2/s) Reasonable Aberg (saline)	Reasonable Beberg and Ceberg (fresh)	Pessimistic All sites
C/HCO_3	0.50	0.05	0.005
Na/Na (I)	0.54	5	0.05
Cl/Cl	0.83	0.08	0.008
Co/Co (II)	0.29	0.29	0.029
Ni/Ni (II)	0.28	0.28	0.028
Se/Se (IV, VI)	0.4	0.4	0.04
Br/Br	0.83	0.08	0.008
Kr (Inert gas)	0.4	0.4	0.04
Sr/Sr (II)	0.33	3	0.03
Zr/Zr (IV)	0.4	0.4	0.04
Nb/Nb (V)	0.4	0.4	0.04
Tc/TcO_4	0.4	0.04	0.004
Tc/Tc (IV)	0.4	0.4	0.04
Pd/Pd (II)	0.4	0.4	0.04
Ag/Ag (I)	0.71	0.71	0.071
Cd/Cd (II)	0.30	0.30	0.030
Sn/Sn (IV)	0.4	0.4	0.04
I/I	0.83	0.08	0.008
Cs/Cs (I)	0.88	9	0.09
Sm/Sm (III)	0.4	0.4	0.04
Eu/Eu (III)	0.4	0.4	0.04
Ho/Ho (III)	0.4	0.4	0.04
Ra/Ra (II)	0.37	0.37	0.037
Ac/Ac (III)	0.4	0.4	0.04
Th/Th (IV)	0.063	0.063	0.0063
Pa/Pa (IV, V)	0.4	0.4	0.04
U/U (IV)	0.4	0.4	0.04
Np/Np (IV)	0.4	0.4	0.04
Pu/Pu (III, IV)	0.4	0.4	0.04
Am/Am (III)	0.4	0.4	0.04
Cm/Cm (III)	0.4	0.4	0.04

Table 2-13. Rock K_d-values /from table 12-1 in Carbol and Engkvist, 1997 and the Data Report/.

Element	Chemical form/ Redox state	K_d (m^3/kg) Reasonable Aberg	Reasonable Beberg and Ceberg	Pessimistic Aberg and Beberg	Pessimistic Ceberg
C	HCO_3^-	0.001	0.001	0.0005	0.0005
Cl	Cl^-	0	0	0	0
Co	Co (II)	0.02	0.1	0.01	0.05
Ni	Ni (II)	0.02	0.1	0.01	0.05
Se	Se (-II, IV, VI)	0.001	0.001	0.0005	0.0005
Kr	inert gas	0	0	0	0
Sr	Sr (II)	0.0002	0.01	0.0001	0.005
Zr	Zr (II)	1	1	0.5	0.5
Nb	Nb (V)	1	1	0.5	0.5
Tc	Tc (IV)	1	1	0.3	0.3
Pd	Pd (II)	0.01	0.1	0.001	0.01
Ag	Ag (I)	0.05	0.5	0.01	0.1
Cd	Cd (II)	0.02	0.1	0.01	0.05
Sn	Sn (IV)	0.001	0.001	0	0
I	I^-	0	0	0	0
Cs	Cs (I)	0.05	0.5	0.01	0.1
Sm	Sm (III)	2	2	1	1
Eu	Eu (III)	2	2	1	1
Ho	Ho (III)	2	2	1	1
Ra	Ra (II)	0.02	0.1	0.01	0.05
Ac	Ac (III)	3	3	1	1
Th	Th (IV)	5	5	1	1
Pa	Pa (IV, V)	1	1	0.5	0.5
U	U (IV)	5	5	1	1
U	U (VI)*	0.005	0.01	0.001	0.005
Np	Np (IV)	5	5	1	1
Np	Np (V)*	0.005	0.01	0.001	0.005
Pu	Pu (III, IV)	5	5	1	1
Am	Am (III)	3	3	1	1
Cm	Cm (III)	3	3	1	1

* Represents value for oxidising conditions. Not relevant here.

1.9 Flow related migration parameters

Table 2-14. Flow related parameters to FARF31. The advective travel time t_w and the flow wetted surface a_w are correlated and cannot be changed independently.

Case	Aberg	Beberg	Ceberg
Travel time, t_w (yrs)			
Reasonable	10	60	2,000
Pessimistic	0.8	3.3	400
Probabilistic	Base case in Walker and Gylling /1998/	Base case in Gylling et al /1999/	Base case in Walker and Gylling /1999/
a_w (m^{-1})			
Reasonable	10^4	10^4	10^3
Pessimistic	10^3	10^3	10^3
Pe			
Reasonable	10	10	10
Pessimistic	2	2	2
Max penetration (m)			
Reasonable	2.0	2.0	20
Pessimistic	0.2	0.2	2.0

1.10 Biosphere

Table 2-15. Biosphere parameters.

Case	Aberg	Beberg	Ceberg
Module			
Reasonable	Peat, with Inner bay of Aberg as variant. For all sites, the reasonable case is also calculated with a site specific well module with a capacity of 300 liters/hour.	Peat. For all sites, the reasonable case is also calculated with a site specific well module with a capacity of 300 liters/hour.	Peat. For all sites, the reasonable case is also calculated with a site specific well module with a capacity of 300 liters/hour.
Pessimistic	Select the module resulting in the highest dose (usually well, peat or agricultural land) for each nuclide, and select highest EDF in the uncertainty interval for these.	Select the module resulting in the highest dose (usually well, peat or agricultural land) for each nuclide, and select highest EDF in the uncertainty interval for these.	Select the module resulting in the highest dose (usually well, peat or agricultural land) for each nuclide, and select highest EDF in the uncertainty interval for these.
EDF for selected module			
Reasonable	Median values	Median values	Median values
Pessimistic	Maximum values	Maximum values	Maximum values

Table 2-16. Reasonable EDF-factors /based on Nordlinder et al, 1999/.

Nuclide	Reasonable EDF-factors (Sv/Bq) Aberg			Beberg		Ceberg	
	Peat area	Well 300l/h	Inner bay	Peat area	Well 300l/h	Peat area	Well 300l/h
Ag-108m	$1.9 \cdot 10^{-11}$	$1.3 \cdot 10^{-12}$	$1.1 \cdot 10^{-15}$	$1.9 \cdot 10^{-11}$	$1.3 \cdot 10^{-12}$	$1.8 \cdot 10^{-11}$	$1.3 \cdot 10^{-12}$
Am-241	$2.0 \cdot 10^{-10}$	$6.8 \cdot 10^{-11}$	$1.6 \cdot 10^{-14}$	$2.0 \cdot 10^{-10}$	$6.8 \cdot 10^{-11}$	$2.0 \cdot 10^{-10}$	$6.7 \cdot 10^{-11}$
Am-243	$1.9 \cdot 10^{-9}$	$1.3 \cdot 10^{-10}$	$1.6 \cdot 10^{-14}$	$1.8 \cdot 10^{-9}$	$1.3 \cdot 10^{-10}$	$1.7 \cdot 10^{-9}$	$1.3 \cdot 10^{-10}$
C-14	$1.1 \cdot 10^{-14}$	$2.4 \cdot 10^{-13}$	$1.7 \cdot 10^{-15}$	$6.5 \cdot 10^{-15}$	$2.4 \cdot 10^{-13}$	$4.6 \cdot 10^{-15}$	$2.4 \cdot 10^{-13}$
Cl-36	$3.6 \cdot 10^{-11}$	$7.3 \cdot 10^{-13}$	$1.6 \cdot 10^{-16}$	$2.2 \cdot 10^{-11}$	$7.2 \cdot 10^{-13}$	$1.5 \cdot 10^{-11}$	$6.3 \cdot 10^{-13}$
Cm-245	$1.2 \cdot 10^{-9}$	$1.6 \cdot 10^{-10}$	$1.6 \cdot 10^{-14}$	$9.8 \cdot 10^{-10}$	$1.6 \cdot 10^{-10}$	$8.1 \cdot 10^{-10}$	$1.6 \cdot 10^{-10}$
Cs-135	$4.4 \cdot 10^{-12}$	$1.9 \cdot 10^{-12}$	$7.8 \cdot 10^{-16}$	$2.7 \cdot 10^{-12}$	$1.9 \cdot 10^{-12}$	$1.8 \cdot 10^{-12}$	$1.7 \cdot 10^{-12}$
Cs-137	$4.0 \cdot 10^{-12}$	$5.6 \cdot 10^{-12}$	$4.8 \cdot 10^{-15}$	$3.5 \cdot 10^{-12}$	$5.6 \cdot 10^{-12}$	$3.1 \cdot 10^{-12}$	$5.6 \cdot 10^{-12}$
Ho-166m	$2.3 \cdot 10^{-12}$	$2.0 \cdot 10^{-12}$	$1.3 \cdot 10^{-16}$	$1.9 \cdot 10^{-12}$	$2.0 \cdot 10^{-12}$	$1.6 \cdot 10^{-12}$	$2.0 \cdot 10^{-12}$
I-129	$5.0 \cdot 10^{-11}$	$9.2 \cdot 10^{-11}$	$1.8 \cdot 10^{-14}$	$3.0 \cdot 10^{-11}$	$9.1 \cdot 10^{-11}$	$2.1 \cdot 10^{-11}$	$7.7 \cdot 10^{-11}$
Nb-94	$3.0 \cdot 10^{-12}$	$3.4 \cdot 10^{-12}$	$2.1 \cdot 10^{-16}$	$2.0 \cdot 10^{-12}$	$3.3 \cdot 10^{-12}$	$1.5 \cdot 10^{-12}$	$2.8 \cdot 10^{-12}$
Ni-59	$4.5 \cdot 10^{-13}$	$5.9 \cdot 10^{-14}$	$2.2 \cdot 10^{-17}$	$2.7 \cdot 10^{-13}$	$5.9 \cdot 10^{-14}$	$1.9 \cdot 10^{-13}$	$5.1 \cdot 10^{-14}$
Ni-63	$1.8 \cdot 10^{-13}$	$6.2 \cdot 10^{-14}$	$5.2 \cdot 10^{-17}$	$1.6 \cdot 10^{-13}$	$6.3 \cdot 10^{-14}$	$1.4 \cdot 10^{-13}$	$6.1 \cdot 10^{-14}$
Np-237	$1.8 \cdot 10^{-10}$	$4.7 \cdot 10^{-11}$	$2.0 \cdot 10^{-15}$	$1.1 \cdot 10^{-10}$	$4.7 \cdot 10^{-11}$	$7.5 \cdot 10^{-11}$	$4.3 \cdot 10^{-11}$
Pa-231	$4.7 \cdot 10^{-9}$	$6.8 \cdot 10^{-10}$	$1.3 \cdot 10^{-14}$	$3.5 \cdot 10^{-9}$	$6.8 \cdot 10^{-10}$	$2.7 \cdot 10^{-9}$	$6.7 \cdot 10^{-10}$
Pd-107	$1.0 \cdot 10^{-13}$	$2.3 \cdot 10^{-14}$	$1.2 \cdot 10^{-18}$	$6.4 \cdot 10^{-14}$	$2.3 \cdot 10^{-14}$	$4.4 \cdot 10^{-14}$	$2.0 \cdot 10^{-14}$
Pu-239	$6.2 \cdot 10^{-10}$	$2.2 \cdot 10^{-10}$	$6.4 \cdot 10^{-15}$	$4.1 \cdot 10^{-10}$	$2.3 \cdot 10^{-10}$	$3.0 \cdot 10^{-10}$	$2.3 \cdot 10^{-10}$
Pu-240	$5.2 \cdot 10^{-10}$	$1.8 \cdot 10^{-10}$	$6.3 \cdot 10^{-15}$	$3.6 \cdot 10^{-10}$	$1.9 \cdot 10^{-10}$	$2.7 \cdot 10^{-10}$	$1.9 \cdot 10^{-10}$
Pu-242	$6.3 \cdot 10^{-10}$	$2.3 \cdot 10^{-10}$	$6.1 \cdot 10^{-15}$	$4.1 \cdot 10^{-10}$	$2.4 \cdot 10^{-10}$	$3.0 \cdot 10^{-10}$	$2.3 \cdot 10^{-10}$
Ra–226	$1.7 \cdot 10^{-9}$	$1.2 \cdot 10^{-10}$	$1.6 \cdot 10^{-14}$	$1.2 \cdot 10^{-9}$	$1.1 \cdot 10^{-10}$	$9.4 \cdot 10^{-10}$	$1.1 \cdot 10^{-10}$
Se-79	$2.7 \cdot 10^{-9}$	$2.7 \cdot 10^{-12}$	$1.4 \cdot 10^{-14}$	$1.7 \cdot 10^{-9}$	$2.7 \cdot 10^{-12}$	$1.2 \cdot 10^{-9}$	$2.1 \cdot 10^{-12}$
Sm-151	$6.4 \cdot 10^{-15}$	$3.2 \cdot 10^{-14}$	$5.9 \cdot 10^{-18}$	$6.0 \cdot 10^{-15}$	$3.2 \cdot 10^{-14}$	$5.7 \cdot 10^{-15}$	$3.2 \cdot 10^{-14}$
Sn-126	$1.4 \cdot 10^{-10}$	$3.9 \cdot 10^{-12}$	$9.9 \cdot 10^{-16}$	$8.6 \cdot 10^{-11}$	$3.9 \cdot 10^{-12}$	$6.1 \cdot 10^{-11}$	$3.1 \cdot 10^{-12}$
Sr-90	$2.1 \cdot 10^{-11}$	$1.3 \cdot 10^{-11}$	$1.3 \cdot 10^{-15}$	$1.8 \cdot 10^{-11}$	$1.3 \cdot 10^{-11}$	$1.6 \cdot 10^{-11}$	$1.2 \cdot 10^{-11}$
Tc-99	$7.0 \cdot 10^{-13}$	$5.5 \cdot 10^{-13}$	$1.7 \cdot 10^{-17}$	$4.2 \cdot 10^{-13}$	$5.5 \cdot 10^{-13}$	$2.9 \cdot 10^{-13}$	$4.7 \cdot 10^{-13}$
Th-229	$7.5 \cdot 10^{-9}$	$4.2 \cdot 10^{-10}$	$1.3 \cdot 10^{-14}$	$7.0 \cdot 10^{-9}$	$4.1 \cdot 10^{-10}$	$6.5 \cdot 10^{-9}$	$4.1 \cdot 10^{-10}$
Th-230	$4.4 \cdot 10^{-9}$	$2.1 \cdot 10^{-10}$	$5.4 \cdot 10^{-15}$	$4.0 \cdot 10^{-9}$	$2.1 \cdot 10^{-10}$	$3.7 \cdot 10^{-9}$	$2.0 \cdot 10^{-10}$
U-233	$1.0 \cdot 10^{-11}$	$1.9 \cdot 10^{-11}$	$2.6 \cdot 10^{-15}$	$6.1 \cdot 10^{-12}$	$1.9 \cdot 10^{-11}$	$4.3 \cdot 10^{-12}$	$1.7 \cdot 10^{-11}$
U-234	$9.8 \cdot 10^{-12}$	$1.8 \cdot 10^{-11}$	$2.5 \cdot 10^{-15}$	$5.9 \cdot 10^{-12}$	$1.7 \cdot 10^{-11}$	$4.1 \cdot 10^{-12}$	$1.7 \cdot 10^{-11}$
U-235	$8.9 \cdot 10^{-12}$	$1.7 \cdot 10^{-11}$	$2.4 \cdot 10^{-15}$	$5.4 \cdot 10^{-12}$	$1.7 \cdot 10^{-11}$	$3.7 \cdot 10^{-12}$	$1.6 \cdot 10^{-11}$
U-238	$8.3 \cdot 10^{-12}$	$1.6 \cdot 10^{-11}$	$2.3 \cdot 10^{-15}$	$5.1 \cdot 10^{-12}$	$1.6 \cdot 10^{-11}$	$3.5 \cdot 10^{-12}$	$1.6 \cdot 10^{-11}$
Zr-93	$6.1 \cdot 10^{-13}$	$3.7 \cdot 10^{-13}$	$9.0 \cdot 10^{-17}$	$4.4 \cdot 10^{-13}$	$3.6 \cdot 10^{-13}$	$3.3 \cdot 10^{-13}$	$3.6 \cdot 10^{-13}$

Table 2-17. Pessimistic EDF-factors. In all cases apart from C-14, the EDFs are those for "pessimistic peat". The C-14 EDF is that of the well with the lowest specific capacity at the respective sites /based on Nordlinder et al, 1999/.

Nuclide	Pessimistic EDF-factors (Sv/Bq)		
	Aberg	Beberg	Ceberg
Ag-108m	$2.3 \cdot 10^{-10}$	$2.3 \cdot 10^{-10}$	$2.2 \cdot 10^{-10}$
Am-241	$2.6 \cdot 10^{-9}$	$2.6 \cdot 10^{-9}$	$2.6 \cdot 10^{-9}$
Am-243	$2.7 \cdot 10^{-8}$	$2.5 \cdot 10^{-8}$	$2.3 \cdot 10^{-8}$
C-14	$5.4 \cdot 10^{-13}$	$2.6 \cdot 10^{-13}$	$2.6 \cdot 10^{-13}$
Cl-36	$3.3 \cdot 10^{-10}$	$2.0 \cdot 10^{-10}$	$1.4 \cdot 10^{-10}$
Cm-245	$1.4 \cdot 10^{-8}$	$1.2 \cdot 10^{-8}$	$9.4 \cdot 10^{-9}$
Cs-135	$3.7 \cdot 10^{-11}$	$2.2 \cdot 10^{-11}$	$1.5 \cdot 10^{-11}$
Cs-137	$3.6 \cdot 10^{-11}$	$2.9 \cdot 10^{-11}$	$2.6 \cdot 10^{-11}$
Ho-166m	$2.3 \cdot 10^{-11}$	$2.0 \cdot 10^{-11}$	$1.8 \cdot 10^{-11}$
I-129	$8.2 \cdot 10^{-10}$	$4.9 \cdot 10^{-10}$	$3.1 \cdot 10^{-10}$
Nb-94	$3.3 \cdot 10^{-11}$	$2.4 \cdot 10^{-11}$	$1.9 \cdot 10^{-11}$
Ni-59	$4.1 \cdot 10^{-12}$	$2.5 \cdot 10^{-12}$	$1.7 \cdot 10^{-12}$
Ni-63	$2.0 \cdot 10^{-12}$	$1.6 \cdot 10^{-12}$	$1.4 \cdot 10^{-12}$
Np-237	$1.7 \cdot 10^{-9}$	$1.0 \cdot 10^{-9}$	$7.0 \cdot 10^{-10}$
Pa-231	$5.2 \cdot 10^{-8}$	$4.3 \cdot 10^{-8}$	$3.4 \cdot 10^{-8}$
Pd-107	$1.1 \cdot 10^{-12}$	$7.1 \cdot 10^{-13}$	$5.0 \cdot 10^{-13}$
Pu-239	$7.7 \cdot 10^{-9}$	$6.4 \cdot 10^{-9}$	$5.0 \cdot 10^{-9}$
Pu-240	$6.4 \cdot 10^{-9}$	$4.9 \cdot 10^{-9}$	$4.1 \cdot 10^{-9}$
Pu-242	$8.3 \cdot 10^{-9}$	$6.8 \cdot 10^{-9}$	$5.0 \cdot 10^{-9}$
Ra-226	$1.9 \cdot 10^{-8}$	$1.6 \cdot 10^{-8}$	$1.2 \cdot 10^{-8}$
Se-79	$2.6 \cdot 10^{-8}$	$1.7 \cdot 10^{-8}$	$1.2 \cdot 10^{-8}$
Sm-151	$8.4 \cdot 10^{-14}$	$8.1 \cdot 10^{-14}$	$7.7 \cdot 10^{-14}$
Sn-126	$1.4 \cdot 10^{-9}$	$9.1 \cdot 10^{-10}$	$6.3 \cdot 10^{-10}$
Sr-90	$2.2 \cdot 10^{-10}$	$1.8 \cdot 10^{-10}$	$1.6 \cdot 10^{-10}$
Tc-99	$1.8 \cdot 10^{-11}$	$1.1 \cdot 10^{-11}$	$7.4 \cdot 10^{-12}$
Th-229	$9.9 \cdot 10^{-8}$	$8.6 \cdot 10^{-8}$	$8.2 \cdot 10^{-8}$
Th-230	$5.7 \cdot 10^{-8}$	$5.0 \cdot 10^{-8}$	$4.5 \cdot 10^{-8}$
U-233	$1.4 \cdot 10^{-10}$	$8.7 \cdot 10^{-11}$	$6.0 \cdot 10^{-11}$
U-234	$1.4 \cdot 10^{-10}$	$8.4 \cdot 10^{-11}$	$5.9 \cdot 10^{-11}$
U-235	$1.3 \cdot 10^{-10}$	$7.6 \cdot 10^{-11}$	$5.3 \cdot 10^{-11}$
U-238	$1.2 \cdot 10^{-10}$	$7.2 \cdot 10^{-11}$	$5.0 \cdot 10^{-11}$
Zr-93	$4.8 \cdot 10^{-12}$	$3.5 \cdot 10^{-12}$	$2.8 \cdot 10^{-12}$

Table 2-18. Pessimistic EDF-factors used in the probabilistic calculations /based on Nordlinder et al, 1999/.

Nuclide	Pessimistic EDF-factor (Sv/Bq)					
	Aberg		Beberg		Ceberg	
	Peat area	Well 300l/h	Peat area	Well 300l/h	Peat area	Well 300l/h
Ni-59	$4.1 \cdot 10^{-12}$	$2.0 \cdot 10^{-13}$	$2.5 \cdot 10^{-12}$	$2.0 \cdot 10^{-13}$	$1.7 \cdot 10^{-12}$	$1.6 \cdot 10^{-13}$
Nb-94	$3.3 \cdot 10^{-11}$	$8.3 \cdot 10^{-12}$	$2.4 \cdot 10^{-11}$	$8.3 \cdot 10^{-12}$	$1.9 \cdot 10^{-11}$	$7.3 \cdot 10^{-12}$
Sn-126	$1.4 \cdot 10^{-9}$	$1.2 \cdot 10^{-11}$	$9.1 \cdot 10^{-10}$	$1.2 \cdot 10^{-11}$	$6.3 \cdot 10^{-10}$	$8.4 \cdot 10^{-12}$
I-129	$4.7 \cdot 10^{-10}$	$3.7 \cdot 10^{-10}$	$2.8 \cdot 10^{-10}$	$3.6 \cdot 10^{-10}$	$2.0 \cdot 10^{-10}$	$2.7 \cdot 10^{-10}$
Ra-226	$1.9 \cdot 10^{-8}$	$2.2 \cdot 10^{-10}$	$1.6 \cdot 10^{-8}$	$2.1 \cdot 10^{-10}$	$1.2 \cdot 10^{-8}$	$1.9 \cdot 10^{-10}$
Th-230	$5.7 \cdot 10^{-8}$	$5.3 \cdot 10^{-10}$	$5.0 \cdot 10^{-8}$	$5.2 \cdot 10^{-10}$	$4.5 \cdot 10^{-8}$	$5.1 \cdot 10^{-10}$
U-234	$1.4 \cdot 10^{-10}$	$2.9 \cdot 10^{-11}$	$8.4 \cdot 10^{-11}$	$2.9 \cdot 10^{-11}$	$5.9 \cdot 10^{-11}$	$2.7 \cdot 10^{-11}$
U-238	$1.2 \cdot 10^{-10}$	$2.6 \cdot 10^{-11}$	$7.2 \cdot 10^{-11}$	$2.5 \cdot 10^{-11}$	$5.0 \cdot 10^{-11}$	$2.4 \cdot 10^{-11}$
Pu-239	$7.7 \cdot 10^{-9}$	$6.0 \cdot 10^{-10}$	$6.4 \cdot 10^{-9}$	$6.0 \cdot 10^{-10}$	$5.0 \cdot 10^{-9}$	$6.0 \cdot 10^{-10}$

Table 2-19. Reasonable EDF-factors for "Open Coast" used in the glacial melting scenario for Aberg /based on Nordlinder et al, 1999/.

Nuclide	Reasonable EDF-factor (Sv/Bq)
Ag-108m	$4.3 \cdot 10^{-18}$
Am-241	$2.0 \cdot 10^{-16}$
Am-243	$2.0 \cdot 10^{-16}$
C-14	$6.7 \cdot 10^{-18}$
Cl-36	$5.7 \cdot 10^{-19}$
Cm-245	$2.1 \cdot 10^{-16}$
Cs-135	$2.9 \cdot 10^{-18}$
Cs-137	$1.8 \cdot 10^{-17}$
Ho-166m	$1.9 \cdot 10^{-18}$
I-129	$1.1 \cdot 10^{-16}$
Nb-94	$1.5 \cdot 10^{-18}$
Ni-59	$9.0 \cdot 10^{-20}$
Ni-63	$2.1 \cdot 10^{-19}$
Np-237	$7.6 \cdot 10^{-18}$
Pa-231	$4.8 \cdot 10^{-17}$
Pd-107	$2.6 \cdot 10^{-20}$
Pu-239	$5.5 \cdot 10^{-17}$
Pu-240	$5.5 \cdot 10^{-17}$
Pu-242	$5.3 \cdot 10^{-17}$
Ra-226	$7.0 \cdot 10^{-17}$
Se-79	$5.3 \cdot 10^{-17}$
Sm-151	$9.1 \cdot 10^{-20}$
Sn-126	$3.8 \cdot 10^{-18}$
Sr-90	$5.0 \cdot 10^{-18}$
Tc-99	$6.1 \cdot 10^{-19}$
Th-229	$4.0 \cdot 10^{-16}$
Th-230	$1.7 \cdot 10^{-16}$
U-233	$1.1 \cdot 10^{-17}$
U-234	$1.1 \cdot 10^{-17}$
U-235	$1.0 \cdot 10^{-17}$
U-238	$9.7 \cdot 10^{-18}$
Zr-93	$9.8 \cdot 10^{-19}$

References: See list of references for Chapter 9.